LOW NO_X EMISSION COMBUSTOR DEVELOPMENT FOR AUTOMOBILE GAS TURBINE ENGINES

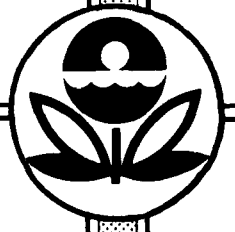

U.S. ENVIRONMENTAL PROTECTION AGENCY
Office of Air and Water Programs
Office of Mobile Source Air Pollution Control
Alternative Automotive Power Systems Division
Ann Arbor, Michigan 48105

APTD-1374

LOW NO_X EMISSION COMBUSTOR DEVELOPMENT FOR AUTOMOBILE GAS TURBINE ENGINES

Prepared By

D.W. Dawson, K.A. Hanson, R.C. Holder

AiResearch Manufacturing Company of Arizona
A Division of The Garrett Corporation
402 S. 36th Street
Phoenix, Arizona 85034

Contract No. 68-04-0014

EPA Project Officer:

R.B. Schulz

Prepared For

U.S. ENVIRONMENTAL PROTECTION AGENCY
Office of Air and Water Programs
Office of Mobile Source Air Pollution Control
Alternative Automotive Power Systems Division
Ann Arbor, Michigan 48105

February 1973

The APTD (Air Pollution Technical Data) series of reports is issued by the Office of Air and Water Programs, U. S. Environmental Protection Agency, to report technical data of interest to a limited number of readers. Copies of APTD reports are available free of charge to Federal employees, current contractors and grantees, and non-profit organizations - as supplies permit from the Air Pollution Technical Information Center, U. S. Environmental Protection Agency, Research Triangle Park, North Carolina 27711 or may be obtained, for a nominal cost, from the National Technical Information Service, U. S. Department of Commerce, 5285 Port Royal Road, Springfield, Virginia 22151.

This report was furnished to the U. S. Environmental Protection Agency by AiResearch Manufacturing Company of Arizona, Phoenix, Arizona, in fulfillment of Contract Number 68-04-0014. The contents of this report are reproduced herein as received from the AiResearch Manufacturing Company of Arizona. The opinions, findings, and conclusions expressed are those of the author and not necessarily those of the Environmental Protection Agency.

Publication Number APTD-1374

TABLE OF CONTENTS

TABLE OF CONTENTS (Contd)

FINAL REPORT
LOW NO_x EMISSION COMBUSTOR DEVELOPMENT FOR AUTOMOBILE GAS TURBINE ENGINES

1. INTRODUCTION AND SUMMARY

1.1 Introduction

The investigation reported herein was performed by AiResearch Manufacturing Company of Arizona, A Division of The Garrett Corporation, to satisfy the Low NO_x Emission Combustor Study for Automobile Gas Turbine Engines under Contract 68-04-0014 for the Environmental Protection Agency, Office of Air and Water Programs, Advanced Automotive Power Systems Development Division.

The purpose of this program was to perform an analytical and experimental study of gas turbine combustors suitable for automotive engines. A chemical kinetics analysis was formulated and performed. Combustors representative of regenerated and nonregenerated automotive gas turbines were analyzed, designed, tested, and evaluated relative to reducing exhaust emissions. The program goal was to establish combustor design data and emission criteria that through test demonstration would aid in achieving the 1976 Federal Emissions Standards tabulated below. The program included emphasis on the reduction of NO_x emissions which for gas turbine combustors is the most difficult emission species to reduce to the 1976 Standards.

1976 Federal Emission Standards

NO_x (as NO_2)	0.40 gm/mi
CO	3.40
HC (as $CH_{1.85}$)	0.41

A number of combustor types were fabricated and evaluated under specified test conditions. When the estimated program cost was expended at 8 months, an extension was negotiated, after a four month hold period to cover 8 tests on two specified combustor configurations. The specified configurations were a vaporizer combustor and a pneumatic-impact injector combustor.

1.2 Acknowledgments

The authors would like to acknowledge major technical contributions given throughout the program by the following individuals: S. C. Hunter, Principal Investigator; C. G. Mackay, Project Engineer; K. W. Benn, J. T. Irwin, Program Managers; Dr's. J. G. Sotter, V. Quan, and C. A. Bodeen of KVB Engineering Inc., Consultant Firm.

1.3 Summary

This document reports on analytical and experimental work performed for the Environmental Protection Agency, Office of Air and Water Programs (formerly Office of Air Programs) under Contract 68-04-0014. The total program, including the four month hold, covered the period from May 11, 1971 to November 30, 1972.

During the contract period 35 combustor configurations were tested to determine emissions characteristics. Six combustor types were checked for emissions characteristics but not extensively investigated.

The goal of demonstrating emissions (NO_x, HC, and CO) lower than the 1976 Federal Emission Standards for Light Duty Vehicles was met, except for NO_x, when utilizing simulated Federal Driving Cycle procedures. A design technique that achieved significant NO_x reductions in a gas turbine combustor was demonstrated. This technique involved the application of recuperator (or regenerator) bypass air directly into the combustor primary zone.

Some difficulties were encountered during the program. One of these was the difficulty of achieving reliable extrapolations of emissions at combustor inlet temperatures higher than the maximum available test temperature. This revealed the desirability of performing combustor emissions tests in facilities capable of providing full-scale air flows with combustor inlet temperatures of at least 1400°F.

Another difficulty related to the method of predicting or simulating the Federal Driving Cycle (FDC) emissions from steady-state test conditions. However, during the course of the program, AiResearch developed a 5-point simulation procedure to predict emissions from steady-state combustor tests. For the vaporizer combustor compared by both procedures with bypass operation, this procedure predicts NO_x emissions almost three times as high as the EPA 6-point procedure. It is also higher than procedures suggested by other EPA sub-contractors. Differences in simulation procedures used by AiResearch and others, including EPA, typically predict orders-of-magnitude differences in the individual species of pollutant. Therefore, comparisons of predicted FDC emissions should be made with the same procedure utilized by all subcontractors. The need for additional study directed toward improvement of the simulation procedure is apparent.

Out of the configurations tested, the vaporizer combustor resulted in the most significant improvement by the use of bypass flow. For combustors with a fixed bypass flow quantity, a bypass of 10 percent appears to be the best selection. Further improvements can be attained by using a combustor with a variable bypass flow. The best results obtained for simulated FDC emissions in gm/mi are as follows:

(Procedure→)	76 Std	AiR 5 Pt 0% BP	AiR 5 Pt 10% BP	AiR 1 Pt 10% BP	EPA 6 Pt 10% BP	EPA 6 Pt Variable BP
NO_x	0.4	6.38	1.73	0.45	0.66	0.78
HC	0.41	0.012	0.005	0.70	0.12	0.09
CO	3.4	0.13	0.071	1.60	1.90	0.90

The results of the program have revealed that the optimum low emissions engine would utilize an engine cycle and variable bypass flow that have been matched to provide the best balance between fuel economy and related emissions.

Significant conclusions of the program include the following:

- Recuperator bypass, correctly applied, is an effective NO_x control technique
  - An 82 percent NO_x reduction has been demonstrated with a vaporizing combustor (SKP26489SD) over the AiResearch 5-point FDC simulation at constant 10 percent bypass.
  - A 73 percent NO_x reduction was demonstrated on the AiResearch 5-point FDC simulation between the vaporizer combustor with the lowest zero-bypass NO_x emissions (SKP26489 M_2) and the vaporizer combustor with the the highest zero-bypass NO_x emissions (SKP26489SD) when operated at a constant 10 percent bypass.
- Recuperator bypass as a NO_x control technique is applicable to a variety of combustor concepts including:
  - Vaporizer
  - Pneumatic impact
  - Atomizer (with air-assist atomization)
  - Premix
- An engine cycle can be optimized to provide the best balance of the emission constituents and fuel economy.

- Variable recuperator bypass is a simple and convenient alternative to variable combustor geometry. The required control system is simpler and has the potential of:

  - Lower cost
  - Higher reliability
  - Better maintainability

- Recuperator bypass does result in higher vehicle fuel consumption. Based on limited testing of non-optimized combustion and without the benefit of cycle optimization considerations, the fuel consumption penalty was about 15 to 20 percent.

2. COMBUSTOR PRELIMINARY DESIGN

2.1 Design Criteria

The program was originally directed to two types or classes of gas turbine engines that exhibit the following characteristics:

Class A	Class B
Low pressure ratio	High pressure ratio
Low turbine inlet temperature	High turbine inlet temperature
Regenerated or recuperated	No form of waste heat recovery

The combustor emission goals originally specified in the "Request For Proposal" (established before the 1976 Federal Emissions Standards were announced) are shown together with the preliminary design criteria for Class A and Class B combustors in Table 2-1.

Conceptual design studies of combustion systems for both the regenerated and nonregenerated applications were conducted on single-can configurations. Conceptual designs proposed for this program were evaluated based on the following criteria:

(a) Capable of operation at low primary zone equivalence ratio to minimize flame temperature

(b) Amenable in itself or by the addition of mixing devices to the establishment of a homogeneous primary zone devoid of local areas of high equivalence ratio

(c) Minimum primary zone residence time

Based on the above criteria, three configurations were selected for further study.

TABLE 2-1

EMISSION LEVEL CRITERIA

	Vehicle Emission Goals grams/mile	Combustion Emission Goals* mg/g fuel	Combustor Emissions Levels, ppm	
			Class A****	Class B****
Hydrocarbons**	0.14	0.48	0.5 to 2.4	1.0 to 4.8
Carbon Monoxide	6.16	21.3	66 to 325	132 to 650
Oxides of Nitrogen***	0.40	1.38	2.6 to 13	5.2 to 26
Particulates	0.03	0.10	-	-

*For 10.0 miles/gal fuel economy and JP-4 fuel (specific gravity = 0.763)

**Total hydrocarbons plus total aldehydes expressed as hexane (C_6H_{14})

***Oxides of nitrogen computed as NO_2

****Parts per million by volume, wet basis

DESIGN CRITERIA FOR GAS TURBINE COMBUSTORS

	Class A		Class B	
	Design Point	Testing Range	Design Point	Testing Range
Heating Rate, Btu/hr	1.386×10^6	2.10×10^5 min	1.880×10^6	2.82×10^5 min
Inlet Air Temperature, °F	1100	200 to 1200	760	400 to 900
Inlet Air Pressure, atm	4.0	2.0 to 6.0	12.0	6.0 to 16.0
Overall Fuel-Air Ratio	0.01	0.003 to 0.015	0.020	0.006 to 0.030
Outlet Temperature, °F	1700	1000 to 2200	1900	1200 to 2400

(a) External Prevaporizing Combustor (Pre-Mix) - The external prevaporizing design (Figure 2-1) incorporates an external chamber into which the fuel is sprayed, vaporized, and mixed with air. The mixture is delivered to the combustion section primary zone through a large number of small connecting tubes. More air is introduced into the primary zone around the tubes to further lean out the mixture prior to combustion. Small recirculating combustion zones are established at the exits of the fuel delivery tubes resulting in a homogeneous primary zone with a very compact flame. Minimizing the combustion zone volume in this manner reduces the length of time the post-flame gases are exposed to high temperature conditions which encourage nitric oxide formation.

(b) Airblast Pneumatic Impact Combustor - A configuration utilizing an air blast injector (Figure 2-2) was designed for the Class B application. By introducing most of the primary air through the injector, maximum atomization and mixing occurs prior to reaching the injector exit.

The airblast injector was sized with the aid of an analytical model developed at AiResearch for the USAAVLABS Advanced, Small, High-Temperature-Rise Combustor Program. The model calculates fuel velocities through the venturi, atomization quality at the injector outlet, and droplet trajectories for five classes of droplet size at the injector exit. At 4.5 percent pressure drop (isothermal conditions) with the Class B fuel flow, an injector geometry consisting of a 3/16-in. diameter fuel delivery tube discharging into the 0.38-in. diameter throat of a 0.65-in. long venturi gave a Sauter mean droplet diameter at the injector exit of 7.5 microns, which is more than adequate atomization for successful combustion operation.

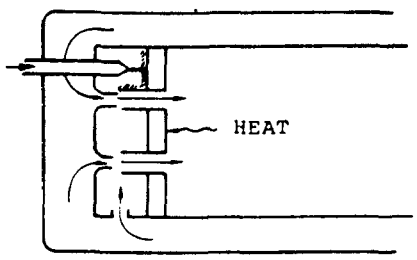

FIGURE 2-1 EXTERNAL PREVAPORIZING COMBUSTOR (PRE-MIX)

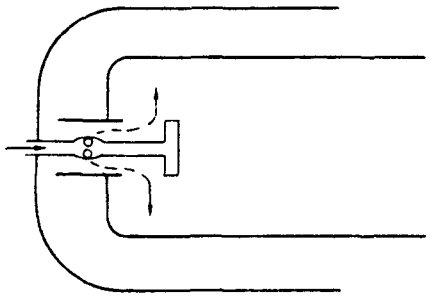

FIGURE 2-2 AIRBLAST PREMIXING COMBUSTOR (PNEUMATIC IMPACT)

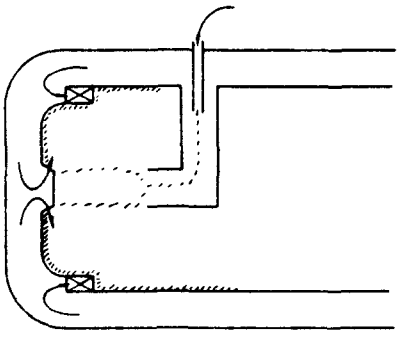

FIGURE 2-3 FILM VAPORIZING COMBUSTOR

(c) Film-Vaporizer Combustor - One film-vaporizing type combustor (Figure 2-3) was designed for each combustor class. Liner open area was sized for a pressure loss of 4.5 percent of inlet total pressure (isothermal) in both cases.

Features of the design incorporated specifically for emission control include a lean primary zone (equivalence ratio = 0.6) to minimize nitric oxide formation rates by reducing flame temperature. Aerodynamic mixing devices are included within the fuel delivery primary pipe to ensure uniform fuel distribution at the pipe exit. Uniform fuel distribution is required to avoid local areas of high equivalence ratio in the primary zone which contribute to high nitric oxide formation rates. In addition, a solid boundary has been introduced between the primary pipe exit and the combustor dome to allow vaporization to begin at an earlier time. The effect is to reduce primary zone residence time by minimizing the effective primary zone length and to allow earlier dilution air introduction to quench emission formation reactions. Figure 2-4 illustrates these effects.

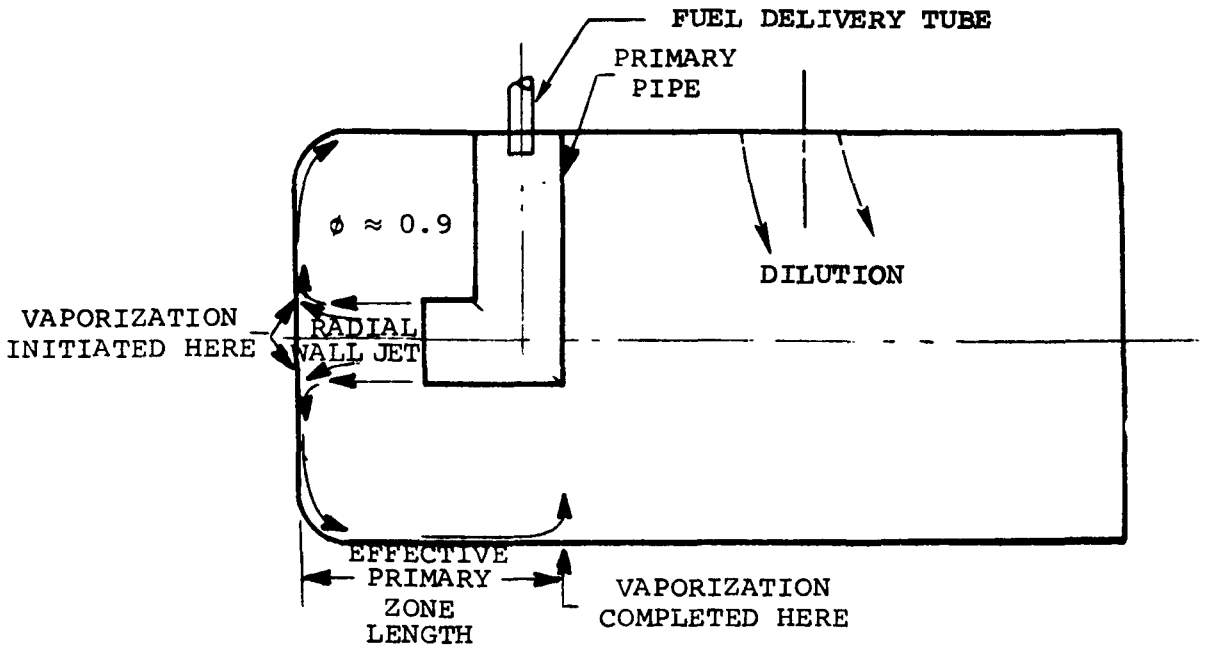

a. CONVENTIONAL FILM-VAPORIZER

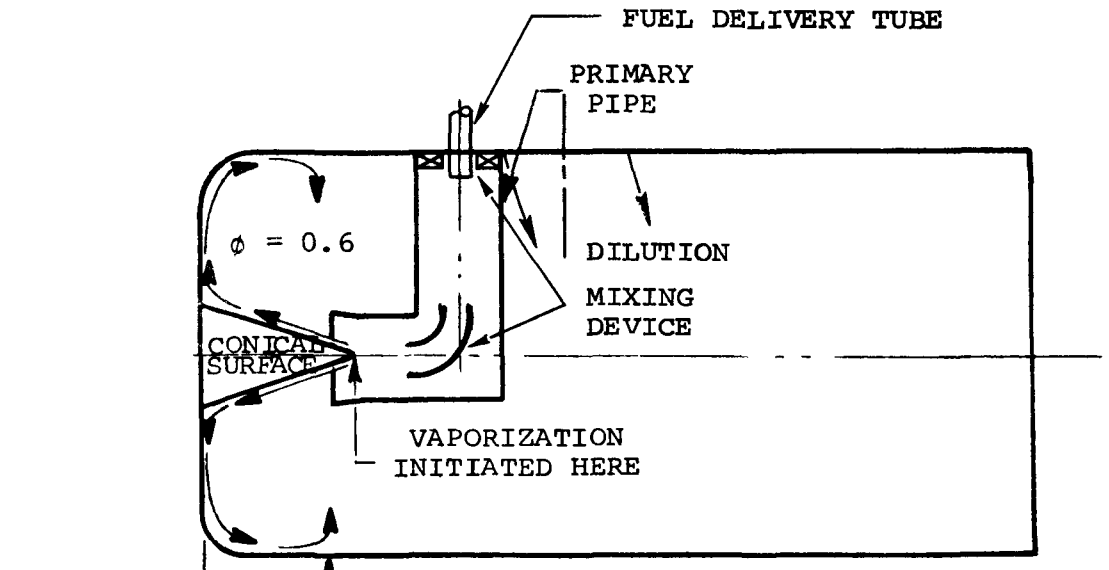

b. LOW NO_x FILM-VAPORIZER

COMPARISON OF CONVENTIONAL AND LOW NO_x FILM-VAPORIZING COMBUSTOR DESIGN FEATURES

FIGURE 2-4

2.2 Engine Design/Off-Design Cycle Analysis

Cycle studies, including design and off-design performance, were conducted to integrate the Class A and Class B combustor preliminary design criteria into representative automotive gas turbine engine applications. The data derived from the cycle analysis were used to establish combustor operating conditions for use in the test program.

(a) Design-Point Cycle Analysis - A compressor-turbine flow match was generated for the Class A and Class B preliminary design criteria utilizing a variable-geometry free-power-turbine engine cycle. The matching studies resulted in a corrected power output for the Class A regenerated engine of 182.5 shp and 124.2 shp for the nonregenerated Class B engine at the design conditions specified. In addition to the design-point calculations, off-design steady-state and transient performance data were also generated for both engine classes.

Because of the wide variation in power output between the two combustor classes, it was recommended and approved that the design criteria be modified to bring the power output of both engines to 150 shp. Consequently, the heat release rate of the Class A combustor was reduced from 1.5×10^6 Btu/hr to 1.396×10^6 Btu/hr, and the Class B heat release was increased from 1.5×10^6 Btu/hr to 1.880×10^6 Btu/hr.

The new design criteria for Class A and Class B are shown in Tables 2-2 and 2-3, respectively.

LOW EMISSION COMBUSTOR ** CLASS A* APCO ASSUMPTIONS-EXCEPT ETA(R) *150 HP ENGINE

LHV	H/C	ALTITUDE	FPS
18500.0	.16786	0.0	0.000

COMPRESSOR				TURBINES 2 IS THE POWER TURBINE				
DRIVING TURBINE	HP	ENERGY CORR. COOLING AIR	WATER	SHAFT HP	ACC HP	HP REQUIRED	MECHANICAL EFFICIENCY	BEFORE MIXING ENTHALPY	BEFORE MIXING TEMP
1	257.46	0.000	0.000	0.0	5.0	262.6	.980	471.49	1860.6
				150.0	1.5	154.6	.980	419.47	1672.3

BURNER	WATER	FUEL FLOW
	0.000	75.46

	CR FLOW	PRESSURE	TEMP	DELTA	THETA	R	ENTHALPY	GAMMA	F/A	W/A	EFF	P/P	DEL P	LEAKAGE	COOLING	
AMBIENT	2.333	14.696	518.7	1.000	1.000	53.349	124.00	1.401		0.0000						AMBIENT
INLET	2.368	14.476	518.7	.985	1.000	53.349	124.00	1.401		0.0000	1.000	1.000	.015	0.000		INLET
COMPRESSR	.706	60.768	841.6	4.135	1.623	53.349	202.01	1.390		0.0000	.808	4.198	0.000	.003	.015	COMPRESSR
DIFFUSER	.713	60.161	841.6	4.094	1.623	53.349	202.01	1.390	0.0000	0.0000			.010			DIFFUSER
REGNR CLD	.944	58.777	1559.5	4.000	3.007	53.349	384.95	1.347		0.0000	.869	1.000	.023	.025		REGEN CLD
BURNER	1.168	56.426	2159.7	3.840	4.164	53.366	555.91	1.316	.0096	0.0000	.980	1.000	.040	0.000		BURNER
TURBINE	2.251	27.346	1850.6	1.864	3.568	53.365	468.66	1.327	.0095	0.0000	.860	2.060	0.000	0.000	.011	TURBINE
DIFFUSER	2.297	26.848	1850.6	1.827	3.568	53.365	468.66	1.327	.0095	0.0000			.020			DIFFUSER
TURBINE	3.515	16.746	1668.3	1.139	3.216	53.365	419.34	1.335	.0095	0.0000	.870	1.603	0.000	0.000	.005	TURBINE
DIFFUSER	3.700	15.909	1668.3	1.083	3.216	53.365	418.34	1.335	.0095	0.0000			.050			DIFFUSER
REGRN HOT	3.198	14.843	981.4	1.010	1.892	53.365	238.13	1.376	.0090	0.0000		1.000	.067	.025		REGNR HOT
DIFFUSER	3.230	14.694	981.4	1.000	1.892	53.365	238.13	1.376	.0090	0.0000			.010			FFUSER

FUEL FLOW	TOTAL	CORRECTED	SFC	POWER	NET	CORRECTED	SPECIFIC
	75.5	76.6	.503		150.0	152.3	64.30

TABLE 2-2

VARIABLE POWER TURBINE GEOMETRY ENGINE

** LOW EMISSION COMBUSTOR **APCO ASSUMPTIONS**CLASS8**150 HP**

ENGINE

LHV	H/C	ALTITUDE	FPS
18500.0	.16786	0.0	0.000

COMPRESSOR

DRIVING TURBINE	HP	ENERGY CORR. COOLING AIR	WATER
1	394.39	0.000	0.000

TURBINES
2 IS THE POWER TURBINE

SHAFT HP	ACC HP	HP REQUIRED	MECHANICAL EFFICIENCY	BEFORE MIXING ENTHALPY	BEFORE MIXING TEMP
0.0	5.0	399.5	.980	438.87	1727.7
150.0	1.5	154.6	.980	365.39	1461.3

BURNER	WATER	FUEL FLOW
	0.000	101.63

	CR FLOW	PRESSURE	TEMP	DELTA	THETA	R	ENTHALPY	GAMMA	F/A	W/A	EFF	P/P	DEL P	LEAKAGE	COOLING	
AMBIENT	1.645	14.696	518.7	1.000	1.000	53.349	124.00	1.401		0.0000						AMBIENT
INLET	1.670	14.476	518.7	.985	1.000	53.349	124.00	1.401		0.0000	1.000	1.000	.015	0.000		INLET
COMPRESSR	.194	176.355	1208.2	12.000	2.329	53.349	293.46	1.368		0.0000	.768	12.306	.010	.021	.050	COMPRESSR
BURNER	.288	169.301	2359.7	11.520	4.549	53.381	520.29	1.304	.0185	0.0000	.980	1.000	.040	0.000		BURNER
TURBINE	1.322	32.801	1706.2	2.232	3.289	53.379	432.53	1.328	.0177	0.0000	.825	5.161	0.000	0.000	.044	TURBINE
DIFFUSER	1.349	32.145	1706.2	2.187	3.289	53.379	432.53	1.328	.0177	0.0000			.020			DIFFUSER
TURBINE	2.583	15.641	1459.6	1.064	2.814	53.379	364.90	1.341	.0175	0.0000	.870	2.055	0.000	0.000	.007	TURBINE
DIFFUSER	2.748	14.702	1459.6	1.000	2.814	53.379	364.90	1.341	.0175	0.0000			.060			DIFFUSER

FUEL FLOW	TOTAL	CORRECTED	SFC
	101.6	103.2	.678

POWER	NET	CORRECTED	SPECIFIC
	150.0	152.3	91.18

TABLE 2-3

VARIABLE POWER TURBINE GEOMETRY ENGINE

(b) Off-Design Cycle Analysis - The following discussion briefly describes the development of combustor test conditions as they evolved during this study program. Also, the method for obtaining mass emissions in grams per mile from combustor rig test data is discussed.

Within the constraints of Table 2-1, an engine cycle design point (Tables 2-2 and 2-3) was generated for each class engine. These data were used to calculate preliminary combustor size. Simultaneous to the preliminary sizing of the two combustor types and the effort to acquire off-design engine performance, an effort was made to adequately represent and simulate the Federal Driving Cycle (FDC) for automobiles.

A mission analysis computer program, formulated during a previous company-sponsored effort, was modified for the automobile gas turbine optimization study (Contract 68-04-0012). The program matched the engine characteristics to the route profile, with due consideration for engine operating speed range, varying transmission efficiency, and vehicle tire adhesion limits. Two versions of the program, one for a single-shaft engine and the other for a free-turbine type, were created to facilitate mathematical modeling of engine dynamic characteristics. The program versions were sufficiently flexible to subject each candidate engine to the various performance tests and driving cycles specified for this study.

A block diagram of the mission analysis program logic applicable to both types of engines is depicted in Figure 2-5. Route profile data was introduced by means of cards designating length, grade, and speed limit for individual route segments. In this manner, it was possible to simulate an

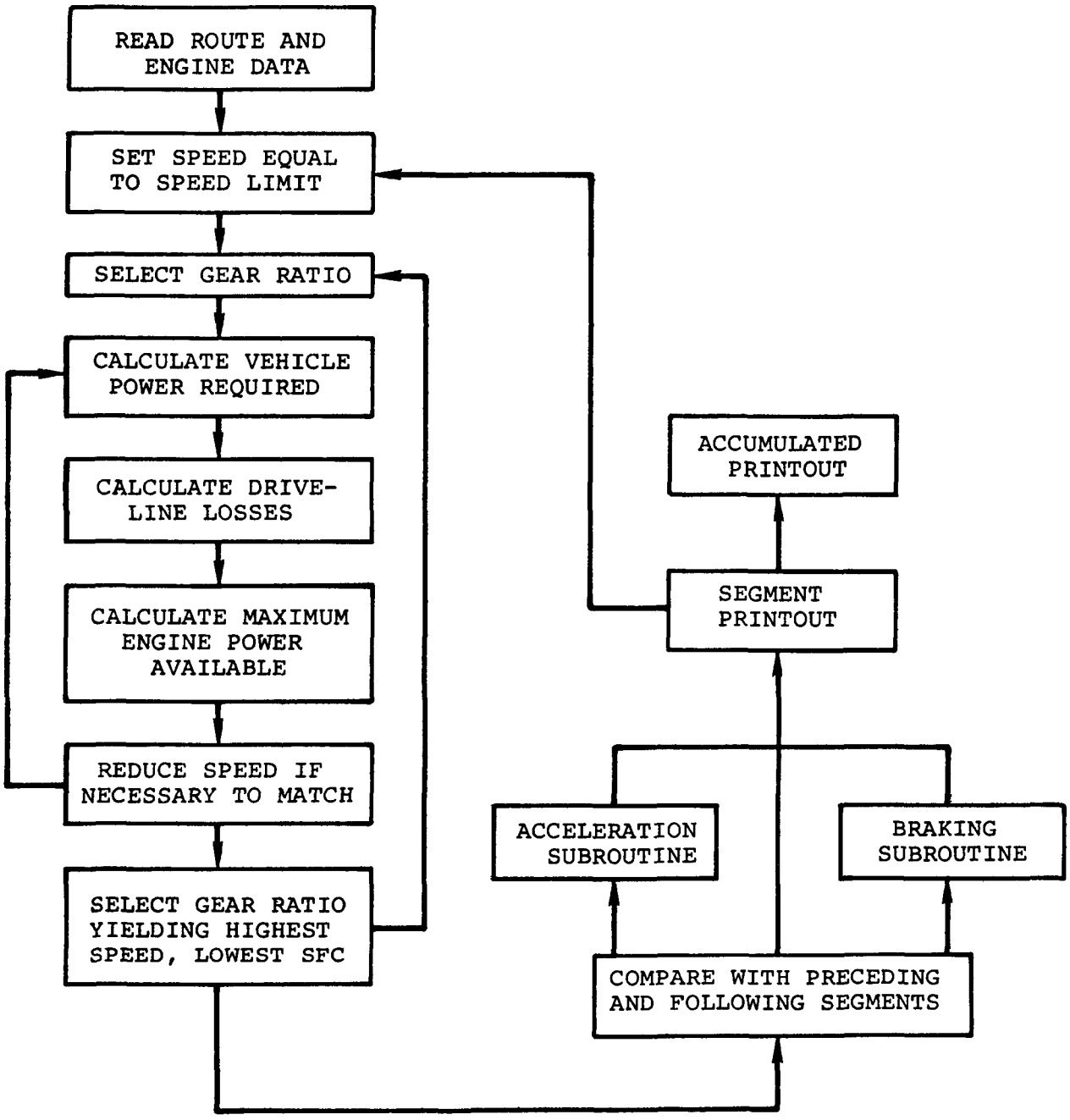

MISSION ANALYSIS PROGRAM LOGIC DIAGRAM

FIGURE 2-5

actual trip with a high degree of accuracy, provided that a sufficient number of route subdivisions were used. The required computation time was a function of both the number of segments and the number of accelerations.

Engine map data consisted of net engine horsepower, fuel flow, gas generator and power turbine speed (where applicable), turbine inlet temperature, and emission indices (gm/kg fuel), all as a function of output speed and throttle setting. Net engine horsepower was defined as gross power output minus the load imposed by engine accessories and the engine-mounted speed reduction gearbox. A separate set of engine map cards was required for each ambient temperature of interest. Fuel consumption for all gas turbine engines in this study was based on a specific gravity of 0.748 (6.25 lb/gal) and a lower heating value of 18,500 Btu/lb. Other input data included; engine-to-transmission speed reduction, maximum vehicle speed at maximum engine speed, engine design speed, gas generator and power turbine inertia, and vehicle total weight.

A 2-dimensional interpolation subroutine determined any desired engine parameter as a function of two other variables. Consequently, the engine was not restricted to a single speed/horsepower operating line, but was free to seek the best match point for a given load condition in accordance with gear-shift logic built into the program.

The initial calculation for a given route segment involved identification of transmission gear ratios that would permit the speed limit to be achieved on a steady-state basis. If the engine power was insufficient to reach the speed limit, a lower match-point vehicle speed was determined by iteration. If it was not possible to attain the speed limit in

any gear ratio, the gear yielding the highest car speed was selected. Conversely, when the speed limit was attainable in more than one gear ratio, the latter was optimized with respect to fuel consumption. Infinitely variable speed mechanical transmissions were simulated by means of a large number of discrete gear splits.

Engine and vehicle inertia were ignored when a computer run was designated as steady-state on the appropriate control card. If such was the case, the calculation proceeded from segment to segment, as described above, until the route was completed. Individual segment printout information included:

- Length
- Grade
- Speed Limit
- Required Engine Horsepower
- Actual Vehicle Speed
- Gear
- Turbine Inlet Temperature
- Power Turbine Speed
- Gas Generator Speed
- Torque Converter Efficiency
- Drive Line Efficiency
- Segment Time
- SFC
- Fuel Economy
- Cumulative Distance and Time
- Weight of Fuel Consumed
- Grams of Individual Pollutants Emitted
- BTU/Mile

The hydrocarbon and NO_x constituents were expressed as equivalent $CH_{1.85}$ and NO_2, respectively.

Segment printouts were optional and could be restricted to a few segments or eliminated altogether. An accumulated data printout containing the following information was displayed after completion of a run:

- Total number of segments
- Total distance, miles
- Total fuel consumed, lb
- Elapsed time, min
- Average fuel consumption, mpg

- Average speed, mph
- Number of gear changes
- Average fuel heat release, Btu/mile
- HC emission, gm/mile
- CO emission, gm/mile
- NO_x emission, gm/mile

In September 1971, the Office of Air and Water Programs suggested the following six point test approach to FDC simulation by the mission analysis program:

Wf, lb/hr	P, psig	$T_{in.}$ °F	Wa lb/sec	Time-Seconds
6	18	1380	0.59	41
8	13	980	0.44	466
10	13	1000	0.44	302
11	13	1000	0.44	302
12	18	1380	0.59	247
20	13	1000	0.44	14

The emissions were to be computed by averaging weighting time with grams/mile to be based on: a total distance of 7.5 miles, a 0.763 fuel specific gravity, and 10.0 miles per gallon fuel economy. However, note that the corresponding output power levels were unknown Subsequently, through engine part-load analysis and combustor test experience AiResearch evolved the following three sets of test conditions/procedures to simulate the FDC:

AiResearch Multiple Extrapolation (ME) 4-Point - December 71
(Based on Free-Turbine Cycle)

(a) Test at 2.18 lb/sec
4 atmospheres pressure
Highest available inlet temperature
0.0096 f/a

In one group of tests, vary f/a
In second group of tests, vary T_{inlet}
In third group of tests, vary $\Delta P/P$

Use data and graphical extrapolation of three variables to obtain emission index at 5.5, 9.5, 18 and 27 hp. Compute grams/mile from grams/mile = $\sum$EI x K

HP	5.5	9.5	18	27
K	0.03606	0.07094	0.04503	0.3031

AiResearch Temperature Extrapolation 4-Point - January 72 - (Based on Free-Turbine Cycle)

(b) Test at reduced hp conditions over a range of inlet temperatures as follows:

HP	Wa, lb/sec	P_1, ATMS	T_1, °R	W_f, lb/hr
5.5	0.47	1.25	1900	4.4
9.5	0.50	1.32	1897	7.6
18	0.635	1.50	1860	12.2
27	0.763	1.69	1809	16.2

These horsepowers were obtained from a time weighted Federal Driving Cycle simulation analysis.

The grams/mile were obtained from

$$\text{Grams/mile} = \sum \text{EI} \times K$$

Using the K values listed for (a), and obtaining the emission index (EI) from extrapolation of EI vs T_{inlet} to the correct inlet temperature. This method involves only one extrapolation on temperature for each test point.

The following final modification to the test procedure was made to conform to the latest optimized engine cycle.* The recommended cycle was a recuperated single-shaft engine with variable inlet guide vanes (labeled NII2V).

AiResearch Temperature Extrapolation (TE) 5-Point - April 72

(c) The gas turbine optimization study (Contract No. 68-04-0012) recommended an engine designated, NII2V, and having characteristics shown on Table 2-4 for a sea level, standard day.

The Federal Driving Cycle (FDC) was simulated by a mission analysis computer program*, as previously described, with each route segment represented by a speed change phase followed by a sustained speed phase to achieve the correct segment average speed and end speed of the automobile. Then the complete mission (FDC) was surveyed to obtain the total time spent within each horsepower range. All horsepower levels were covered, using 1-hp intervals to 31 hp, and 3-hp intervals from 30 hp to 91 hp. For the Federal Driving Cycle, the NII2V Engine does not operate at more than 91 hp at any time on a sea level, 85°F day. Under these conditions this gas turbine engine meets the performance requirements specified by the Environmental Protection Agency document "Prototype Vehicle Performance Specification" 3 January 1972.

From the mission analysis program output, a set of test conditions can be chosen that satisfactorily represents the ranges in fuel flow, pressure, and temperature over which the engine combustion system must operate. Table 2-5 presents each of five test conditions selected to represent a range of operating variables over the range

*Refer to "Automobile Gas Turbine Optimization Study," Final Report (AT-6100-R7), Contract 68-04-0012.

TABLE 2-4

MODIFIED NII 2 V ENGINE FOR COMBUSTION STUDY FEB 7

NE

LHV	A/C	ALTITUDE	FPS
18300.0	.16786	0.0	0.000

	COMPRESSOR					TURBINE		BEFORE MIXING	
DRIVING TURBINE	HP	ENERGY CORR. COOLING AIR	WATER	SHAFT HP	ACC HP	HP REQUIRED	MECHANICAL EFFICIENCY	ENTHALPY	TEMP
1	186.35	0.000	0.000	155.0	6.0	350.6	.980	446.93	1767.9

BURNER	WATER	FUEL FLOW
	0.000	62.45

	CR FLOW	PRESSURE	TEMP	DELTA	THETA	R	ENTHALPY	GAMMA	F/A	W/A	EFF	P/P	DEL P	LEAKAGE	COOLING	
AMBIENT	1.484	14.696	518.7	1.000	1.000	53.349	124.00	1.401		0.0000						AMBIENT
INLET	1.506	14.476	518.7	.985	1.000	53.349	124.00	1.401		0.0000	1.000	1.000	.015	0.000		INLET
COMPRESSR	.194	72.374	885.5	4.925	1.707	53.349	212.78	1.387		0.0000	.818	5.000	0.000	.004	.015	COMPRESSR
DIFFUSER	.190	71.654	885.5	4.876	1.707	53.349	212.78	1.387	0.0000	0.0000			.010			DIFFUSER
REGEN CLD	.541	70.006	1625.1	4.764	3.133	53.349	402.45	1.344		0.0000	.850	1.000	.023	0.000		REGEN CLD
BURNER	.537	67.206	2359.7	4.573	4.549	53.369	615.19	1.309	.0119	0.0000	.999	1.000	.040	0.000		BURNER
TURBINE	2.414	16.747	1755.7	1.140	3.305	53.369	443.44	1.329	.0117	0.0000	.880	4.013	0.000	0.000	.015	TURBINE
DIFFUSER	2.541	15.910	1755.7	1.083	3.305	53.369	443.44	1.329	.0117	0.0000			.050			DIFFUSER
REGEN HOT	2.117	14.844	1061.0	1.010	2.046	53.369	258.79	1.369	.0117	0.0000		1.000	.067	0.000		REGEN HOT
DIFFUSER	2.138	14.696	1061.0	1.000	2.046	53.369	258.79	1.369	.0117	0.0000			.010			DIFFUSER

FUEL FLOW	TOTAL	CORRECTED	SFC	POWER	NET	CORRECTED	SPECIFIC
	62.4	63.4	.403		155.0	157.4	106.47

COMBUSTOR FLOW AREA = 3.90 IN^2

COMBUSTOR VOLUME = 219 IN^3

FOR SEA LEVEL, 85°F DAY, DESIGN SPEED, SHP = 122

TABLE 2-5

TABLE OF 5-POINT TEST EVALUATION

Test Points	HP	Airflow, lb/sec	Temperature, T_1, °R	Pressure, P_1, psia	Fuel Flow, lb/hr	Fuel/Air
Min	1.3	0.331	1960	20.5	3.64	0.00305
1 Av	1.3	0.331	1960	20.5	3.64	0.00305
Max | Min	6.5	0.392	1935	21.9	5.30	0.00373
2 Av	8.5	0.412	1915	22.5	5.85	0.00394
Max | Min	18.5	0.506	1850	25.8	9.30	0.00500
3 Av	29.5	0.615	1780	29.3	13.40	0.00605
Max | Min	38.5	0.705	1722	32.8	17.00	0.00705
4 Av	53.5	0.850	1660	38.2	23.50	0.00768
Max | Min	62.5	0.935	1632	42.0	27.00	0.00835
5 Av	80.5	1.080	1580	49.4	35.00	0.00900
Max	121.0	1.380	1485	65.0	54.00	0.01050

of engine operation during the Federal Driving Cycle simulation analysis. Likewise, one or more of these conditions were applied to the combustor development tests during this program. Note that the test points selected minimize the cycle parameter variation between the output power extremes, thus ensuring maximum accuracy in the conversion from measured emmission index to grams of pollutant per mile. Table 2-6 summarizes these data.

The use of the 5-point evaluation accounts for all steady-state conditions, including a detailed integration of horsepower versus time during engine accelerations and decelerations. It does not account for the exhaust emissions that would be generated during the one cold and one hot engine start in the 1975 Federal Driving Cycle nor the variation in emissions associated with any other engine transient operation.

The effect of the new driving cycle simulation is to increase the predicted emission levels in grams-per-mile. This is illustrated by values calculated according to the OAP-suggested procedure compared with values from the two AiResearch procedures (original 4-point simulation versus revised 5-point simulation). Calculations for the vaporizer combustor (SKP26489-M_2) yield the following values:

FDC Simulation	NO_x (as NO_2) gm/mi	Percent
AiR 5-pt	6.38	137
AiR 4-pt	5.46	117
OAP	4.67	100

TEST CONDITIONS – SIMULATED FEDERAL DRIVING CYCLE

TABLE 2-6

POWER, HP	1.30	8.50	29.50	53.5	80.5
RANGE, HP	0–6	6–18	18–37	37–61	61–121
TIME, PERCENT	12.2	64.7	18.1	4.5	0.5
W_a, LB/SEC	0.33	0.41	0.62	0.85	1.08
P_1, PSIA	20.5	22.5	29.3	38.2	49.4
T_1, ^oR	1960	1915	1780	1660	1580
W_f, LB/HR	3.64	5.85	13.40	23.50	35.00
f/a	0.00310	0.00395	0.00618	0.00783	0.00900
FUEL, LB	0.169	1.441	0.926	0.402	0.063
K	0.0103	0.08811	0.0565	0.0246	0.0038

GRAMS MILE = Σ EMISSION INDEX X K FOR THE FIVE TEST POINTS

$$K = \frac{\text{FUEL BURNED IN SEGMENT, LBS}}{1000} \times \frac{453.6 \text{ GM/LB}}{7.50 \text{ MI OVER FDC}}$$

$$\text{EMISSION INDEX, LB/1000 LB FUEL} = \frac{1 + f/a}{f/a} \times S \times \frac{M_s}{M_e} \times 10^3$$

f/a = FUEL/AIR WEIGHT RATIO

S = FRACTIONAL VOLUME OF POLLUTANT = $\frac{\text{PPM} \times 10^{-6}}{1}$

M_s = MOLECULAR WEIGHT OF POLLUTANT

M_e = MOLECULAR WEIGHT OF EXHAUST = 29

2.3 Preliminary Sizing

Based on the combustor operating data derived from the engine cycle analysis, preliminary designs of each of the candidate combustion systems were accomplished using existing design techniques. Combustor preliminary sizing was accomplished by conventional methods for both combustors in the following manner:

(a) A combustor jet velocity was calculated assuming one velocity head loss across the combustor at a pressure drop of 3 percent of inlet total pressure.

(b) An outside annulus area was computed assuming a maximum annulus velocity head equal to one-half of the jet velocity head from (a). The minimum outside annulus area can then be calculated from the volume flow rate and the maximum velocity.

(c) Combustor volume was calculated based on an assumed heat release rate limit of 5×10^6 Btu/hr-ft^3-atm. The combustor cross-sectional area was then determined using assumed values of length-to-diameter ratio for each case and setting a practical limit of 250 fps for the combustor discharge velocity.

(d) Minimum combustor reference area is then the sum of the annulus area from (b) and the combustor area from (c).

The above computational method is applicable to turbine engines operating at essentially constant speed and constant combustor throughflow. When engine performance for the variable-geometry free-turbine cycle was calculated over the Federal Driving Cycle, however, it was determined that most engine operating time was spent at part-power conditions less than 40 shp with correspondingly reduced throughflow, pressure ratio, and engine speed. At these conditions combustor loading, Q, is increased and, therefore, a correction to increase combustor

volume was made to reduce Q to ensure that a reasonable combustion efficiency could be attained at these more severe operating conditions. Therefore, the volume was based on idle output power condition which corresponds to a combustor loading, Q, range of values between 0 and 0.1. Figure 2-5 was the design basis used for combustor sizing. The resultant vaporizer combustor geometry for Class A and Class B combustors are shown in Figures 2-6 and 2-7. Table 2-7 presents a summary of preliminary vaporizer combustor design parameters.

During the test program, it was determined that the measured combustion efficiencies were higher at a given aerodynamic loading parameter Q than shown on the design curve. The measured efficiencies indicated that a design line passing through a combustion efficiency of 92.5 percent at Q = 0.8 could have been conservatively used. This compares to the design line predicting 80 percent combustion efficiency at Q = 0.8. This indicated that a Class A combustor volume of 100 $in.^3$ would have been adequate rather than the 247 $in.^3$ used. If the combustor were reduced in size, lower NO_x emissions (and higher CO and HC emissions) than those reported in the following test results should be achieved.

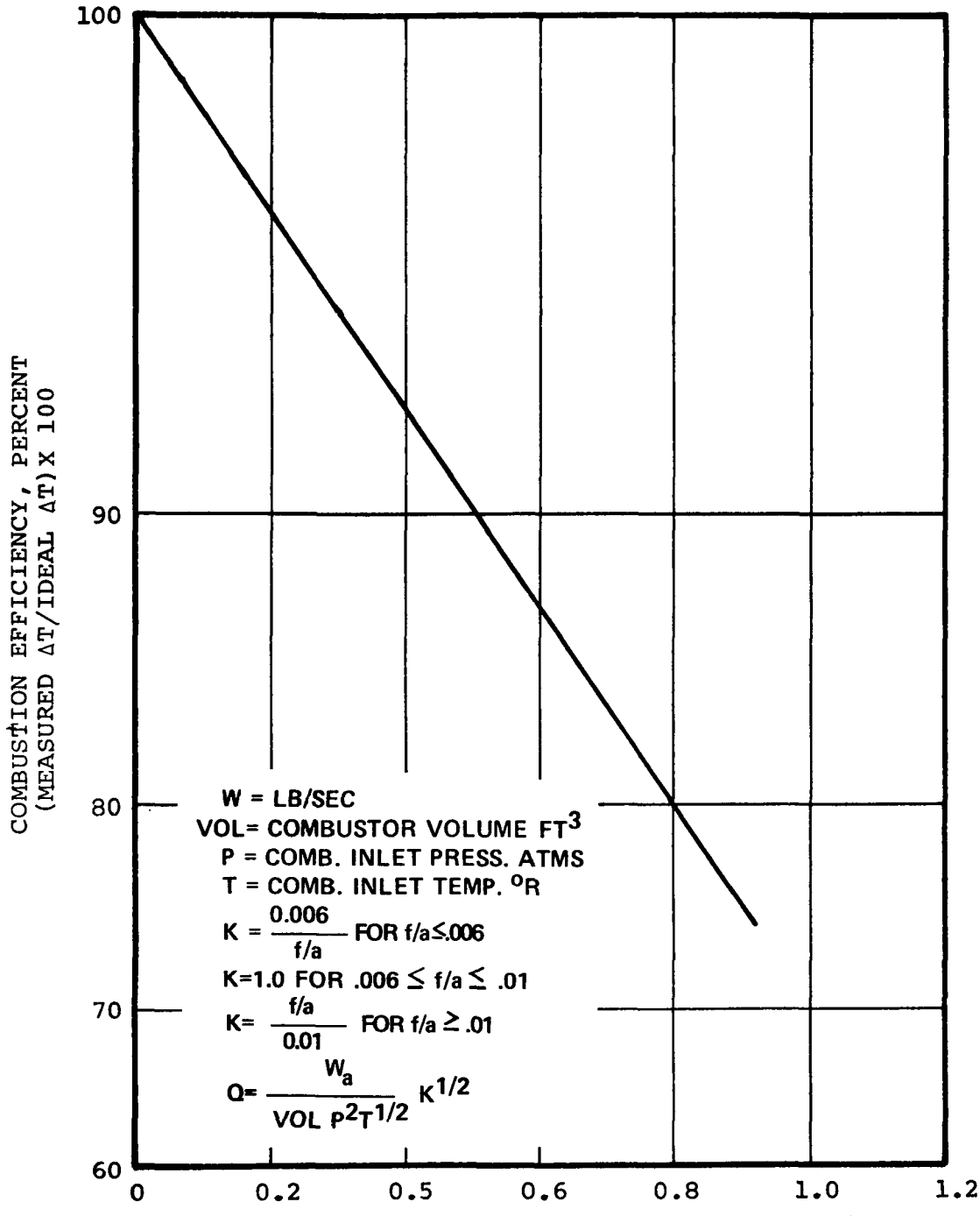

COMBUSTION EFFICIENCY VERSUS AERODYNAMIC LOADING

FIGURE 2-5

TABLE 2-7

SUMMARY OF PRELIMINARY VAPORIZER COMBUSTOR DESIGN PARAMETERS

	Class A	Class B
Heat rate, Btu/hr	1.396×10^6	1.88×10^6
Inlet air temperature, °F	1100	760
Inlet air pressure, atm	4.0	12.0
Fuel air ratio	0.0096	0.0185
Outlet temperature, °F	1700	1900
Fuel flow rate, lb/hr (1)	75.5	101.6
Airflow rate, lb/sec	2.178	1.525
Volume flow rate, cu ft/sec	21.4	3.86
Reference diameter, in.	6.1	3.7
Liner diameter, in.	4.8	3.25
Liner length, in.	13.7	10.0
Length/diameter ratio	1.5	2.0
Reference velocity, fps	106	52.3
Liner discharge velocity, fps	250	138
Characteristic residenct time, ms (2)	2.40	3.92
Combustor volume, cu ft	0.143	0.481
Heat intensity, Btu/hr/ft^3/atm	4.6×10^6	5.0×10^6

NOTES:

(1) Fuel lower heating value = 18,500 Btu/lb

(2) Characteristic residence time - liner length/liner discharge velocity

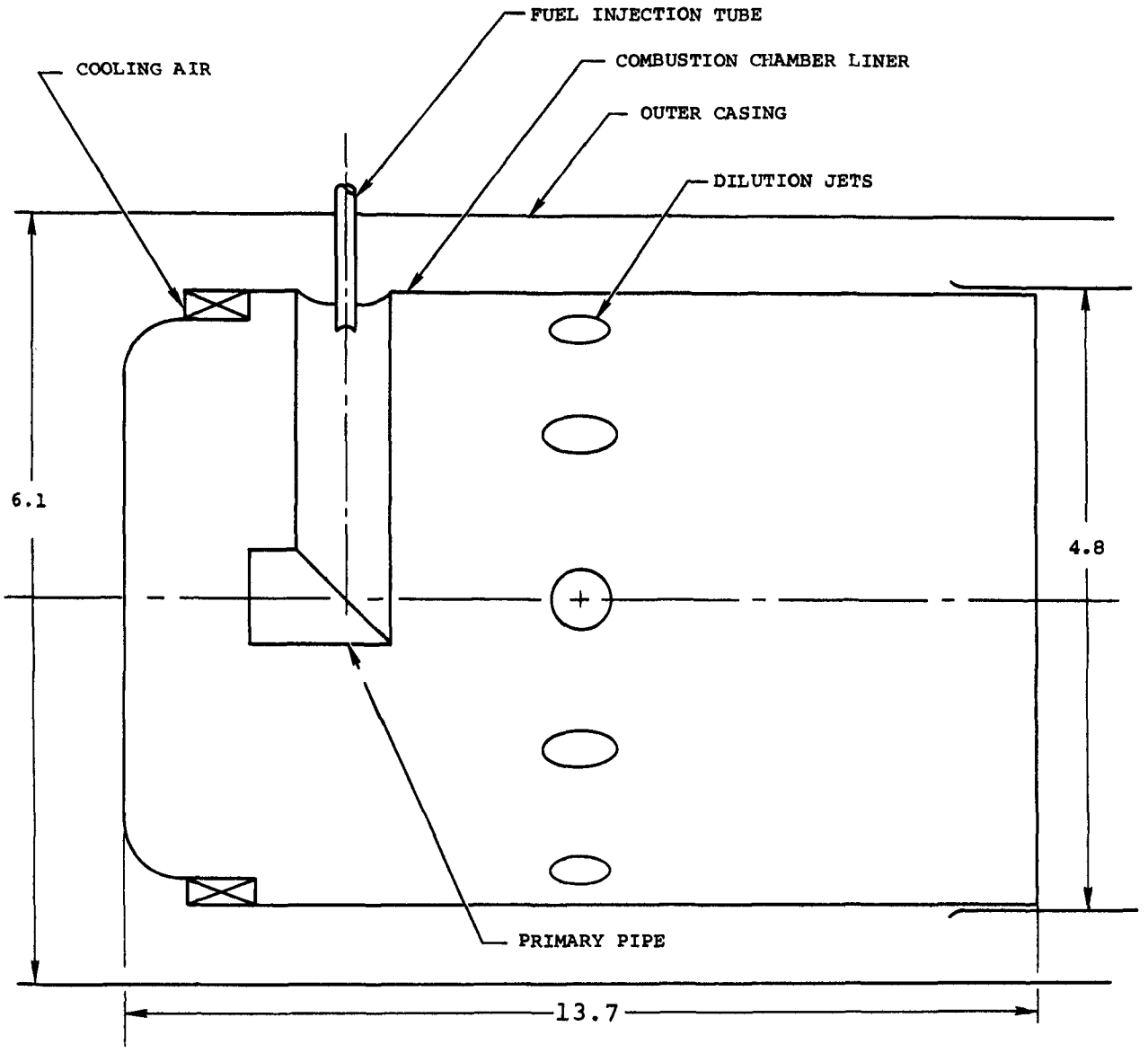

PRELIMINARY VAPORIZER COMBUSTOR DESIGN - CLASS A
(NO SCALE)

FIGURE 2-6

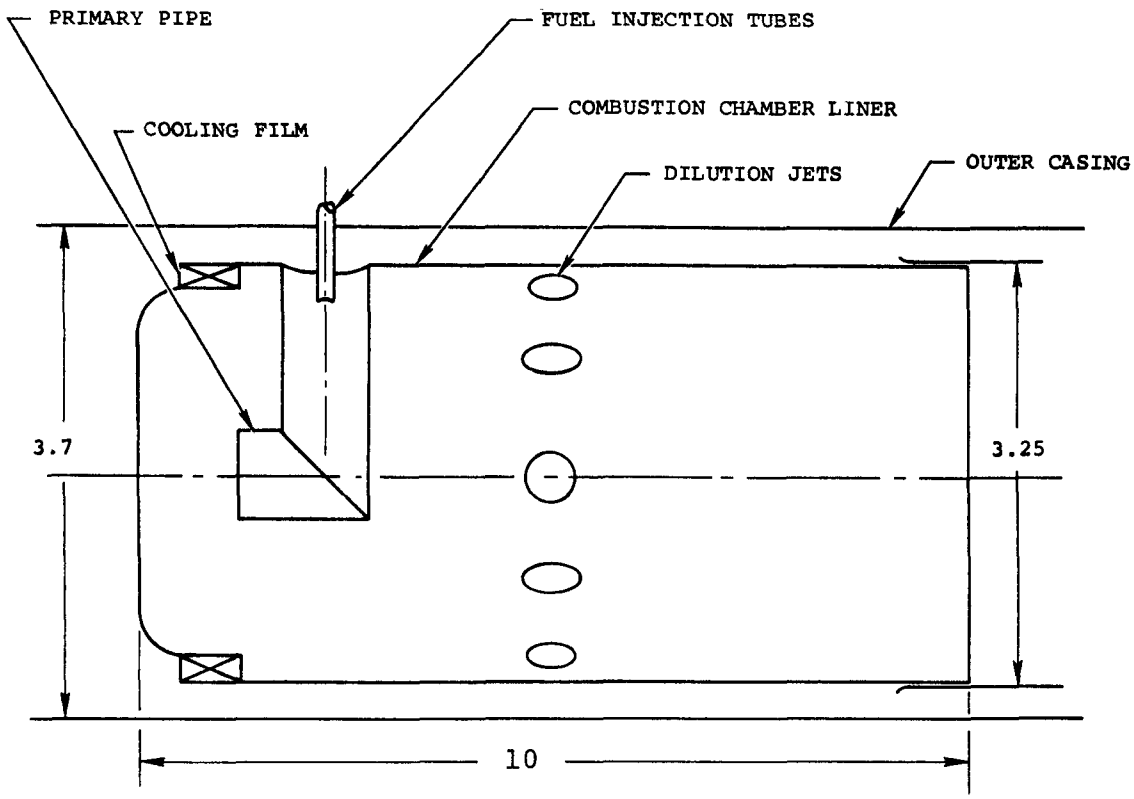

PRELIMINARY VAPORIZER COMBUSTOR DESIGN - CLASS B
(NO SCALE)

FIGURE 2-7

2.4 Analytical Design Techniques

Internal flow fields of the preliminary combustor designs were predicted with the use of an existing two-dimensional finite-element gas flow computation program from Gosman[1]. Figure 2-8 presents the basis used for flow-field calculations. The results of this analysis provided velocities, temperatures, and mixture concentrations over the range of combustor operating conditions defined in the cycle analysis.

An existing Gosman computer program provides time, temperature, and mixture maps and equations for nitric oxide kinetics which were incorporated into the Gosman computer program. Results from this program were compared on a limited basis with results from an existing one-dimensional method of analysis.

The combustion of fuel and the formation of carbon monoxide were computed from overall rates based on stirred reactor experimental data.

2.4.1 Flow Pattern Numerical Analysis

Flow pattern analysis was conducted on the preliminary combustor designs. The analysis initially concentrated on the primary zone region where nitric oxide formation predominates. Grid node patterns and boundary conditions were established. Computations were conducted for both cold flow (no combustion) and hot flow conditions for comparison with the flow visualization experimental analysis. Hot flow conditions can be computed assuming local chemical equilibrium for which combustion rates are limited only by mixing processes or by a two-step global kinetic process utilizing stirred reactor combustor rates. The

[1] Gosman, A. D., W. M. Pun, A. K. Runchal, D. B. Spalding, and M. Wolfshtein, Heat and Mass Transfer in Recirculating Flows, Academic Press, 1969.

FINITE DIFFERENCE ANALYSIS

DERIVED FROM THE METHODS OF GOSMAN, SPALDING AND WOLFSHTEIN

PROVIDES MEANS OF CALCULATING RECIRCULATING FLOW

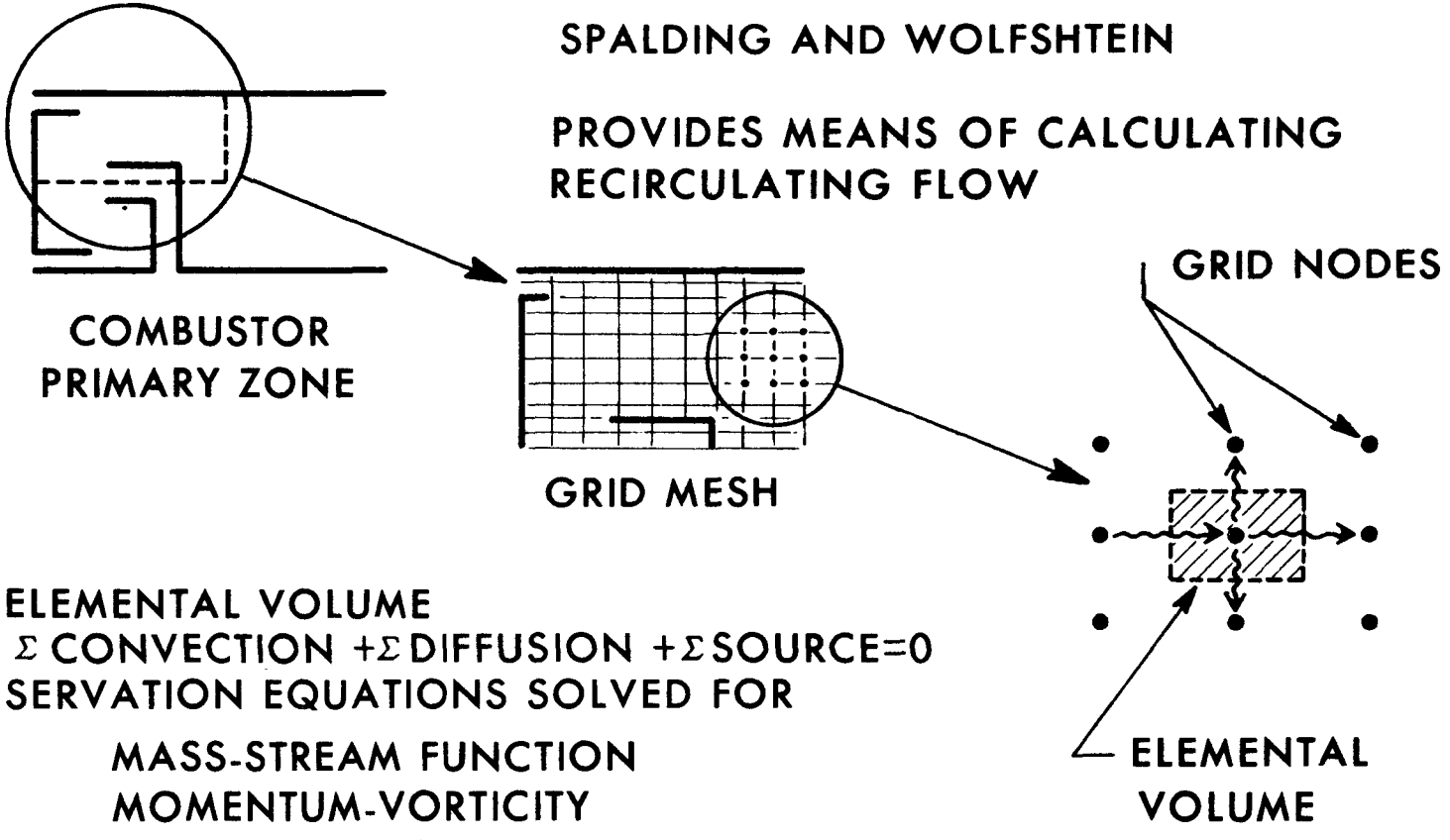

FOR ELEMENTAL VOLUME

Σ CONVECTION $+\Sigma$ DIFFUSION $+\Sigma$ SOURCE $=0$

CONSERVATION EQUATIONS SOLVED FOR

- MASS-STREAM FUNCTION
- MOMENTUM-VORTICITY
- ENERGY-ENTHALPY
- SPECIES-MASS FRACTIONS

FIGURE 2-8

latter process allows an assessment of the relative effects of mixing and kinetics and was selected for use in this program. The global rate source terms were incorporated into the finite difference computer program to calculate rates of fuel conversion to carbon monoxide and subsequent conversion to carbon dioxide. Resulting combustion efficiency calculations for a simplified configuration compared favorably with both stirred reactor and practical combustor data.

Primary zone isothermal flow patterns were computed for the film vaporizing combustor for the Class B engine. Figure 2-9 shows the flow streamlines and velocity profiles. Air and fuel from the primary pipe form a radial wall jet which is entrained into the cooling air wall jet. The ejecting action of the primary pipe air results in formation of a recirculation zone. High velocities are maintained along the combustor walls by judicious introduction of high energy air to delay combustion until mixing to a lean fuel-air ratio is complete, thereby averting combustion at high equivalence ratios which results in high nitric oxide formation rates. Once a flame is stabilized in the recirculation zone, propagation to the higher equivalence ratio regions near the walls is prevented by the high velocity gradients shown in Figure 2-9.

The computed flow pattern was utilized to calculate primary zone fuel mixing rates and hot flow patterns. These data were then coupled with the KVB analytical model that computes nitrogen compound concentrations and are discussed in the following paragraphs.

2.4.2 Chemical Kinetic Analysis

The chemical kinetic analysis of nitric oxide and nitrogen dioxide formation was conducted by KVB engineering under subcontract to AiResearch. The kinetic formation equations were expressed in a form suitable for inclusion in a two-dimensional recirculating flow

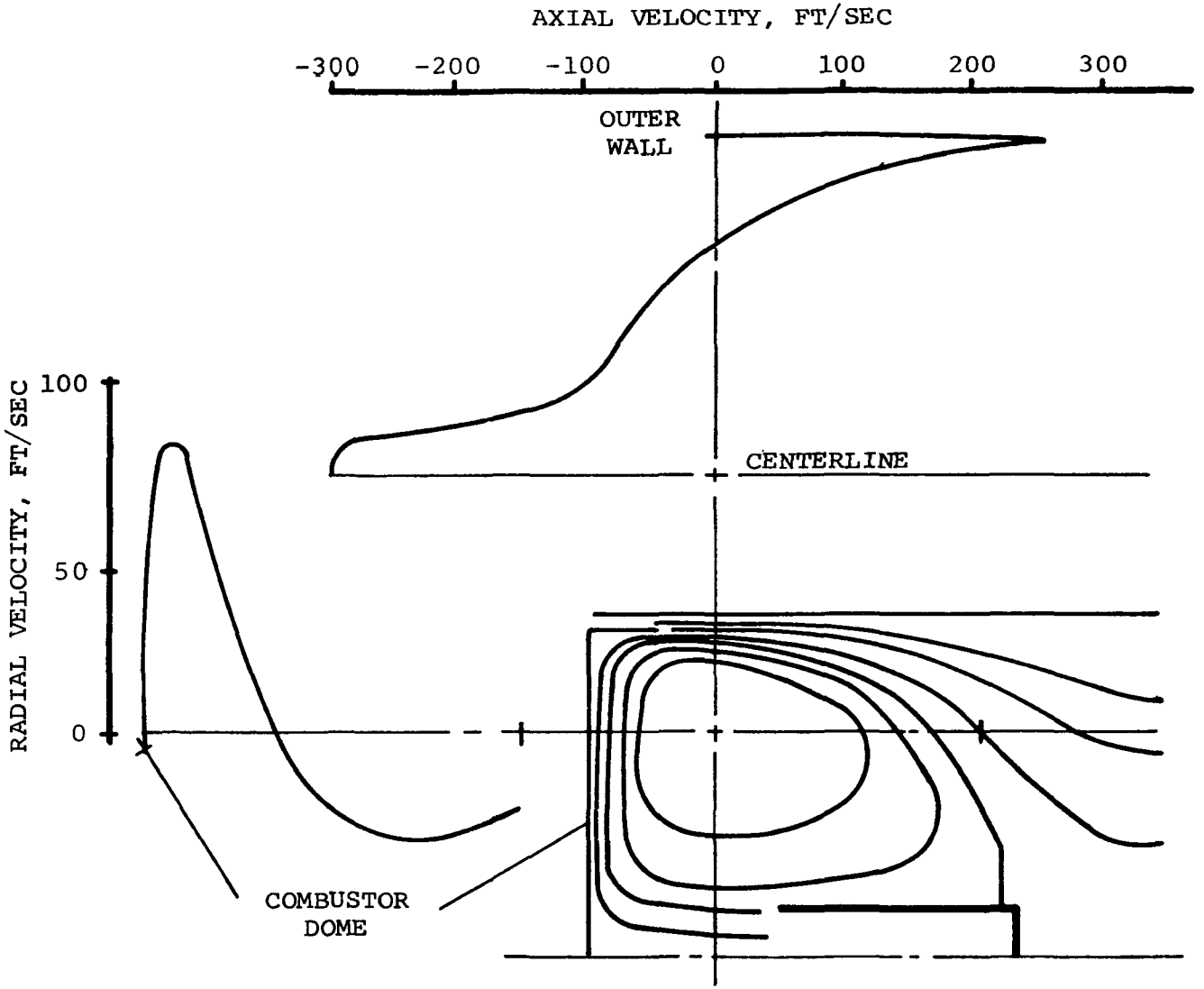

CALCULATED BY		
TRACED BY		8-25-71
CHECKED BY		
APPROVED BY		
UNIT NO.		

CLASS B COMBUSTOR
PRIMARY ZONE FLOW PATTERN
AND VELOCITY PROFILES

FIGURE
2-9

analysis of a gas turbine combustion chamber primary zone with nonuniform fuel-air ratio distribution. Chemical equilibrium may or may not be attained at various locations in the flow field. The kinetic analysis includes the following six reactions leading to nitric oxide formation and two reactions for the oxidation of nitric oxide to nitrogen dioxide:

$$N_2 + O \rightleftarrows NO + N \quad (1)$$

$$N + O_2 \rightleftarrows NO + O \quad (2)$$

$$N + OH \rightleftarrows NO + H \quad (3)$$

$$N_2 + OH \rightleftarrows N_2O + H \quad (4)$$

$$N_2 + O_2 \rightleftarrows N_2O + O \quad (5)$$

$$O + N_2O \rightleftarrows 2NO \quad (6)$$

$$NO + O + M \rightleftarrows NO_2 + M \quad (7)$$

$$NO + O_2 \rightleftarrows NO_2 + O \quad (8)$$

For preliminary assessment of the initial combustor designs, a simplified time step integration of the pertinent nitric oxide formation equations was performed by AiResearch. Nitric oxide formation rates were computed at the design conditions of the Class A and Class B combustors for a range of primary zone equivalence ratios assuming mixture conditions constant at the adiabatic flame temperatures. At 0.6 equivalence ratio the formation rates were 14 ppm per millisecond and 3.1 ppm per millisecond for the Class A and Class B combustors, respectively. Characteristic primary zone residence times were computed by dividing primary zone volume by the burned gas volumetric

flow rate. These times were 3.0 and 3.6 milliseconds for the Class A and Class B combustors, respectively. For the assumed conditions formation rates are constant up to 10 milliseconds. Multiplying the formation rates by the characteristic residence times results in primary zone exit concentrations of 42 and 11 ppm for the two combustors. These amounts reduce to 10 ppm and 5 ppm when adjusted by the dilution zone mixing process. Conversion of the 0.4 gm/mile requirement for oxides of nitrogen to a ppm basis for the two designs gives 8.2 ppm and 15.8 ppm, respectively. The estimated formation rates are within reasonable agreement with these requirements. This analysis is of course highly simplified primarily in terms of neglecting mixture non-uniformity. Analysis of data on existing combustors by this procedure is planned to evaluate the merits of such a comparison.

Programming of the nitrogen oxide reaction mechanism was completed by KVB Engineering. A final report describing this effect is included as Appendix II for your reference. This computation was intended to be attached to the flow analysis program which solves the flow pattern and hydrocarbon chemistry equations simultaneously. After convergence, the nitrogen compound reaction equations were to be solved. Introduction of the nitrogen oxide kinetic analysis after convergence of the Gosman recirculating flow analysis was to provide independent development of these two analytical models; therefore, reduce computation time. For reference, the complete chemical mechansim is shown in Table 2-8.

As a means of providing initial insight into the ability to solve for NO, a simplified model was programmed to solve the NO formation for the two-reaction Zeldovich mechanism consisting of the first two nitrogen chemistry reactions listed in Table 2-8. The combustor was configured with a central methane fuel jet surrounded by a concentric air annulus. Figure 2-10 shows the computed flow pattern and lines of constant NO concentration. The peak level of 434 ppm is typical of that expected at the primary zone exit prior to dilution air introduction.

TABLE 2-8

FINITE DIFFERENCE FLOW PROGRAM
CHEMICAL KINETIC MECHANISM

Hydrocarbon Chemistry

$$CH_X + \left(\frac{1}{2} + \frac{X}{4}\right) O_2 \rightarrow CO + \frac{X}{2} H_2O$$

$$CO + \frac{1}{2} O_2 \rightarrow CO_2$$

Atomic Species

$$CO + OH \overset{\rightarrow}{\leftarrow} CO_2 + H$$

$$O + OH \overset{\rightarrow}{\leftarrow} O_2 + H$$

$$OH + OH \overset{\rightarrow}{\leftarrow} H_2O + O$$

Nitrogen Chemistry

$$N + NO \overset{\rightarrow}{\leftarrow} N_2 + O$$

$$N + O_2 \overset{\rightarrow}{\leftarrow} NO + O$$

$$N + OH \overset{\rightarrow}{\leftarrow} NO + H$$

$$H + N_2O \overset{\rightarrow}{\leftarrow} N_2 + OH$$

$$O + N_2O \overset{\rightarrow}{\leftarrow} N_2 + O_2$$

$$O + N_2O \overset{\rightarrow}{\leftarrow} NO + NO$$

$$NO + O + M \overset{\rightarrow}{\leftarrow} NO_2 + M$$

$$NO_2 + O \overset{\rightarrow}{\leftarrow} NO + O_2$$

SIMPLIFIED FLOW MODEL

$N_2 + O \longrightarrow NO + N\cdot$ $\qquad N_2 = .72$

$N + O_2 \longrightarrow NO + O$ $\qquad O_2 = .01$

$$\text{REACTION RATE} = \rho A e^{-B/T} (N_2)(O_2)^{1/2} \left(\frac{P}{T}\right)^{1/2}$$

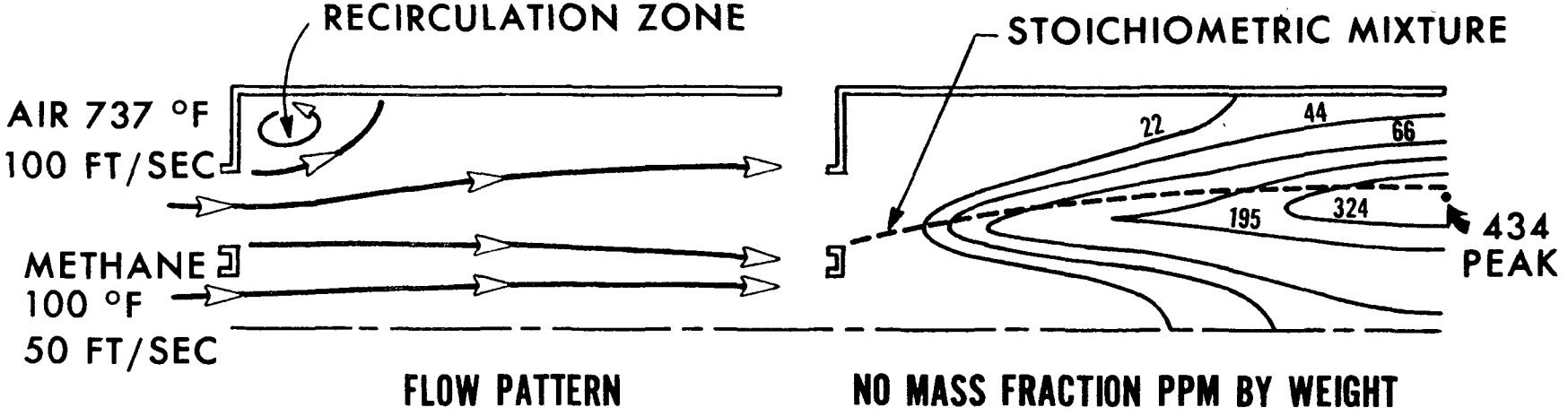

FIGURE 2-10

2.4.3 Flow Pattern and Chemical Kinetic Analysis

The following is a discussion of the integration of the oxides of nitrogen computation procedure provided by KVB Engineering with the AiResearch flow computation program. Several test cases were run to check out the program on simple geometric configurations. The oxides of nitrogen computations were found to converge at a rate comparable to the fluid flow and mass fraction computations. The program was then applied to the primary zone geometry for the Class B combustor for which flow patterns without combustion had previously been computed. A coarse 21-by-10 grid pattern was used for more economical computation during program checkout. This grid and the portion of the combustor which it covers are shown in Figure 2-11. The computations are performed in cylindrical coordinates with the axis of symmetry at the axis of the cylindrical can combustor. Air enters through two inlets. One, on the axis, represents the air-blast fuel insertion device through which the fuel-air mixture enters the primary zone; the second inlet, at the outer radius, represents the first cooling band.

The equations that are to be solved include vorticity (conservation of total momentum), stream function (conservation of total mass), fuel conservation parameter (conservation of all species and enthalpy), mass fraction of unburned fuel, mass fraction of carbon dioxide, and mass fractions of NO and NO_2. Solution of these equations is dependent on proper specification of boundary conditions, turbulent mixing relations, and reaction rates for interconversion of the various species.

The boundary conditions are specified for four types of boundaries: inlets, exits, solid walls, and the axis of symmetry. At the inlets the vorticity is determined from the specified inlet velocity profile. The stream function is determined by integrating the mass flow rate across each inlet. If premixed conditions are being considered, the fuel conservation parameter and fuel mass fraction are set

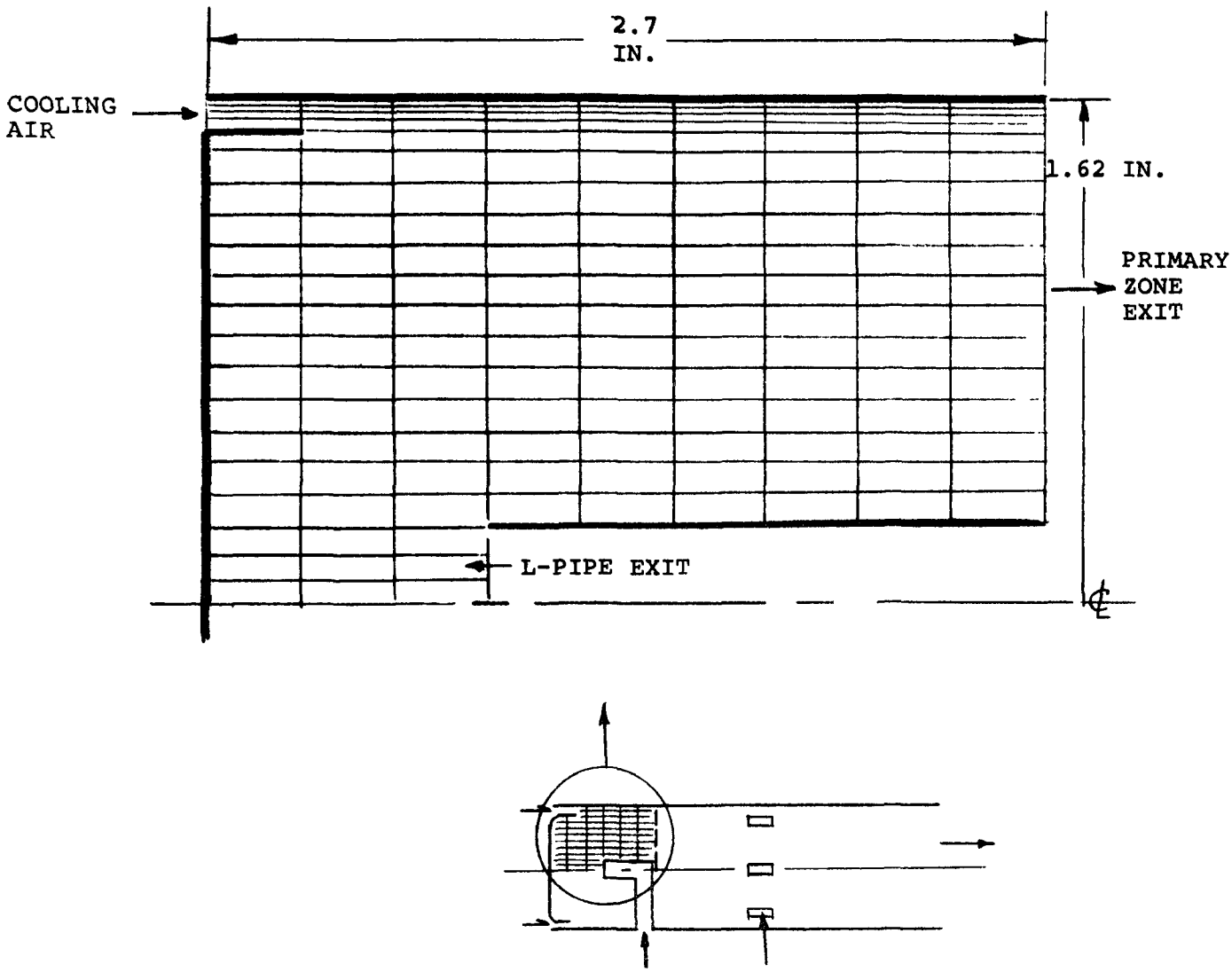

PREPARED	SCH	10/71	CLASS B COMBUSTOR PRIMARY ZONE COARSE GRID PATTERN	FIGURE 11
WRITTEN				
APPROVED				

FORM P709A-1

equal to the mass fraction of fuel vapor in air at the inlet. Carbon dioxide and nitrogen oxides are set to zero. It is assumed that the inlet air is dry. Humid air can be considered in the program, but will be neglected for initial predictions.

Boundry conditions at the exit are specified such that the stream lines are parallel to the axis and mass fraction gradients are zero in the axial direction. Vorticity is determined from the radial exit velocity profile.

On solid walls the vorticity is computed by an implicit technique from Reference (1), assuming a linear vorticity variation between the wall and the first interior grid node. Stream function is constant along a wall since the flow is parallel to it. Mass fraction gradients normal to the wall are zero for impermeable walls. Computation assumes adiabatic conditions so that enthalpy is directly related to fuel-air ratio. An alternate procedure is to specify the boundary temperature and solve a conservation equation for enthalpy. The axis of symmetry is a streamline and because of symmetry there are no mass fraction gradients, so boundary conditions are identical to solid walls except that the vorticity is zero.

Rates of turbulent mixing are specified in terms of an effective turbulent eddy viscosity. For turbulent flow the rates of mixing for all the conserved properties (mass, momentum, mass fractions, and enthalpy) are of the order of unity. Accordingly, all the turbulent Prandtl and Schmidt numbers are set to 1.0. The turbulent eddy viscosity is computed from the Prandtl-Komologrov hypothesis relating eddy viscosity to turbulent kinetic energy and length scale of turbulence. The turbulent kinetic energy is assumed proportional to the square of the inlet velocities, and length scale is assumed proportional to the size of the inlets. Details of this computation are given by Wolfshtein (Reference 2) and Gosman, et al (Reference 1).

The hydrocarbon-air kinetic interconversion of species is handled by the following assumed two-step reaction mechanism:

$$CH_x + (\frac{1}{2} + \frac{X}{4})\ O_2 \longrightarrow CO + \frac{X}{2}\ H_2O$$

$$CO + \frac{1}{2}\ O_2 \longrightarrow CO_2$$

Reaction rates are taken from Williams (Reference 3). Since there are two reaction rates, the conservation equations for the mass fraction of two species must be solved. The species CH_x and CO_2 are used in the present program. The mass fractions of the remaining species plus inert nitrogen are then directly related through stoichiometry to these two mass fractions.

Provision has been made in the procedure for fuel addition by film vaporization from the wall. The formation of the fuel film is computed by the method detailed in NACA Report 1087 (Reference 4). Rates of vaporization are computed by the method of NASA Report TR-R-67 (Reference 5). Velocities and temperatures in the primary zone are required inputs to the film formation and vaporization computations. The computation is then iterated until temperatures are compatible with the rates of vaporization.

Initial computations for program checkout with the coarse grid have been restricted to premixed fuel vapor and air entering the two inlets. Computations with internal vaporization should be performed after checkout of the integrated program is complete. However, this phase was never completed. These two procedures for fuel introduction provide a comparison of premixing and internal vaporization in terms of the resultant emissions formation.

The computed flow pattern for conditions of the Class B combustor full power design point is shown in Figure 2-12. The curves

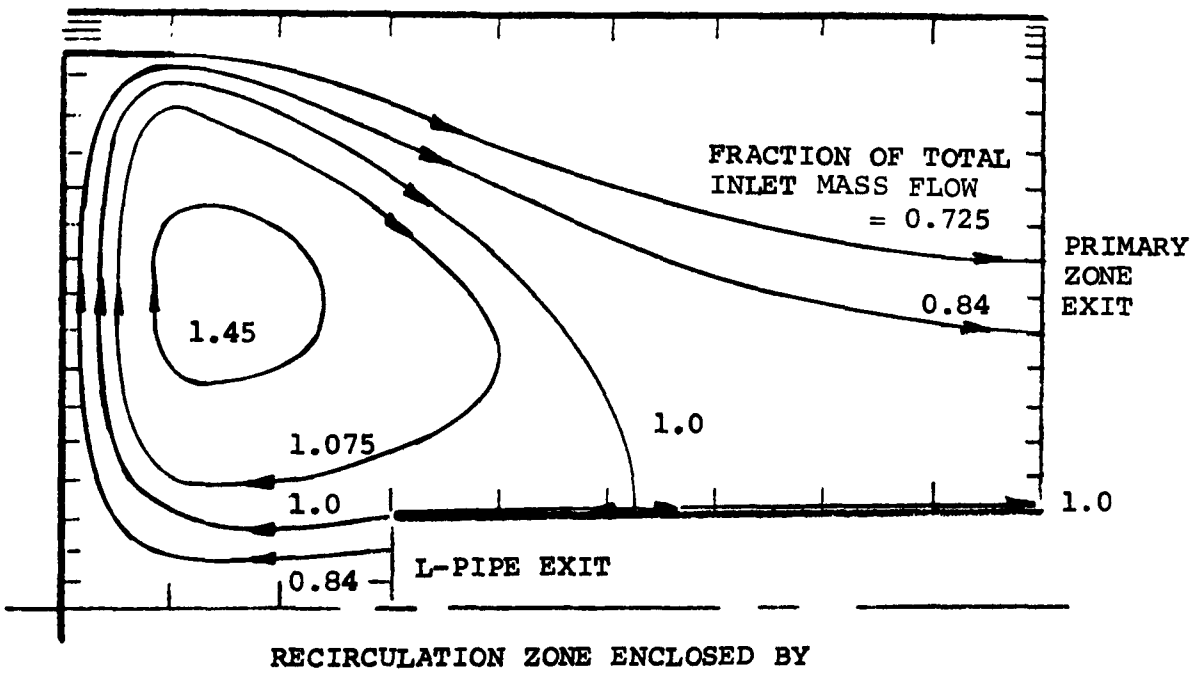

RECIRCULATION ZONE ENCLOSED BY
STREAMLINE = 1.0

INLET VELOCITY = 300 FT/SEC

PREPARED	SCH	11-71	CLASS B COMBUSTOR PRIMARY ZONE HOT FLOW PATTERN	FIGURE 2-12
WRITTEN				
APPROVED				

FORM P703A-1

F = FUEL CONSERVATION PARAMETER

= MASS FRACTION OF CONSERVED CARBON AND HYDROGEN IN FUEL AND COMBUSTION PRODUCTS

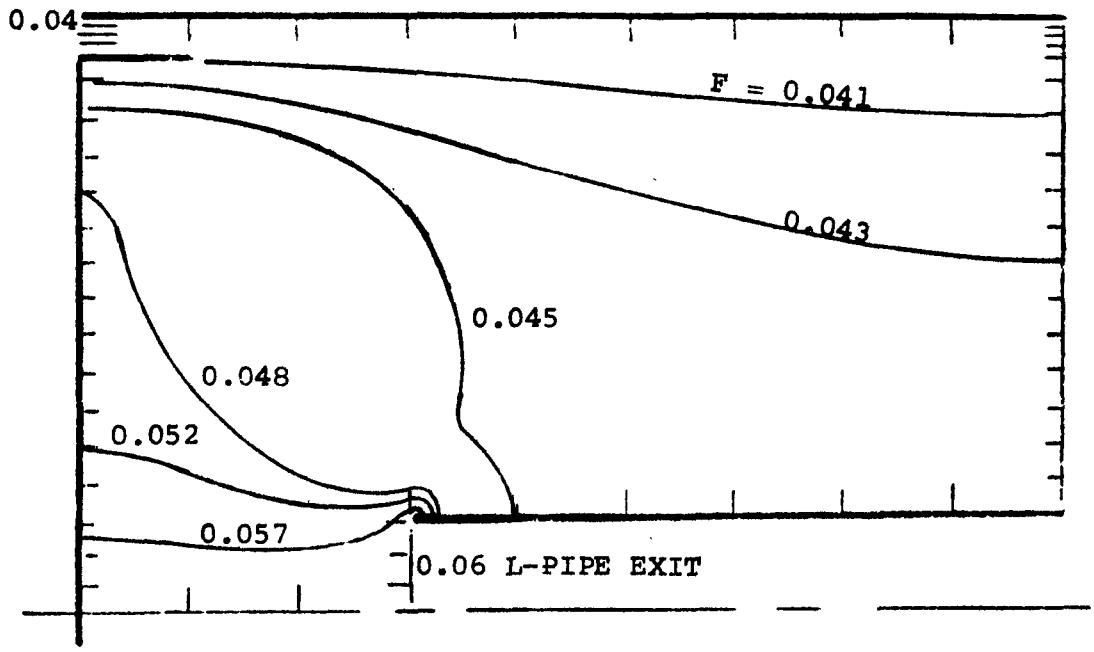

PREMIXED VAPOR-AIR MIXTURE
AT BOTH INLETS

PREPARED	SCH	11-71	CLASS B COMBUSTOR PRIMARY ZONE FUEL CONSERVATION PARAMETER	FIGURE 2-13
WRITTEN				
APPROVED				

FORM P708A-1

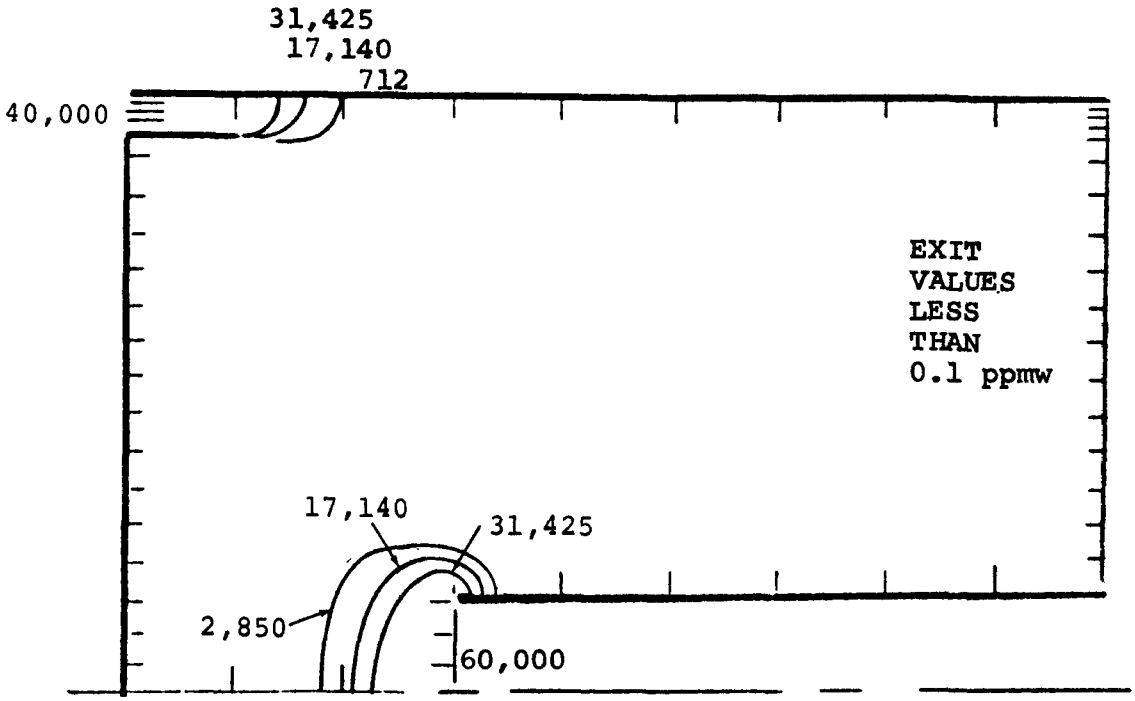

CONCENTRATION C_XH_Y (PPM BY WEIGHT)

PREMIXED VAPOR-AIR MIXTURE
AT BOTH INLETS

PREPARED	SCH	11-71	CLASS B COMBUSTOR PRIMARY ZONE UNBURNED HYDROCARBONS	FIGURE 2-14
WRITTEN				
APPROVED				

FORM P708A-1

represent lines of constant stream function so that a fixed amount of mass flow exists between two lines. The hot flow pattern is quite similar to the cold flow pattern presented in Figure 2-9, and is qualitatively consistent with patterns observed in the plexiglass model flame visualization test and water model tests of the Shelldyne film-vaporizing combustor.

The computation was performed with premixed mass fractions of 0.06 (0.95 equivalence ratio) at the L-pipe inlet and 0.04 (0.63 equivalence ratio) at the second inlet. Figure 2-13 shows the distribution of the fuel conservation parameter that expresses the rate of mixing between the two inlet flows and the circulation zone. The fuel conservation parameter is essentially an indication of the local fuel-air ratio. It is the determination of the local fuel conservation parameter that is the key to balancing mixing and fuel introduction so that lean combustion is maintained for low NO emission. If both inlets were set to the same value of initial premixed fuel mass fraction, the fuel conservation parameter would be constant throughout the field. With different values at the two inlets, local grid values are intermediate between the inlet values. When internal vaporization is introduced, local vaporization rates may be sufficiently high to produce rich regions. It is the express purpose of this analytical procedure to determine the combustor geometric changes necessary to eliminate rich and near stoichiometric regions.

Figure 2-14 shows the mass fraction of unburned hydrocarbons. For the premixed condition, hydrocarbon is converted to CO within a very short distance from the inlets. Hydrocarbon emission at the primary zone exit is less than 0.1 ppm. Conversion of CO to CO_2 also occurs rapidly with less than 1 ppm CO emission. Resultant combustion efficiency is over 99.6 percent.

The original Gosman-Spalding program assumed constant specific heats of the gaseous species. Since temperature has a significant effect on the reaction rates for both the hydrocarbon and nitrogen reactions, the temperature calculation was improved by incorporating variable specified heats through the use of sixth order equations obtained from NASA SP-3001 (Reference 6). Figure 2-15 shows the computed temperature distribution. For the calculation presented, temperatures in the recirculation zone are of the order of 3500°F. Peak temperatures occur at the exit of the air blast injection pipe where the fuel-air ratio os near stoichoimetric.

After solutions are obtained for the flow pattern, species mass fractions, and temperature, the conservation equations for formation of NO and NO_2 are solved. The procedure for solution is discussed in the KVB Engineering Final Report (included as Appendix II of this report). Figure 2-16 shows the distribution of lines of constant NO mass fraction. Peak levels occur in the highest temperature region near the air-blast injector inlet. Summation of the concentrations at the exit weighted by the mass flow at each radius give a primary zone exit NO level of 3 ppm by weight. This is well below the levels required to meet the program goals. However, the calculation presented was performed for program checkout only when further work was halted. Further computations should be conducted with refined finite difference grid patterns, internal fuel vaporization, and at other engine operating conditions for both the Class A and Class B combustors. Approximately 8 engineering hours and 6 computer hours would be required to complete the analysis.

In addition to the foregoing analysis, a simplified procedure for extrapolation of emissions from empirical data has been developed. This procedure is being evaluated as a means of reducing the number of test points required to assess the emission characteristics of a given test combustor modification. This procedure has been integrated with engine cycle mission analysis programs to allow rapid assessment of emissions over the Federal Driving Cycle.

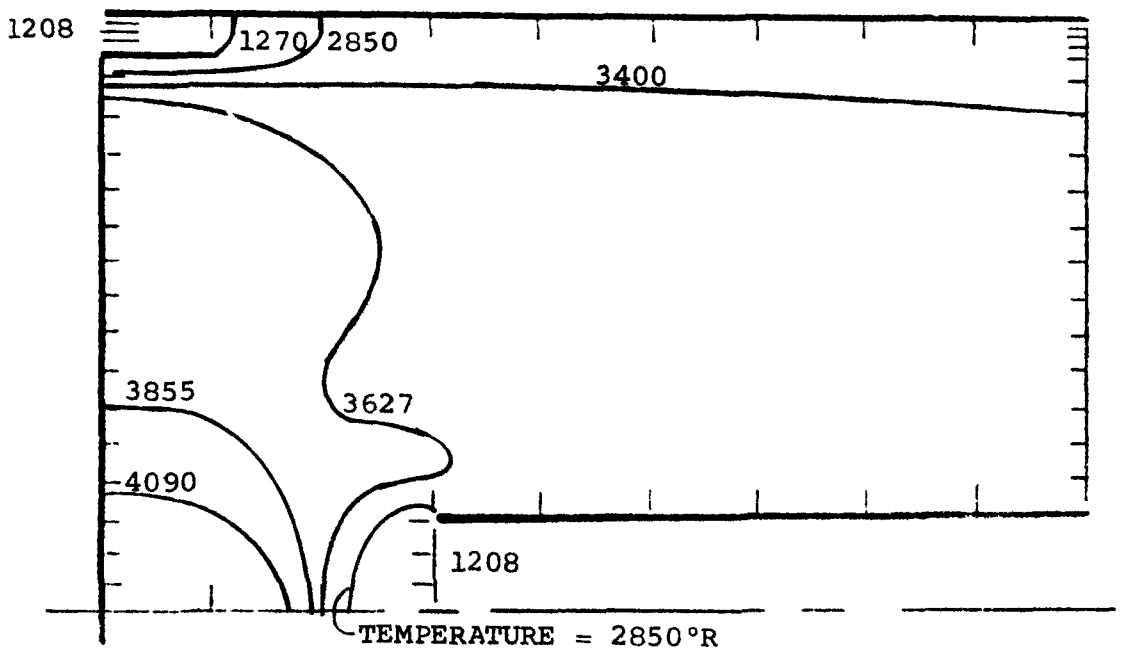

PREPARED	SCH	11-71	CLASS B COMBUSTOR PRIMARY ZONE TEMPERATURE DISTRIBUTION	FIGURE 2-15
WRITTEN				
APPROVED				

FORM P703A-1

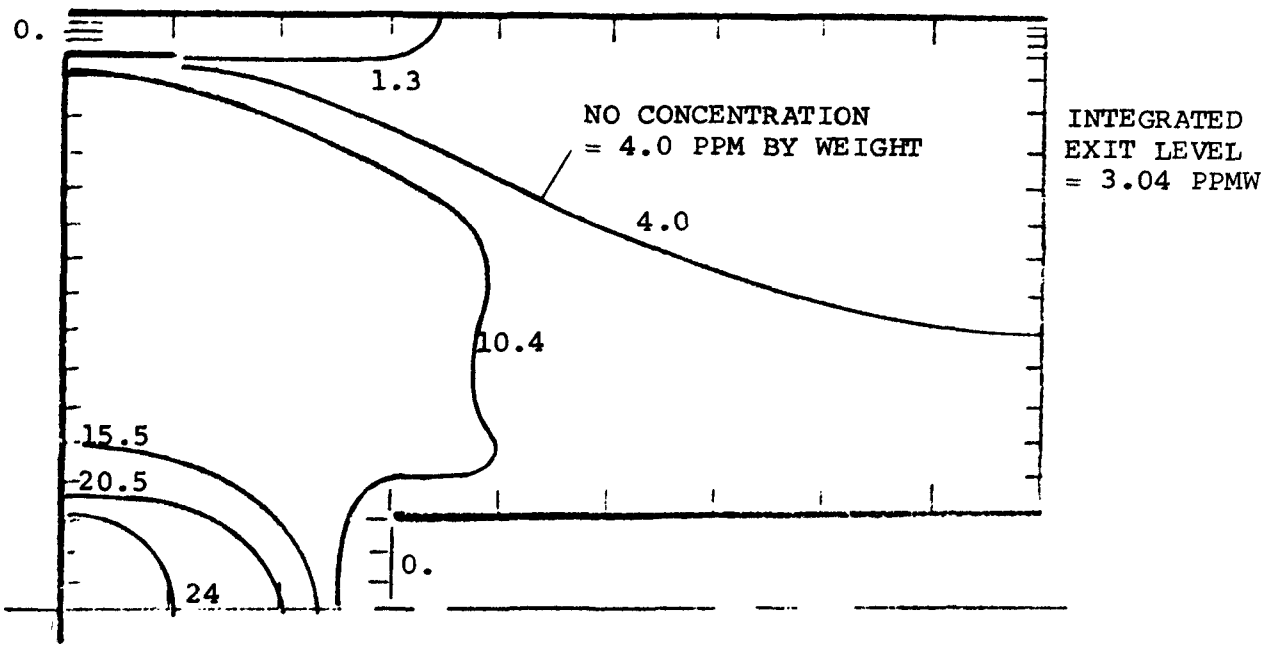

PREMIXED VAPOR-AIR MIXTURE
AT BOTH INLETS

PREPARED	SCH 11-71	CLASS B COMBUSTOR PRIMARY ZONE DISTRIBUTION OF NITRIC OXIDE	FIGURE 2-16
WRITTEN			
APPROVED			

FORM P709A-1

2.5 Experimental Flow Visualization Model

A plexiglass model of a preliminary film vaporizing combustor design was employed in flow visualization tests to verify internal flow pattern computations by the Gosman method. The model was installed in a three-dimensional water rig and the flow patterns were analyzed with tracer particles. Figures 2-17 and 2-18 are photographs of the test rig, Assembly No. SKP26283, as installed in the test facility.

In addition, high-speed motion pictures were taken of the flame development during operation of the model in an ambient pressure airflow rig. The plexiglass model of a film-vaporizing combustor was installed in the ambient airflow test rig, and air was drawn through the model with a vacuum header. Motion pictures of the flame-stabilization process within the combustor were taken at 4000 and 8000 frames per second during two-second operation tests. The motion picture of the film-vaporizing combustor flame stabilization process was presented at the EPA in Ann Arbor, Michigan on August 24, 1971. Minimal-volume intense recirculation and absence of combustion in the high velocity fuel film along the combustor wall are illustrated in the film.

The primary zone flow pattern observed during operation of the model correlated very closely with the calculated streamlines from the flow pattern analysis, thereby providing reasonable confirmation of the analysis by the Gosman method. Further testing was conducted on the three-dimensional water analog model to establish primary zone flow patterns for comparison with the analytical model. Figures 2-19 and 2-20 are photographs of the trajectories of tracer particles used to define the flow path inside the combustor. An overlay for Figure 2-19 has been made to indicate the direction of motion. Note the similarity between the flow pattern of Figure 2-19 and the analytical results shown in Figure 2-21.

THREE-DIMENSIONAL WATER ANALOG RIG

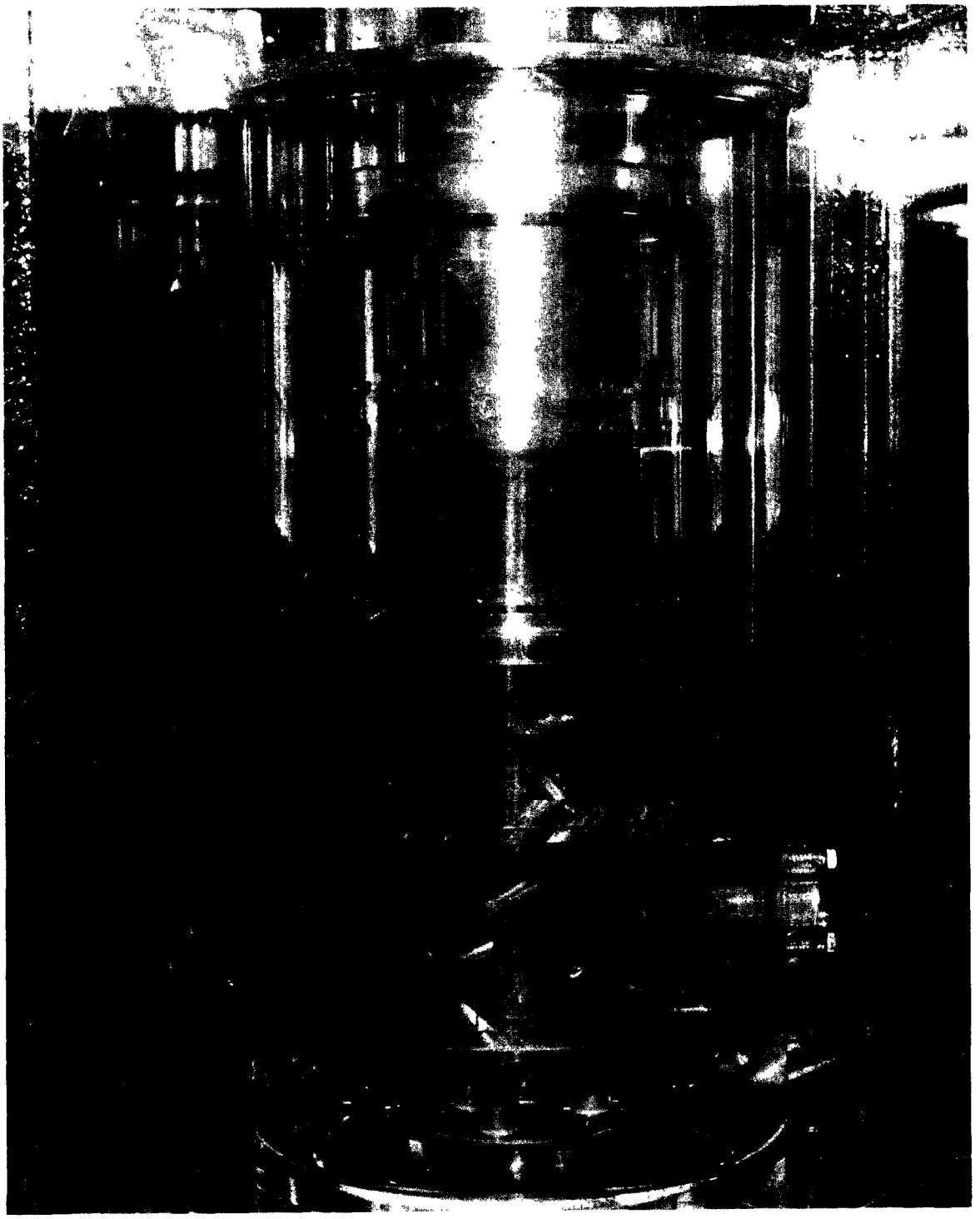

SHOWING CLOSEUP OF INSTALLED COMBUSTOR MODEL

FIGURE 2-17

THREE-DIMENSIONAL WATER ANALOG RIG

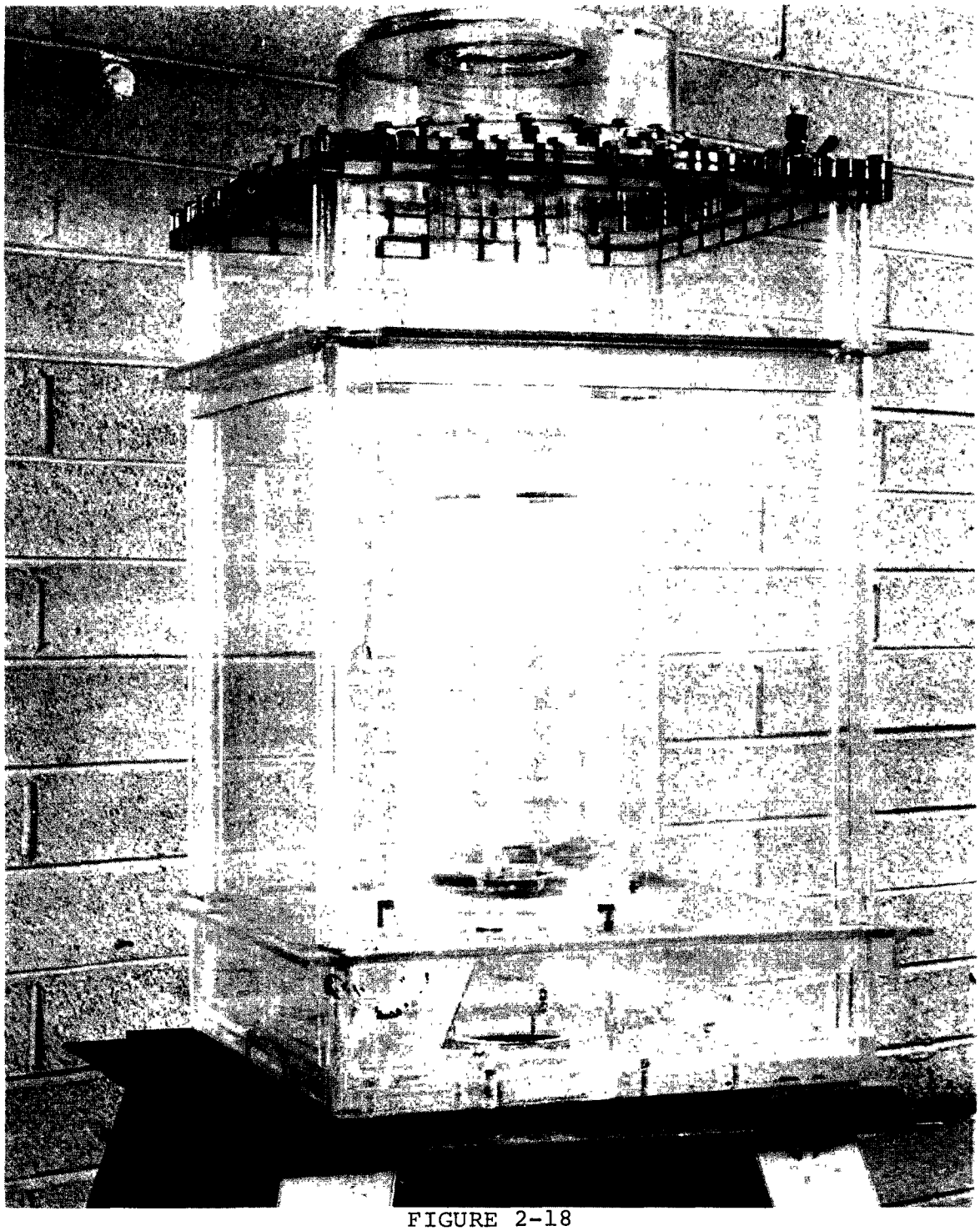

FIGURE 2-18

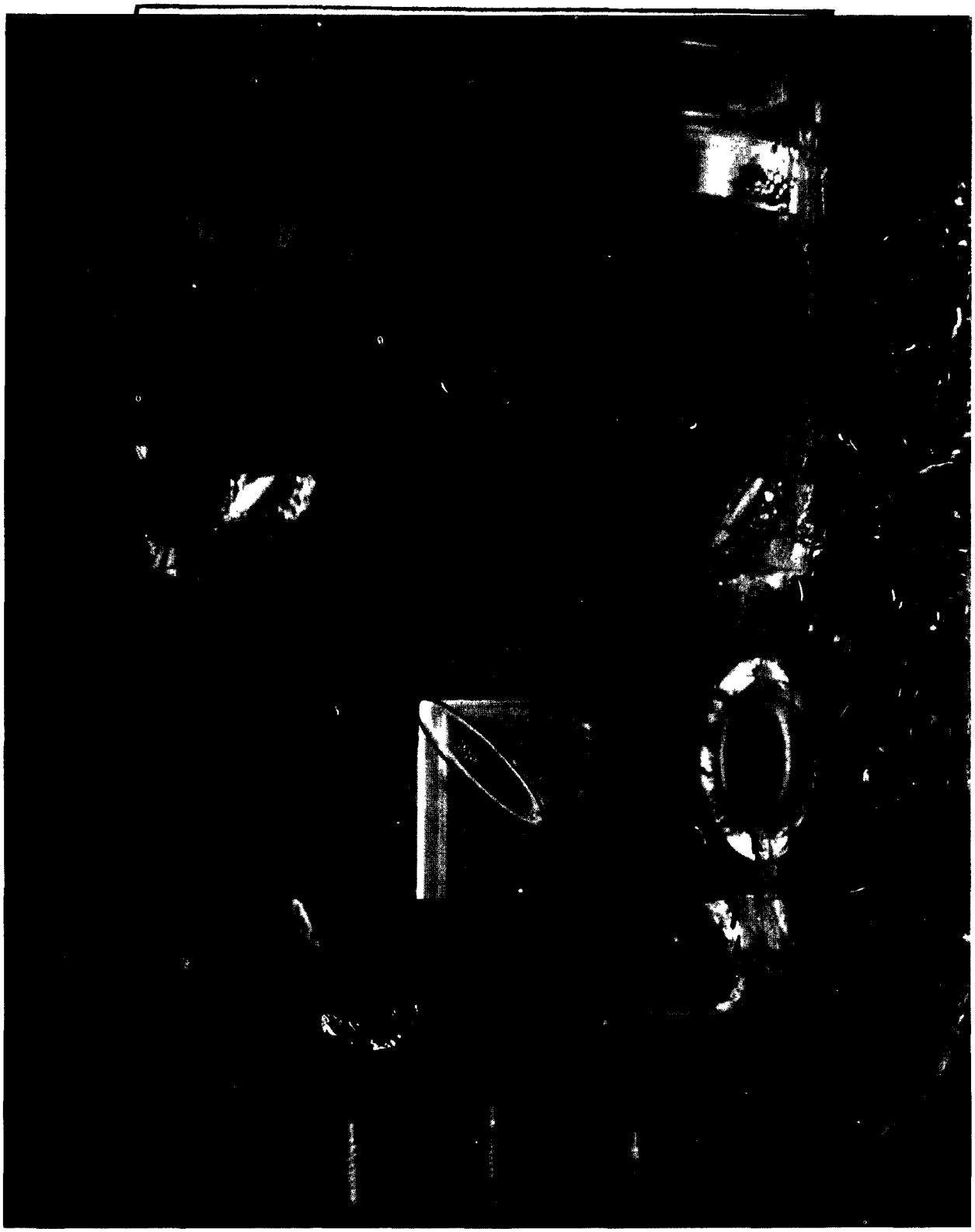

FIGURE 2-19

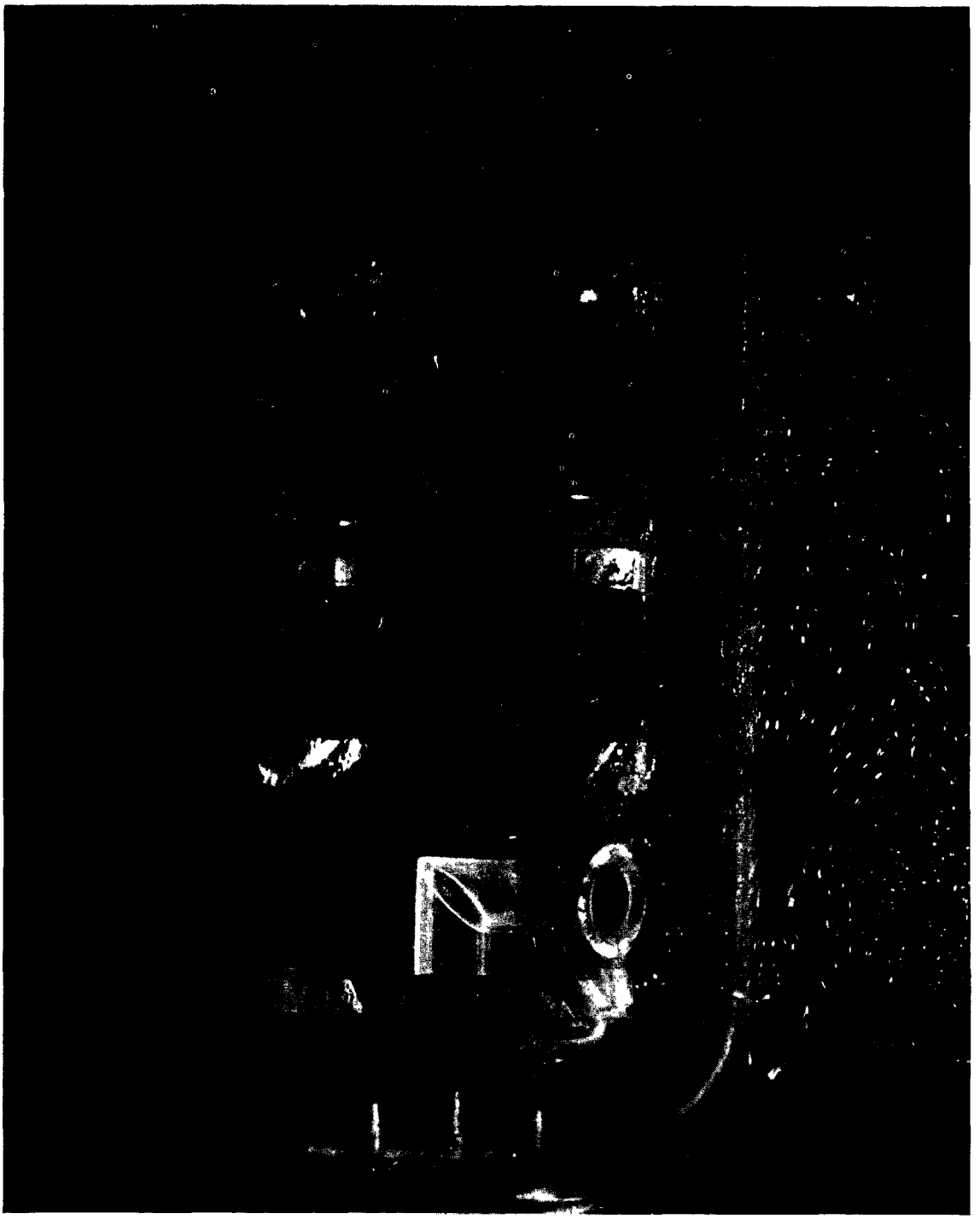

FLOW PATTERN RECORD COMBUSTOR OVERALL VIEW 3-D WATER ANALOG
LOW EMISSION COMBUSTOR STUDY

FIGURE 2-20

COMPUTED FLOW PATTERN

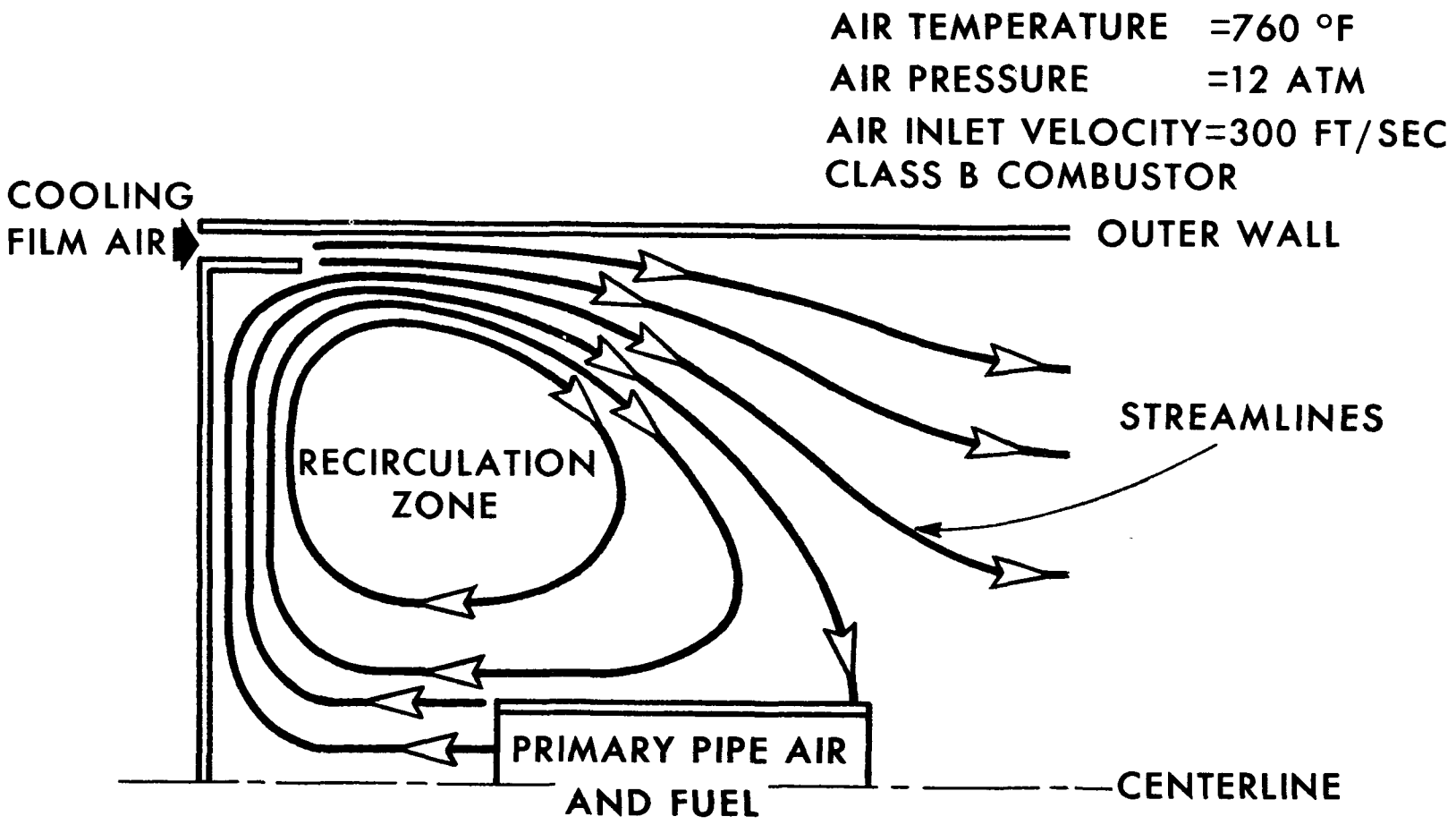

FIGURE 2-21

The test was conducted at a Reynolds number of 1.42×10^5 based on the combustor mean diameter. For Reynolds similarity with the Class B combustor design condition, a Reynolds number of 4.02×10^5 would have been required. Once the Reynolds number is sufficiently high to ensure turbulence, however, the flow pattern becomes independent of Reynolds number, so the test condition was set up only to establish turbulent flow ($Re_d > 10^5$).

The photographs were obtained by introducing small polystyrene spheres with a density approximately equal to that of water into the rig inlet and allowing them to circulate continuously. The tracers were illuminated as they passed through the combustor by projecting a two-dimensional beam of light from a 1000-watt quartz lamp through the combustor along the centerline of one set of orifices. Then with an appropriate adjustment to the camera shutter speed a tracer direction of travel was established by noting that the brightest illumination of the particle occurs just as the shutter opens and then trails off in the direction of motion of the tracer as the shutter closes.

Because of the two-dimensionality of the light beam and the photograph, it is impossible to determine whether the tracers are moving into, out of, or completely within the flow pattern plane being photographed. It is, therefore, impossible to record the effect of swirl other than by actual visual observation of the model. In this case, difficulty with plugging of the cooling air swirl passages with tracer particles was encountered.

3. COMBUSTOR TEST RIG AND INSTRUMENTATION

A full-scale test fixture with a removable test section, capable of operating over the combustor operating range as determined from the cycle analysis, was designed for use in the test program. A separate component test section to simulate critical flow paths around the combustion chamber was designed for both combustors. Each test section was designed into a section of standard-diameter pipe flanged at both ends to allow common inlet and exhaust plumbing.

A clean air supply that is capable of achieving combustor inlet temperatures typical of recuperated engine cycle operation was provided for this program in three steps.

(a) From the start of the program to November 17, 1971, the existing laboratory facility heater (a gas-fired heat exchanger) was used to obtain a maximum temperature of 740°F.

(b) Added capability was achieved (up to 1000°F) by using the discharge air from a cross-flow exhaust recuperator.

(c) Finally, by early November 1972, a new preheater (Model 1030) was installed at the test facility. A combustor inlet temperature of 1200°F was thought achievable, but, subsequent test experience demonstrated only a 1030°F maximum temperature was achievable at the test airflow rates.

3.1 Rig Design and Fabrication

It was decided to test the combustors in an 8-inch diameter pipe to eliminate any effects due to non-uniform external flow conditions and to ensure that combustor performance measured will be affected by combustor design features only.

Figures 3-1 and 3-2 show a section layout and a photograph of the combustion high-pressure test rig respectively. Common inlet and exhaust plumbing are used for both classes of combustors with a separate test section for each. A pressure drop is taken across a screen installed ahead of the test section to ensure uniform distribution of the incoming airflow. The two test sections are fabricated from short sections of standard diameter pipe flanged at both ends to facilitate installation into the test cell. The combustor is mounted on four half-inch unreaded rods located at the inlet end of the test section and slips into an exhaust collector at the discharge end. The mounting rods can be positioned to accommodate various length combustors. fill the gap between combustor delivery and high-pressure combustion rig hardware delivery a simple low-pressure rig was designed and fabricated in-house.

The low-pressure rig was assembled and installed in the test facility as shown in Figure 3-3. A single-point probe capable of traversing across the combustor exit in a single plane was used to measure exhaust gas temperature and to pick up an emissions sample simutaneously.

3.2 Instrumentation

The combustor rig test sections were instrumented to measure total and static pressure and temperature at combustor inlet and discharge. All temperatures were measured by ungrounded-junction, shielded, high-recovery factor, thermocouples; combustor discharge-temperature-measuring thermocouples were aspirated. Combustion chamber liner temperatures were measured with temperature-indicating paint. A weight-flow rate system was used for fuel flow measurements, and standard orifice measuring sections was used for airflow measurement.

COMBUSTOR TEST RIG FOR EMISSION STUDY

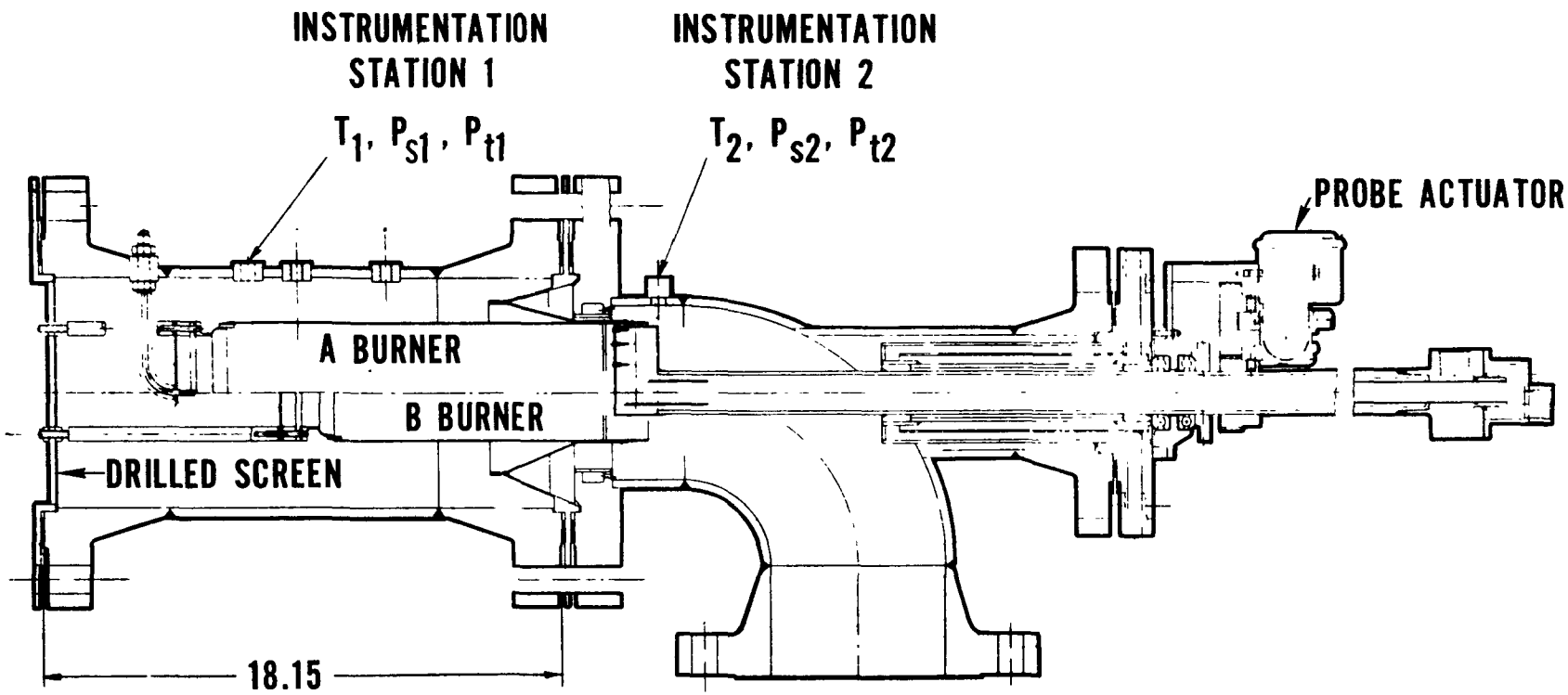

FIGURE 3-1

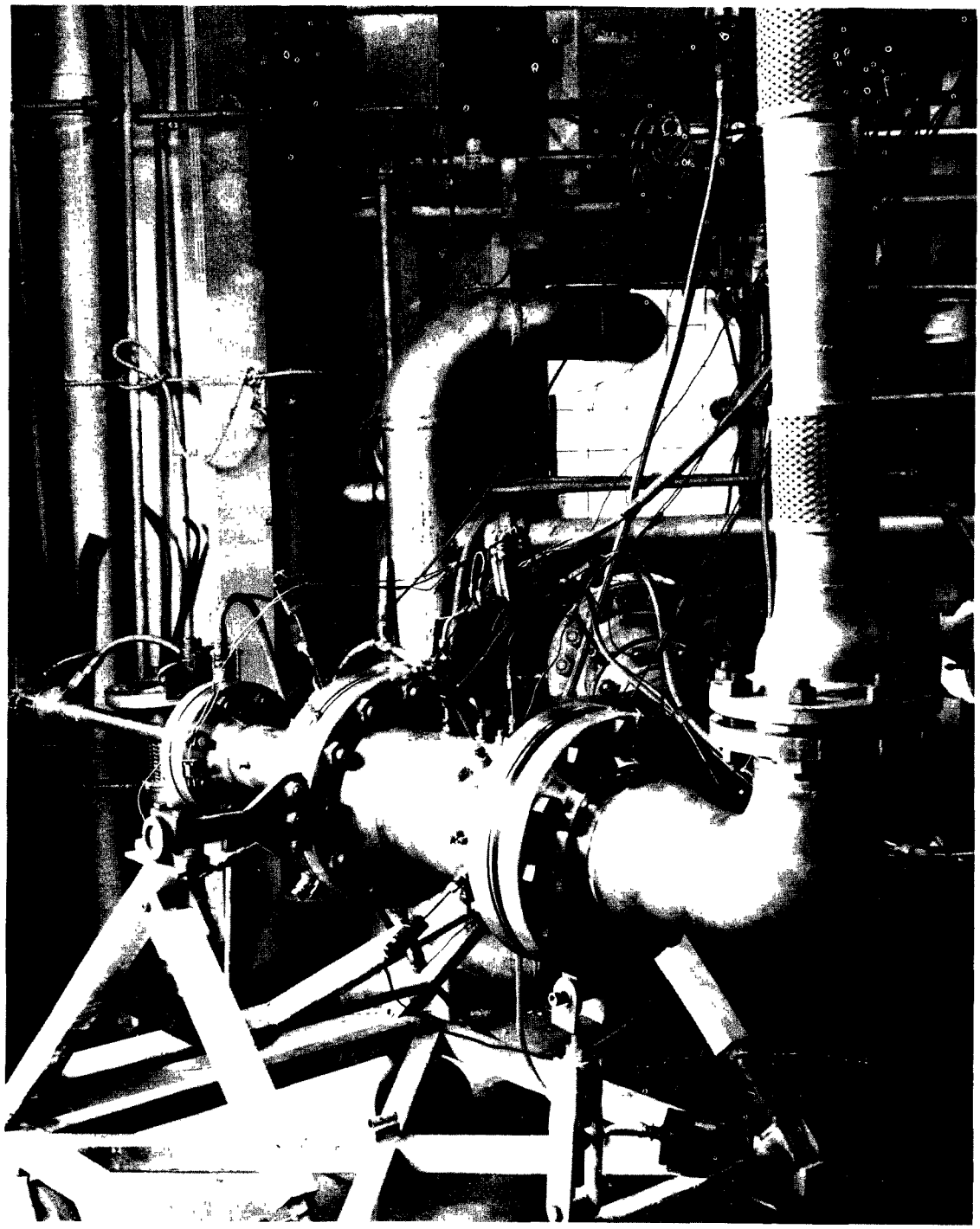

LOW EMISSIONS COMBUSTOR STUDY, HIGH-PRESSURE TEST RIG

FIGURE 3-2

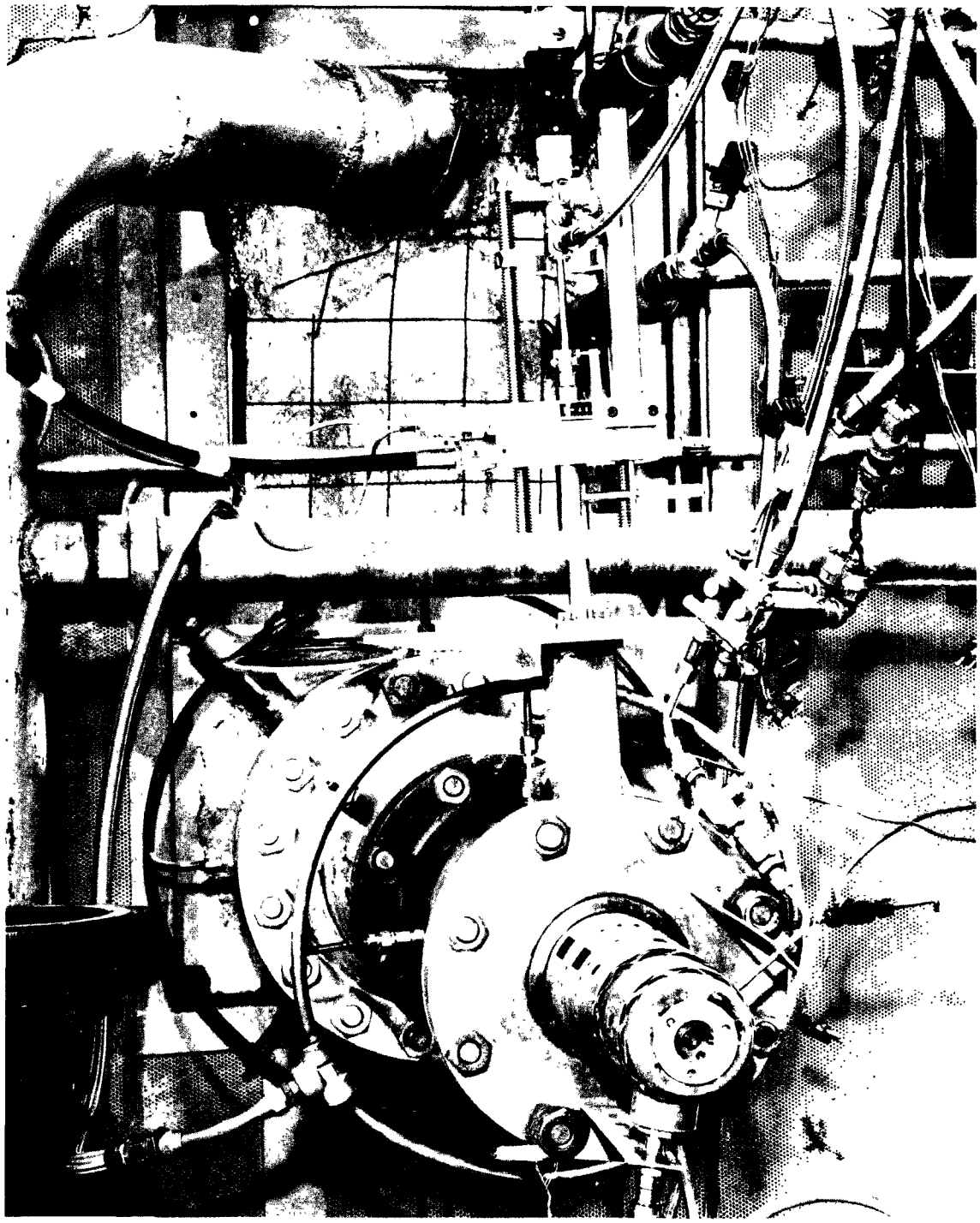

LOW-PRESSURE (ATMOSPHERIC) TEST RIG

FIGURE 3-3

3.2.1 Combustor Performance

Performance data were measured by the instrumentation described below and recorded on data sheets shown in Appendix III.

(a) Pressure Measurements - Static pressure measurements were taken with wall static taps, four each equally spaced at both combustor inlet and discharge. Total pressures were measured with Kiel-type total pressure probes, one each corresponding to each static tap. The pressure readouts were either vertical water or mercury manometers graduated in 0.1 in. increments or Wallace and Tiernan Bourdon-type gauges graduated in 0.5-in. increments to 300 in. Hg. Advertised accuracy of the gauge readouts is ±0.1 percent of full scale.

(b) Temperature Measurements - Inlet temperatures were measured with shielded high-recovery factor iron-constantan thermocouples to 800°F and with similar chromel-alumel thermocouples to 1200°F. One thermocouple corresponding to each total pressure pickup was installed. Discharge gas temperatures up to 2000°F were measured with a separated chromel-alumel thermocouples and with platinum/platinum-10 percent rhodium thermocouples above 2000°F/ Eight equally spaced two-point probes located at the area centers of equal areas were used to determine the temperature distribution factor. The temperatures were read out on Brown recorders: 0-1000°F with ±2 deg accuracy for the I-C, 0-2400°F with ±5 deg accuracy for the C-A, and 0-3000°F with ±2 deg accuracy for the Pt/Pt-10 Rh. Capability to record temperature data automatically with a digital acquisition system was also provided.

(c) Air and Fuel Flow Rates - Airflows were determined by standard, regularly-calibrated orifice measuring sections with flange taps. Two sections, an 8.0-in. and a 3.0-in. are available as an integral part of the test facility depending upon the required airflow and were used for test conditions not requiring a heat exchanger. For inlet temperatures exceeding 700°F, a heat exchanger was plumbed into the system with a 6.0-in. measuring section between it and the section.

Fuel flow was measured by a Cox Flowmeter. This instrument determined fuel weight flow rate directly by measuring the amount of time required to pass a specified weight of fuel. The fuel weight was automatically measured on a balance scale, with the known weight input by the operator.

(d) Metal Temperature Measurements - Combustor metal temperatures were measured with the aid of temperature-indicating paint.

(e) Emissions Sampling Probe - The gas sampling probe consisted of three individual probes on a common support capable of being traversed circumferentially and positioned axially up to the combustor primary zone exit. The pickup points were located at the area centers of equal areas such that a separate probe was required for each combustor class. The probe was actuated by a rotary gear drive (Figure 3-4) supported on the rig discharge elbow, and the positions were controlled microswitches on the actuator mechanism. The probe positioning shaft was sealed with "O"-rings encased in a cooling water manifold.

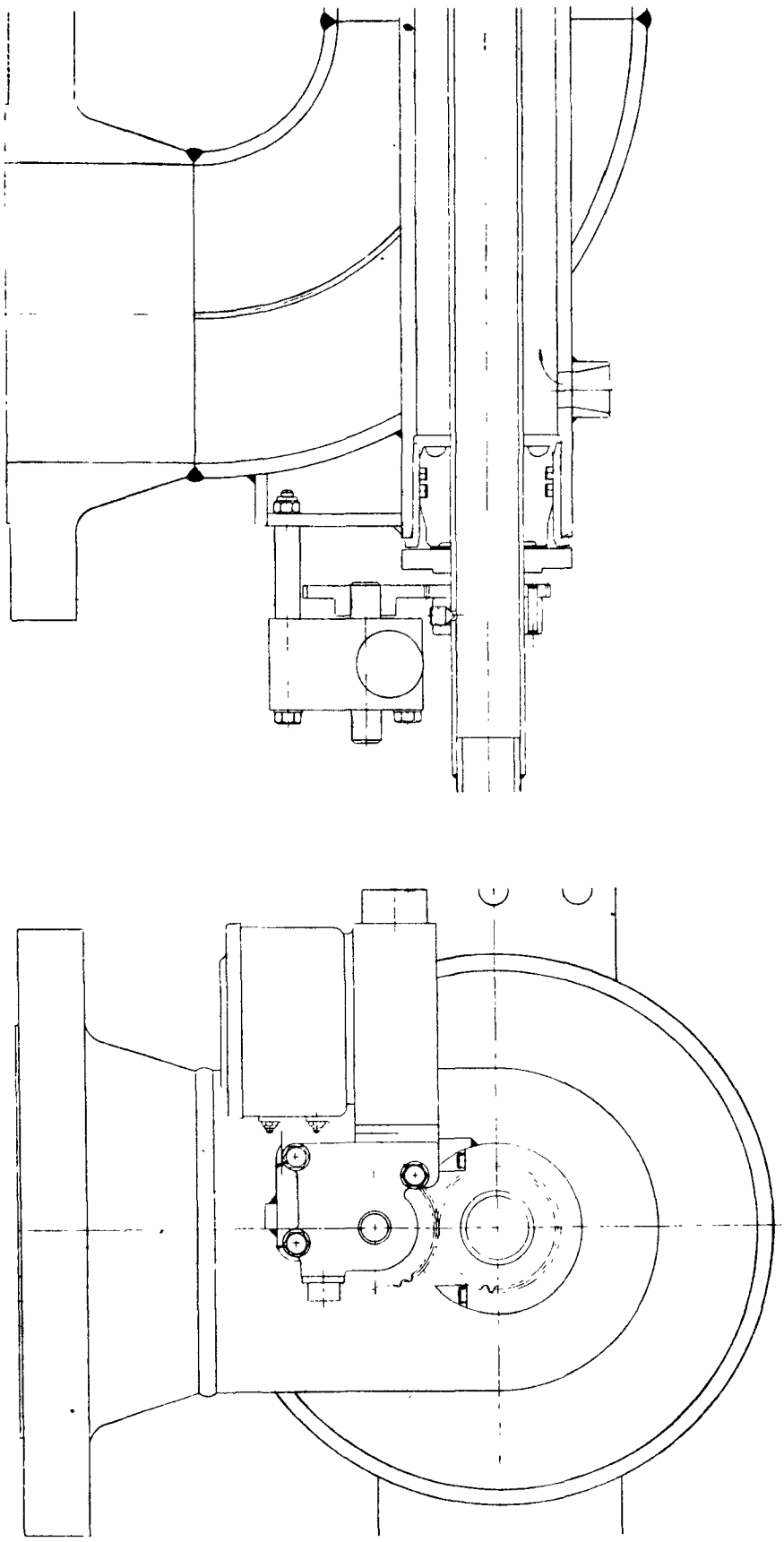

EMISSIONS PROBE ACTUATOR

FIGURE 3-4

The probe body construction consisted of three separate 1/16-in. diam probes individually valved with remotely controlled solenoids. The probes terminated in a common support as shown in Figure 3-5. Cooling air was delivered to the probe plenum through the outside passage formed by two concentric tubes which made up the rotating shaft and discharged back through the center passage. The probe heads incorporated a convergent-divergent nozzle at the inlet to assist the coolant flow in reducing the exhaust sample temperature by increasing the sample velocity, thereby quenching any reactions continuing at the combustor exit. Reaction quenching assured that the composition of the sample did not change significantly between the probe inlet and the analyzing equipment. Use of air as the coolant ensured that the probe temperature did not drop below the 300°F required to avoid condensation of the heavy hydrocarbons on the probe walls.

Later, to expedite testing, the emissions samples were taken from the thermocouple aspirated flow (eight two-point probes) as shown in Figure 3-6.

3.2.2 Emissions Analyzing Equipment

Continuous monitoring of pollutant levels was performed during the test phase with the equipment described in this section. Manufacturer's data, including principles of operation and model specifications, are presented in Appendix II. The emissions-analyzing equipment was installed in a truck (Figure 3-7) equipped with an environmental control system. Figure 3-8 shows the instrumentation installed in the truck. The following paragraphs briefly describes this equipment.

(a) Carbon Dioxide and Carbon Monoxide Analysis - Carbon dioxide and carbon monoxide concentrations were measured by the nondispersive infrared method. Concentrations were measured on

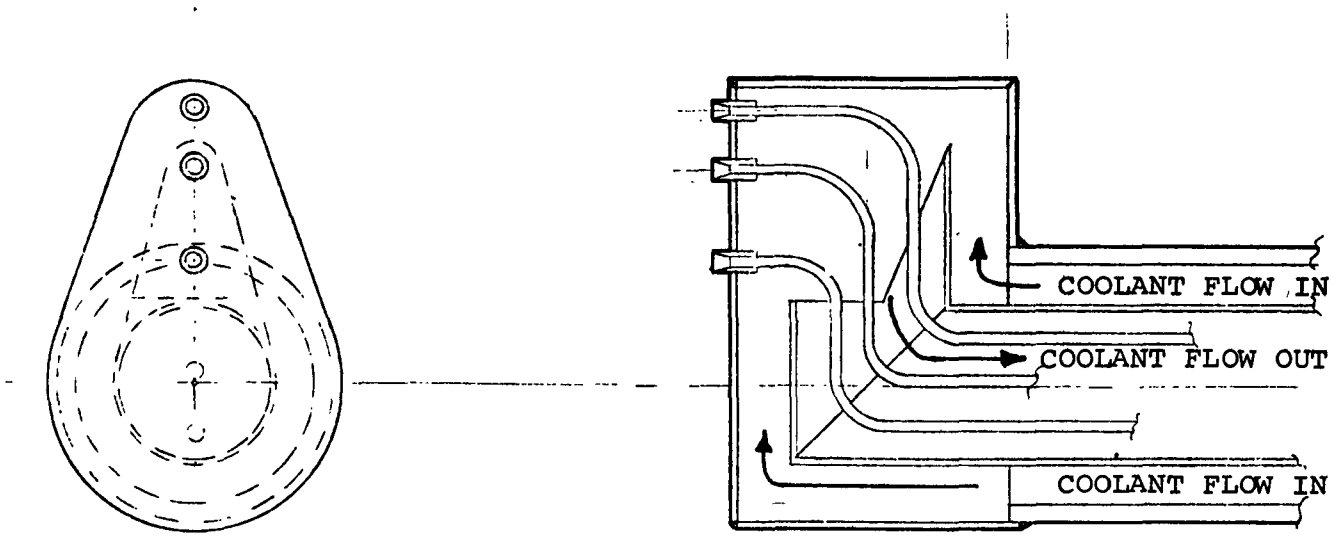

EMISSIONS SAMPLING PROBE TIP

FIGURE 3-5

STATIONARY PROBES - INSTRUMENTATION

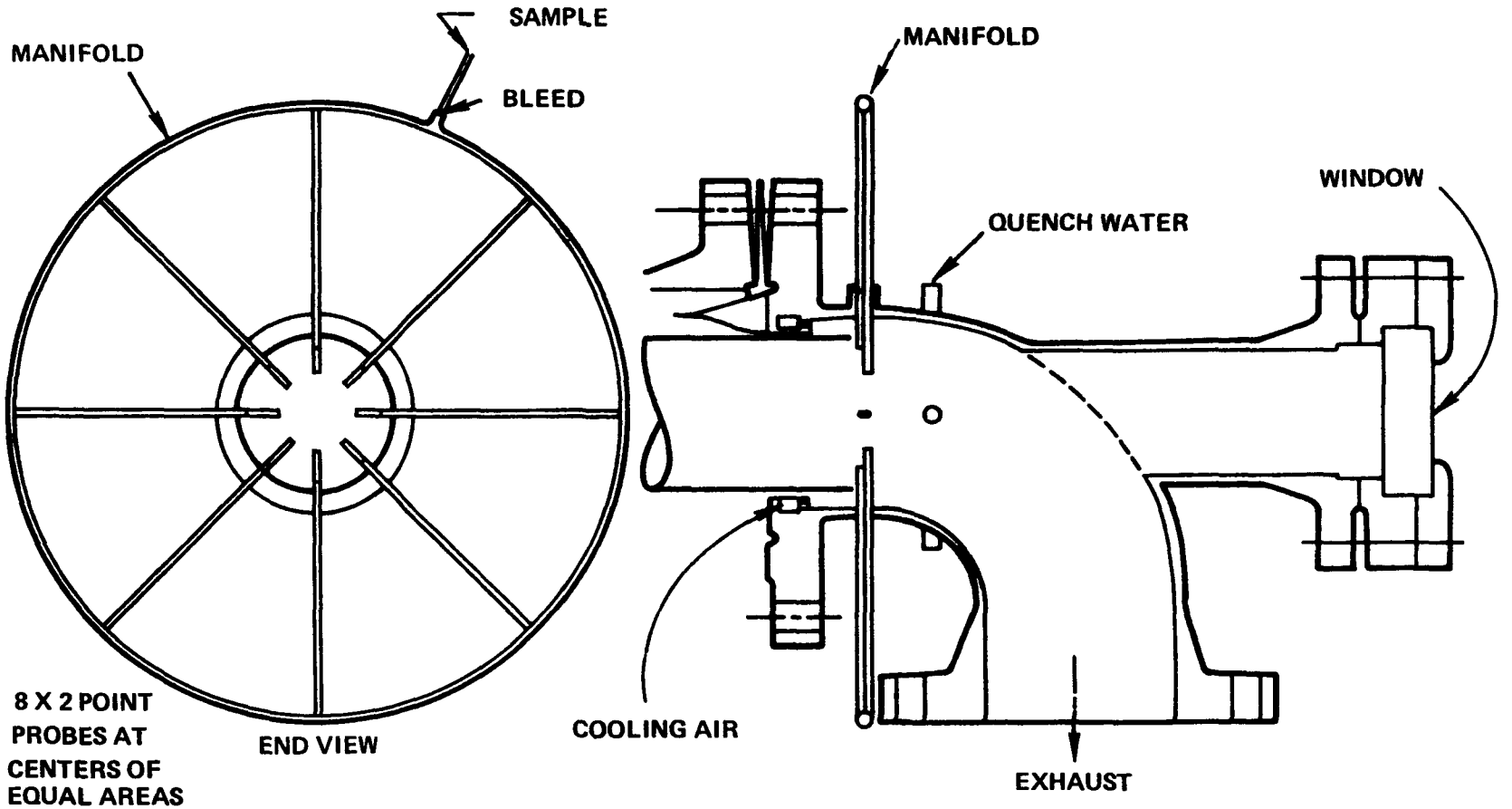

COMBINATION T_2 MEASUREMENT AND AVERAGING EMISSION SAMPLING

FIGURE 3-6

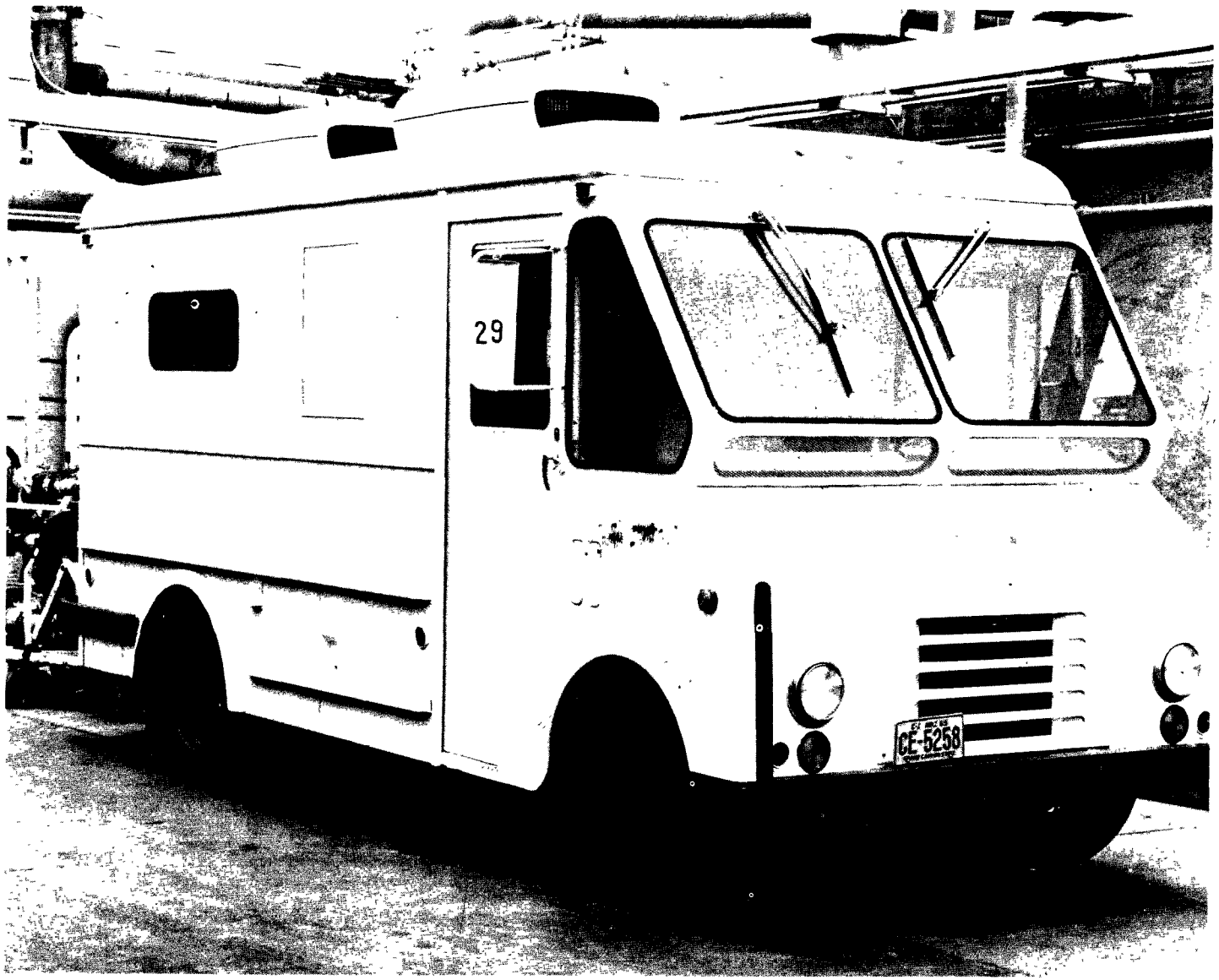

AIRESEARCH EXHAUST EMISSIONS ANALYZING TRUCK

FIGURE 3-7

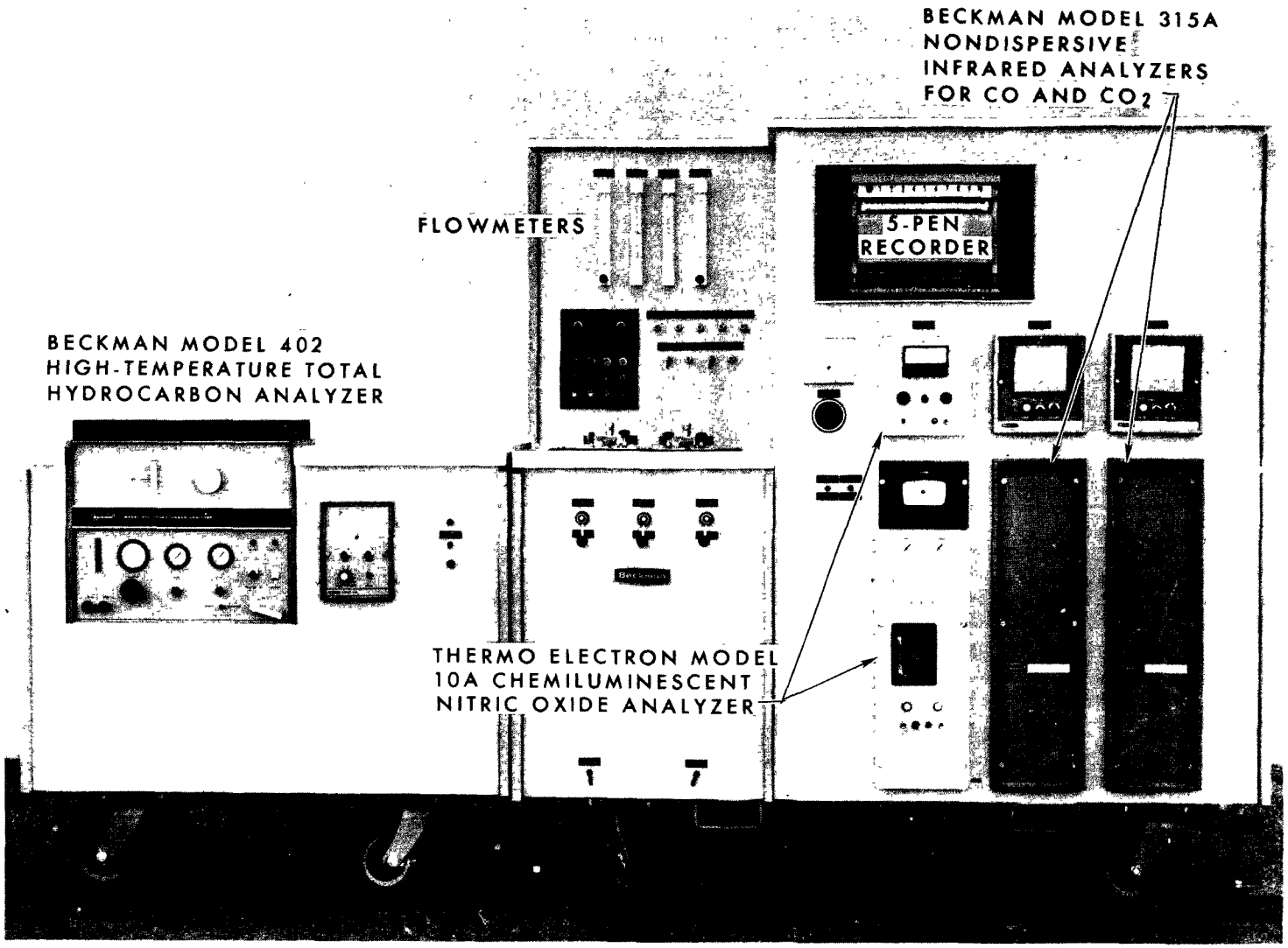
BECKMAN MODEL 315A
NONDISPERSIVE
INFRARED ANALYZERS
FOR CO AND CO_2
FLOWMETERS
5-PEN
RECORDER
BECKMAN MODEL 402
HIGH-TEMPERATURE TOTAL
HYDROCARBON ANALYZER
THERMO ELECTRON MODEL
10A CHEMILUMINESCENT
NITRIC OXIDE ANALYZER

FIGURE 3-8

a dry exhaust products basis since dessicants are used to remove excess water vapor from the sample to minimize interference. Beckman Model 315A Nondispersive Infrared Analyzers with the following specified ranges and accuracies were used:

Range: Carbon monoxide; 0-100 ppm, 0-500 ppm, and 0-2500
Carbon dioxide; 0-2 percent, 0-5 percent, 0-15 percent

Accuracy: 2 percent full scale for 100 ppm CO range
1 percent full scale for 500 and 2500 ppm CO range
1 percent full scale for 2 percent and 5 percent CO_2 range

(b) Oxides of Nitrogen Analysis - Nitrogen oxide concentration were measured by the homogeneous chemiluminescent method. Water vapor was removed from the sample prior to entering the analyzer so results were measured on the basis of dry exhaust concentrations. A Thermo Electron Model 10A was equipped with a thermal converter to break down NO_2 to NO and O_2, thereby making it possible to monitor total oxides of nitrogen, (NO_2 + NO = NO_x) instead of nitric oxide only. The instrument has the following advertised range and accuracy:

Range: 3-10,000 ppm
Accuracy: ±1 percent full scale (±1 ppm)

(c) Unburned Hydrocarbon Analysis - Unburned hydrocarbon concentrations were measured on a wet basis with a heated flame ionization detector to minimize response errors due to absorption-desorption of the heavy hydrocarbon molecules between the probe and the analyzer. A Beckman Model 402 High-Temperature Total Hydrocarbon Analyzer was used. This

instrument came equipped with an integral heated 10-ft long sample line, thermostatically controlled at approximately 200°C. Advertised range and accuracy are:

Range:	0-5 ppm to 0-5000 ppm (as methane)
Accuracy:	1 percent full scale

4. DATA REDUCTION METHODS AND PRESENTATION

The following analytical procedures were used to reduce the data obtained during combustor performance testing. Data reduction was computerized where practical.

4.1 Combustor Performance Data Reduction

Conventional combustor performance parameters including pressure loss, temperature distribution, lean stability, efficiency, and metal temperature levels were measured at selected test conditions. Data were reduced according to the following procedures.

(a) Pressure Loss

Combustor pressure drop was calculated as

$$(P_{T_{in}} - P_{T_{out}})/P_{T_{in}}$$

where $P_{T_{in}}$ and $P_{T_{out}}$ represent total pressures at the combustor inlet and outlet, respectively. The pressure used in the denominator was a circumferentially averaged value from the individual probes while the numerator value was obtained from a pressure gauge. The measured values of inlet total pressure were checked against values calculated from a measured static pressure, airflow rate, and inlet temperature with the aid of Mach tables.

(b) Temperature Distribution

Discharge gas temperature distribution was calculated as a Temperature Spread Factor (TSF) defined as

$$TSF = \frac{T_{max} - T_{mean}}{T_{mean} - T_{inlet}}$$

where T_{max} and T_{mean} are the maximum measured and average measured total temperatures at the combustor discharge, respectively, and T_{inlet} is the combustor inlet total temperature, all in degrees F.

(c) Ignition and Lean Stability

Ignition limits were determined as minimum fuel-air ratio required to light as a function of combustor airflow. Combustor lean stability was calculated as fuel-air ratio at lean blowout at the specified test condition. The values of airflow and fuel flow were measured. Both ignition and lean blowout were determined by monitoring combustor temperature rise.

(d) Combustion Effficiency

Combustion efficiency was calculated as

$$\eta = \frac{(f/a)_{ideal}}{(f/a)_{actual}}$$

where $(f/a)_{ideal}$ is the ideal fuel-air ratio required to obtain the measured combustor temperature rise. This value is obtained from constant pressure combustion charts. $(f/a)_{actual}$ is the actual fuel-air ratio from measured air and fuel flow rates at the test condition.

The efficiency calculated from the above expression was checked against an efficiency computed using the measured levels of carbon monoxide and unburned hydrocarbons, assuming these constituents are the only products of incomplete combustion.

(e) Combustor Metal Temperature

Metal temperatures were determined directly as isotherms on a thermindex-painted combustor.

A computer program available at AiResearch for engine emission data reduction was modified to allow computerized data reduction of combustion rig data. Both emission index and pollutant generation rate in lb/hr are calculated. The emissions concentrations are corrected to concentrations in wet exhaust from a combustion process with dry air. In addition, combustion efficiency is calculated from the measured carbon monoxide and unburned hydrocarbon concentrations. A typical computer printout is shown in Figure 4-1.

It should be noted that unburned hydrocarbon weights are calculated as methane, CH_4. If it is necessary to convert the emission indices to equivalent $CH_{1.85}$ or C_6H_{14}, the printed weight values should be multiplied by 0.865 or 0.895, respectively.

In the reduction of the exhaust emission data, carbon monoxide, carbon dioxide, and oxides of nitrogen volume concentrations will be considered dry analysis data because of the use of a dessicant or condenser in the sampling train. Total hydrocarbons concentrations, however, will include the water vapor initially in the air plus the water vapor formed by the combustion process. For the purpose of reducing the data on a volumetric basis, the concentration levels will be corrected to percent (or parts-per-million) by volume of wet exhaust gas from a combustion process with dry air. Accordingly, the wet analysis data will be initially corrected to dry conditions as follows:

$$S' = \frac{S''}{1 - \nu - \omega} \qquad (1)$$

AIRESEARCH EMISSION TEST SUMMARY

ENGINE=EPA S/N=0AP COMB P/N=SKP26489SDTEST DATE 6-19-72 FUEL=JP-4 P BARO= 28.60
RAT THR= 0. RA EGT,F= 0. RAT SPD= 0. DEW PT,F= 15. REL HUM= 0.00 SPEC HUM= .001758
FUEL H/C= 1.9[illegible]0 STOI F/A= .06781 L H V= 18520. S LN T,F= 0.0 FLO,L/M= 0.000 SL TIM,S= 0.0000

Data Point Number	1	2	3A	3	4A	4	5	6
Percent Bypass	2.9	5.0	9.9	9.8	15.0	15.0	5.0	4.9
Bypass Air Temperature, 300°							200°	400°
Burner Inlet Temp., Deg F	1060	1062	1060	1062	1060	1050	1055	1047
FA RATIO CALC. FROM EMISSION	.0065	.0063	.0072	.0064	.0082	.0058	.0062	.0063
EQUIVALENCE RATIO	.096	.093	.106	.094	.120	.085	.091	.093
COMB EFFIC FROM EMISSIONS	99.892	99.932	99.570	97.688	96.586	93.010	99.909	99.924
SUMMARY OF REDUCED EMISSION DATA								
CARBON DIOXIDE								
PERCENT BY VOLUME, WET	1.33	1.29	1.47	1.27	1.59	1.03	1.27	1.29
PERCENT BY VOLUME, DRY	1.35	1.31	1.49	1.29	1.62	1.05	1.29	1.31
LB. CO2 PER LB. OF FUEL	3.13	3.14	3.12	3.04	3.00	2.73	3.13	3.14
WEIGHT FLOW, LB./HR.	50.8	50.8	55.9	49.2	64.4	45.1	50.8	50.8
CARBON MONOXIDE								
PPM BY VOLUME, WET	27.6	15.6	51.9	227.0	377.4	1330.9	21.6	17.6
PPM BY VOLUME, DRY	28.0	15.8	52.7	229.9	383.6	1346.4	21.9	17.8
LB. PER 1000 LB. OF FUEL	4.138	2.417	7.009	34.587	45.126	224.017	3.392	2.724
WEIGHT FLOW, LB./HR.	.067	.039	.125	.560	.970	3.696	.055	.044
UNBURNED HYDROCARBONS- PPM AS CARBON, WEIGHTS AS CH4								
PPM BY VOLUME, WET	1.5	1.5	39.1	195.6	391.1	204.6	1.5	1.5
PPM BY VOLUME, DRY	1.5	1.5	39.7	198.1	397.5	207.0	1.5	1.5
LB. PER 1000 LB. OF FUEL	.129	.133	3.019	17.032	26.733	19.683	.135	.133
WEIGHT FLOW, LB./HR.	.002	.002	.054	.276	.575	.325	.002	.002
RATIO LB HC/LB CO	.0312	.0551	.4308	.4924	.5924	.0879	.0398	.0489
NITRIC OXIDE (NO) + WEIGHTS AS NO2								
PPM BY VOLUME, WET	58.2	33.1	6.5	2.0	9.0	4.0	31.6	35.6
PPM BY VOLUME, DRY	59.0	33.5	6.6	2.0	9.2	4.1	32.0	36.1
LB. PER 1000 LB. OF FUEL	14.336	8.416	1.446	.502	1.773	1.109	8.155	9.052
WEIGHT FLOW, LB./HR.	.232	.136	.026	.008	.038	.018	.132	.147
NITROGEN DIOXIDE (NO2)								
PPM BY VOLUME, WET	6.0	3.5	2.5	1.5	11.0	0.0	3.5	3.0
PPM BY VOLUME, DRY	6.1	3.6	2.5	1.5	11.2	0.0	3.6	3.0
LB. PER 1000 LB. OF FUEL	1.483	.893	.556	.377	2.167	0.000	.906	.765
WEIGHT FLOW, LB./HR.	.024	.014	.010	.006	.047	0.000	.015	.012
TOTAL OXIDES OF NITROGEN (NO+NO2) AS NO2								
PPM BY VOLUME, WET	64.2	36.6	9.0	3.5	20.1	4.0	35.1	38.6
PPM BY VOLUME, DRY	65.1	37.1	9.2	3.6	20.4	4.1	35.6	39.1
LB. PER 1000 LB. OF FUEL	15.819	9.309	2.002	.879	3.940	1.109	9.061	9.817
WEIGHT FLOW, LB./HR.	.256	.151	.036	.014	.085	.018	.147	.159

NOTES 1.ALL EMISSIONS CONCENTRATIONS CORRECTED TO CONCENTRATION IN WET OR DRY EXHAUST FROM COMBUSTION WITH DRY AIR.
2.EQUIVALENCE RATIO CALCULATED FROM CO2,CO,AND HC DATA AND FUEL COMPOSITION.
3.MASS EMISSIONS OF NO, NO2, AND NO+NO2 CALCULATED AS NO2 FROM CONCENTRATIONS WITH MOLECULAR WEIGHT OF NO2 (46.01).
4.COMBUSTION EFFICIENCY CALCULATED FROM CO,AND UHC AS VAPORIZED ORIGINAL FUEL ON LB/ LB FUEL BASIS.

FIGURE 4-1

where:

S' - volumetric concentration of pollutant species in dry exhaust gas

S" - volumetric concentration of pollutant species in wet exhaust gas containing water vapor in rig inlet air plus water vapor formed by combustion process

ν - mole fraction of water vapor in exhaust from initial conditions of inlet air = h (M_e/M_ω)

ω - mole fraction of water vapor formed from combustion process = R/2 (a' + b' + d') = 2d'

h - lb water vapor/lb dry air at rig inlet determined from relative humidity of inlet air

M_e - molecular weight of exhaust products = 29.0 lb/lb-mole

M_ω - molecular weight of water vapor = 18.02 lb/lb-mole

a' - mole fraction of carbon dioxide in dry exhaust

b' - mole fraction of carbon monoxide in dry exhaust

d' - mole fraction of total hydrocarbons including total aldehydes (expressed as CH_4) in dry exhaust. Use d" in Equation (1)

R - hydrogen/carbon ratio of atoms in fuel

The volume concentrations so determined and the dry analysis carbon dioxide, carbon monoxide, and nitrogen oxide data will then be corrected to fraction by volume of wet exhaust gas from combustion with dry air by the following procedure:

$$S = S' \ (1 - \omega) \qquad (2)$$

where

S - volumetric concentration of pollutant species in wet exhaust gas containing only the water vapor formed by the combustion process

An emission index expressed as pounds of pollutant per thousand pounds of fuel consumed (equivalent to an index expressed as mg/gm fuel consumed) will then be calculated according to the following equation:

$$EI_S = \frac{(1 + f) \ S \ M_S}{f \ M_e} \times 10^N$$

where terms not previously defined are:

N = 3 if S is fractional
N = -3 if S is in parts/millions

EI_S - emission index, lb pollutant species S per 1000 lb of fuel consumed

f - fuel-air weight ratio determined from measured fuel and air-flow rates at the specified test condition, lb fuel/lb dry air

M_S - molecular weight of pollutant species S, lb/lb-mole

= 86.17 for C_6H_{14}
= 44.01 for CO_2
= 28.01 for CO
= 16.04 for CH_4
= 30.01 for NO
= 46.01 for NO_2

Total oxides of nitrogen on an emission index basis will be computed as NO_2 to comply with the 1976 Federal Standards.

The expression for the fuel-air ratio, as shown below, will be used to cross-check the measured values:

$$f = \frac{M_C + RM_H}{M_A} \cdot \frac{a' + b' + d'}{1 + \frac{aR}{4} + \frac{b}{2}\left(\frac{R}{2} - 1\right) + d\left(\frac{R}{4} - 2\right)} \qquad (4)$$

where terms not previously defined are:

M_A - molecular weight of air = 28.9 lb/lb-mole

M_C - atomic weight of carbon = 12.01 lb/lb-atom

M_H - atomic weight of hydrogen = 1.008 lb/lb-atom

Pollutant emission rates were also calculated to allow computerized integration over specific driving cycles to obtain an emissions index in terms of pollutant weight per vehicle mile. The emission rates were calculated by the following expression:

$$F_S = EI_S \times W_f \qquad (5)$$

where

F_S - emission rate of pollutant species S, lb/hr

W_f - measured test condition fuel flow rate, lb/hr

The vehicle mass emission rate as a function of the driving cycle was then computed from:

$$P_S = 2.205 \times 10^{-3} \frac{F_S}{V} \quad (6)$$

where

P_S - vehicle mass emission rate, gm of pollutant species S per vehicle mile

V - vehicle speed, mile/hr

4.3 Humidity Corrections to Emissions Results

It is known that moisture in the air at combustion inlet can have an significant effect on the emissions from a combustor. NO_X emissions are particularly affected. However, quantitative corrections for these effects have not been established. Therefore, other than the small volumetric corrections discussed in Section 4.2, Gaseous Emissions Data Reduction, no attempt has been made to correct the emission test results to any other combustor inlet condition than the dry air condition under which it was tested (0.0006 lb water vapor/lb dry air).

5. COMBUSTOR DEVELOPMENT AND EVALUATION

The experiment program has been divided into four test periods for purposes of discussion of the test results. This division combines groups of tests generally having common available test facilities and program direction.

The first two test periods, May 12, 1971 through December 10, 1971 and December 11, 1971 through January 31, 1972, cover the preliminary testing conducted prior to the contract hold period. The third test period, February 1, 1972 through August 10, 1972 covers work conducted by AiResearch during the contract hold period and up until a heater failure occurred. The fourth test period covers the final calibration test series conducted after the heater facility repair.

5.1 Test Period (5-12-71 to 12-10-71)

Preliminary tests were conducted on an atmospheric test rig on four combustor configurations to compare combustion efficiency at high loading with predicted levels. Atmospheric air was drawn through the rig by the application of a vacuum to the combustor discharge. The first test was conducted on a modified film-vaporizing combustor that was initially designed for a high-velocity, high-heating-value-per-unit volume fuel (Shelldyne-H) under a contract with the Air Force Systems Command. The combustor was modified by the addition of a conical surface on the baseplate with the apex of the cone located at the plane of discharge of the primary pipe. The second configuration was a baseline, unmodified configuration.

The combustors were tested at the Class A design point corrected flow conditions to ensure a reasonable pressure drop during operation. The pressure drop would have been too low at the Class B flow conditions since the effective open area of the test combustors were approximately three times that of the Class B design and two-thirds that of

the Class A. Purpose of the test was to compare lean stability and combustion efficiency of the film-vaporizer combustor with and without the cone. The test results showed that performance of the combustor with the cone was superior in both respects and also had a shorter ignition delay. Specifically, lean limit blowout fuel-air ratio decreased from 0.0045 to 0.003 and combustion efficiency increased from 74 to 82 percent at the Class A design-point corrected flow conditions.

Emissions data were taken solely for the purpose of calculating combustion efficiency since the rig had insufficient instrumentation for a thermodynamic efficiency determination based on the measured temperature rig. The emission level was obtained by averaging the value measured by a single-point probe as it traversed across the combustor exit plane. The efficiency was then calculated from an enthalpy balance using the actual measured combustion products.

The ideal enthalpy change per pound of fuel consumed is equal to the heat of reaction or fuel lower heating value. The actual enthalpy change is the lower heating value of the fuel minus the heating value of each non-ideal combustion product formed. The efficiency is then:

$$\eta = \frac{(LHV)_F - \Sigma W_P \, (HV)_P}{(LHV)_F} \times 100$$

where:

η = combustion efficiency, percent

$(LHV)_F$ = fuel lower heat value, Btu/lb

W_P = weight concentration of non-ideal combustion product, lb/lb fuel

$(HV)_P$ = heating value of non-ideal combustion product, Btu/lb

= 18,500 Btu/lb for JP-4

= 4345.2 Btu/lb for carbon monoxide

= 18,646 Btu/lb for $CH_{1.85}$ per Federal test requirements

The effect of oxides of nitrogen is negligible. Therefore:

$$\eta = \frac{18{,}500 - 4345.2\ W_{CO} - 18{,}646\ W_{HC}}{18{,}500} \times 100$$

$$= 100 - 23.48\ W_{CO} - 100.8\ W_{HC}$$

or on an emission index (EI) basis in terms of pounds pollutant per thousand pounds of fuel burned,

$$\eta = 100 - 0.02348\ EI_{CO} - 0.1008\ EI_{HC}$$

The emission index was calculated from the measured data using the method detailed in Section 4.2 of this report.

Figure 5-1 shows the efficiency levels of the two test combustors as a function of aerodynamic loading parameter superimposed on the published efficiency map that was generated during the development program. An increase in efficiency at both of the test conditions established was observed for the conical-domed configuration. In addition, the efficiency values were consistent with the earlier data.

Both the cone-domed and flat-domed versions of the Class B combustor (SKP26312) were also tested on the vacuum rig. Figure 5-2 shows the efficiency of the combustors compared with both the predicted

P = INLET PRESSURE, ATMOSPHERES
T = INLET TEMPERATURE, °F
V = VOLUME PER CUBIC FOOT
W = AIRFLOW, POUNDS PER SECOND
FUEL-TO-AIR RATIO = 0.020

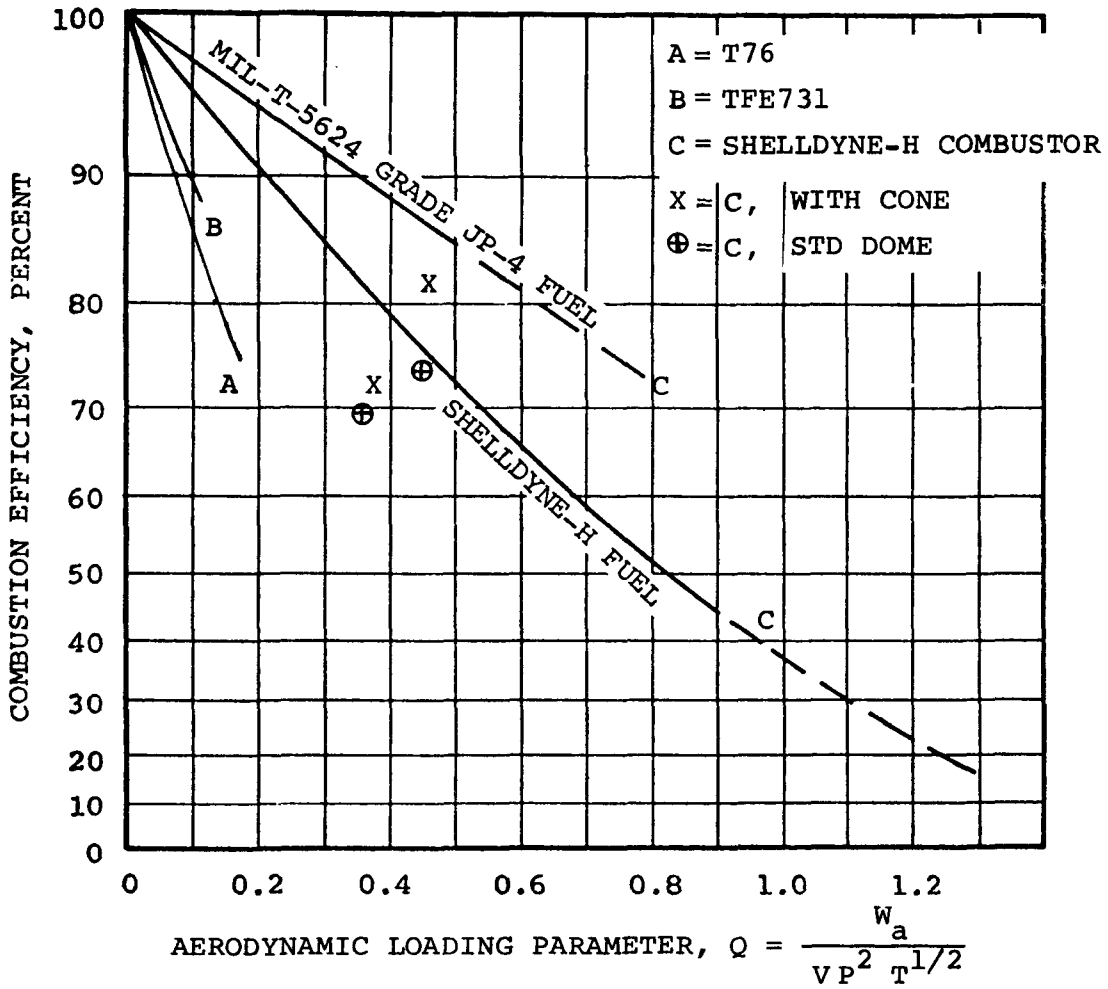

PERFORMANCE COMPARISON

COMBUSTOR EFFICIENCY COMPARISON

FIGURE 5-1

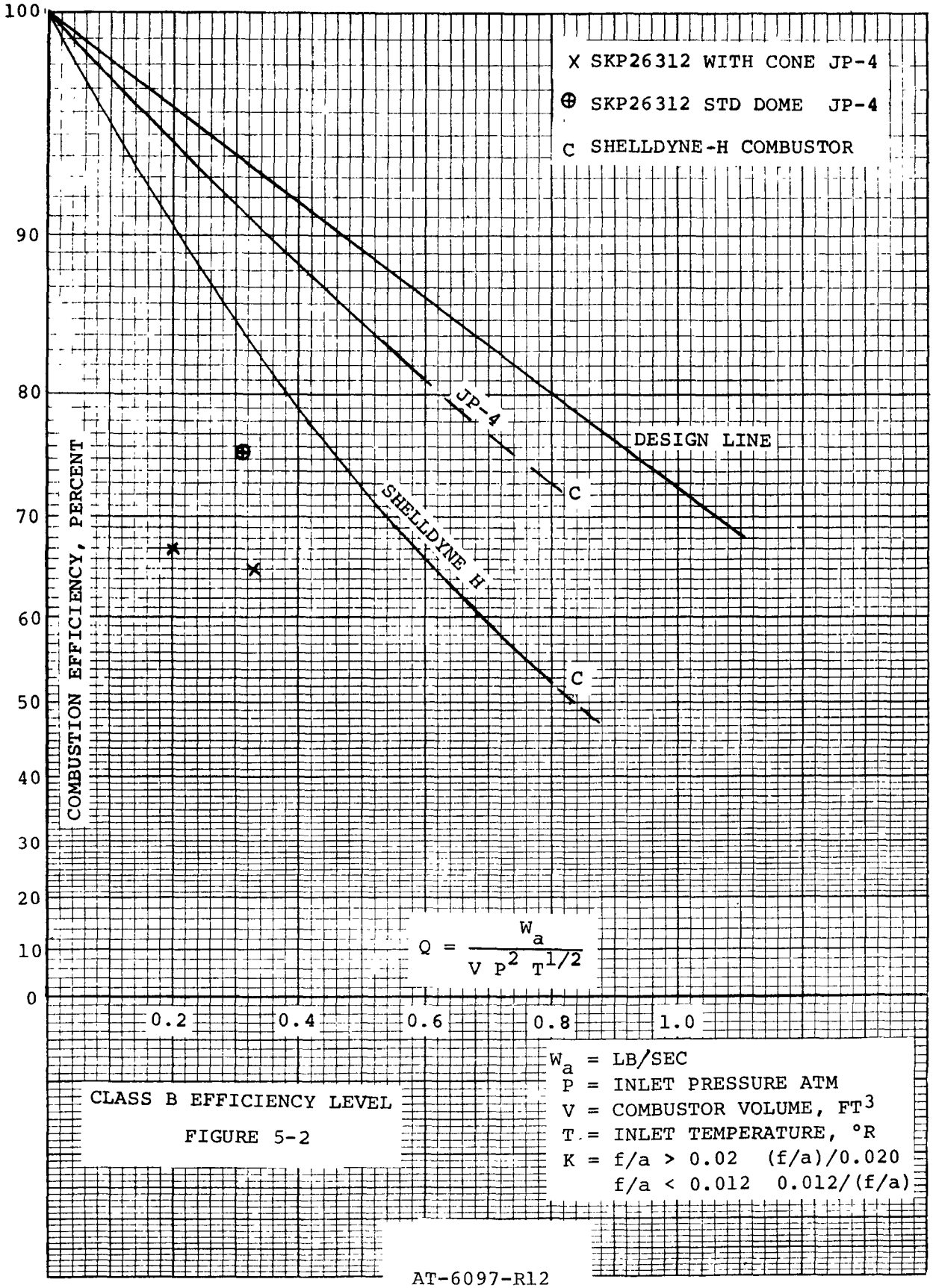

CLASS B EFFICIENCY LEVEL

FIGURE 5-2

values and the curve from Figure 5-1. The data indicates that development effort is required to improve the efficiency to the to the desired level, but that the efficiency is not significantly worse than the more highly developed Shelldyne configuration. The data did indicate, however, that the flat-domed configuration was slightly more efficient, but the low overall efficiency levels, in general, are attributed to fuel maldistribution within the primary zone that was observed during the testing.

Following the completion of this series of tests, the high-pressure test rig was completed and installed at the combustion laboratory. High-pressure combustion rig testing was therefore started (November 17, 1971) on the Class B film vaporizing combustor, P/N SKP26312. The test results are shown in Figure 5-3. Note in Figure 5-3 that the effect of pressure is the reverse of what would be expected from simple kinetic theory. Figure 5-4 shows a typical chart recording of emission readings.

These results are converted to grams/mile for the simulated Federal Driving Cycle which reflects the variable geometry, free power turbine engine performance as follows:

(a) Figure 5-5 gives data on the Class B engine assembled in accordance with contract specified items and to provide 150 hp.

(b) Figure 5-6 summarizes data extracted from the optimization study (68-04-0012) and provides the basis for selecting 5.5, 9.5, 18, and 27 hp conditions to represent the Class B engine over the Federal Driving Cycle.

(c) Table 5-1 tabulates the Class B test points and gives the constants used to convert the emission index (EI) from combustor test results to grams/mile for the Federal Driving Cycle.

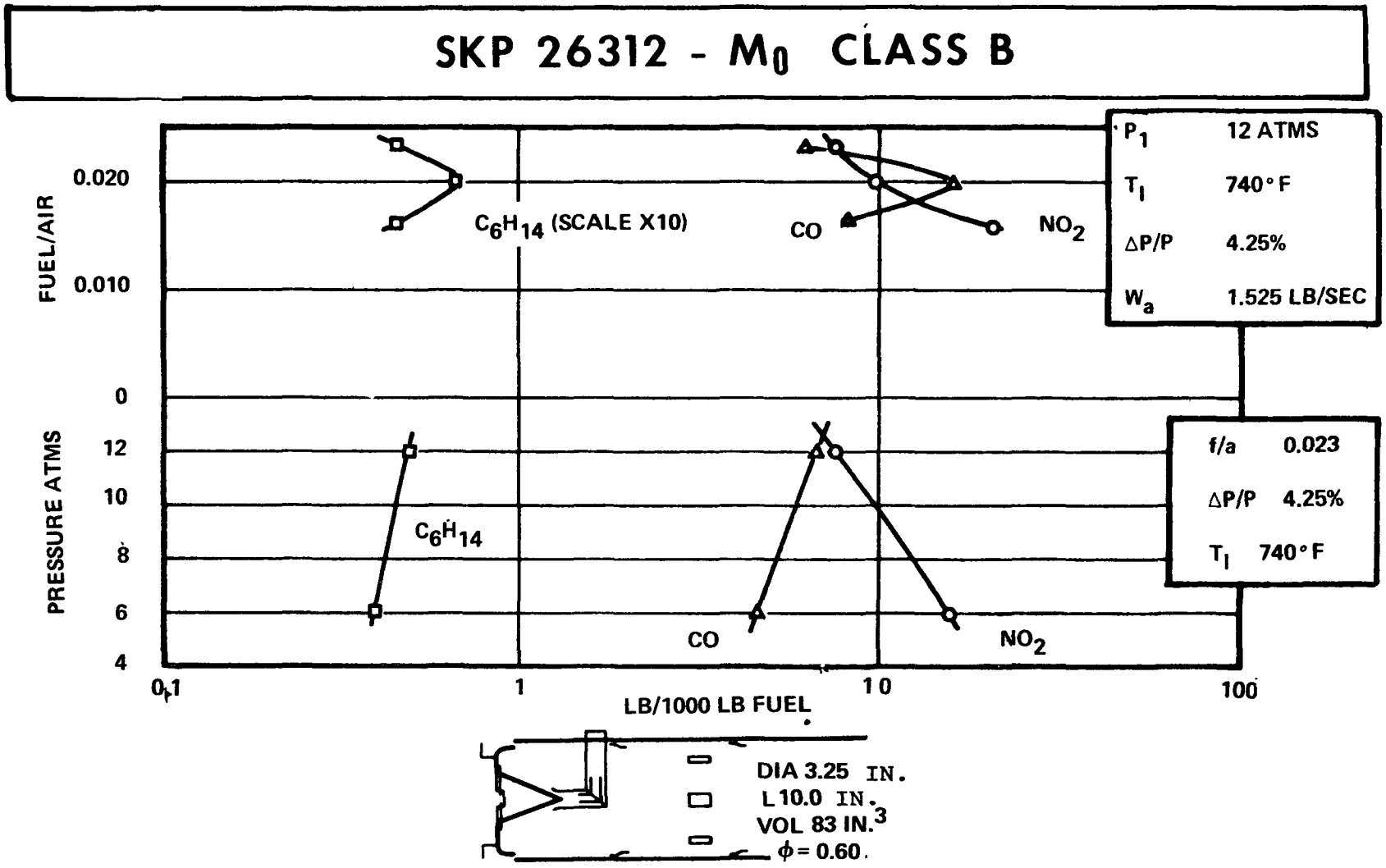
SKP 26312 - M_0 CLASS B
FUEL/AIR
0.020
0.010
0
PRESSURE ATMS
12
10
8
6
4
0.1
1
10
100
LB/1000 LB FUEL
C_6H_{14} (SCALE X10)
CO
NO_2
C_6H_{14}
CO
NO_2
P_1 12 ATMS
T_1 740° F
ΔP/P 4.25%
W_a 1.525 LB/SEC
f/a 0.023
ΔP/P 4.25%
T_1 740° F
DIA 3.25 IN.
L 10.0 IN.
VOL 83 IN.^{3}
ϕ = 0.60

FIGURE 5-3

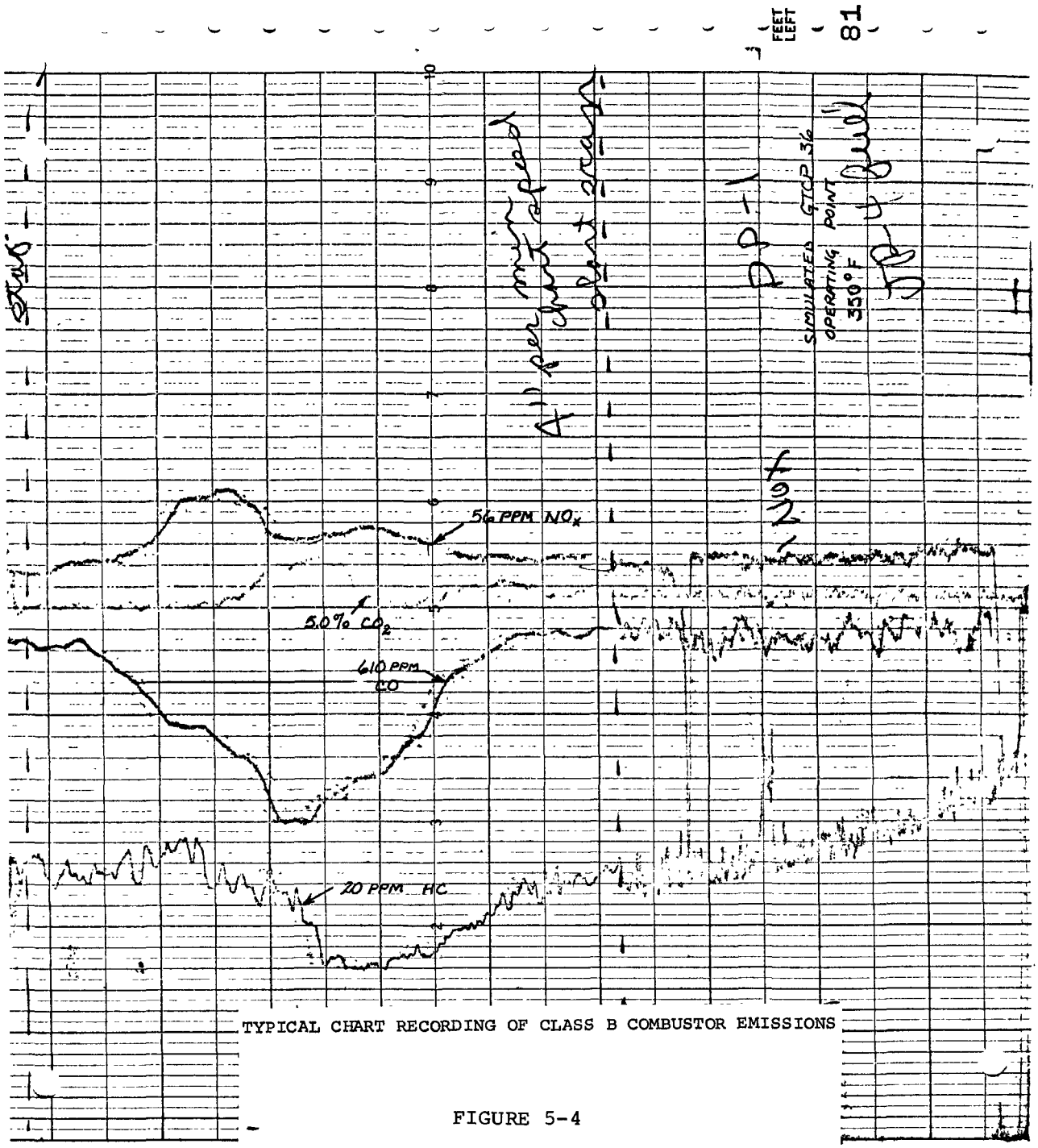

TYPICAL CHART RECORDING OF CLASS B COMBUSTOR EMISSIONS

FIGURE 5-4

AT-6097 CLASS B ENGINE CYCLE

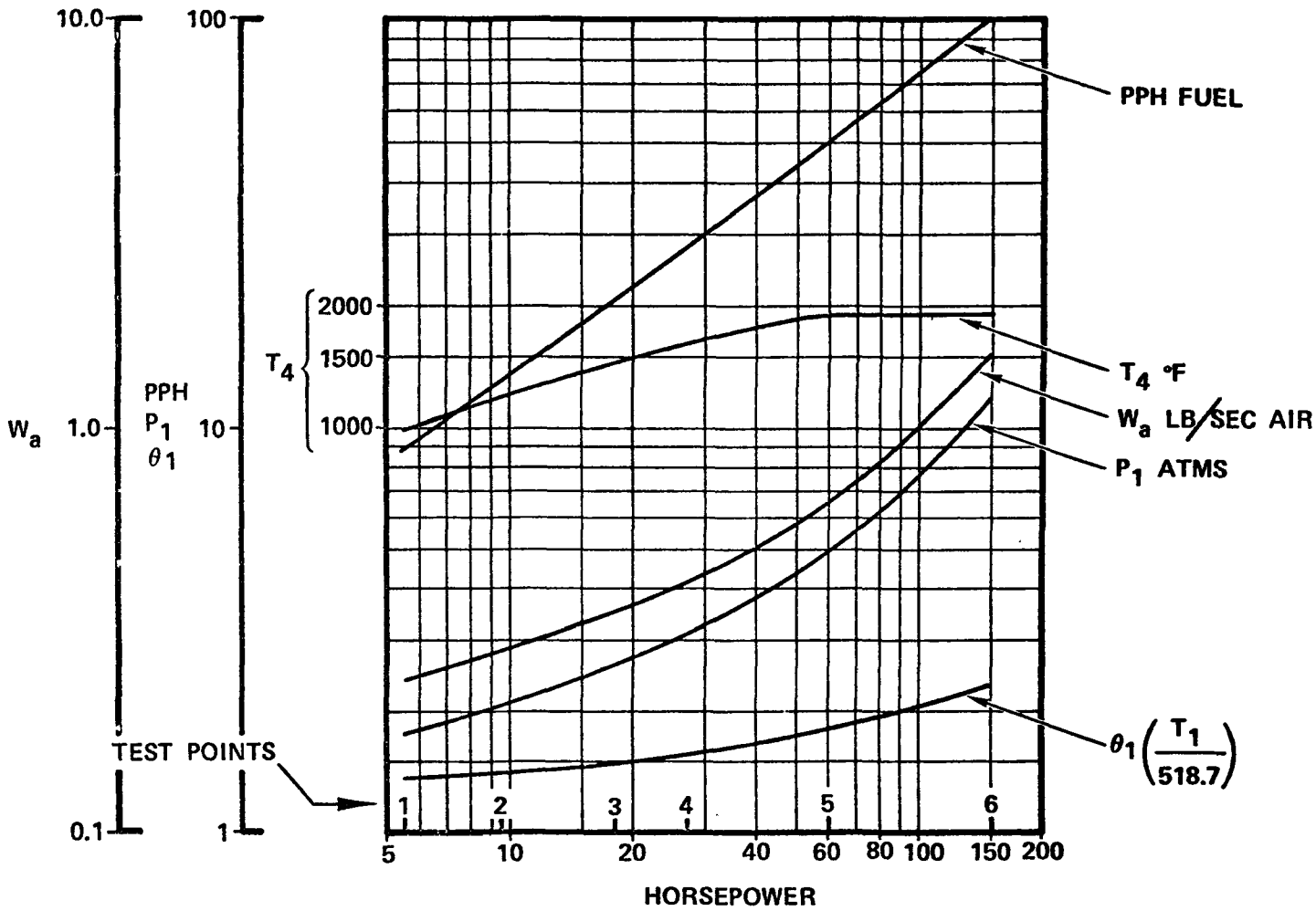

FIGURE 5-5

HORSEPOWER SPECTRUM FOR FEDERAL DRIVING CYCLE

FROM CONTRACT 68-04-0012

		TRANSIENTS	CLASS B	
		COLD START	ONE COLD START	
DISTANCE	7.435 MILES	ACCELERATIONS	5.5 HP	FUEL FLOW 9.0 TO 11.2 PPH 27 TIMES
ELAPSED TIME	22.709 MINUTES		9.5 HP	FUEL FLOW 13.2 TO 15.0 PPM 34 TIMES
AVERAGE SPEED	19.64 MPH		18 HP	FUEL FLOW 21.0 TO 26.0 PPM 8 TIMES
		DECELERATIONS	9.5 HP	FUEL FLOW 13.2 TO 10.5 PPH 33 TIMES
			18	FUEL FLOW 21.0 TO 18.0 PPH 11 TIMES
			27	FUEL FLOW 28.0 TO 26.0 PPH TIMES

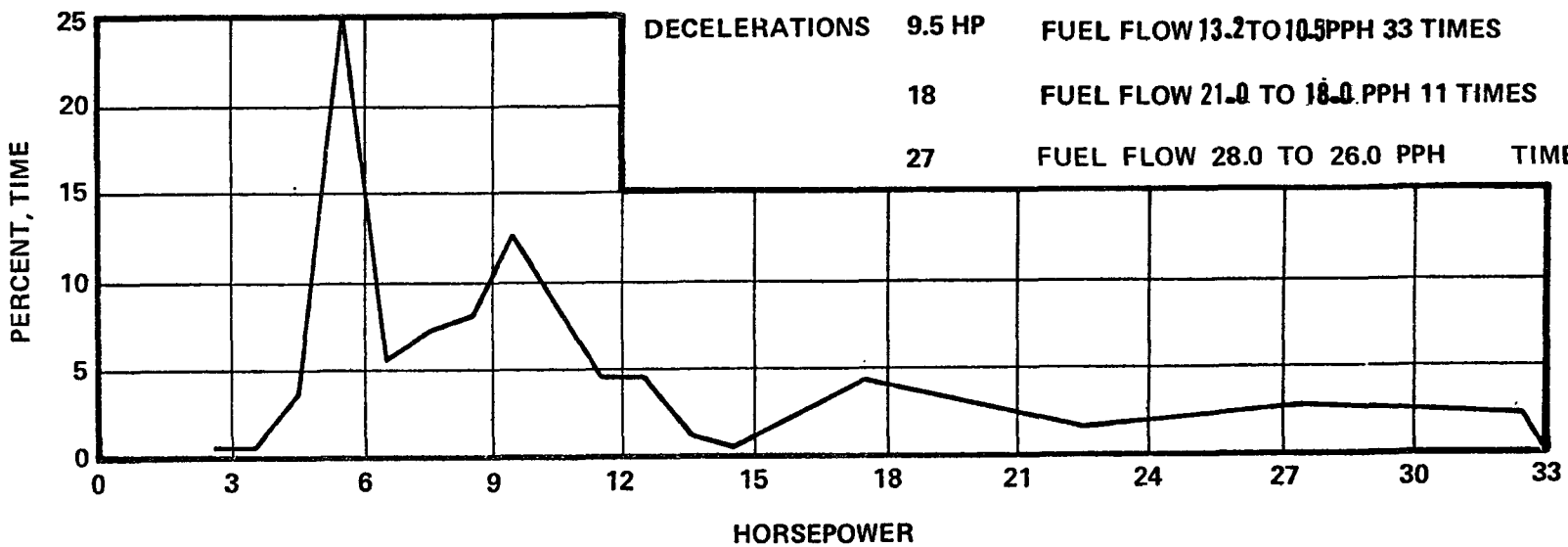

FIGURE 5-6

TABLE 5-1

TEST POINTS - CLASS B COMBUSTOR

HP	W_a, lb/sec	P_3 ATMS	T_3°R	T_4 °R	PPH	$\frac{W}{P^2 T^{1/2}} = Q \times Vol$
5.5	0.24	1.75	715	1460	9.0	0.002931 - Sets Combustor Volume
9.5	0.28	2.08	733	1660	13.2	0.002390
18	0.352	2.62	777	1910	21	0.001840
27	0.42	3.10	820	2070	28	0.001526
60	0.66	5.00	938	2360	51	0.000862
150	1.55	12.00	1218	2360	105	0.000308

Emissions grams/mile = $EI_{5.5} \times 0.0738 + EI_{9.5} \times 0.1232 + EI_{18} \times 0.0775 + EI_{27} \times 0.0524$

FOR FEDERAL DRIVING CYCLE
VEHICLE DATA FROM CONTRACT 68-04-0012
AND THE ABOVE ENGINE DATA

Note that the constants were derived as follows: At 5.5 hp, time is 8.06 min out of a total of 22.709 min and 7.435 miles for the FDC. With a flow of 9.0 pph, 1.209 lb of fuel (JP-4) is burned. Then,

$$EI_{5.5} \text{ (lb/1000 lb)} \times \frac{1.209}{1000} \times \frac{453.6}{7.435} = 0.0738 \times EI_{5.5}$$

is the grams/mile contribution of the emission for the 5.5 hp segment of the Federal Driving Cycle.

This procedure, using trend data from the Class A combustor allows the data of Figure 5-3 to be converted to 5.0 grams/mile of NO_2. The CO and HC values were not converted because of the possible unreliability of a value obtained from trend data of another combustor. However, the values are believed to be below the 1976 Federal Standards for carbon monoxide and hydrocarbons.

Finally, the TSF, $\left(\frac{T_{max} - T_2}{T_2 - T_1} \right)$, was not measured in these tests.

The collection of data for the Class B combustor was terminated because of damage to the combustor. Figure 5-7 shows a hole burned in the downstream end of the combustor. In addition, a crack developed in the exit elbow of the rig.

After repairing the rig, testing was resumed using the Class A combustor. Use of only the Class A combustor for further testing was justified for the following reasons:

(a) The Class A engine is preferred as a result of the automobile engine optimization study (EPA Contract No. 68-04-0012).

(b) It is generally more difficult to meet the 1976 Federal NO_X Standard with the Class A combustor, because of the higher combustor inlet temperature of a regenerated engine.

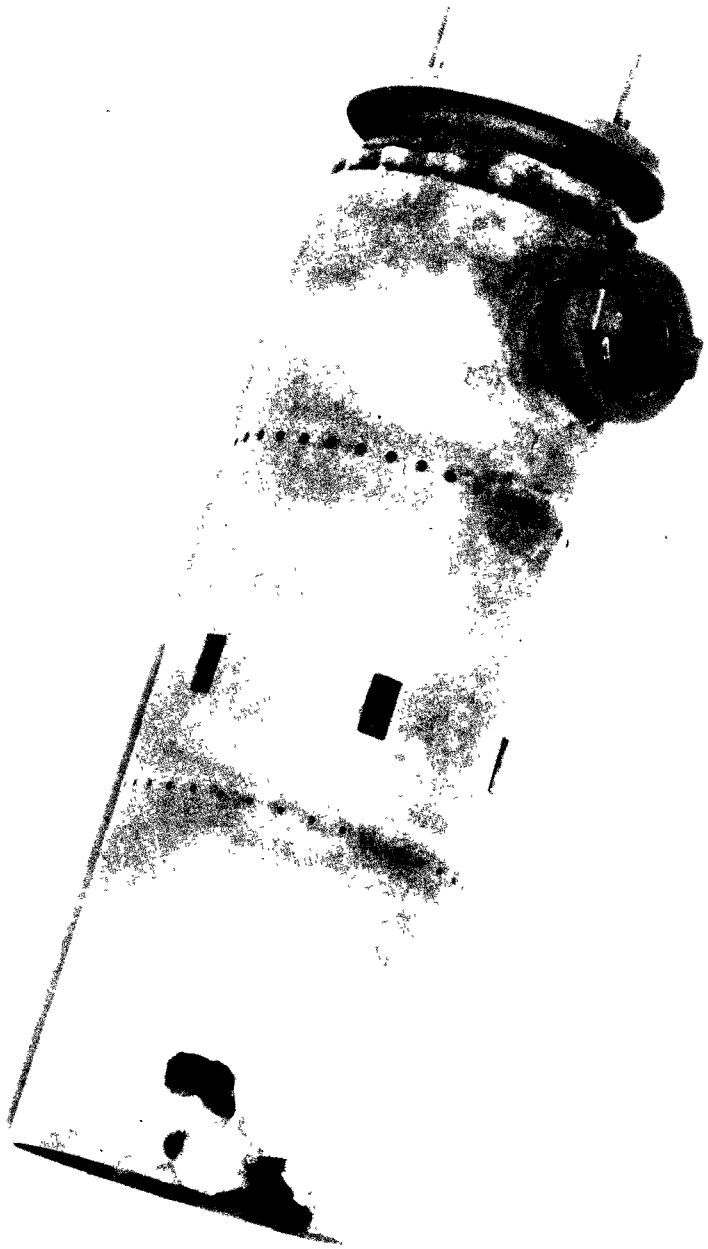

CLASS B COMBUSTION CHAMBER, P/N SKP26312 SHOWING DISCHARGE LIP BURN-OUT

FIGURE 5-7

5.2 Test Period (12-11-71 to 1-31-72)

5.2.1 Emissions Performance

Thirteen Class A combustor tests were conducted during this test period, including various modifications of the following basic combustor configurations:

(a) SKP26259 Vaporizer (7)

(b) PAP218770 Premix (2)

(c) SKP26489 Vaporizer (3)

(d) SKP26489 Pneumatic Impact (1)

Test results are presented graphically and discussed in the following paragraphs. Test data were converted to a grams per mile basis using the AiResearch 4-point test procedure (January 1972) defined in Section 2.2 of this report.

(a) SKP26259 Vaporizer

Notable features of the baseline SKP26259 M_0 (Cone Dome) Test, Figure 5-8, were NO_2 increasing at low fuel-air ratios, and CO and C_6H_{14} decreasing at high fuel-air ratios with decreasing NO_2. A further observation was NO_2 emission index considerably below the emission index for the Class B combustor. This was attributed to the dilution ports being closer to the primary zone (on an L/D basis) in the Class A burner.

SKP26259-M_0 CLASS A

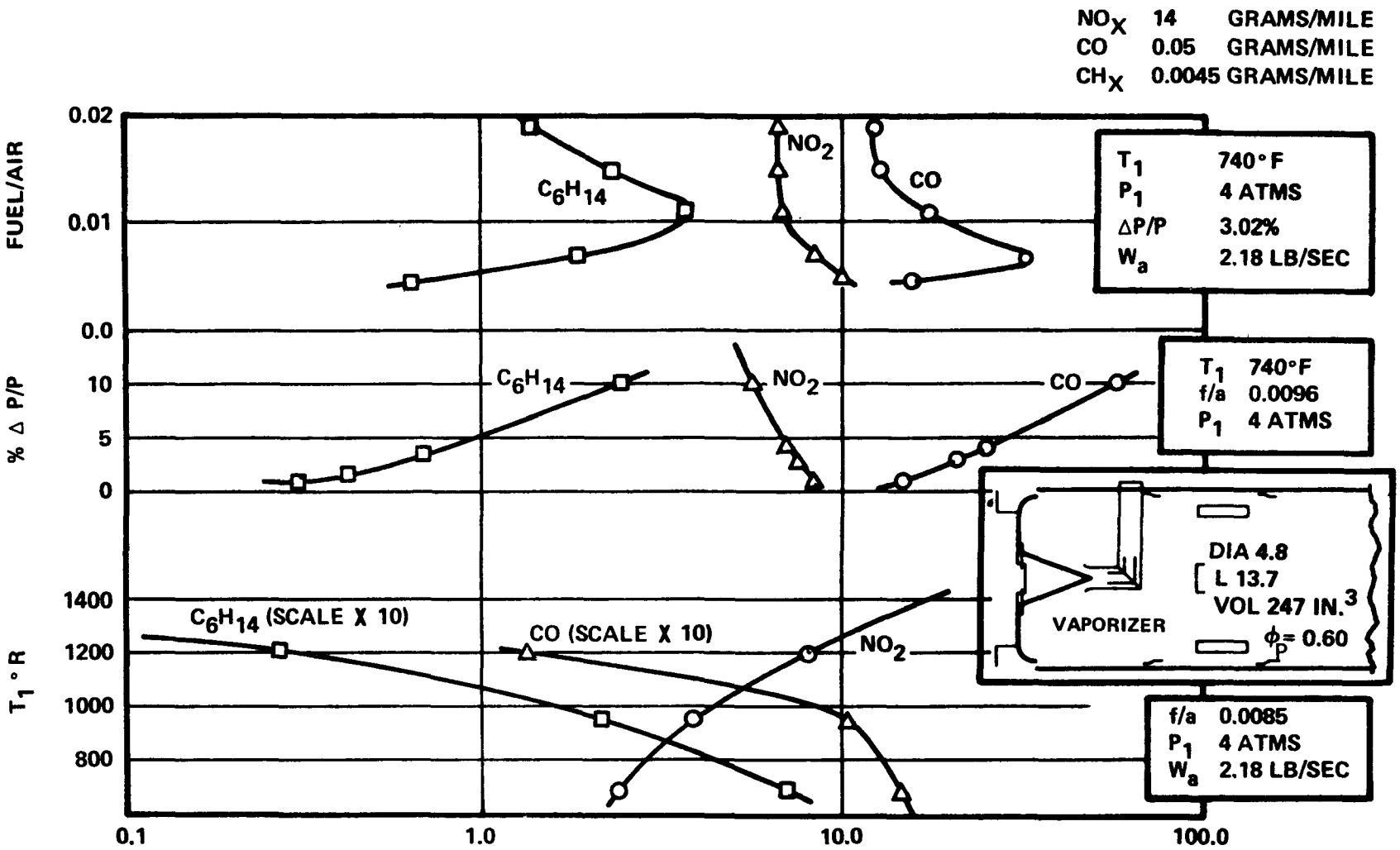

FIGURE 5-8

The first modification (M_1), Figure 5-9, was directed at running a lean primary zone, high pressure drop and low primary zone residence time. The result was no change in NO_x, which was not the expected result.

The second modification (M_2), Figure 5-10, removed the cone and moved the primary pipe closer to the base plate. This is a change in the direction of more conventional vaporizers. The result was an improvement primarily due to reshaping the NO_2 versus fuel-air ratio curve.

The third modification (M_3), Figure 5-11, moved the dilution ports closer to the primary zone following a trend noticed earlier. The result was a substantial improvement, and what was not expected was an improvement in combustion efficiency and temperature spread factor.

Modification 4, Figure 5-12, consisted of removing the primary pipe and injecting fuel and air into a plenum chamber attached to the combustor baseplate. The mixture was injected into the chamber through the radial air distributor forming the vaporizer impact plate. The intent was to improve the fuel-air mixing process to ensure a lean mixture and to try to avoid bringing the fuel and air together from opposite directions as in the L-pipe injection method, which has a tendency to establish near-stoichiometric combustion interfaces through diffusion. This modification exhibited unsatisfactory lean stability, and a subsequent modification intended to improve the stability did not result in sufficient improvement to warrant further investigation.

SKP26259-M_1 CLASS A

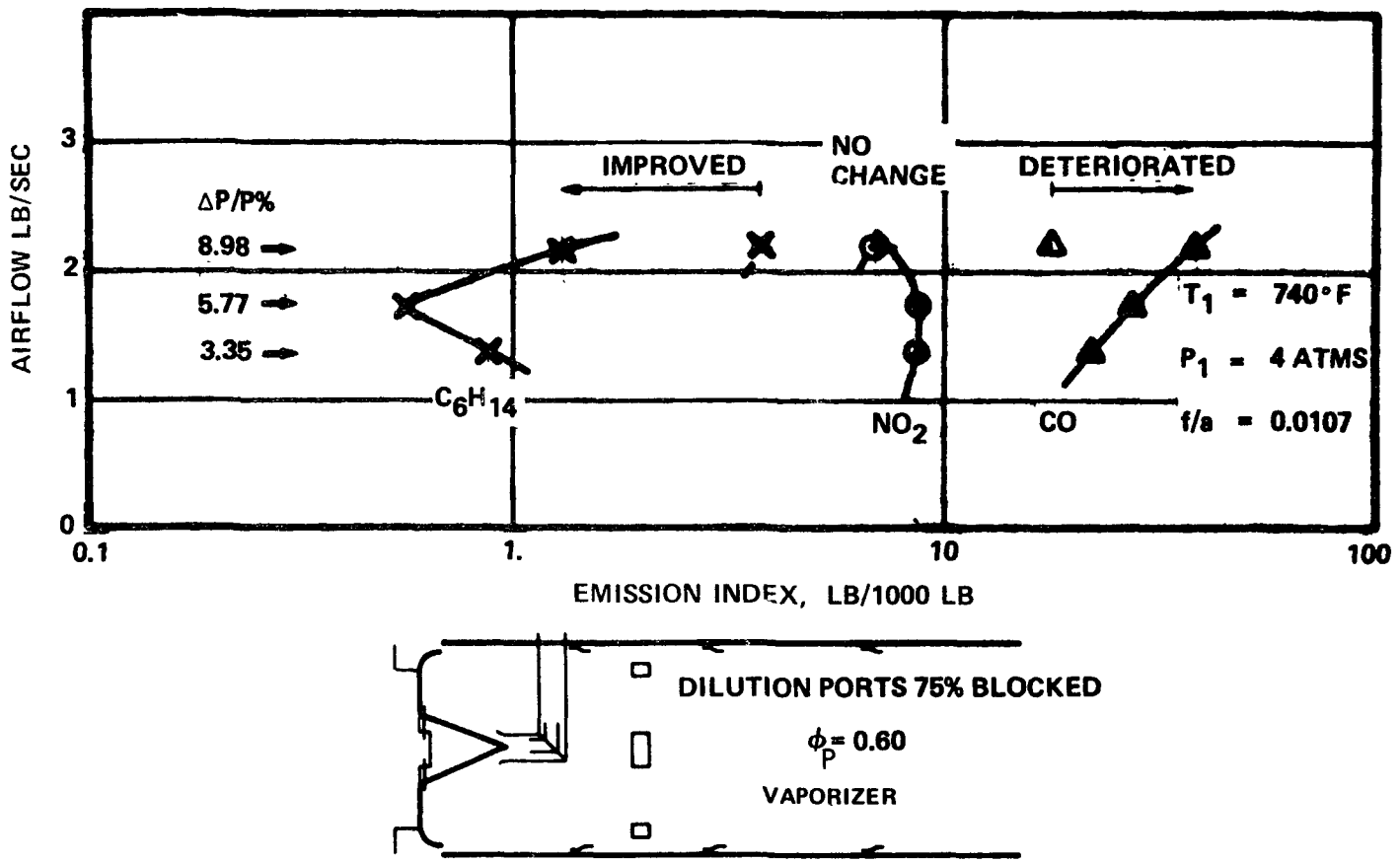

FIGURE 5-9

SKP26259-M_2 CLASS A

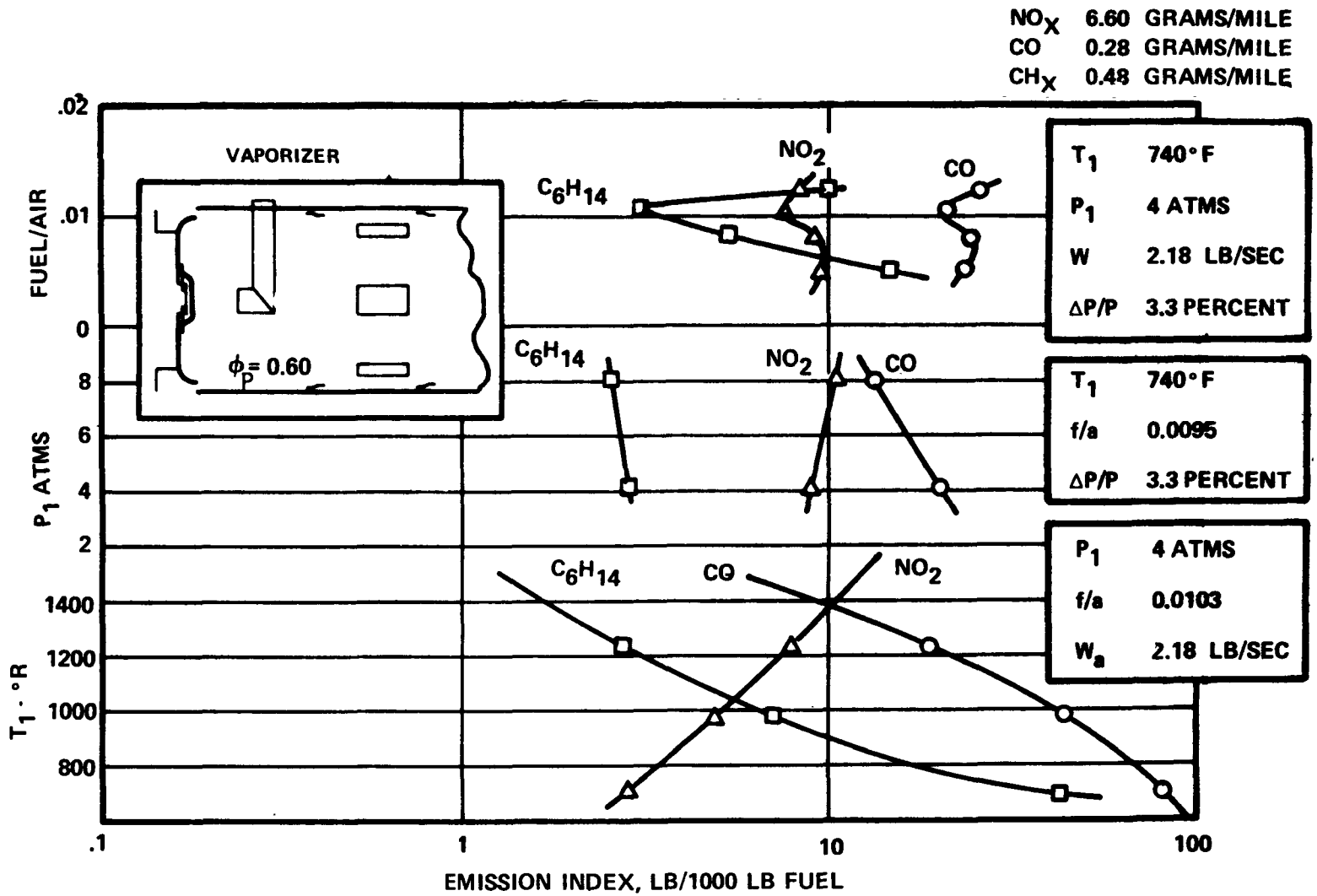

FIGURE 5-10

SKP 26259-M_3 CLASS A

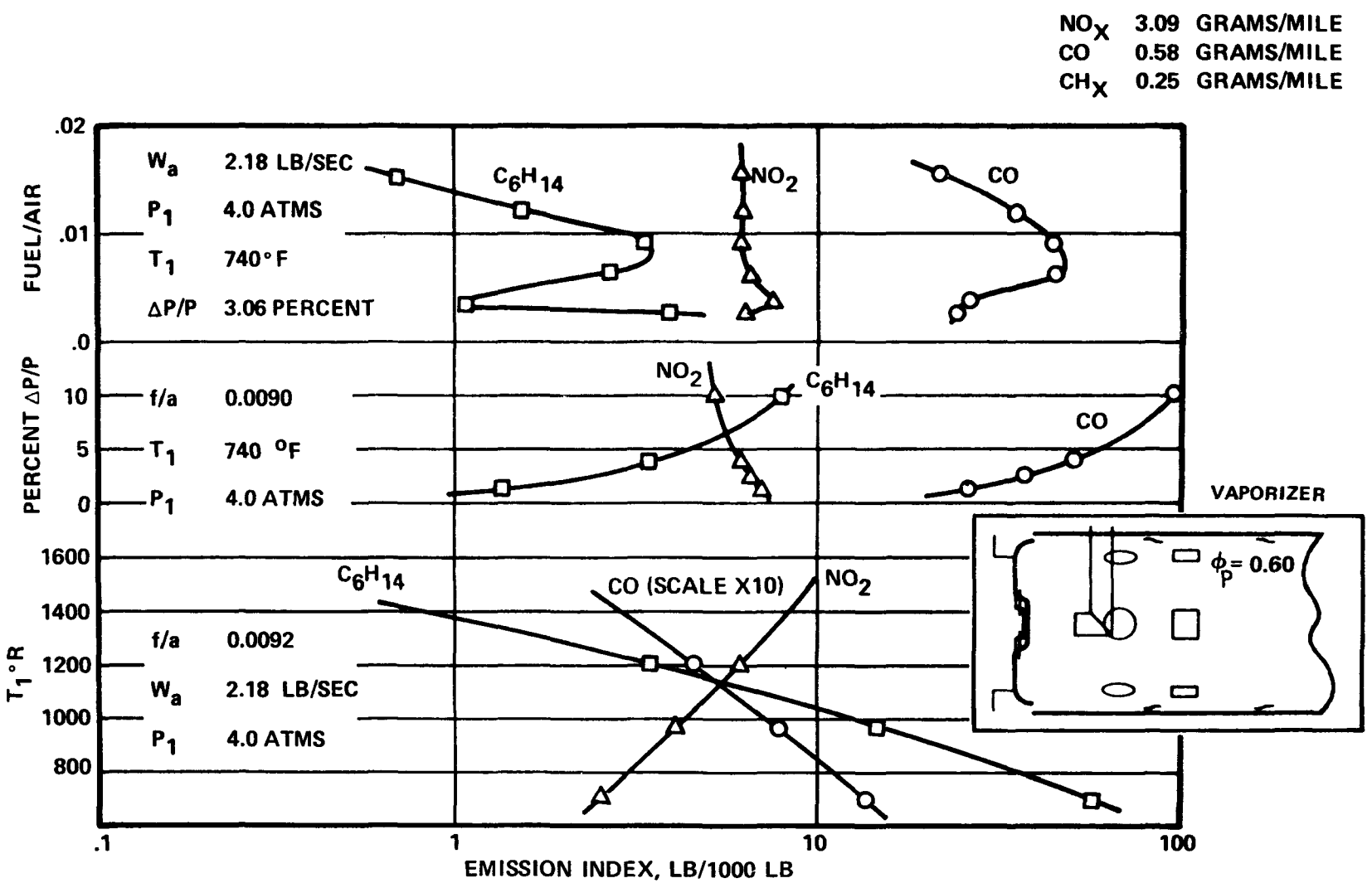

FIGURE 5-11

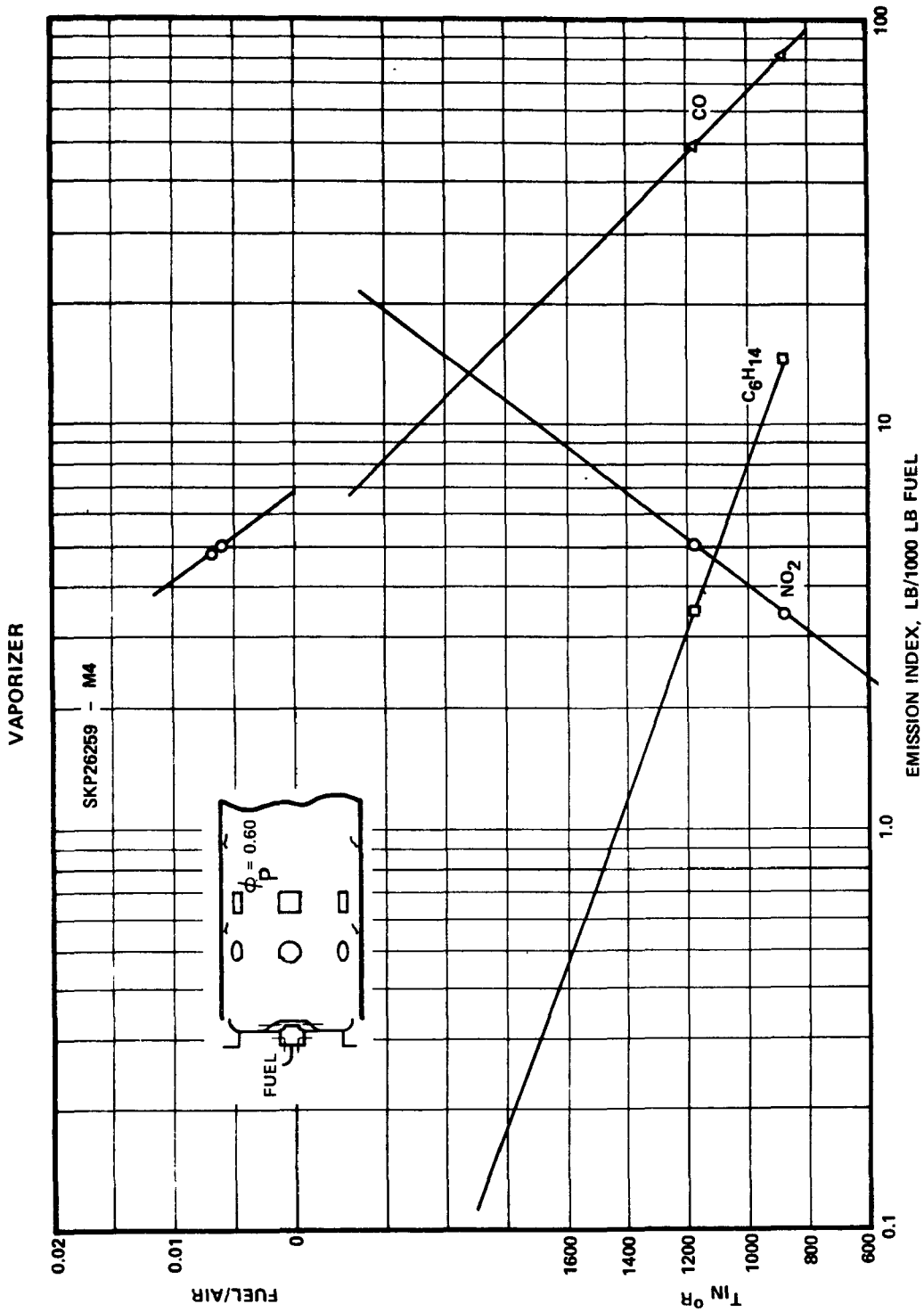
VAPORIZER
SKP26259 - M4
Φ_P = 0.60
FUEL
CO
C_6H_{14}
NO_2
EMISSION INDEX, LB/1000 LB FUEL
100
10
1.0
0.1
FUEL/AIR
0.02
0.01
0
T_{IN} °R
1600
1400
1200
1000
800
600

FIGURE 5-12

(b) PAP218770 Premix

This combustor (PAP218770) had originally been designed for natural gas operation for an in-house research program on combustion noise reduction. The first test, Figure 5-13, was conducted on natural gas as a baseline evaluation since prior testing on the vaporizer combustors had shown little effect of fuel type on NO_x emission and because the combustor had previously exhibited stability problems during operation on liquid fuel. The preliminary data was very encouraging.

A modification (intended to reduce the premix chamber fuel-air ratio) was then made to the combustor. Concurrently the combustor orifice pattern was modified to reduce the open area to that required by the Class A combustor in order to test at the correct flow conditions. Test results, Figure 5-14, showed changes in NO_x and CO emission as a function of fuel-air ratio that resulted in higher grams-per-mile values. The change is attributed to the blockage of primary ports in the combustor main chamber during the open area reduction process. Apparently the ports had been effective in both oxidizing primary-zone-generated CO and in partially freezing the NO reactions.

(c) SKP26489 Vaporizer

The SKP26489 combustor was a vaporizer design derived from a combustor developed for burning viscous fuel (Shelldyne H).

The first test on the secondary-pipe dome configuration (M_0), Figure 5-15, resulted in a burned primary pipe and severe distortion of the baseplate. Despite the failure, emissions measurements indicated that HC and CO emissions were very low (see Figure 5-15), corresponding to 92.5 percent

PAP218770 CLASS A

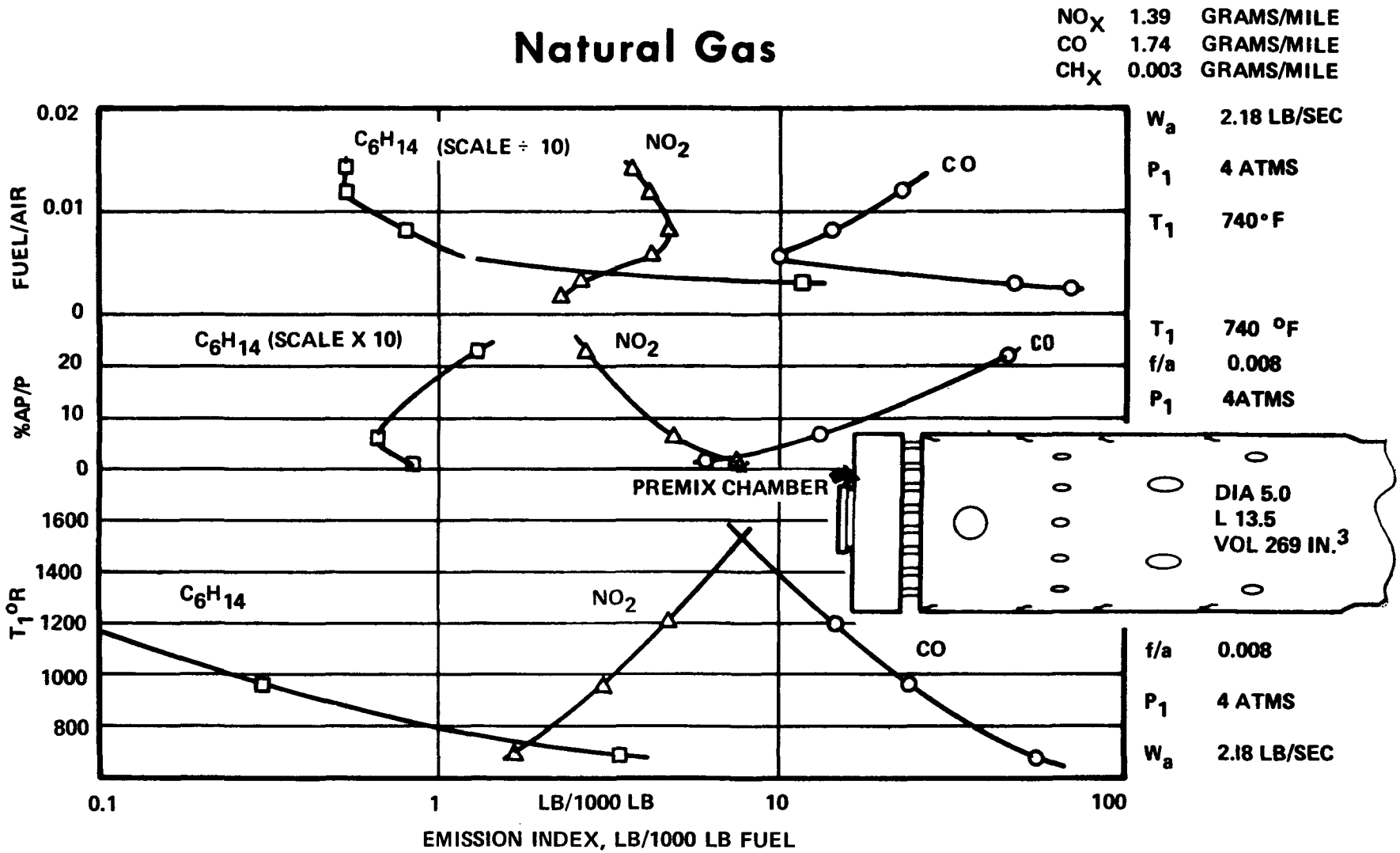

FIGURE 5-13

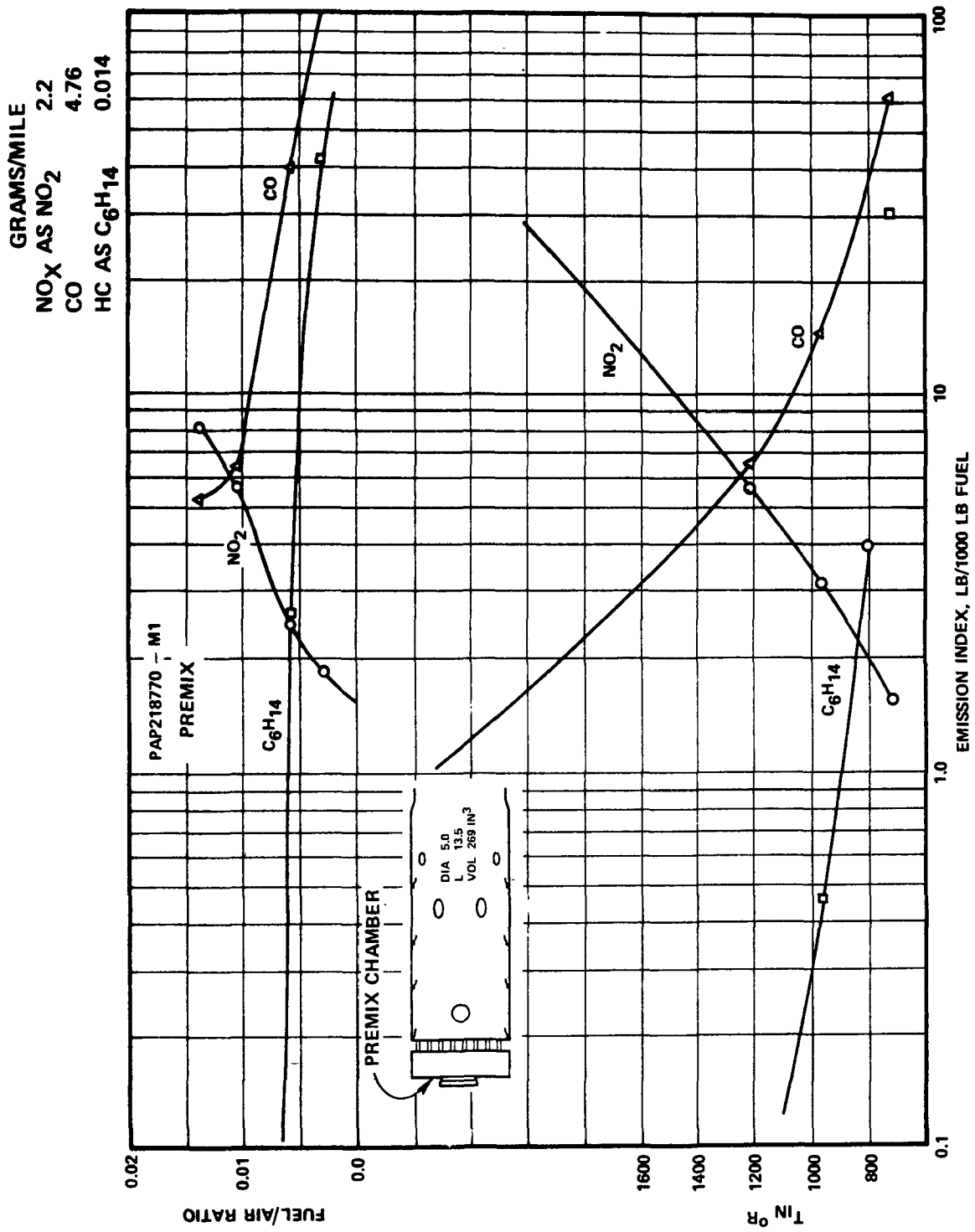
GRAMS/MILE
NO_X AS NO_2 2.2
CO 4.76
HC AS C_6H_{14} 0.014
PAP218770 – M1
PREMIX
NO_2
CO
C_6H_{14}
PREMIX CHAMBER
DIA 5.0
L 13.5
VOL 269 IN^3
FUEL/AIR RATIO
0.02
0.01
0.0
T_{IN} °R
1600
1400
1200
1000
800
EMISSION INDEX, LB/1000 LB FUEL
100
10
1.0
0.1

FIGURE 5-14

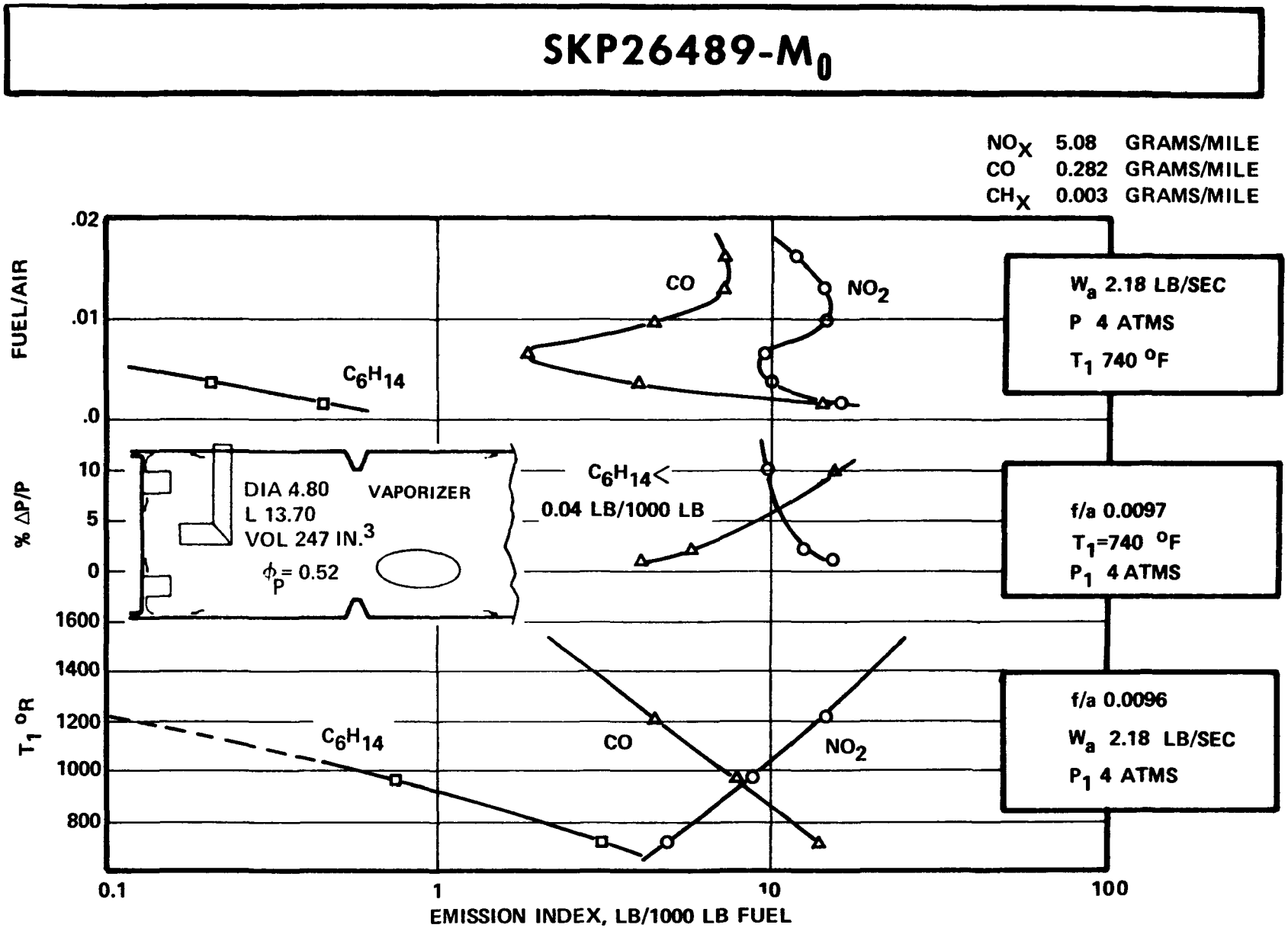
SKP26489-M0
NOX 5.08 GRAMS/MILE
CO 0.282 GRAMS/MILE
CHX 0.003 GRAMS/MILE
FUEL/AIR
.02
.01
.0
C6H14
CO
NO2
Wa 2.18 LB/SEC
P 4 ATMS
T1 740 °F
% ΔP/P
10
5
0
DIA 4.80
L 13.70
VOL 247 IN.3
VAPORIZER
ϕP = 0.52
C6H14 <
0.04 LB/1000 LB
f/a 0.0097
T1=740 °F
P1 4 ATMS
T1 °R
1600
1400
1200
1000
800
C6H14
CO
NO2
f/a 0.0096
Wa 2.18 LB/SEC
P1 4 ATMS
0.1
1
10
100
EMISSION INDEX, LB/1000 LB FUEL

FIGURE 5-15

efficiency at a loading parameter of $Q = W/Vol\ P^2\ G^{1/2} = 0.80$. Eighty percent efficiency at Q = 0.80 had been used in sizing the combustor. This indicated that a combustor of this type with only 100 $in.^3$ volume (40 percent of the existing 247 $in.^3$ volume) would still meet the HC and CO standards.

The combustor was rebuilt to the M1 configuration by adding primary pipe cooling and a strengthened baseplate. Somehow, the improved cooling with perhaps reduced airflow to the primary zone resulted in an increase in NO_x as shown in Figure 7-16.

At this time, a new high temperature air preheater (heat exchanger adapted for rig use) was installed in the lab which provided up to 1000°F combustor inlet air temperature capability as compared to 740°F. As a result, two measures were taken to take advantage of this capability.

(1) The FDC emissions simulation test procedure was changed from a multiple extrapolation involving temperature, pressure, and fuel-air ratio (AiResearch 4-point test procedure ME, - December 71) to an extrapolation on temperature only (AiResearch 4-point test procedure TE, - January 72). As is described in Section 2.2, the later test procedure involves setting the actual conditions of airflow and inlet pressure and testing at 500°F, 740°F, and 1000°F combustor inlet temperature. Once the measured emissions data taken at these points was reduced and plotted (EI versus $T_{in.}$), the emission index, EI, at the correct combustor inlet temperature corresponding to the test points selected to represent the engine cycle, was obtained by graphical extrapolation.

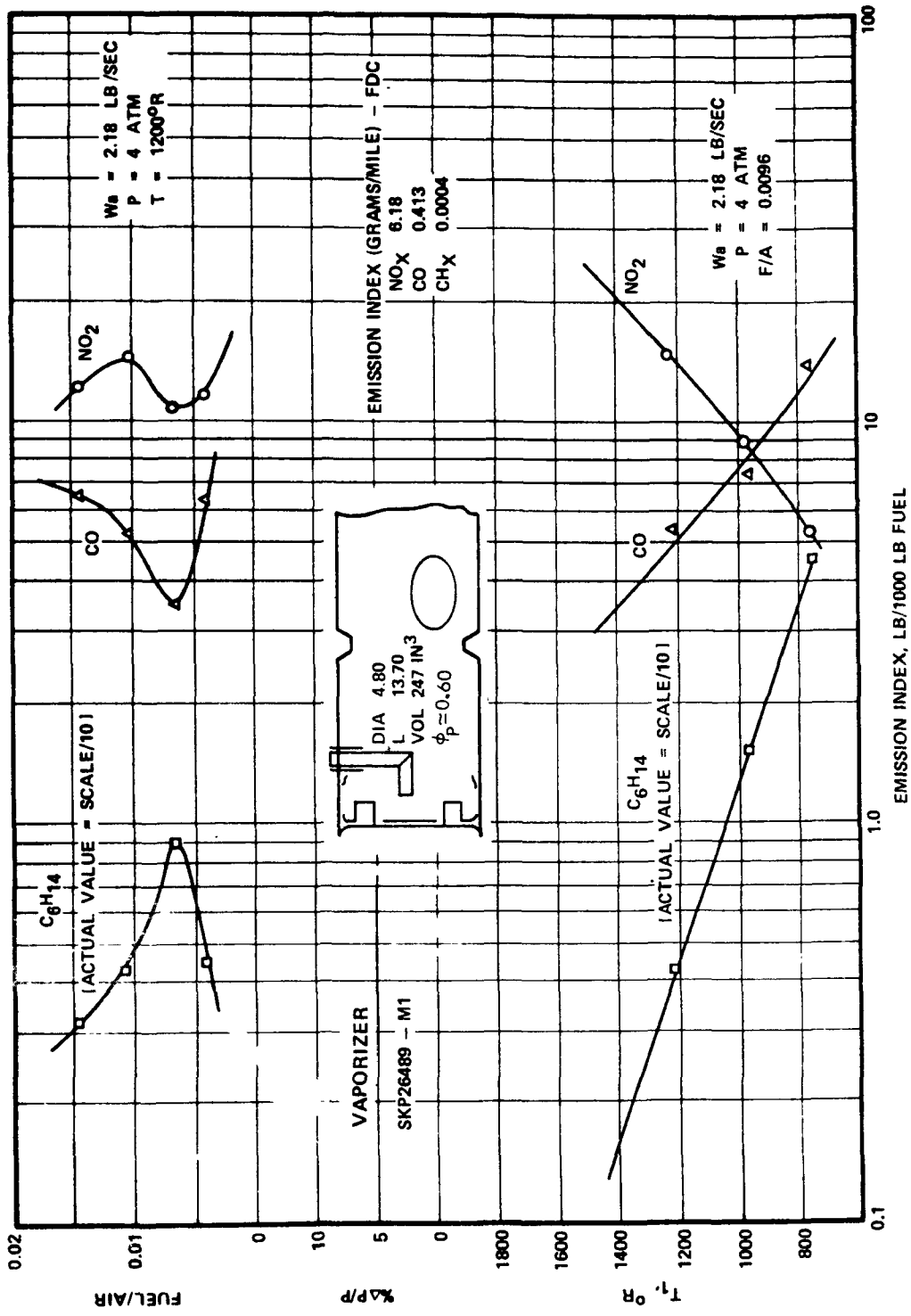
Wa = 2.18 LB/SEC
P = 4 ATM
T = 1200°R
EMISSION INDEX (GRAMS/MILE) – FDC
NOx 6.18
CO 0.413
CHx 0.0004
NO2
CO
C6H14
(ACTUAL VALUE = SCALE/10)
DIA 4.80
L 13.70
VOL 247 IN3
φp=0.60
VAPORIZER
SKP26489 – M1
Wa = 2.18 LB/SEC
P = 4 ATM
F/A = 0.0096
FUEL/AIR
%ΔP/P
T1, °R
EMISSION INDEX, LB/1000 LB FUEL
0.02
0.01
0
10
5
0
1800
1600
1400
1200
1000
800
100
10
1.0
0.1

FIGURE 5-16

(2) *For comparison, this same combustor (SKP26489-M1)* was tested using both the old and the new test procedures. Figure 5-17 presents the new procedure (TE) test results. The mass emissions levels in grams per mile were determined for each and are presented below:

SKP26489-M1	NO_x (as NO_2)	GM/mi CO	CH_x (as C_6H_{14})
Test Method 1 (ME)	6.18	0.413	0.0004
Test Method 2 (TE)	4.19	0.570	0.104

Note that the simpler and more reliable second method yields lower NO_x mass emissions and far greater unburned hydrocarbon levels. The slope variations observed in the plots of unburned hydrocarbons versus temperature illustrates that extrapolation on temperature at constant fuel-air ratio and inlet pressure, as in Test Method 1, may lead to inaccurate results. Therefore, it is imperative that all testing be conducted at the correct combustor inlet conditions, if possible. Test results obtained using the first test method (AiResearch 4-point, December 1972) should therefore be examined carefully with regard to interpretation.

(d) SKP26489 Pneumatic Impact

The test on this configuration was shortened because of fuel dribbling problems associated with the injector that resulted in high carbon monoxide and unburned hydrocarbon emissions. Emission index data as a function of fuel-air ratio are shown in Figure 5-18; the data were taken at 500°F combustor inlet temperature.

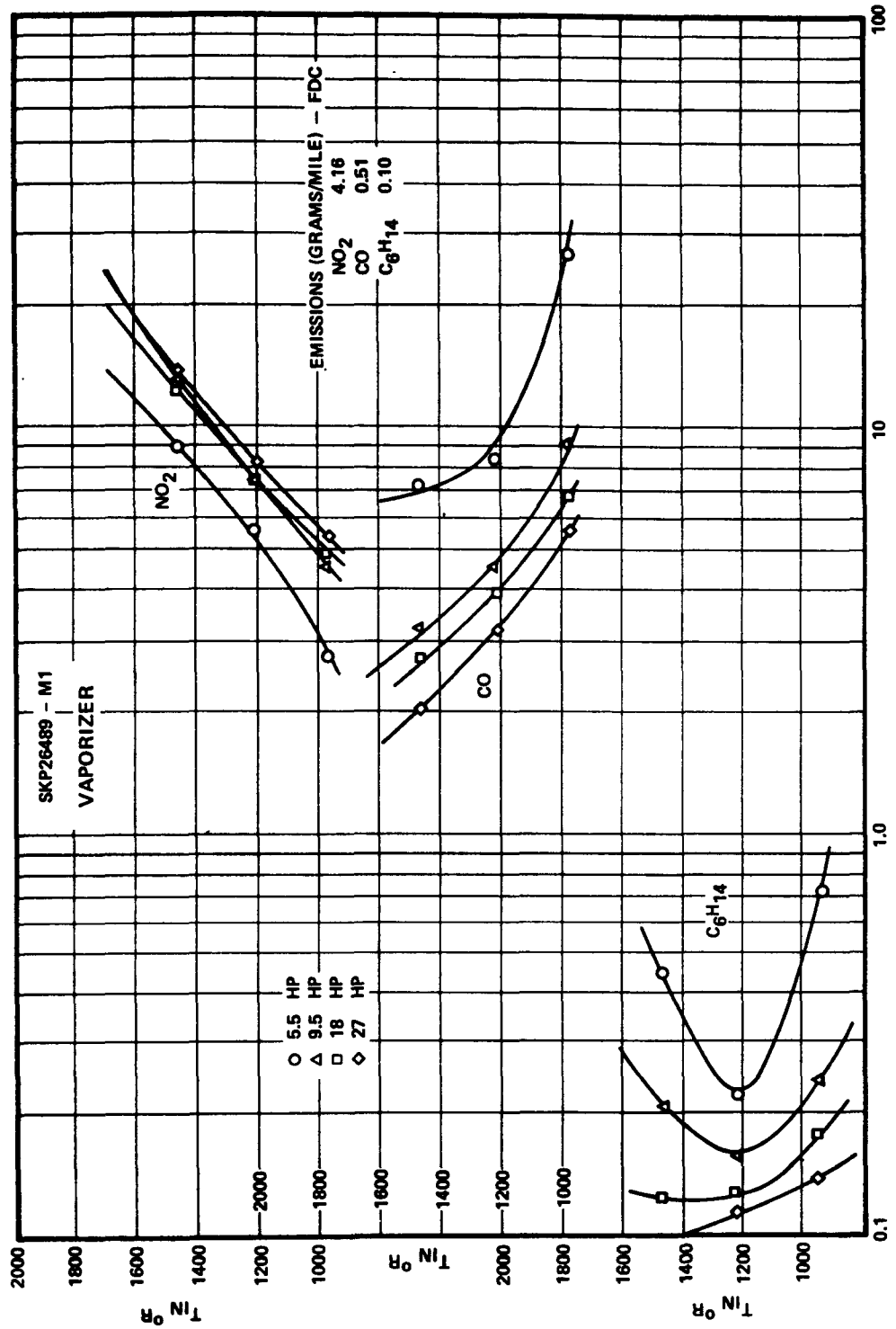
SKP26489 - M1
VAPORIZER
EMISSIONS (GRAMS/MILE) – FDC
NO2 4.16
CO 0.51
C6H14 0.10
NO2
CO
C6H14
5.5 HP
9.5 HP
18 HP
27 HP
T IN °R
EMISSION INDEX, LB/1000 LB FUEL
100
10
1.0
0.1
2000
1800
1600
1400
1200
1000

FIGURE 5-17

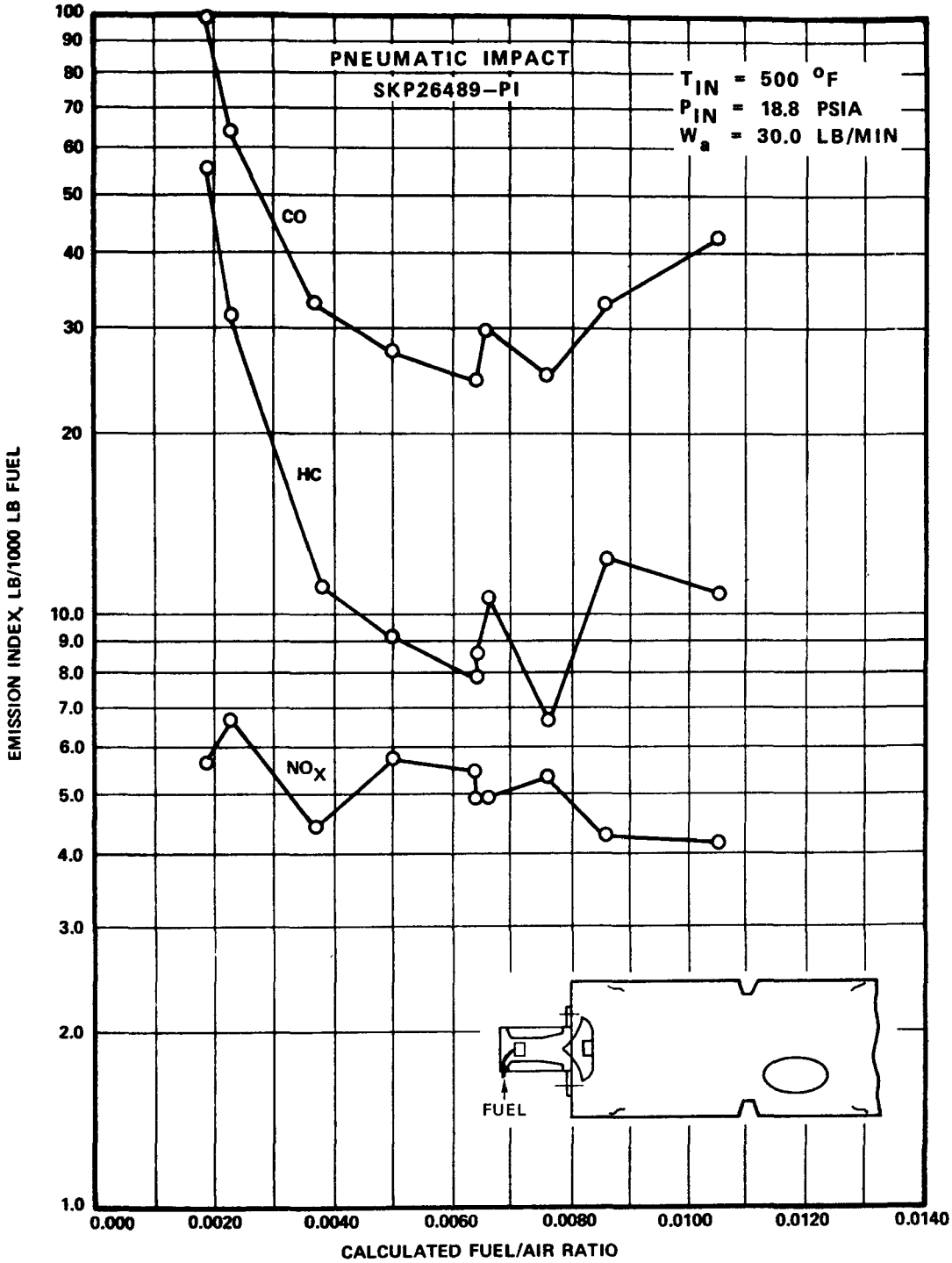
PNEUMATIC IMPACT
SKP26489–PI
T_{IN} = 500 °F
P_{IN} = 18.8 PSIA
W_a = 30.0 LB/MIN
CO
HC
NO_X
FUEL
EMISSION INDEX, LB/1000 LB FUEL
CALCULATED FUEL/AIR RATIO
100
90
80
70
60
50
40
30
20
10.0
9.0
8.0
7.0
6.0
5.0
4.0
3.0
2.0
1.0
0.000
0.0020
0.0040
0.0060
0.0080
0.0100
0.0120
0.0140

FIGURE 5-18

The injector was modified (SKP26489PIM1) to eliminate the fuel dribbling problem but was not retested until later in the test program.

5.2.2 Emission Pickup Probe Conversion

It was determined early in this test period that an unsatisfactory correlation existed between emissions profiles measured with the rotating emissions probe and temperatures measured during succeeding tests with the same combustor and the rotating probe removed. This lack of correlation was attributed to airflow distortion effects introduced by blockage resulting from the probe presence at the downstream combustor support discharge plane. For this reason a fixed probe, drawing its sample from the discharge thermocouple aspiration air, was fabricated. An average sample obtained from 8 circumferential pickup points at each of two radii resulted. The new setup allowed both conventional performance and emissions performance data to be acquired simultaneously during each test.

The new probe was checked out on a previously tested combustor to determine if the 16-point pickup represented a true average sample. Data were compared against the average emissions measured at equivalent conditions with the rotating probe. It was concluded that the new probe was satisfactory because of the higher values obtained in this manner, as evidenced by the data tabulated below:

COMPARISON OF EMISSION INDICES MEASURED
BY TRAVERSING AND FIXED PROBES

Emission Index, EI, lb/1000 lb						
Condition	NO_x		CO		HC (as C_6H_{14})	
	Rot	Fixed	Rot	Fixed	Rot	Fixed
1	2.75	2.75	77.8	78.5	32.2	37.0
2	4.47	4.67	44.2	46.5	6.5	7.3

5.2.3 Conventional Performance (Non-Emissions)

After the conversion to the fixed emissions probe was made, conventional combustor performance parameters were also checked where convenient. Among these were pressure drop, temperature spread, and lean stability.

(a) Pressure Drop

The vaporizer combustors were initailly sized for 4-percent loss of inlet total pressure at 150 hp (free-turbine engine cycle) conditions. This value converts to 3.08 percent at the reduced inlet temperature test condition. The following pressure drops were measured as compared with the 3.08-percent value:

Combustor	Measured Pressure Drop, percent
SKP26259 M0	3.02
M1	8.98 High $\Delta P/P$ mod
M2	3.30
M3	3.06
SKP26489 M0	3.60
M1	3.37
PAP218770 M1	3.22

The effect of combustor pressure drop on NO_x emission index is illustrated quantitatively in Figure 5-19 for 5 combustors. In general the L-pipe vaporizers have the same slope.

$$EI \propto \left(\frac{\Delta P}{P}\right)^{-0.176}$$

The slope of the line for the PAP218770 premix

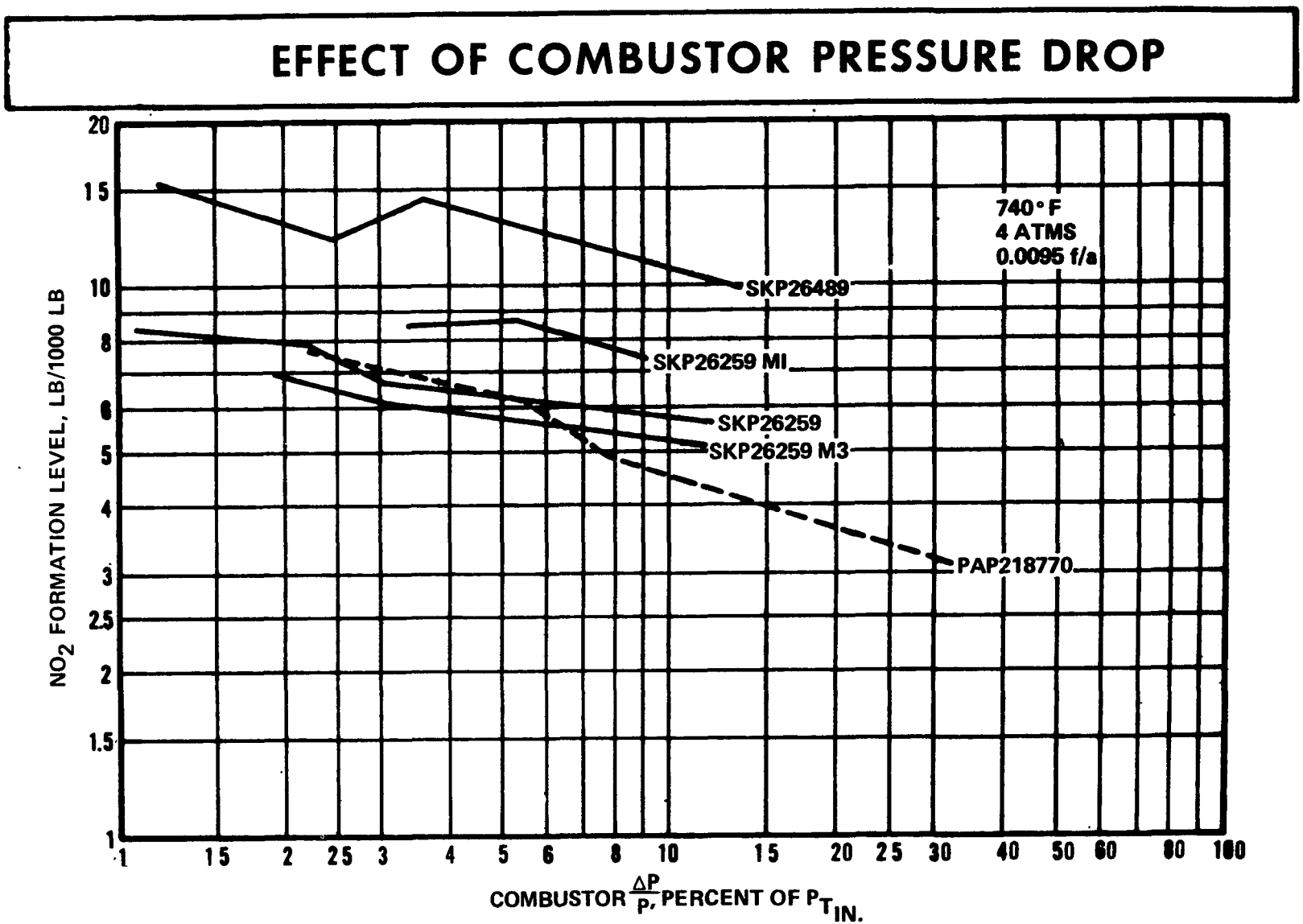
EFFECT OF COMBUSTOR PRESSURE DROP
740° F
4 ATMS
0.0095 f/a
SKP26489
SKP26259 MI
SKP26259
SKP26259 M3
PAP218770
NO2 FORMATION LEVEL, LB/1000 LB
20
15
10
8
6
5
4
3
2.5
2
1.5
1
.1
.15
.2
.25
.3
.4
.5
.6
.8
1.0
1.5
2.0
2.5
3.0
4.0
5.0
6.0
8.0
10.0
COMBUSTOR ΔP/P, PERCENT OF PT IN.

FIGURE 5-19

combustor is slightly steeper, and the exponent on percent pressure drop is -0.327. No quantitative, theoretical, or physical significance has been determined for these exponents, although qualitatively the fact that NO_x decreases with increasing pressure drop can be attributed to the lower residence time that occurs due to the higher combustor velocities associated with higher pressure drop. Probably more important, the higher pressure drop also promotes improved mixing and hence more uniform primary zone fuel-air ratio which may also reduce NO_x emission.

(b) Discharge Gas Temperature Spread

The combustor discharge temperature spread was also measured by 16 aspirated C-A thermocouples, 8 at each of two radii in the discharge factor (TSF) defined by

$$TSF = \frac{T_{max} - T_{avg}}{T_{avg} - T_{inlet}}$$

where all temperatures are in °F. Typical results for the various combustors tested are as follows:

Combustor	TSF
SKP26259 M0	0.400
M2	0.317
M3	0.135
SKP26489 M0	0.078
M1	0.118
PAP218770 M0	0.230
M1	0.113
SKP26489 PI	0.345

(c) Lean Stability

Because of the low fuel-air ratios associated with recuperated engine cycles, lean blowout was checked on several of the combustors to determine whether they were suitable for the particular application. Idle fuel-air ratio for the AiResearch engine was to be 0.0025, so 0.002 was arbitrarily set as an acceptable lower limit. Measured results for the combustors tested are tabulated below.

Combustor	Test Conditions			Fuel-Air Ratio At Lean Blowout
	T_{in}, °F	P_{in}, psia	W_a, lb/sec	
SKP26259 M0	750	58.8	2.18	0.0032
M1		Same as M0		0.0027
M2		Same as M0		0.0015
M3		Same as M0		0.0016
M4	500	22.0	0.64	0.0058
M5	500	22.0	0.64	0.0045
SKP26489 M0	750	58.8	2.18	0.0019
M1	990	18.4	0.47	0.0019
SKP26489 PI	500	24.7	0.76	0.0019

No lean blowout tests were conducted on the PAP218770 premix combustor because it was felt that the combustor would not yield representative results on natural gas fuel. Also note that the tests of the M4 and M5 modifications to the SKP26259 vaporizer were terminated prematurely according to the unsatisfactory lean blowout criterion.

On February 3, the program was placed on hold, and further contract work suspended pending discussions and negotiations with OAP/EPA.

5.3 Test Period (February 1, 1972 to August 10, 1972)

5.3.1 Test and Analysis Activity

The test period covers a contract hold period (February 1, 1972 to May 15, 1972) in which experimental combustor evaluation sponsored by AiResearch continued during the official contract suspension period. The testing was conducted using the EPA-contract combustion rig per agreement with the EPA and is reported in the sections that follow. Contract activity was then reinitiated in May 1972.

During the period of AiResearch-sponsored testing, a series of emissions tests were conducted on a baseline pressure-atomizing combustor typical of the AiResearch Model GTCP85 Engine combustors. Several other tests including vaporizing and premix combustion systems were also conducted.

Subsequent to the reinitiation of the contract effort in accordance with Amendment No. 3, four tests on the SKP26489 vaporizer configuration, including one that simulated recuperator bypass air injection into the burner for a given engine configuration, and one test on the pneumatic impact combustor, were conducted. These tests were performed under off-design operating conditions as defined by the "Automobile Gas Turbine Optimization Study" under EPA/OAP Contract 68-04-0012.

A new Federal Driving Cycle simulation technique was incorporated in an existing mission analysis computer program which should closely approximate the engine transient performance required for the vehicle accelerations and decelerations of the FDC. On the basis of this simulation technique and with an assumed part-load operating schedule for an engine, vehicle mass emissions (grams/mile) were predicted from the combustor emission indexes.

Table 2-6 showed the new test conditions as determined from the selected engine cycle performance that resulted from the simulated Federal Driving Cycle portion of this study. Additional details on this AiResearch 5-point simulation procedure are presented in Section 2.

5.3.2 Test Results

Emissions test results are presented graphically on an emission index (EI) basis defined as pound of pollutant per 1000 lb of fuel burned. For comparison purposes, the average EI corresponding to the FDC standards were determined by the following relationship:

$$\frac{gm}{mi} = \frac{0.454\ D_f\ (EI)}{(MPG)}$$

where

D_f = fuel density, lb/gal

(MPG) = vehicle fuel economy, mi/gal

(EI) = emission index, lb/1000 lb fuel or gm/kg fuel

The average allowable EI values, based on 14 miles/gal and a fuel density of 6.25, are as follows:

1976 Federal Emission Standards

Emission Specie	gm/mi	EI, lb/1000 lb fuel
NO_x (as NO_2)	0.40	1.98
CO	3.40	16.80
HC (as $CH_{1.85}$)	0.41	2.03
HC (as CH_4)	0.474	2.34

The allowable EI values were superimposed on the test results which follow.

(a) Baseline Atomizer Tests (P/N 899930)

Baseline atomizer test results are presented in Figure 5-20. When compared to vaporizer data at similar test conditions, Figure 5-21, the atomizer exhibits slightly higher NO_x emission with a greater fuel-air ratio dependence at the higher inlet temperatures and substantially increased CO and unburned hydrocarbon (CH_x) emissions. These results are attributed to the fact that the test conditions were not typical of those for which the combustion system was initially designed, and consequently, the primary side of the dual-orifice atomizer being used was oversized for the application involved. Corresponding grams-per-mile levels calculated by the procedure defined in AT-6097-R9 (Page 6) for both the atomizer and vaporizer combustors are tabulated below:

Combustor	Gm/Mi		
	NO_x (as NO_2)	CO	CH_x (as CH_4)
P/N 899930 (Atomizer)	4.18	5.65	1.31
SKP26489 (Vaporizer)	3.36	1.98	0.04
1976 Federal Standards	0.40	3.4	0.475 (0.41 as $CH_{1.85}$)

(b) Premix Combustor Tests (PAP 218770)

A modification to the PAP218770 premix combustor tested earlier in the program was made to improve its performance on liquid fuel. A successful liquid fuel test was then conducted on JP-4 injected into the combustor prechamber through a pressure atomizer. Poor efficiency attributed to unsatisfactory atomization of the fuel in the prechamber resulted in excessively high CO and unburned hydrocarbon emission.

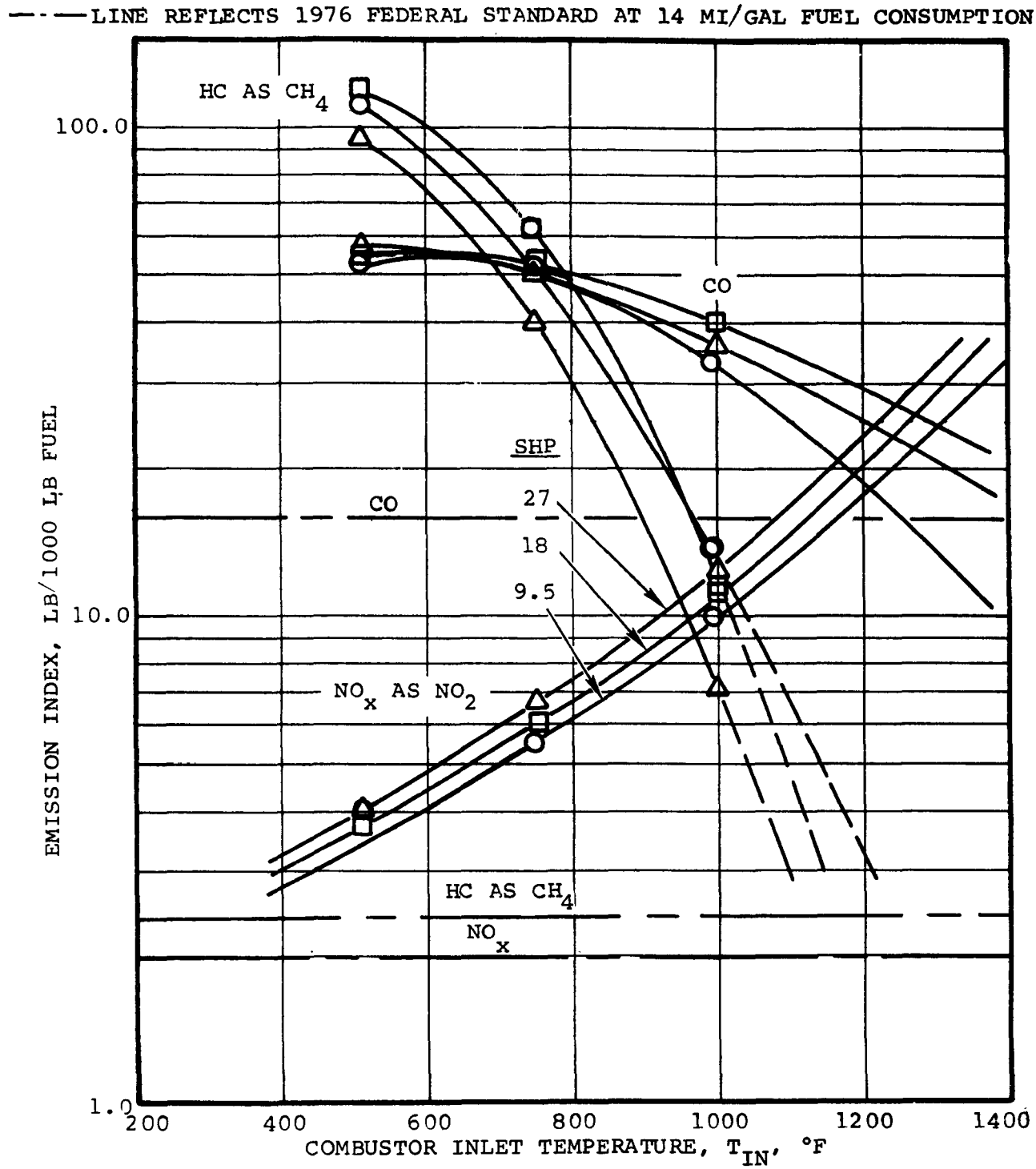

ATOMIZER COMBUSTOR P/N 899930
(FROM GTCP85-118 ENGINE)

FIGURE 5-20

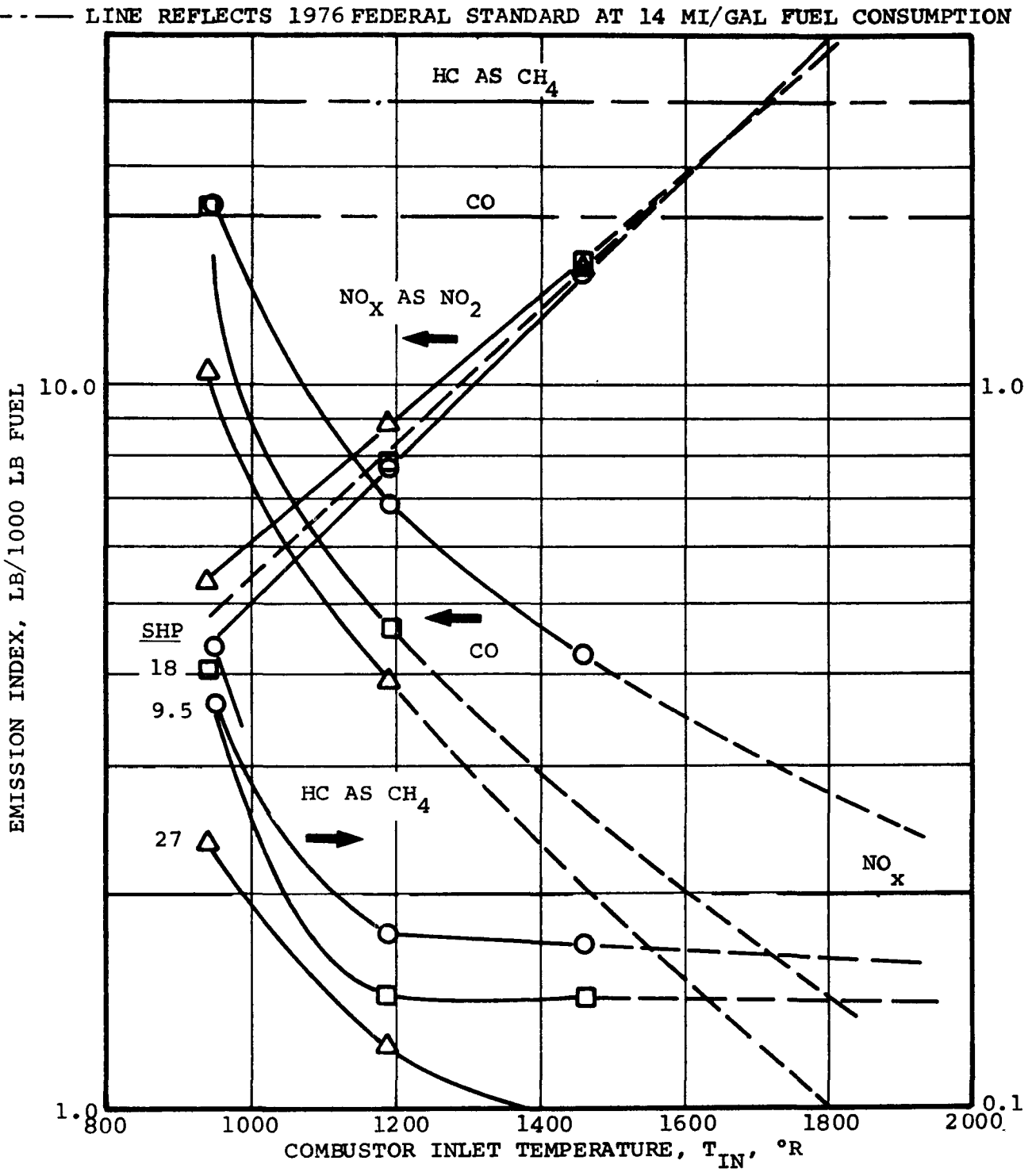

VAPORIZER COMBUSTOR - SKP26489

FIGURE 5-21

NO_x emission was correspondingly very low-estimated at 0.84 gm/mi over the Federal Driving Cycle. NO_x emission index as a function of combustion efficiency based on the test data is shown in Figure 5-22. The allowable Federal Standards require a combustor efficiency of 99.4%. Increasing NO_x with increasing combustion efficiency is attributed to the higher flame temperature associated with increased heat release.

(c) Vaporizer Testing

A series of tests were conducted on a recuperated AiResearch Engine Model GTPR36-61 to determine the effect of recuperator bypass air (expressed as percent of total engine flow) on NO_x emission levels. The major tests associated with this program consisted of the following:

(1) An atomizer combustor baseline

(2) A vaporizer combustor baseline (PAP226608)

(3) 1.5-percent bypass air to the vaporizer combustor primary pipe or L-pipe (PAP226608)

(4) 3.0-percent bypass air, half to L-pipe and half to baseplate (PAP226608)

(5) 3.0-percent bypass air plus early quench (PAP226608)

Test results are shown in Figure 5-23. With respect to the atomizer baseline, the vaporizer showed a 28-percent increase in NO_x at 900°F. With respect to the vaporizer baseline, the bypass air and early quench modifications resulted in the NO_x reductions shown in Table 5-2. It should be noted here that pressure losses in the test setup limited the maximum bypass flow available to 3 percent of the total engine flow. The engine performance was unaffected by the recuperator bypass setup, however.

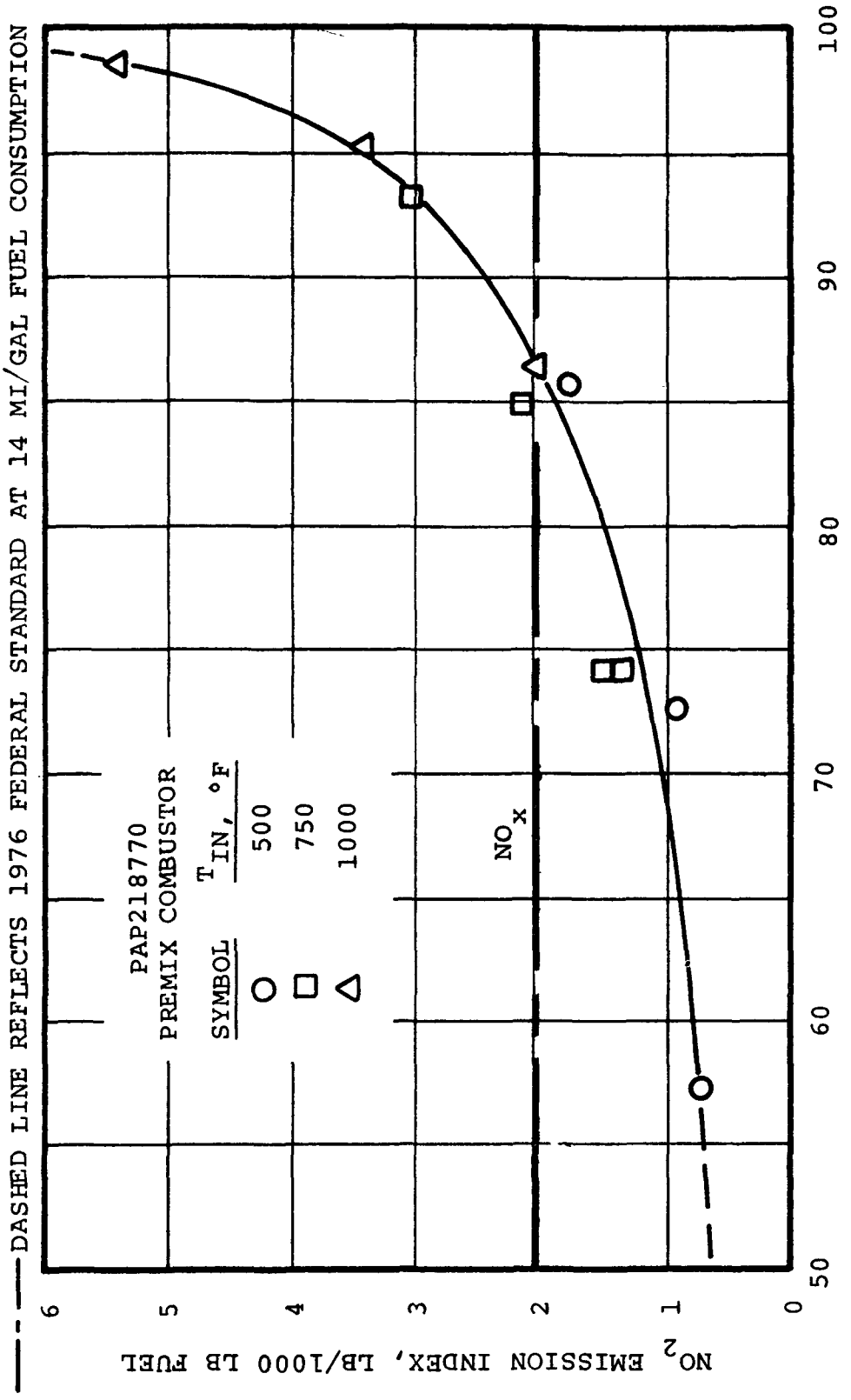
DASHED LINE REFLECTS 1976 FEDERAL STANDARD AT 14 MI/GAL FUEL CONSUMPTION
PAP218770
PREMIX COMBUSTOR
SYMBOL
T_{IN}, °F
500
750
1000
NO_x
NO_2 EMISSION INDEX, LB/1000 LB FUEL
COMBUSTION EFFICIENCY
0
1
2
3
4
5
6
50
60
70
80
90
100

FIGURE 5-22

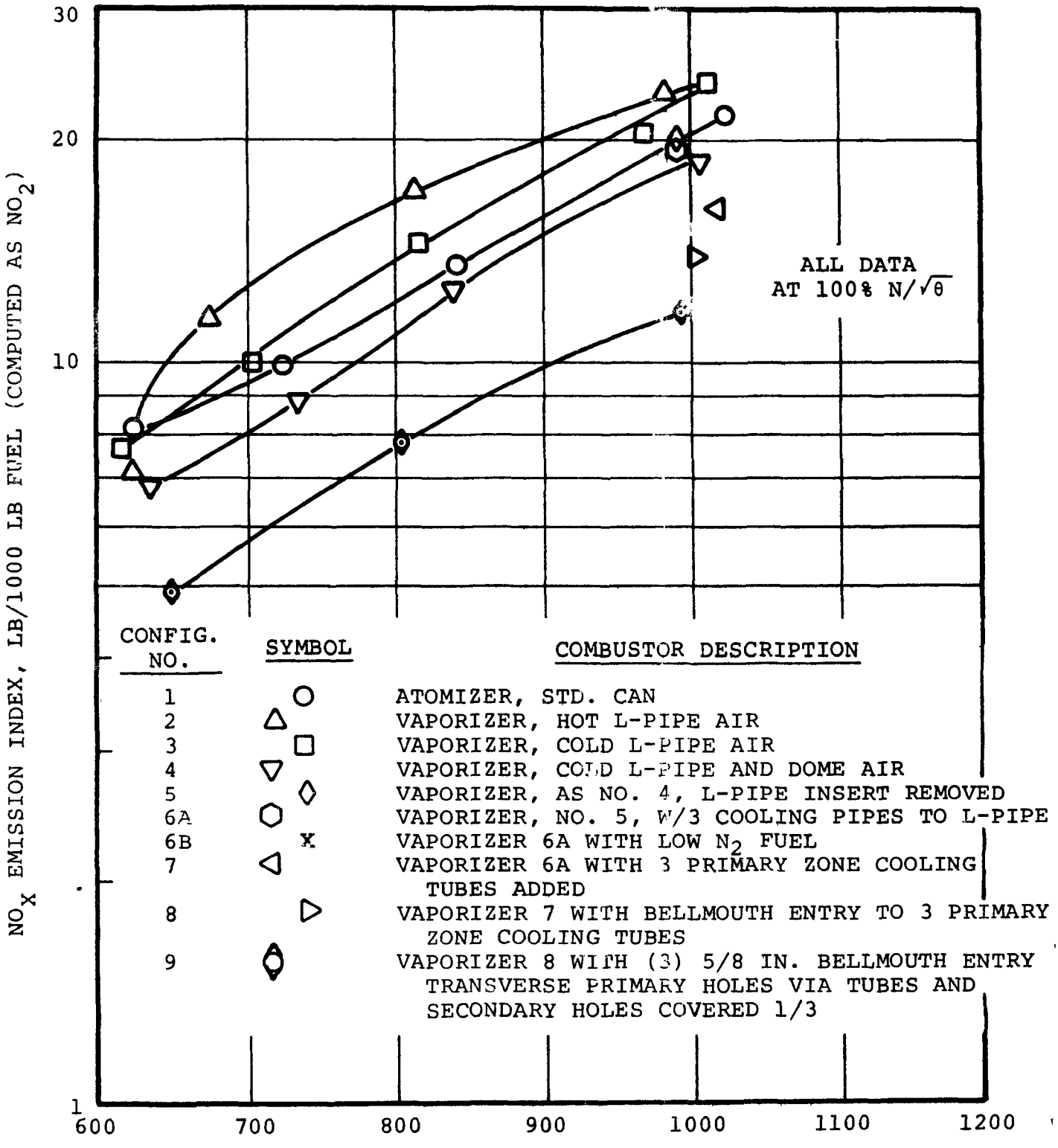

DEVELOPMENT PROGRESS ON THE
L-PIPE VAPORIZER COMBUSTOR PAP226608

FIGURE 5-23

TABLE 5-2

PERCENT NO_x REDUCTION OBTAINED ON GTPR36-61
ENGINE TESTS WITH BYPASS AIR AND EARLY QUENCH

PAP226608 Combustor	Percent NO_x Reduction at	
Configuration	T_{in} = 900°F	1000°F
1.5% bypass	10.5	4
3.0% bypass	26	22
3.0 % bypass + early quench	51	51

(d) L-Pipe Patternation Tests

Patternation tests were conducted on a vaporizer primary pipe to determine what modifications would improve the fuel distribution from the primary or L-pipe.

The configuration which gave the most uniform distribution of fuel is detailed in Figure 5-24.

The test setup and a comparison of test results from eight circumferential positions for two L-pipes and the improved L-pipe are presented in Figure 5-25 and 5-26, respectively. Table 5-3 presents a quantitative comparison of the resultant fuel rates per unit time at the eight positions.

TABLE 5-3

Configuration	L-Pipe No. 1	L-Pipe No. 2	Modified L-Pipe
Max-Min	1.579	1.819	0.64
$\sum \frac{\lvert \text{Reading-Avg} \rvert}{8}$	0.484	0.484	0.170

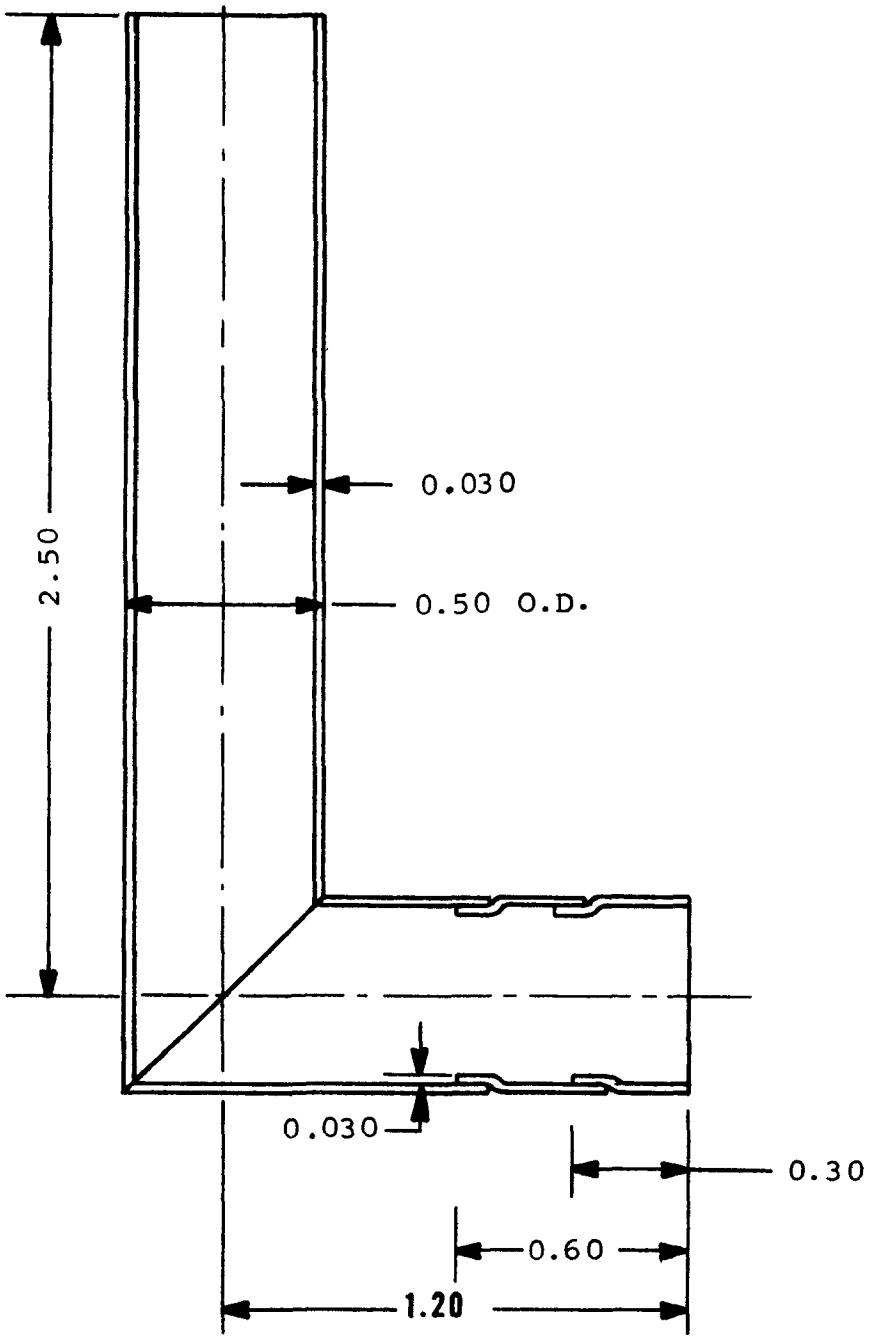

IMPROVED PRIMARY PIPE

FIGURE 5-24

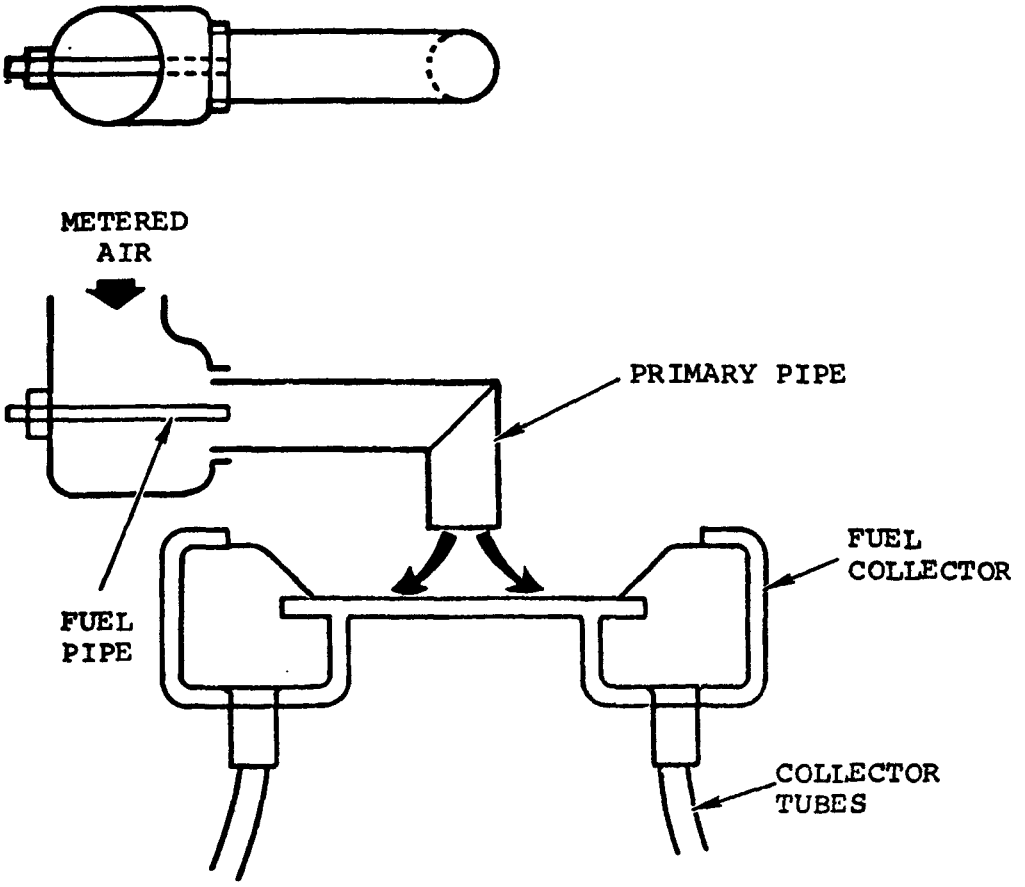

ATMOSPHERIC FUEL PATTERNATION
TEST RIG

FIGURE 5-25

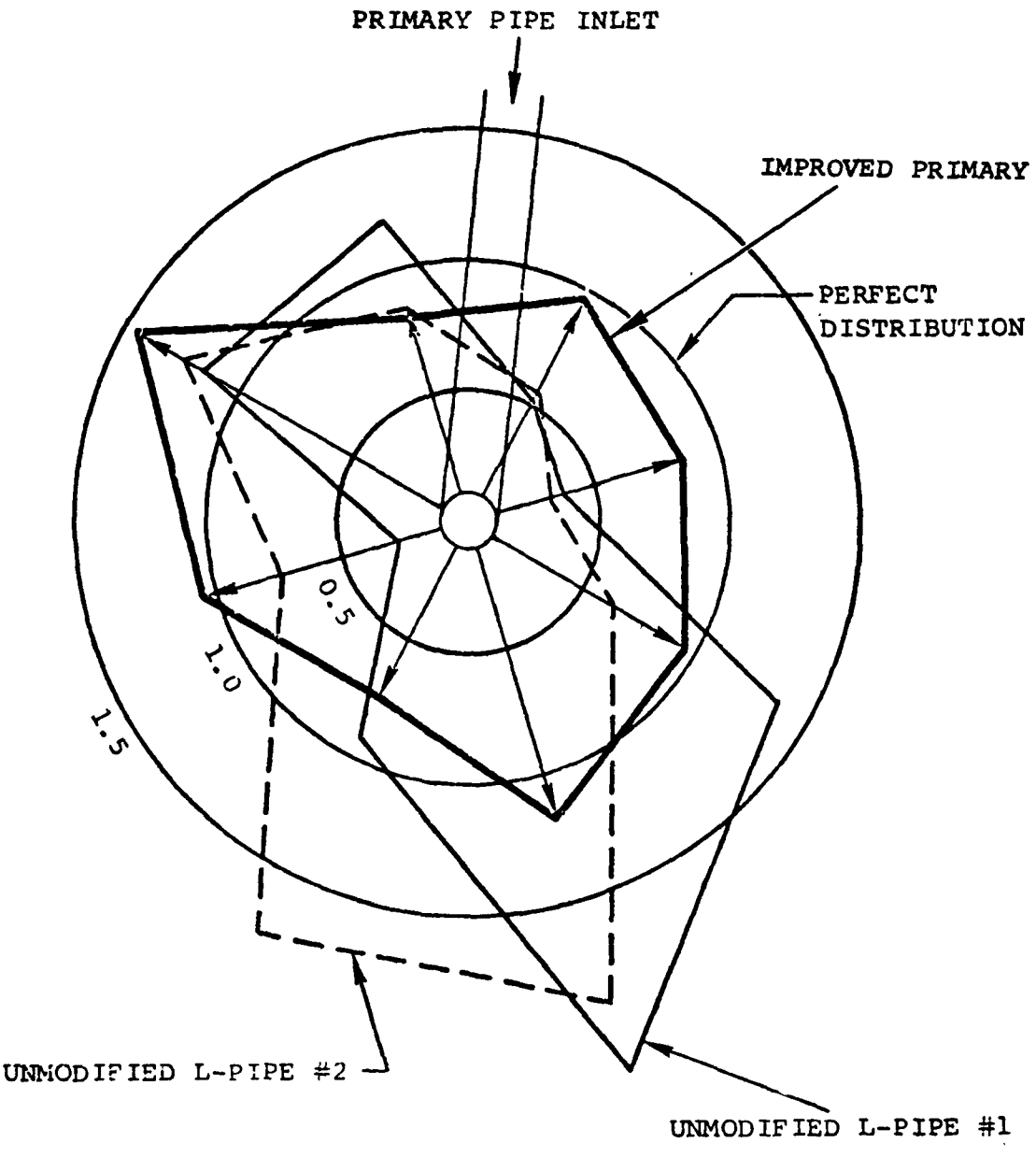

FUEL PATTERNATION TESTS.
ON L-TYPE PRIMARY PIPE
WITH DOUBLE WEIRS

FIGURE 5-26

(e) SKP26489 Vaporizer Tests

Four tests were conducted on the SKP26489 vaporizer combustor. The first test consisted of a baseline run of the original configuration with an additional radial cooling skirt on the combustion baseplate. The test was conducted per the conditions shown on Table 5-1. Figure 5-27 shows the basic dimensions to the SKP26489-M2 configuration tested, and Figure 5-28 shows the test results. Representative shaft horsepower (shp) loads shown on this and the following curves are based on N112V engine cycle performance demonstrated over the simulated Federal Driving Cycle (shown in Table 5-1) as determined from the "Automobile Gas Turbine Optimization Study" (EPA/OAP Contract 68-04-0012). N112V denotes a 1975 technology single-shaft engine cycle with recuperation and variable inlet guide vanes. the resultant emissions reflect an increase in NO_x, gm/mi, which is attributed to the test and calculation procedure change discussed in Section 5.3.3(a).

As a result of thermal distress noted on the combustor baseplate, particularly on the ends of the secondary pipes, a baseplate redesign, without the secondary pipes, was constructed for subsequent test. Figure 5-29 is a detail sketch of the redesign and Figure 5-30 shows a photograph of the new design. Test results for this configuration, Figure 5-31, showed a slight increase in carbon monoxide and unburned hydrocarbons attributed to a slight drop in combustion efficiency and essentially no change in NO_x emission.

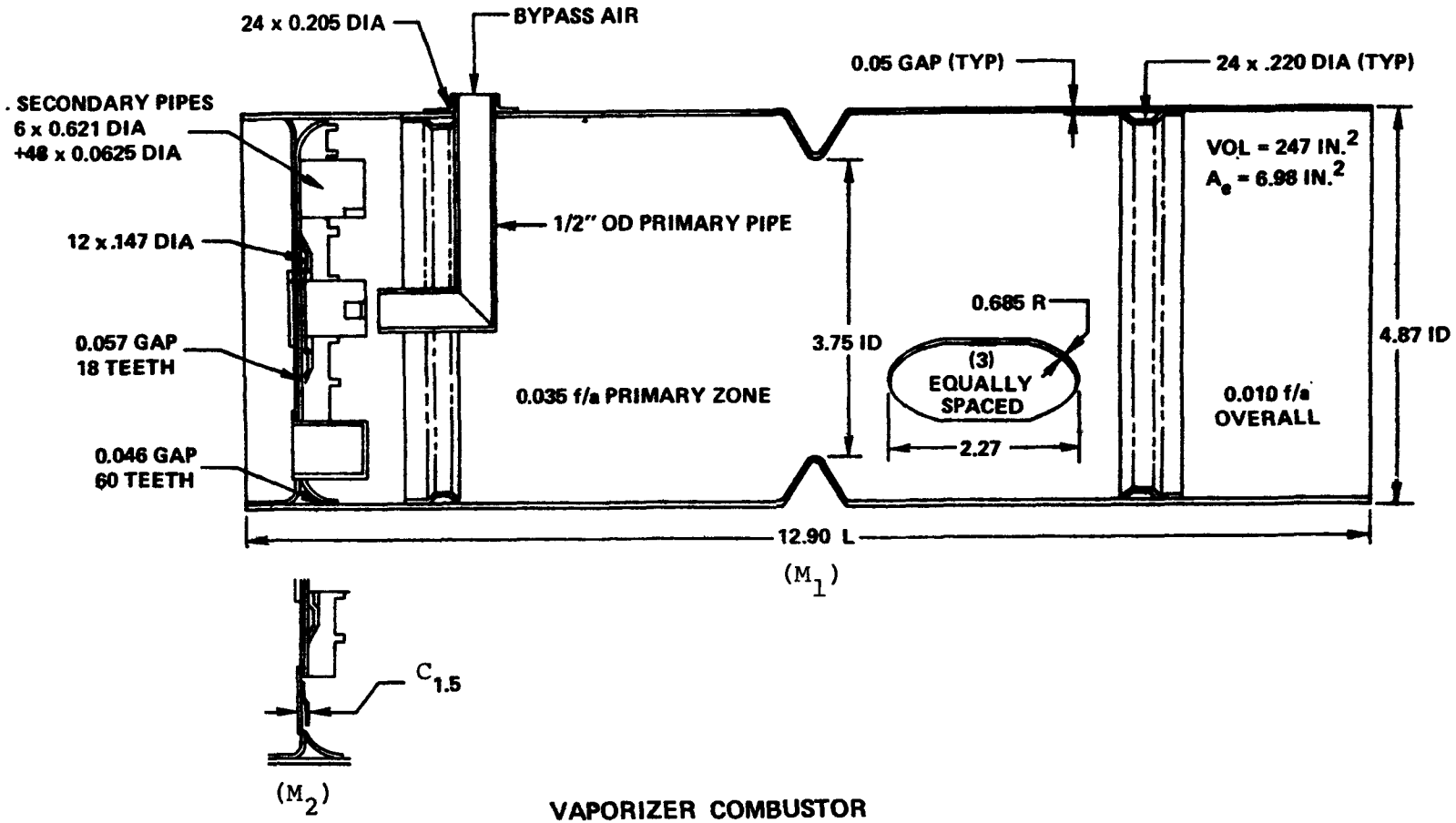

VAPORIZER COMBUSTOR
SKP26489-M1 & SKP26489-M2

FIGURE 5-27

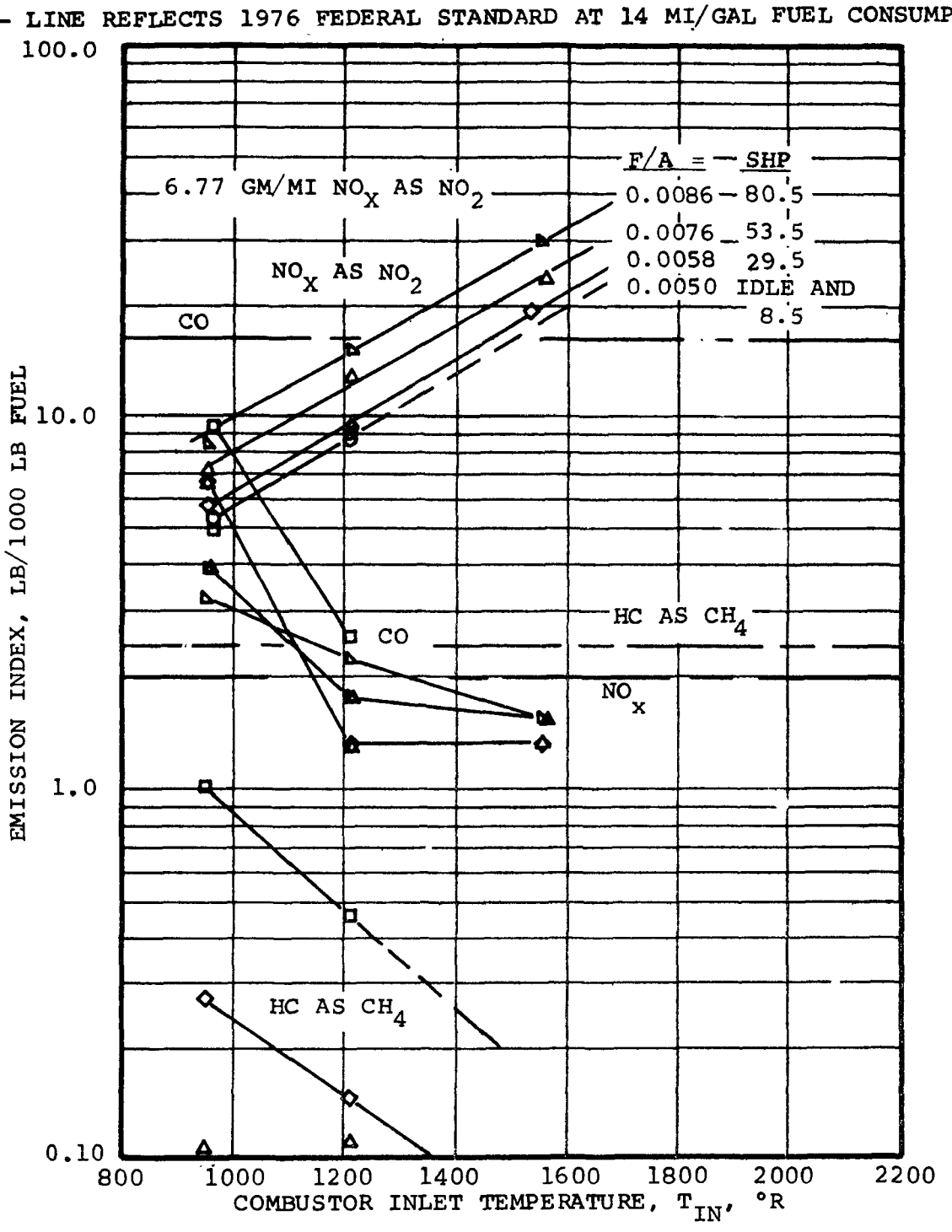

VAPORIZER COMBUSTOR - SKP26489-M2

FIGURE 5-28

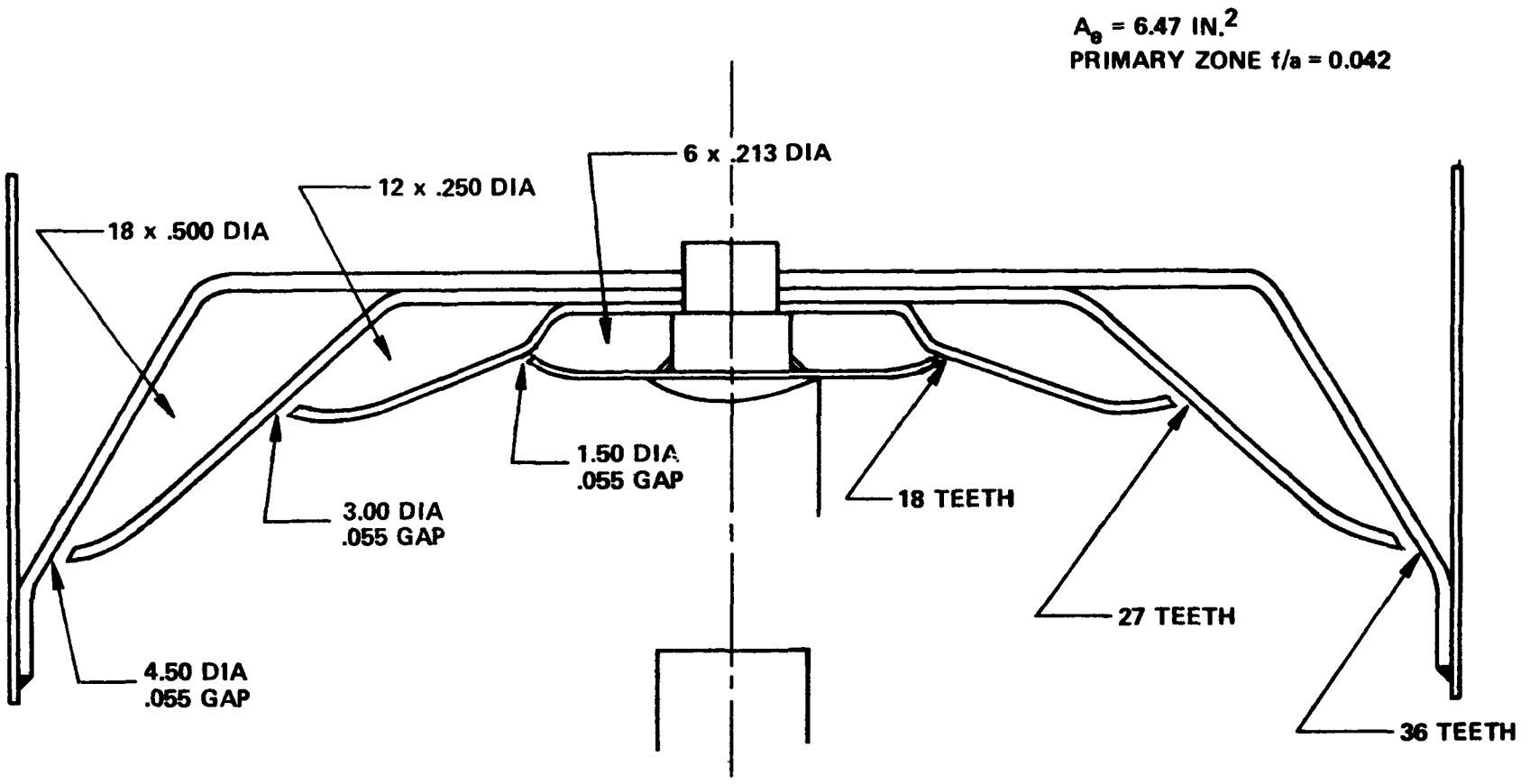

FIGURE 8-A

STAGED DOME
(USED IN SKP26489SD)

FIGURE 5-29

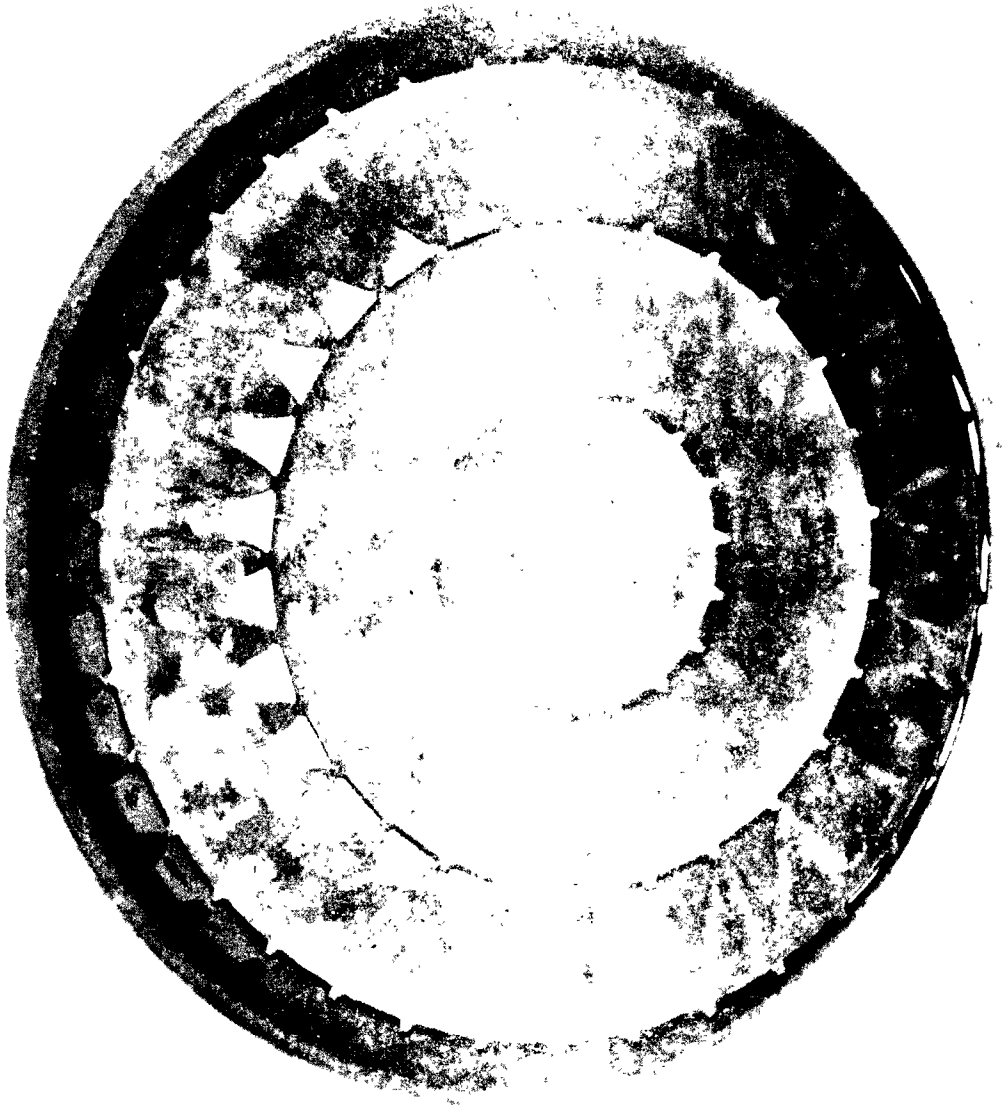

VAPORIZER COMBUSTOR BASEPLATE REDESIGN
P-45410
(USED IN SKP26489SD)

FIGURE 5-30

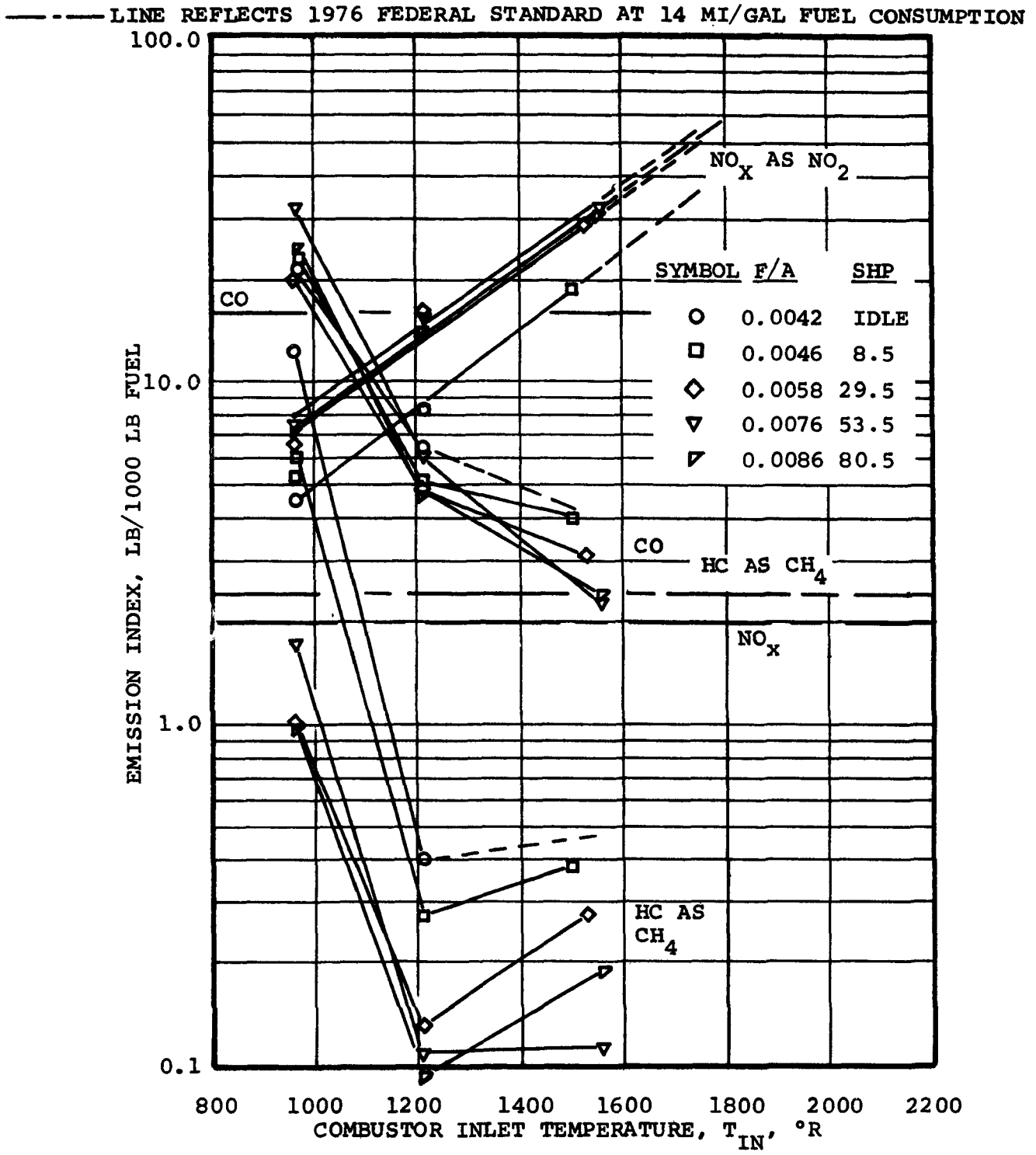

VAPORIZER COMBUSTOR - SKP26489SD

FIGURE 5-31

The combustor was then fitted with a new primary pipe equipped with an internal weir to improve fuel distribution. Test results, Figure 5-32, were essentially unchanged from the baseline test of the new baseplate design. An overtemperature failure of the primary pipe occurred during the test, as shown in Figure 5-33, and since the test data indicated that no benefit was obtained from the new L-pipe design, the combustor was repaired with a conventional L-pipe with no internal devices.

(f) Recuperator Bypass Simulation

To more fully explore the GTPR36-61 Engine recuperator bypass test results, a recuperator bypass test was simulated in the combustion rig by delivering cooled air to the L-pipe. The test condition was the 29.5 hp point from Table 2-6. The effects of both bypass air (percent of total engine flow) and bypass air temperature were determined.

Test results are presented in Figure 5-34. NO_x emission was reduced 93 percent with 10-percent bypass flow (300°F) and a combustor inlet temperature of 1060°F (1520°R). A comparison of emissions obtained at 10-percent bypass flow with emissions that would be obtained with 300°F combustor inlet temperature is presented below.

COMPARISON OF EMISSION INDEX VALUES

	NO_x (as NO_2)	CH_x (as CH_4)	CO
Emissions at 10-percent bypass; 1060°F combustor inlet	2.02	3.02	7.01
Emissions at 300°F combustor inlet	4.0	6.0	60.0

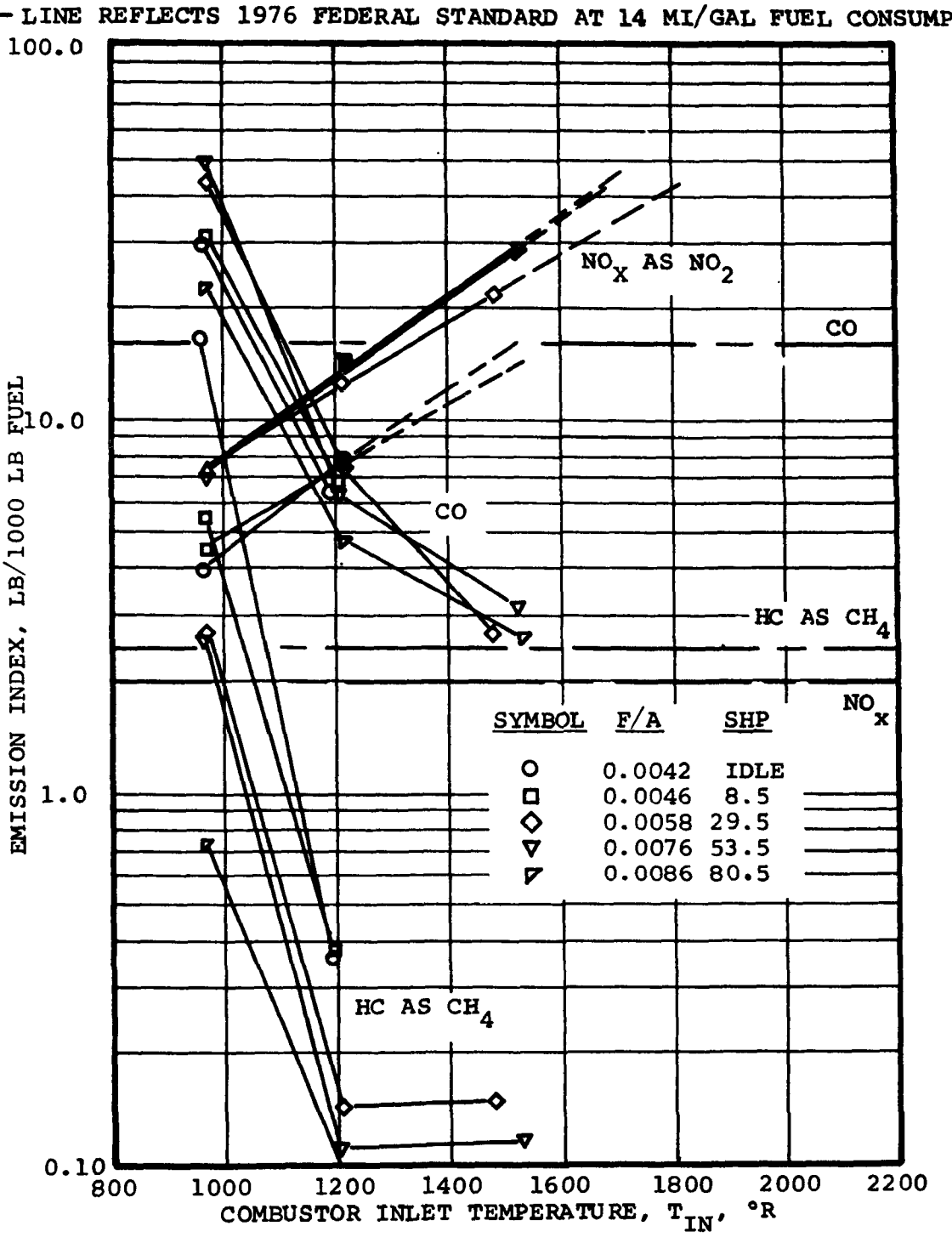

L-PIPE VAPORIZER WITH WEIR
COMBUSTOR - SKP26489 NL

FIGURE 5-32

PRIMARY PIPE OVERTEMPERATURE FAILURE
P-45425-1

FIGURE 5-33

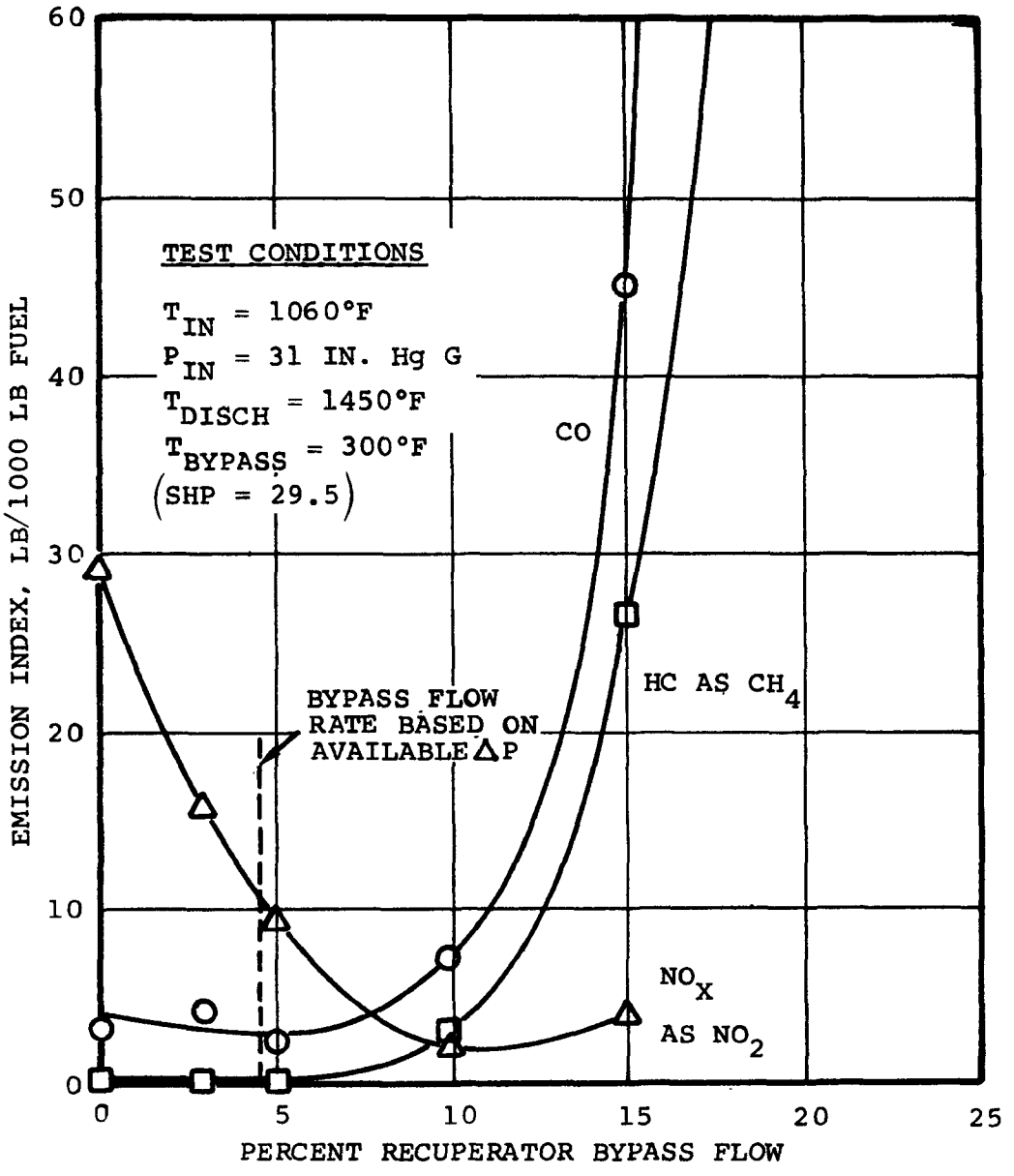

EFFECT OF RECUPERATOR BYPASS AIR
ON EMISSIONS OF SKP26489-SD COMBUSTOR

FIGURE 5-34

The introduction of 10% bypass air at 300°F into the primary zone achieved lower NO_x levels than were obtained with all the combustor inlet air at 300°F. There are several reasons that could account for the lower NO_x levels of the bypass test compared to NO_x levels with all combustor inlet air at the same temperature. The most important of these are primary zone equivalence ratio and primary zone turbulence level.

The introduction of 10% bypass air into the L-pipe while the combustor pressure drop is essentially constant adds 45% extra air to the primary zone. This reduces the primary zone fuel-air ratio from a calculated 0.042 to 0.029 (PZ equivalence ratio from 0.62 to 0.43). With a combustor inlet temperature of approximately 1000°F, this change in primary zone fuel-air ratio would reduce the equilibrium combustion temperature from 3350°R to 2750°R and the corresponding equilibrium concentration of NO by a factor of two[1]. Therefore, the change in primary zone equivalence ratio is sufficient to account for most, if not all, of the measured 2/1 reduction in NO_x from an E_I value of 4.0 to 2.0. The availability of increased quantities of excess oxygen with the leaner primary zone would also account for the lower measured quantity of CO emission.

An increase in general turbulence level would be expected as the result of the high airflow rate and high pressure drop in the L-pipe at 10% bypass. This higher turbulence level could improve the mixture homogenity and would improve primary zone mixing and combustion temperature uniformity in cases where substantial variations were present during no-bypass operation. A subsequent test (reported in Figure 5-50) indicated that the turbulence effect on NO_x formation rate was a relatively minor one in this case.

(1) "A Combustion system for a Vehicular Regenerative Gas Turbine Featuring Low Air Pollutant Emissions", SAE Paper 670936, (1967) by Cornelius, Stivender and Sullivan.

Figure 5-35 shows the effect on NO_x emission index of varying the temperature of the bypass air at 5 percent bypass flow from its nominal value of 300°F. At 200°F, the NO_x reduction was 2.7 percent compared to 300°F bypass air temperature. At 400°F, the NO_x increased 5.5 percent.

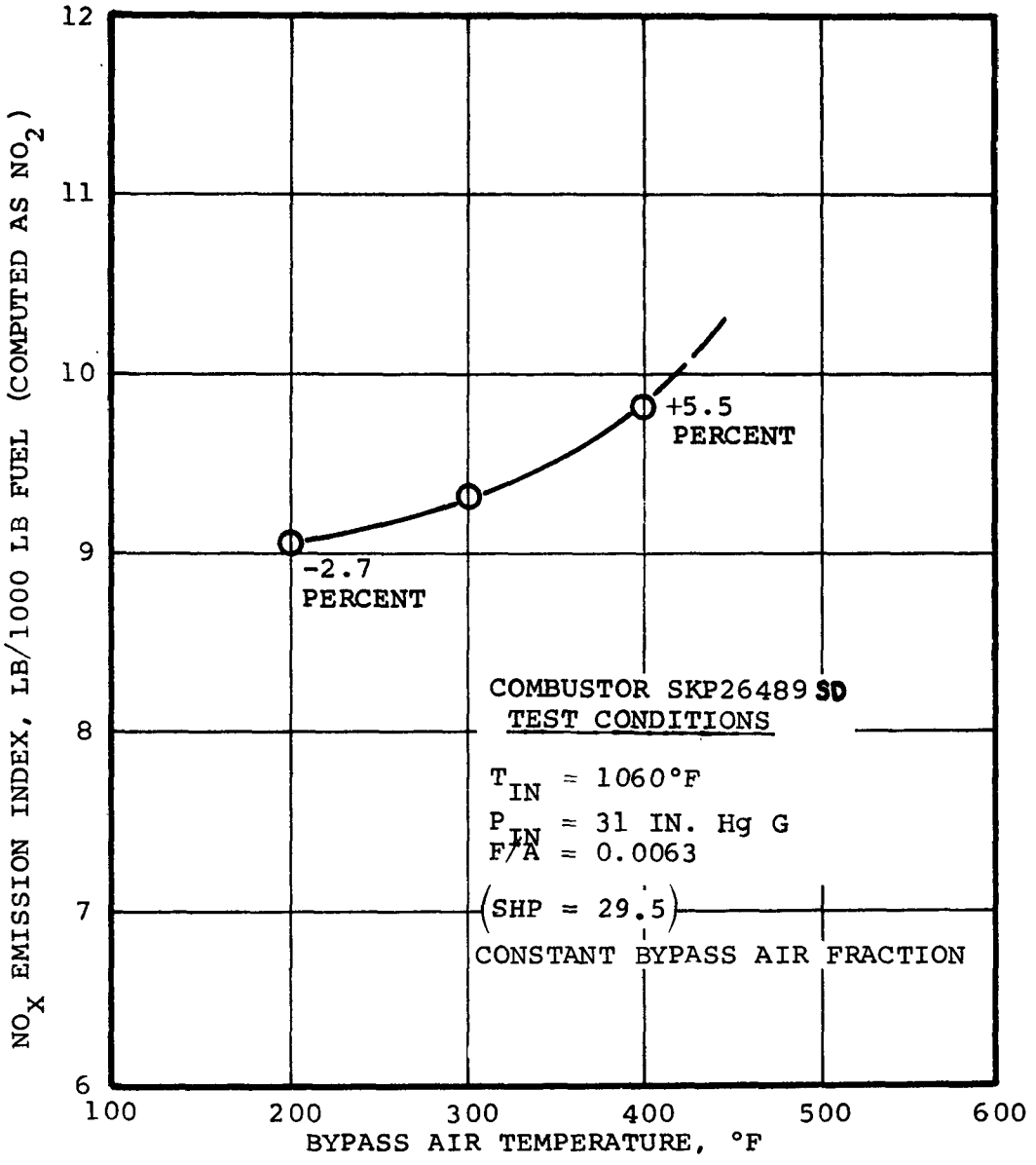

EFFECT OF BYPASS AIR TEMPERATURE ON
NO_X EI AT 5 PERCENT RECUPERATOR BYPASS FLOW

FIGURE 5-35

By comparison, the results shown above reflect a larger than expected decrease in NO_x emission index than for the same configuration under the same conditions without recuperator bypass flow [based on data extrapolated to 300°F (760°R) combustor inlet temperature (shown on Figure 5-31)]. Possible reasons include increased turbulence and mixing because of high pressure drop, and higher primary zone equivalence ratios.

The test results also verified that an engine performance penalty must be paid in the form of increased fuel flow for control of NO_x emission by the recuperator bypass method. For example, an increase in fuel-air ratio from 0.0063 to 0.0072 was required to maintain a constant combustor discharge temperature of 1450°F at 10-percent bypass flow. The increased fuel-air ratio did have the added benefit of delaying the drop-off in combustion efficiency associated with cooling and leaning the combustor primary zone as illustrated in Figure 5-36. These results were further investigated in the cycle studies reported in Section 5.3.3(b).

In order to determine the optimum amount of bypass air, the EI values with bypass from Figure 5-34 were converted to grams-per-mile and plotted versus percent bypass, as shown in Figure 5-37. This conversion takes into account the increased fuel flow required when using bypass, and assumes that the 29.5 hp condition is representative of the emissions over the complete range of operation. For the fixed bypass air temperature case, the influence of nonbypassed air from the recuperator into the burner was assumed to be negligible, although an air temperature difference of 260°F was observed between the fixed bypass air temperature test condition and the 29.5 hp shaft load operating condition. It can be seen from the plot that the optimum bypass air percentage is approximately 9 to 10 percent. This could be achieved with a 3/4-in. primary pipe instead of 1/2 in. The final calibration will be done at 10-percent bypass, based on the above, to verify the results obtained and to determine if bypass is as effective at other horsepower points.

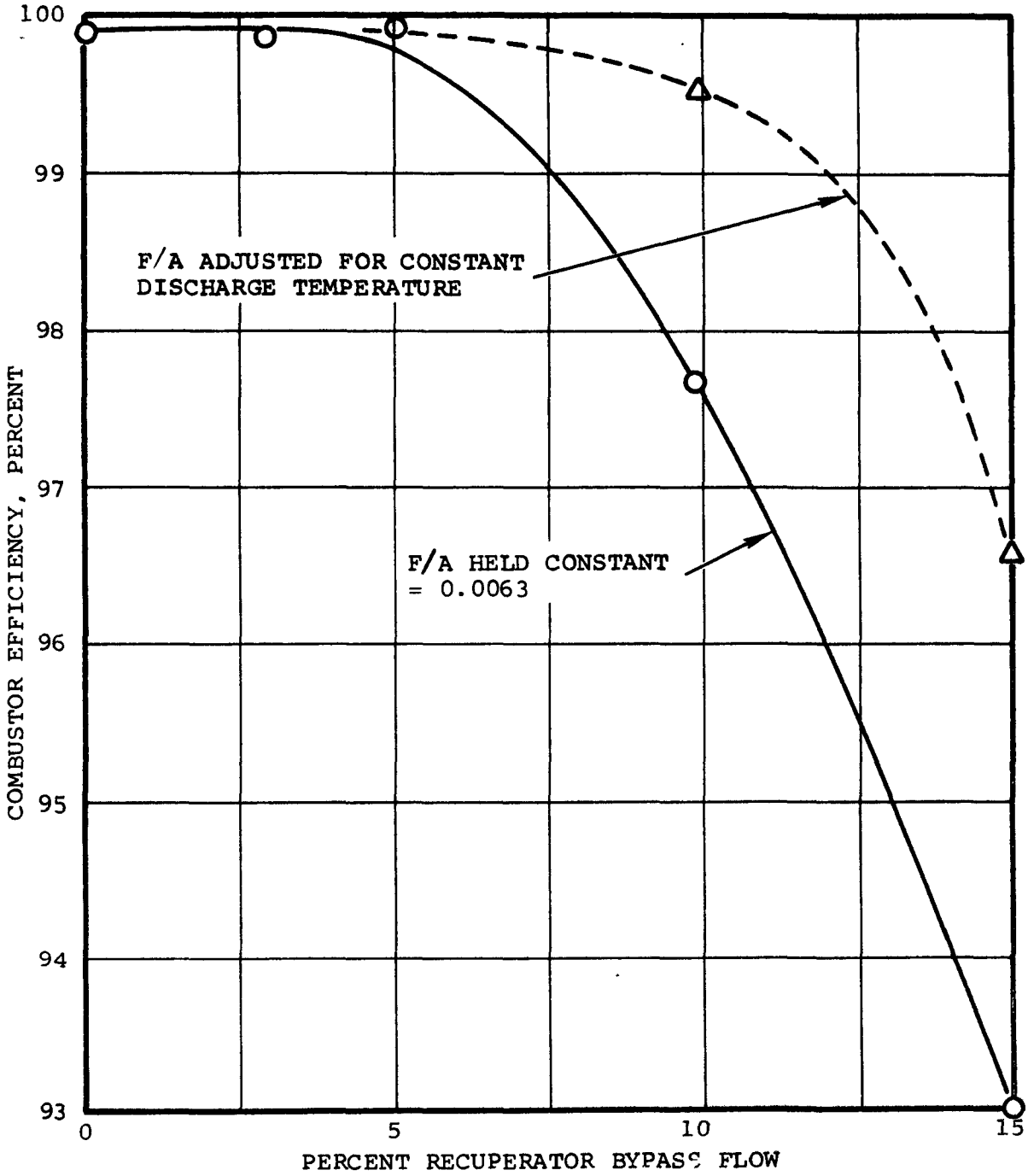

EFFECT OF BYPASS AIR ON
SKP26489-SD COMBUSTOR EFFICIENCY

FIGURE 5-36

1976 FEDERAL EMISSIONS STANDARDS

NO_x (AS NO_2)	0.40 GM/MI
CO	3.40
HC (AS $CH_{1.85}$)	0.41
HC (AS CH_4)	0.474

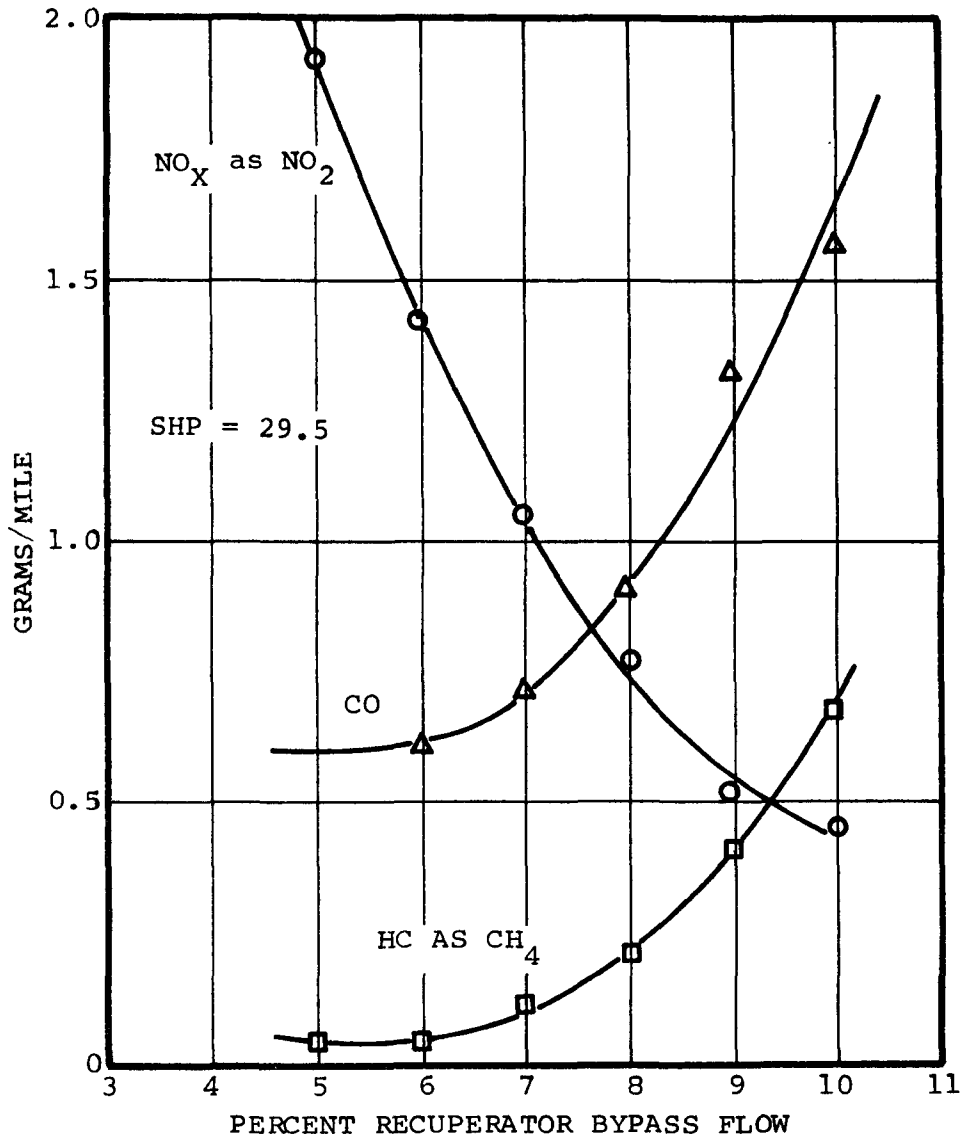

EFFECT OF BYPASS FLOW ON EMISSIONS
FROM SKP26489 COMBUSTOR ON
A GRAMS/MILE BASIS

FIGURE 5-37

(g) Pneumatic Impact Testing

The fuel injector of the pneumatic impact combustor configuration was modified by the addition of a flow diverting cone welded to the impact plate to prevent coalescing of the fuel droplets in the center of the plate as had been observed during earlier bench testing of the atomizer. The fuel delivery pipe was then modified for radial fuel injection to minimize eccentricity problems between the apex of the flow-directing cone and the delivery tube centerline. Additionally a shroud was added around the radial spray ports of the fuel tube to keep the fuel from impinging on the atomizer venturi walls. These modifications are illustrated in Figure 5-38.

The modified injector was then bench tested at atomospheric conditions. Test results indicated that the fuel dribbling noted on the unmodified injector had been eliminated.

The new configuration was then tested in the rig. Test data, Figure 5-39, showed that carbon monoxide and unburned hydrocarbon emissions were substantially reduced, but the NO_x level was high, estimated at nearly 9 gm/mi. In addition stability problems were encountered at the low power test conditions.

An examination of the data showed that the injector passed too much air resulting in unacceptable fuel-air ratios near the idle condition. However, the unburned hydrocarbons and CO emissions are sufficiently low enough that the injector could be resized to give lower NO_x without exceeding the CH_x and CO limits. This work, however, was not done.

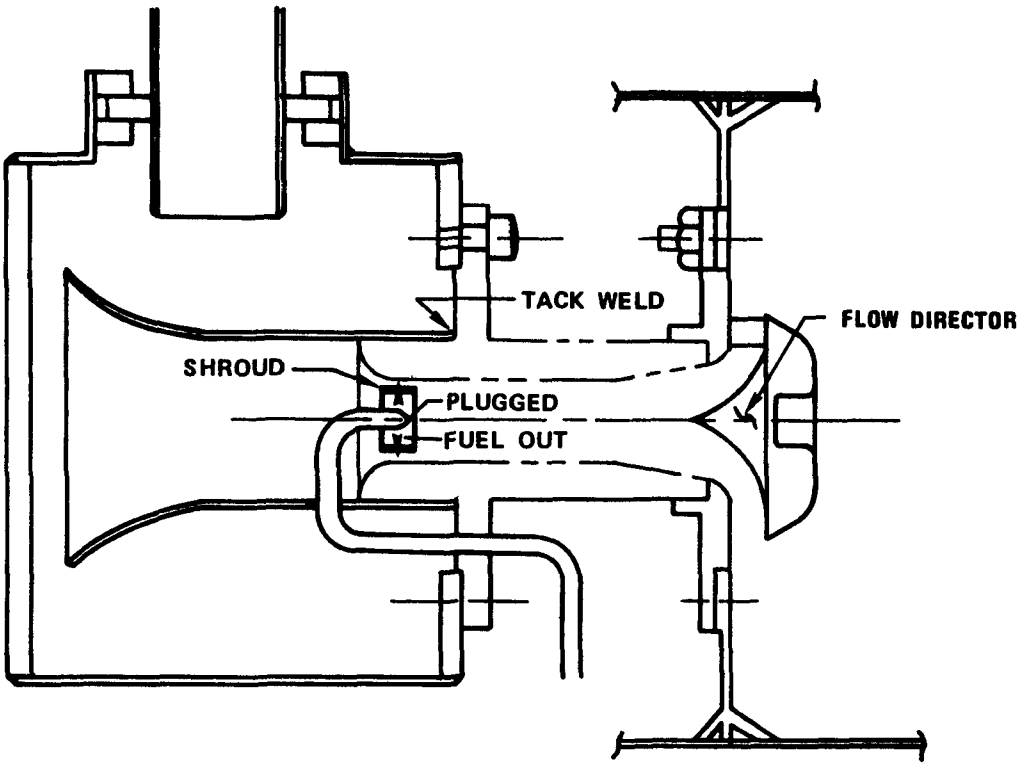

MODIFIED PNEUMATIC IMPACT
FUEL INJECTOR

FIGURE 5-38

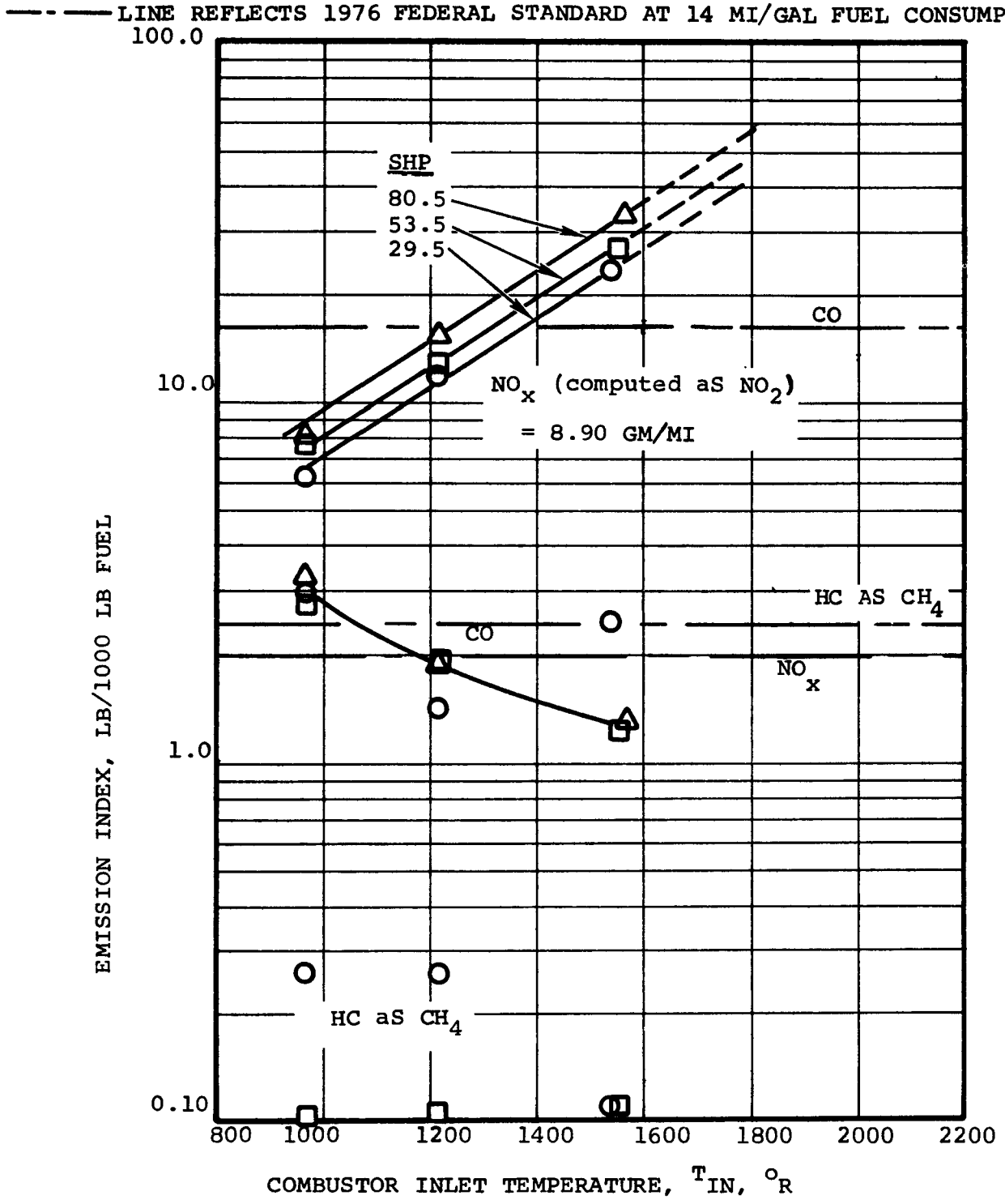

PNEUMATIC IMPACT COMBUSTOR
SKP26489-PI

FIGURE 5-39

5.3.3 Analytical Effort

(a) Federal Driving Cycle Simulation for Optimized Engine Cycle

The following modification to the test procedure was made to incorporate new test conditions based on the optimized engine cycle.* The recommended cycle was a recuperated single-shaft engine with variable inlet guide vanes (labeled NII2V).

The Federal Driving Cycle (FDC) was simulated by a mission analysis computer program* with each route segment represented by a speed change phase followed by a sustained speed phase to achieve the correct segment average speed and end speed of the automobile. Then the complete mission (FDC) was surveyed to obtain the total time spent within each horsepower range. All horsepower levels were covered, using 1-hp intervals to 31 hp, and 3-hp intervals from 30 hp to 121 hp. For the Federal Driving Cycle, the NII2V Engine does not operate at more than 91 hp at any time.

From the mission analysis program output, a set of test conditions can be chosen that satisfactorily represents the ranges in fuel flow, pressure, and temperature over which the engine combustion system must operate. A 5-point representation was chosen as shown in Table 2-6 the end points of the horsepower ranges that are simulated by the 5 test points are shown in Table 5-4. It can be seen from the table that the points were chosen so as to minimize the range of operating variables associated with each point in order to ensure maximum accuracy in the conversion to grams-per-mile.

*Refer to "Automobile Gas Turbine Optimization Study," Final Report (AT-6100-R7), Contract 68-04-0012.

TABLE 5-4

TABLE OF 5-POINT TEST EVALUATION

Test Points		HP	Airflow, lb/sec	Temperature, T_1, °R	Pressure, P_1, psia	Fuel Flow, lb/hr	Fuel/Air
	Min	1.3	0.331	1960	20.5	3.64	0.00305
1	Av	1.3	0.331	1960	20.5	3.64	0.00305
	Max Min	6.5	0.392	1935	21.9	5.30	0.00373
2	Av	8.5	0.412	1915	22.5	5.85	0.00394
	Max Min	18.5	0.506	1850	25.8	9.30	0.00500
3	Av	29.5	0.615	1780	29.3	13.40	0.00605
	Max Min	38.5	0.705	1722	32.8	17.00	0.00705
4	Av	53.5	0.850	1660	38.2	23.50	0.00768
	Max Min	62.5	0.935	1632	42.0	27.00	0.00835
5	Av	80.5	1.080	1580	49.4	35.00	0.00900
	Max	121.0	1.380	1485	65.0	54.00	0.01050

The use of the 5-point evaluation above accounts for all steady-state conditions, including a detailed integration of horsepower vs time during engine accelerations and decelerations. It does not account for exhaust emissions present during cold and hot engine starts nor the variation in emissions associated with engine transient operation.

The effect of the new driving cycle simulation is to increase the predicted emission levels in grams-per-mile. This is illustrated by values calculated according to the OAP-suggested procedure compared

with values from the two AiResearch procedures (original 4-point simulation versus revised 5-point simulation). Calculations for the SKP26489 vaporizer yield the following values:

FDC Simulation	NO_x (as NO_2) gm/mi	Percent
AiR 5-pt	6.38	137
AiR 4-pt	5.46	117
OAP	4.67	100

(b) Engine Cycle-Recuperator Bypass Study

Off-design cycle studies were conducted on the NII2V Engine to determine the effect of recuperator bypass on engine performance. Performance data were generated for bypass percentages of 0, 5, and 10 percent of total engine flow at each of the 5-power points in the driving cycle simulation. The increase in recuperator effectiveness as a result of decreased throughflow was included. Small secondary effects resulting from pressure drop changes were assumed to be negligible. Results of the cycle study are presented in Table 5-5; the data show that the effect of recuperator bypass decreases as engine power increases because of the increased combustor temperature rise at higher power conditions.

The fuel flow rate (W_f) data shown in Table 5-5 has been plotted against output power for 0-, 5-, and 10-percent recuperator bypass flows (Figure 5-40). Fuel consumption penalties are small at the higher power levels. The penalties can be significant at low power levels,

TABLE 5-5

RECUPERATED SINGLE-SHAFT, VIGV AUTO ENGINE
SIMULATED OFF-DESIGN PERFORMANCE AT SEA LEVEL,
85° 1700°F T_4 FOR RECUPERATOR
BYPASS FLOWS OF: 0%, 5%, 10%

Engine design point match at T_4 = 1900°F
Sea level, standard day, $(\Delta P/P)_B$ = 4%

HP	1.3	8.5	29.5	53.5	80.5
$\Delta P/P_{Burner}$	0.0282	0.0333	0.0431	0.0433	0.0420
$T_{comp\ disch}$ °R	641.3	650.7	709.7	773.8	832.5
$T_{rec\ out}$ °R					
0%	1968.8	1916.4	1783.4	1676.4	1591.2
5%	1997.6	1942.0	1807.0	1686.9	1609.5
10%	2012.9	1964.6	1829.1	1716.9	1627.7
*$T_{burn-in}$ °R					
0%	1968.8	1916.4	1783.4	1676.4	1591.2
5%	1934.6	1881.9	1756.7	1653.0	1572.2
10%	1885.0	1841.9	1723.0	1627.0	1551.3
ε_{regen}					
0%	0.9582	0.9508	0.9227	0.8996	0.8778
5%	0.9790	0.9700	0.9430	0.9200	0.8990
10%	0.9900	0.9870	0.9620	0.9400	0.9200
W_f, lb/hr					
0%	3.4	5.8	14.0	23.4	34.5
5%	4.0	6.61	15.0	24.5	35.6
10%	4.9	7.56	16.2	25.7	36.8
f/a					
0%	0.0031	0.0040	0.0061	0.0077	0.0091
5%	0.0037	0.0046	0.0065	0.0081	0.0094
10%	0.0044	0.0052	0.0070	0.0085	0.0097

*$T_{burn-in}$ includes mixing of recuperator bypass flow.

depending on the amount of bypass required to achieve the desired NO_x emission reduction at these lower power levels. This can be seen from the plot of percent fuel consumption penalty vs output power in Figure 5-40. If a 9-percent bypass flow is needed at low power levels, the fuel consumption penalty would range from about 6 percent at 80 hp to 39 percent at idle. While the results shown in Figure 5-31 would indicate that bypass flows of 9 percent might be desirable, several factors could make the optimum bypass flow lower than that value. The test represented in Figure 5-40 was run at a fixed power condition and with the bypass temperature fixed at 300°F. If the bypass air temperature is assumed to be at compressor discharge temperature, the range of bypass temperature expected is from 180°F to 370°F. Because of the low temperature of the bypass air at low power conditions, the amount of bypass flow may be reduced for a desired NO_x reduction. Figure 5-41 shows a comparison between 5 percent bypass flow and 9 percent bypass flow with respect to fuel consumption penalty.

(c) Data Reduction Program

During the contract hold period, a computer program available at AiResearch for engine emission data reduction was modified to allow computerized data reduction of rig data. Both emission index and pollutant generation rate in lb/hr are calculated. The emissions concentrations are corrected to concentrations in wet exhaust from a combustion process with dry air. In addition, combustion efficiency is calculated from the measured carbon monoxide and unburned hydrocarbon concentrations. A typical computer printout is shown in Figure 5-42.

It should be noted that unburned hydrocarbons are calculated as methane, CH_4. If it is necessary to convert the emission indices to equivalent $CH_{1.85}$ or C_6H_{14}, the printed values should be multiplied by 0.865 or 0.895, respectively.

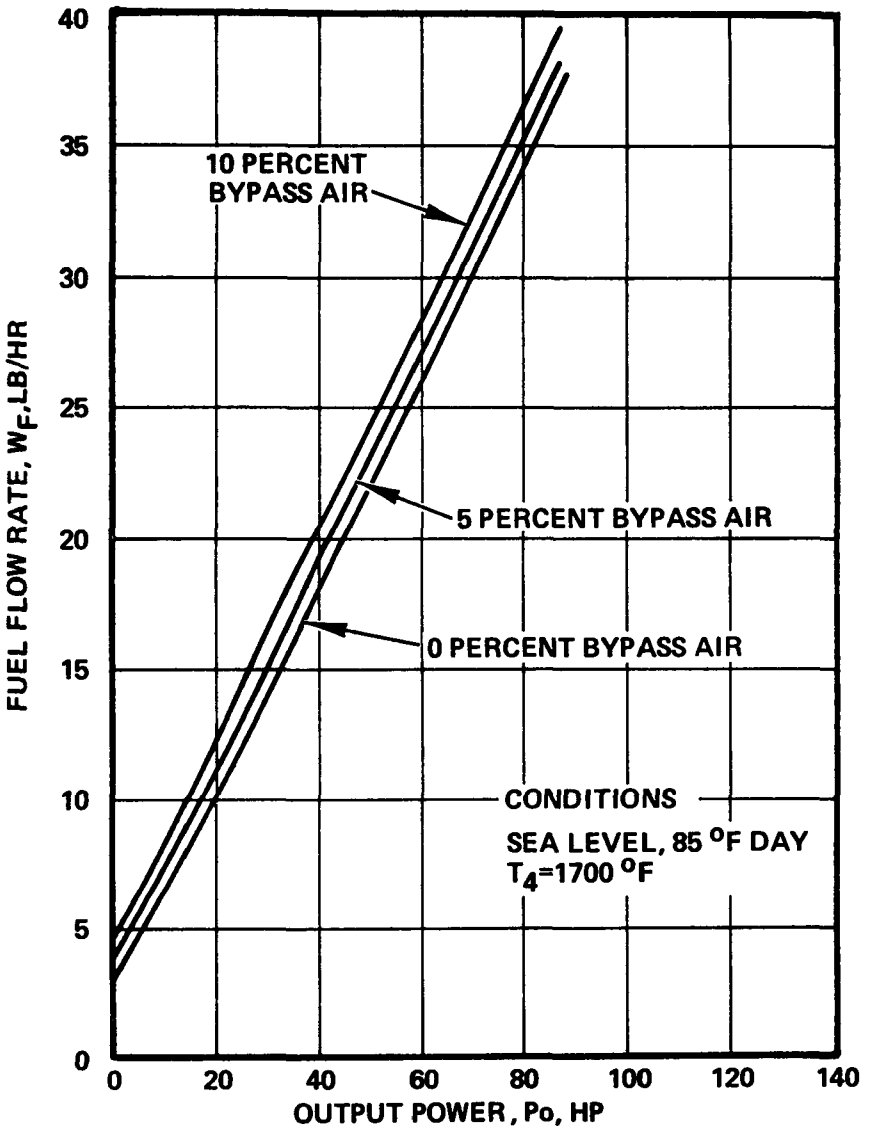

FIGURE 5-40

FUEL FLOW RATE VS OUTPUT POWER FOR 0%, 5%, 10% RECUPERATOR BYPASS AIR

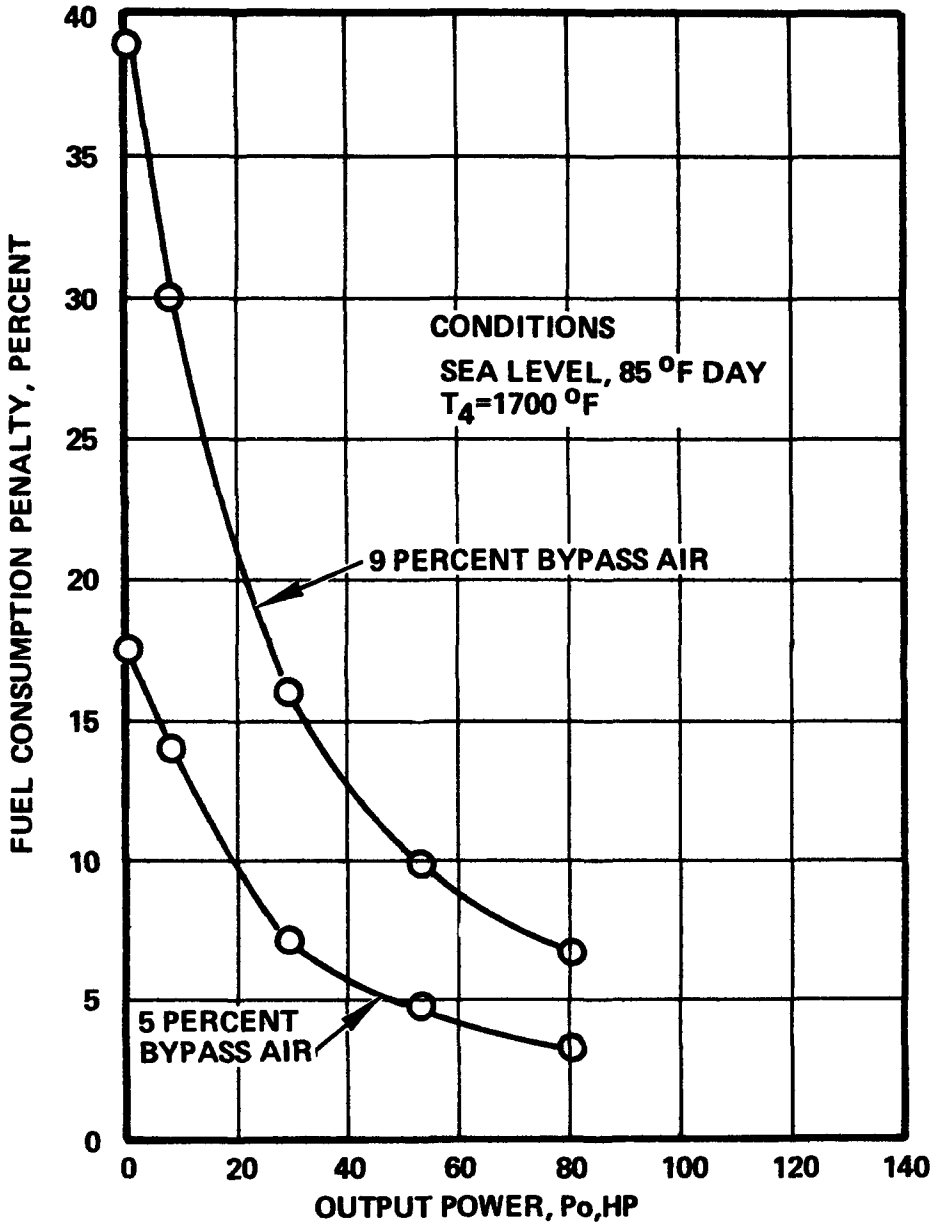

FIGURE 5-41

EFFECT OF RECUPERATOR BYPASS AIR ON PART LOAD FUEL CONSUMPTION

AIRESEARCH EMISSION TEST SUMMARY

ENGINE=EPA S/N=0AP COMB P/N=SKP26489SDTEST DATE 6-19-72 FUEL=JP-4 P BARO= 28.60
RAT THR= 0. RA EGT,F= 0. RAT SPD= 0. DEW PT,F= 15. REL HUM= 0.00 SPEC HUM= .001758
FUEL H/C= 1.9900 STOI F/A= .06781 L H V= 18520. S LN T,F= 0.0 FLO,L/M= 0.000 SL TIM,S= 0.0000

Data Point Number	1	2	3A	3	4A	4	5	6
Percent Bypass	2.9	5.0	9.9	9.8	15.0	15.0	5.0	4.9
Bypass Air Temperature, 300°							200°	400°
Burner Inlet Temp., Deg F	1060	1062	1060	1062	1060	1050	1055	1047
FA RATIO CALC. FROM EMISSION	.0065	.0063	.0072	.0064	.0082	.0058	.0062	.0063
EQUIVALENCE RATIO	.096	.093	.106	.094	.120	.085	.091	.093
COMB EFFIC FROM EMISSIONS	99.892	99.932	99.570	97.688	96.586	93.010	99.909	99.924
SUMMARY OF REDUCED EMISSION DATA								
CARBON DIOXIDE								
PERCENT BY VOLUME, WET	1.33	1.29	1.47	1.27	1.59	1.03	1.27	1.29
PERCENT BY VOLUME, DRY	1.35	1.31	1.49	1.29	1.62	1.05	1.29	1.31
LB. CO2 PER LB. OF FUEL	3.13	3.14	3.12	3.04	3.00	2.73	3.13	3.14
WEIGHT FLOW, LB./HR.	50.8	50.8	55.9	49.2	64.4	45.1	50.8	50.8
CARBON MONOXIDE								
PPM BY VOLUME, WET	27.6	15.6	51.9	227.0	377.4	1330.9	21.6	17.6
PPM BY VOLUME, DRY	28.0	15.8	52.7	229.9	383.6	1346.4	21.9	17.8
LB. PER 1000 LB. OF FUEL	4.138	2.417	7.009	34.587	45.126	224.017	3.392	2.724
WEIGHT FLOW, LB./HR.	.067	.039	.125	.560	.970	3.696	.055	.044
UNBURNED HYDROCARBONS- PPM AS CARBON, WEIGHTS AS CH4								
PPM BY VOLUME, WET	1.5	1.5	39.1	195.6	391.1	204.6	1.5	1.5
PPM BY VOLUME, DRY	1.5	1.5	39.7	198.1	397.5	207.0	1.5	1.5
LB. PER 1000 LB. OF FUEL	.129	.133	3.019	17.032	26.733	19.683	.135	.133
WEIGHT FLOW, LB./HR.	.002	.002	.054	.276	.575	.325	.002	.002
RATIO LB HC/LB CO	.0312	.0551	.4308	.4924	.5924	.0879	.0398	.0489
NITRIC OXIDE (NO) - WEIGHTS AS NO2								
PPM BY VOLUME, WET	58.2	33.1	6.5	2.0	9.0	4.0	31.6	35.6
PPM BY VOLUME, DRY	59.0	33.5	6.6	2.0	9.2	4.1	32.0	36.1
LB. PER 1000 LB. OF FUEL	14.336	8.416	1.446	.502	1.773	1.109	8.155	9.052
WEIGHT FLOW, LB./HR.	.232	.136	.026	.008	.038	.018	.132	.147
NITROGEN DIOXIDE (NO2)								
PPM BY VOLUME, WET	6.0	3.5	2.5	1.5	11.0	0.0	3.5	3.0
PPM BY VOLUME, DRY	6.1	3.6	2.5	1.5	11.2	0.0	3.6	3.0
LB. PER 1000 LB. OF FUEL	1.483	.893	.556	.377	2.167	0.000	.906	.765
WEIGHT FLOW, LB./HR.	.024	.014	.010	.006	.047	0.000	.015	.012
TOTAL OXIDES OF NITROGEN (NO+NO2) AS NO2								
PPM BY VOLUME, WET	64.2	36.6	9.0	3.5	20.1	4.0	35.1	38.6
PPM BY VOLUME, DRY	65.1	37.1	9.2	3.6	20.4	4.1	35.6	39.1
LB. PER 1000 LB. OF FUEL	15.819	9.309	2.002	.879	3.940	1.109	9.061	9.817
WEIGHT FLOW, LB./HR.	.256	.151	.036	.014	.085	.018	.147	.159

NOTES 1.ALL EMISSIONS CONCENTRATIONS CORRECTED TO CONCENTRATION IN WET OR DRY EXHAUST FROM COMBUSTION WITH DRY AIR.
2.EQUIVALENCE RATIO CALCULATED FROM CO2,CO,AND HC DATA AND FUEL COMPOSITION.
3.MASS EMISSIONS OF NO, NO2, AND NO+NO2 CALCULATED AS NO2 FROM CONCENTRATIONS WITH MOLECULAR WEIGHT OF NO2 (46.01).
4.COMBUSTION EFFICIENCY CALCULATED FROM CO,AND UHC AS VAPORIZED ORIGINAL FUEL ON LB/ LB FUEL BASIS.

FIGURE 5-42

5.4 Test Period (8-10-72 to 11-15-72)

5.4.1 Test Results

Tests were conducted during the test period on several vaporizer combustor configurations and on the pneumatic impact injector combustor. The testing included operation with simulated recuperator bypass operation as well as at the zero bypass flow condition. The combustion rig modified for bypass simulation is shown in Figure 5-43.

(a) Bypass Simulation Plus Transverse Primary Jets - Fuel build-up on the outlet leg of the primary pipe at low fuel flows was observed during primary pipe fuel distribution tests. The combustor that had undergone the recuperator bypass simulation test was therefore modified (SKP26489M_3 SD) by the addition of three primary ports arranged as in Figure 5-44 to inject air at the primary pipe outlet leg to eliminate fuel cohesion at the pipe outlet at low power conditions and to reduce the local fuel-air ratio at the primary pipe discharge plane. This test was suggested by trends noted during testing on an earlier vaporizer configuration and substantiated by subsequent testing with recuperator bypass in an AiResearch GTPR36-61 Engine.

The GTPR36-61 engine tests had indicated that NO_x emission reductions could be attained by increasing the amount of air being injected through the primary ports. This trend held true up to the point where an additional 30 percent primary air was being introduced; beyond that point the combustor stability deteriorated. From these data it was decided that transverse primary ports injecting an additional 25 percent primary air would be satisfactory for the combustion rig recuperator bypass simulation test, and the combustor was so modified. The dilution ports were blocked off an equivalent amount to maintain the same overall pressure drop.

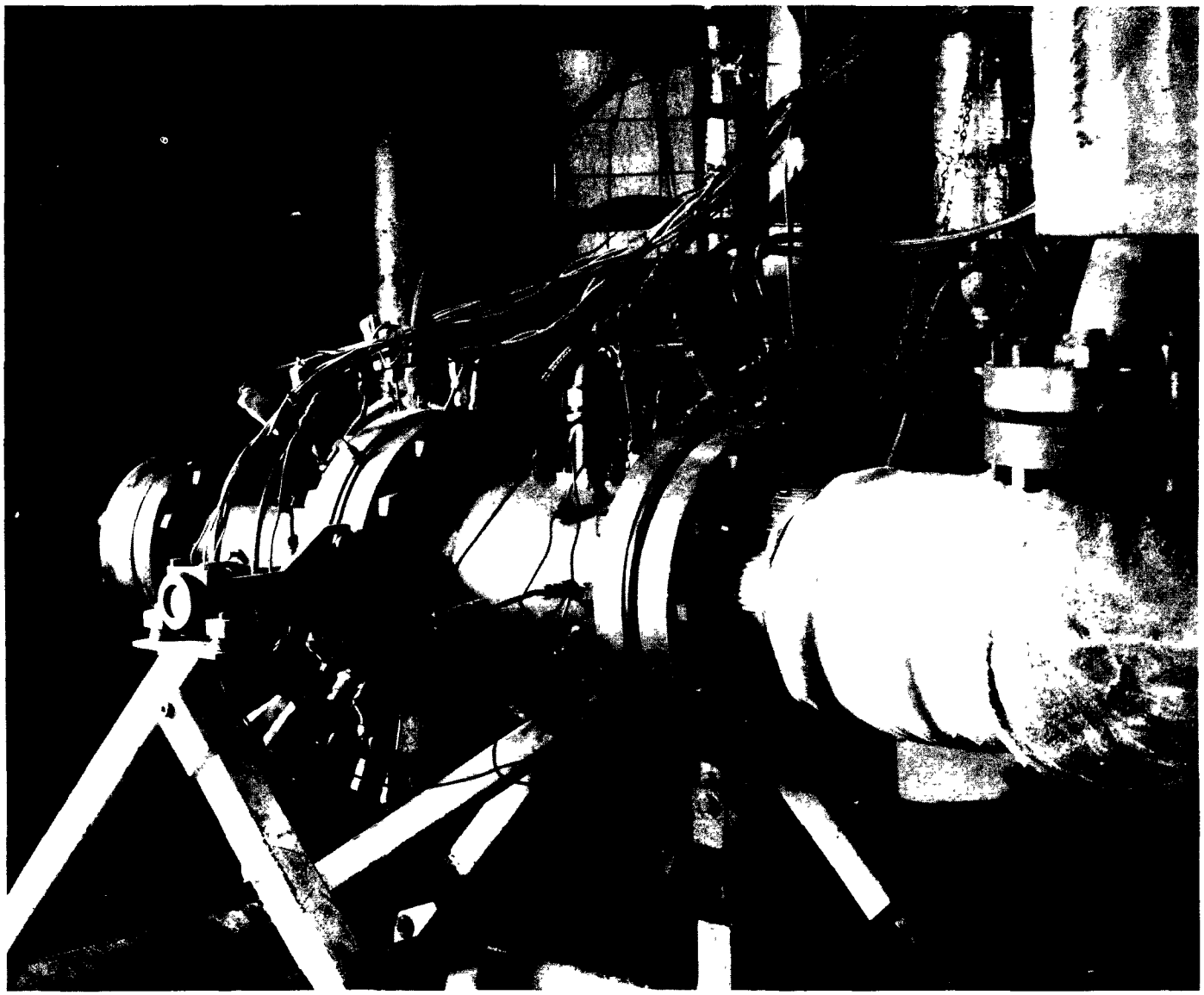

COMBUSTION RIG MODIFIED FOR BYPASS SIMULATION

FIGURE 5-43

EARLY QUENCH COMBUSTOR

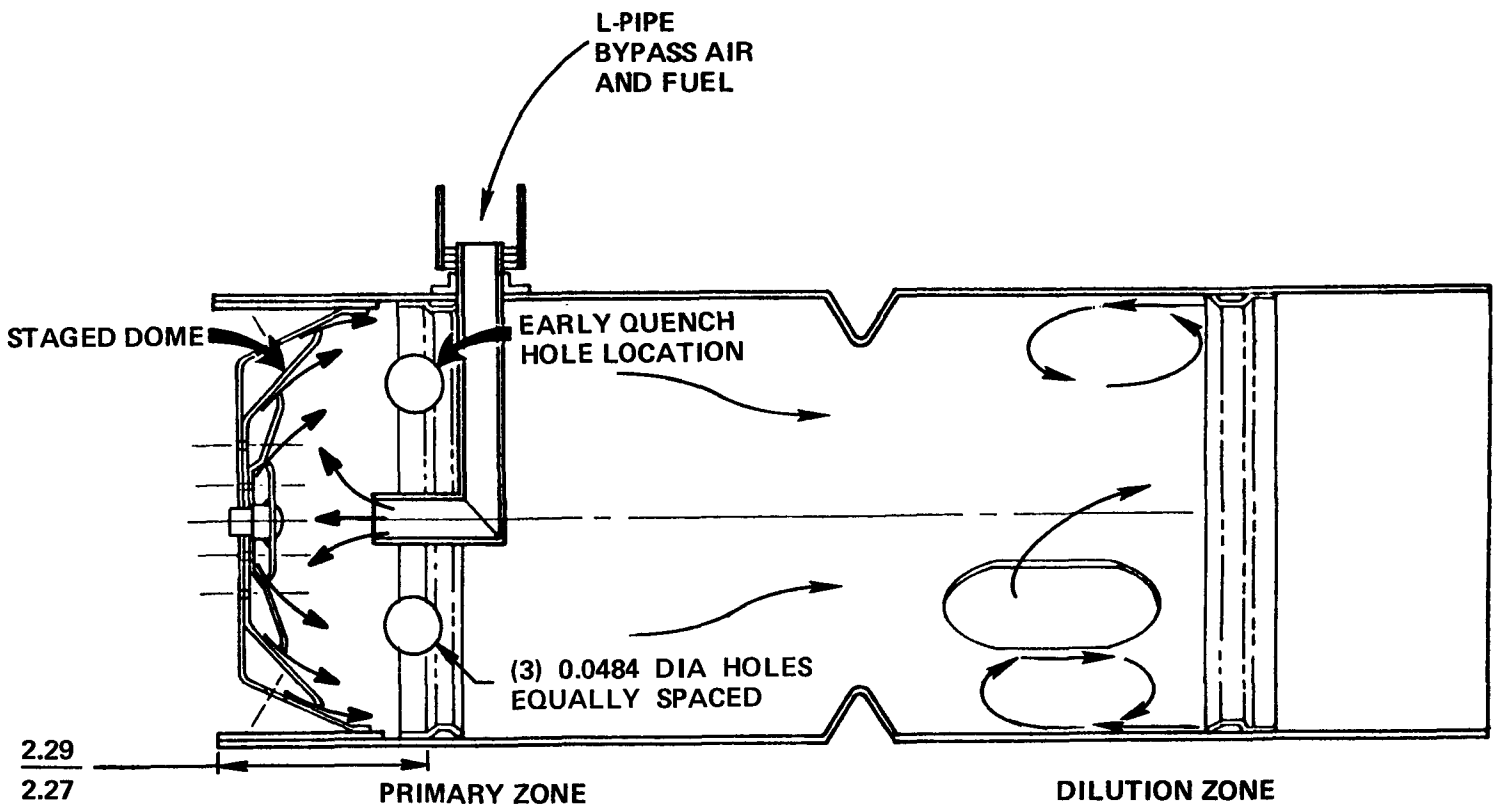

SKP26489-M3(SD)
L-PIPE COMBUSTOR (STAGED DOME) WITH
EARLY PRIMARY ZONE QUENCHING HOLES

FIGURE 5-44

FEATURE

PROVIDE EARLY N–O REACTION QUENCHING

The test was conducted at pressure and flow conditions corresponding to the 29.5 hp power condition in order to compar results with the original bypass test without primary jets. Test results are compared in Figures 5-45, 5-46, and 5-47. The data showed similar NO_x reduction potential to the earlier test, but the drop-off in combustion efficiency associated with bypass operation occurred at 10 percent rather than 15 percent bypass flow. This is because the primary jet configuration provides a leaner primary zone. Since the primary zone with transverse jets is already more lean than the nonjet combustor and the fact that bypass operation reduces the primary zone equivalence ratio and average temperature, less bypass flow may be added in a primary-port combustor before the stability limit of the combustor is reached.

(b) Bypass to Primary Pipe and Dome - Since the bypass test with primary jets verified that 10 percent bypass still gave the maximum NO_x reduction, it was concluded that without a change in the engine cycle, it was impractical to attempt to take advantage of the additional reduction potential demonstrated at lower bypass percentages. Instead, a modification was made to the combustor to attempt to introduce the bypass air into the combustor at lower pressure drop. To this end an additional bypass line was added to the system that delivered bypass air to a plenum attached to the combustor baseplate. A schematic of the dual-bypass combustor is shown in Figure 5-48 and a photograph of the dual-bypass combustion rig is shown in Figure 5-49. The bypass flow split was controlled by the area ratio between the L-pipe and the center baseplate rosette discharge annulus. This flow split was approxi mately 58 percent through the dome, and 42 percent through the L-pipe.

EARLY QUENCH RESULTS

TEST CONDITIONS

T_{IN} = 1060°F

P_{IN} = 31 IN. Hg G

T_{DISCH} = 1450°F

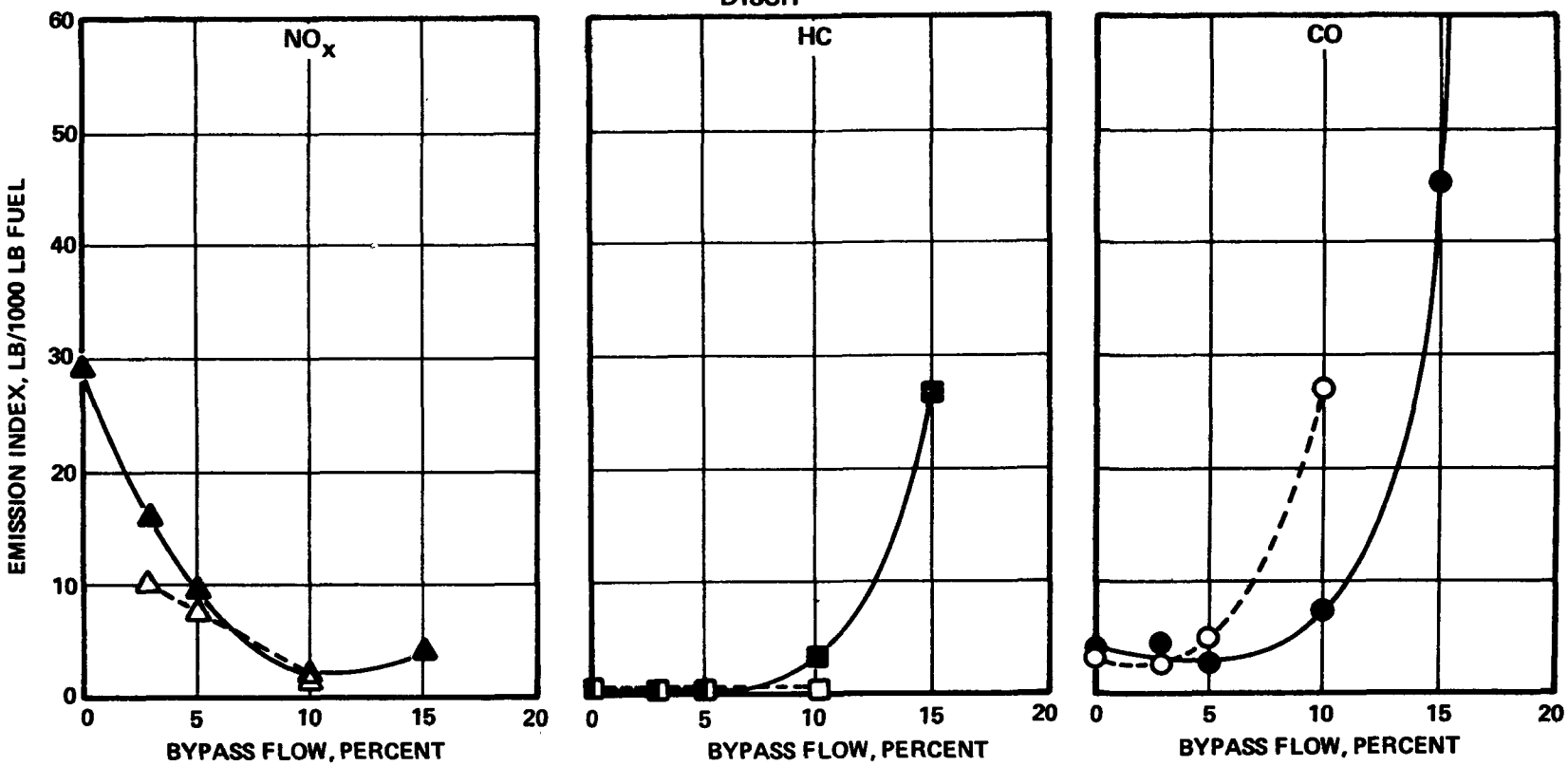

L-PIPE VAPORIZER (STAGED DOME) WITH BYPASS (SKP26489-SD)

L-PIPE VAPORIZER (STAGED DOME) WITH BYPASS PLUS TRANSVERSE PRIMARY AIR JETS (EARLY QUENCH) (SKP26489-M3 (SD)

FIGURE 5-45

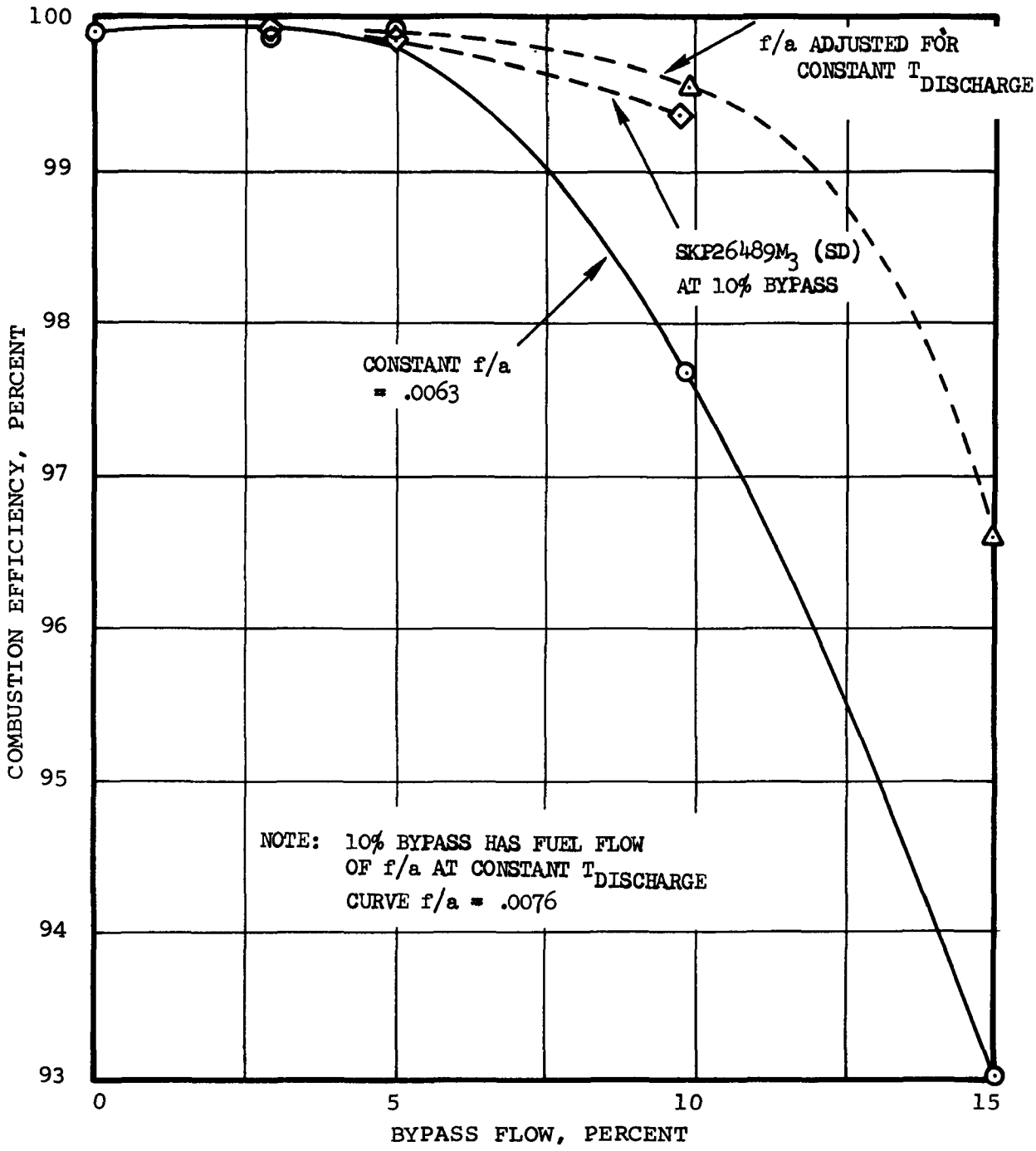

COMBUSTION EFFICIENCY COMPARISON BETWEEN VAPORIZOR COMBUSTORS MODIFIED FOR BYPASS ONLY AND BYPASS PLUS TRANSVERSE PRIMARY AIR JETS

FIGURE 5-46

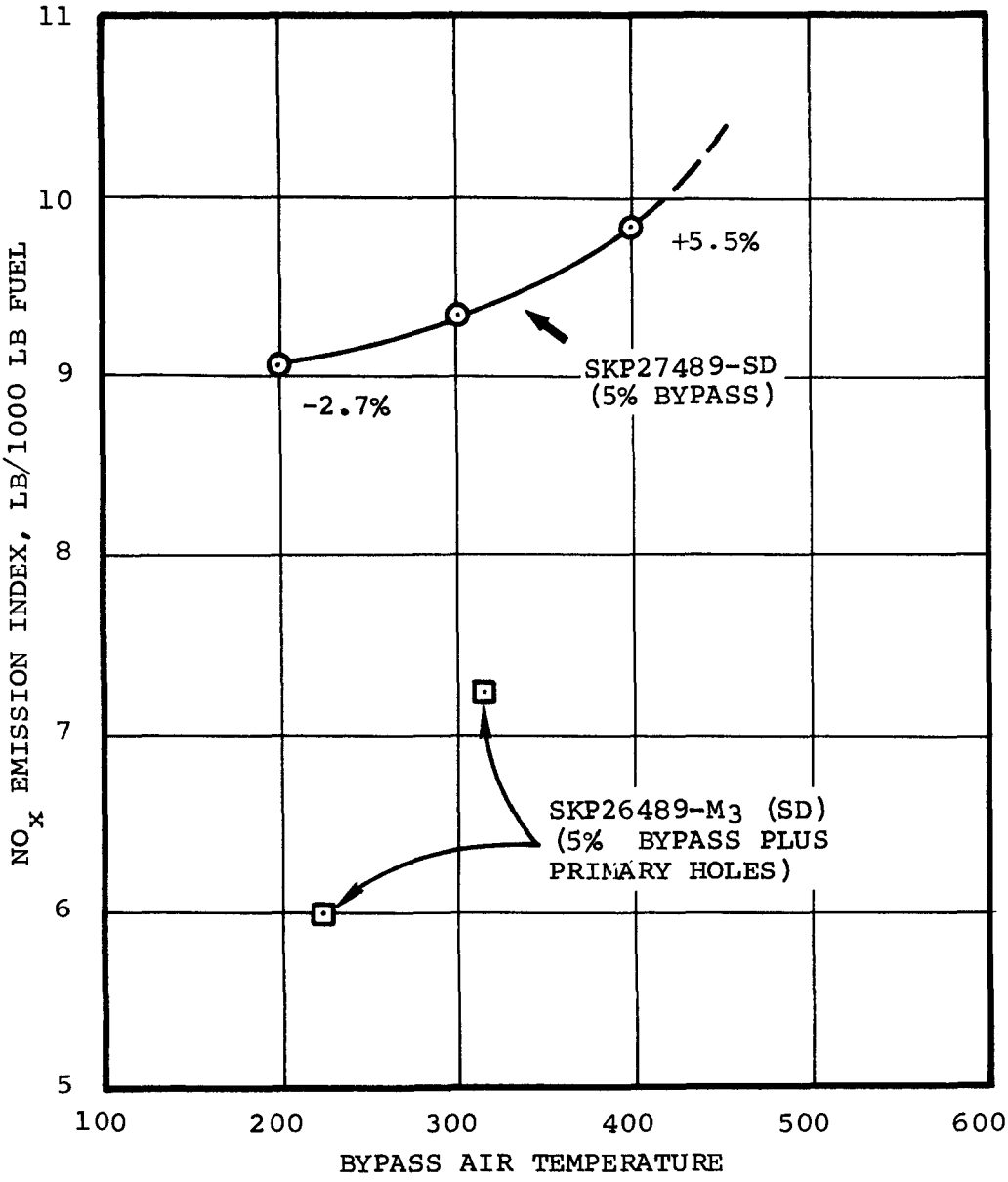

NO_x EMISSIONS COMPARISON BETWEEN VAPORIZER COMBUSTORS WITH 5% BYPASS AND 5% BYPASS PLUS PRIMARY HOLES

FIGURE 5-47

DUAL BYPASS CONCEPT

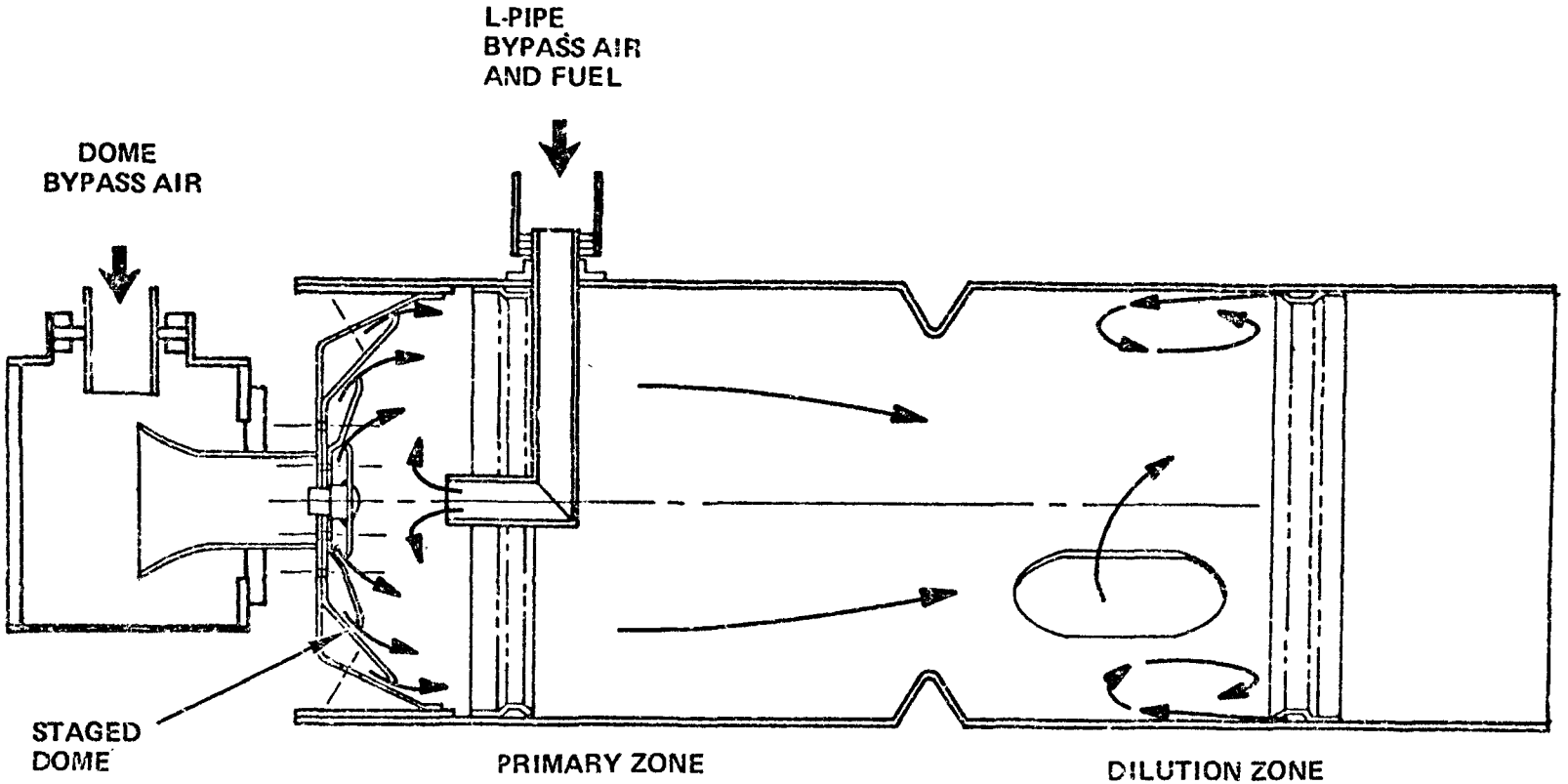

L-PIPE VAPORIZER COMBUSTOR (STAGED DOME)
WITH DUAL BYPASS AIR DELIVERY METHOD
[SKP26489-M3(SD)]

FIGURE 5-48

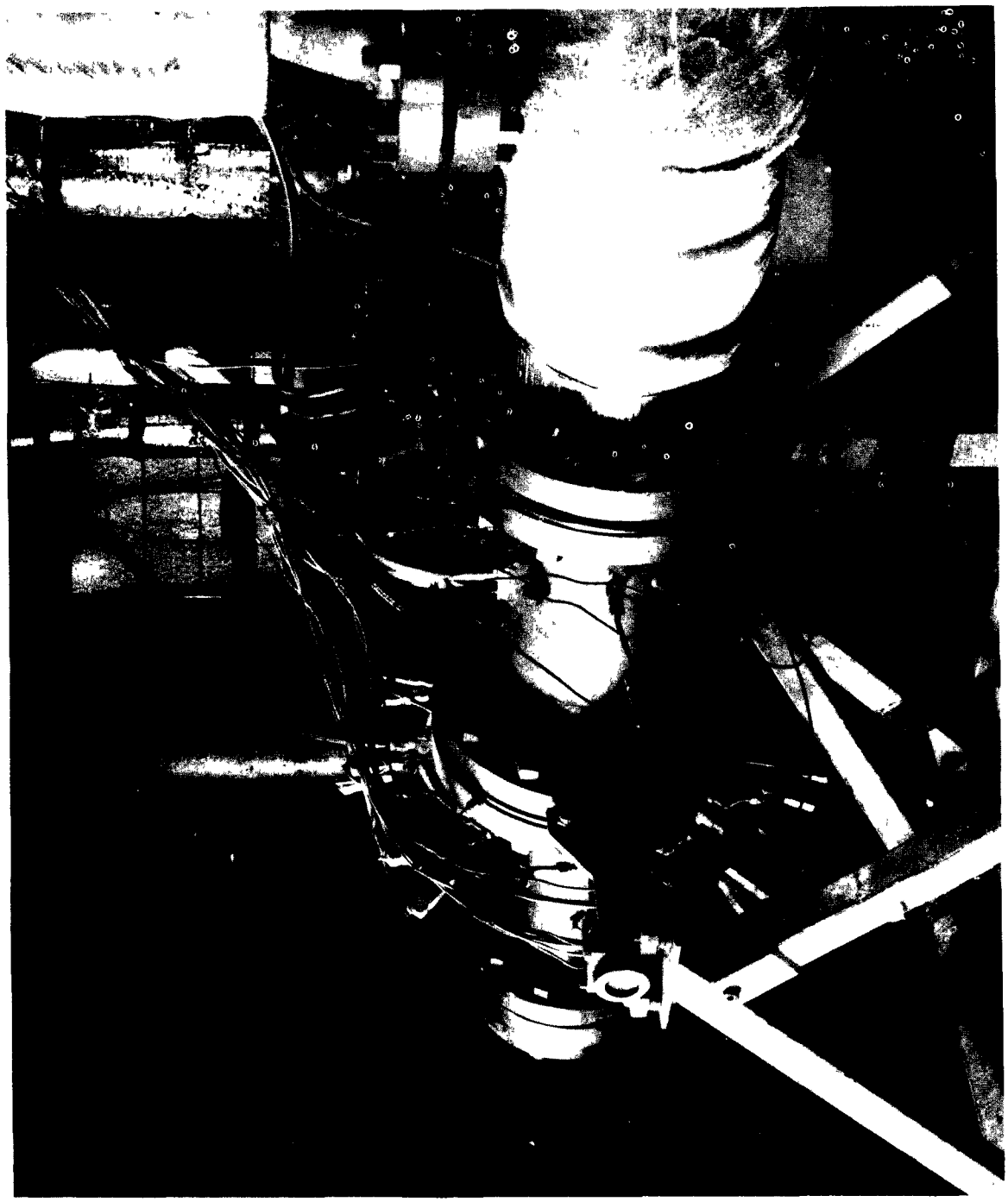

DUAL BYPASS COMBUSTION RIG

FIGURE 5-49

Test results for this configuration, again at the 29.5 hp flow and pressure conditions and maximum facility inlet temperature, are shown in Figure 5-50. The data essentially repeated that obtained with the original configuration with bypass through the primary pipe only, except that the deterioration in combustion efficiency at 15 percent bypass was more severe with the dual-bypass system (88.5 percent compared with 93.0 percent).

(c) L-Pipe Vaporizer With Staged Dome, SKP26489SD - Final Calibration - Because the dual bypass test indicated that by injecting all bypass air through the primary pipe at high pressure drop was not causing artificially low NO_x readings and because there appeared to be no advantage from an emissions standpoint in retaining the dual bypass system, it was decided to conduct the final test at 10 percent bypass through the primary pipe only. The primary objective of the test was to evaluate the effect of the recuperator bypass NO_x control concept at test conditions other than the 29.5 hp condition and to generate sufficient emissions data to predict a grams-per-mile value for the Federal Driving Cycle (FDC).

The test procedure consisted of testing at the pressure levels defined for the 5-point FDC simulation defined in Section 2.2. The flows were corrected up by a constant factor to maintain 3 percent combustor pressure drop, and the fuel flows were increased by a similar amount. Ten percent bypass flow was delivered through the primary pipe at a temperature corresponding to compressor discharge pressure at each of the 5 test conditions. The fuel flow was again increased to account for the performance penalty incurred as a result of the recuperator bypass operation; resultant fuel flow increase as a function of bypass percentage is shown in Figure 5-51.

DUAL BYPASS RESULTS

TEST CONDITIONS

T_{IN} = 1060°F

P_{IN} = 31 IN. Hg G

T_{DISCH} = 1450°F

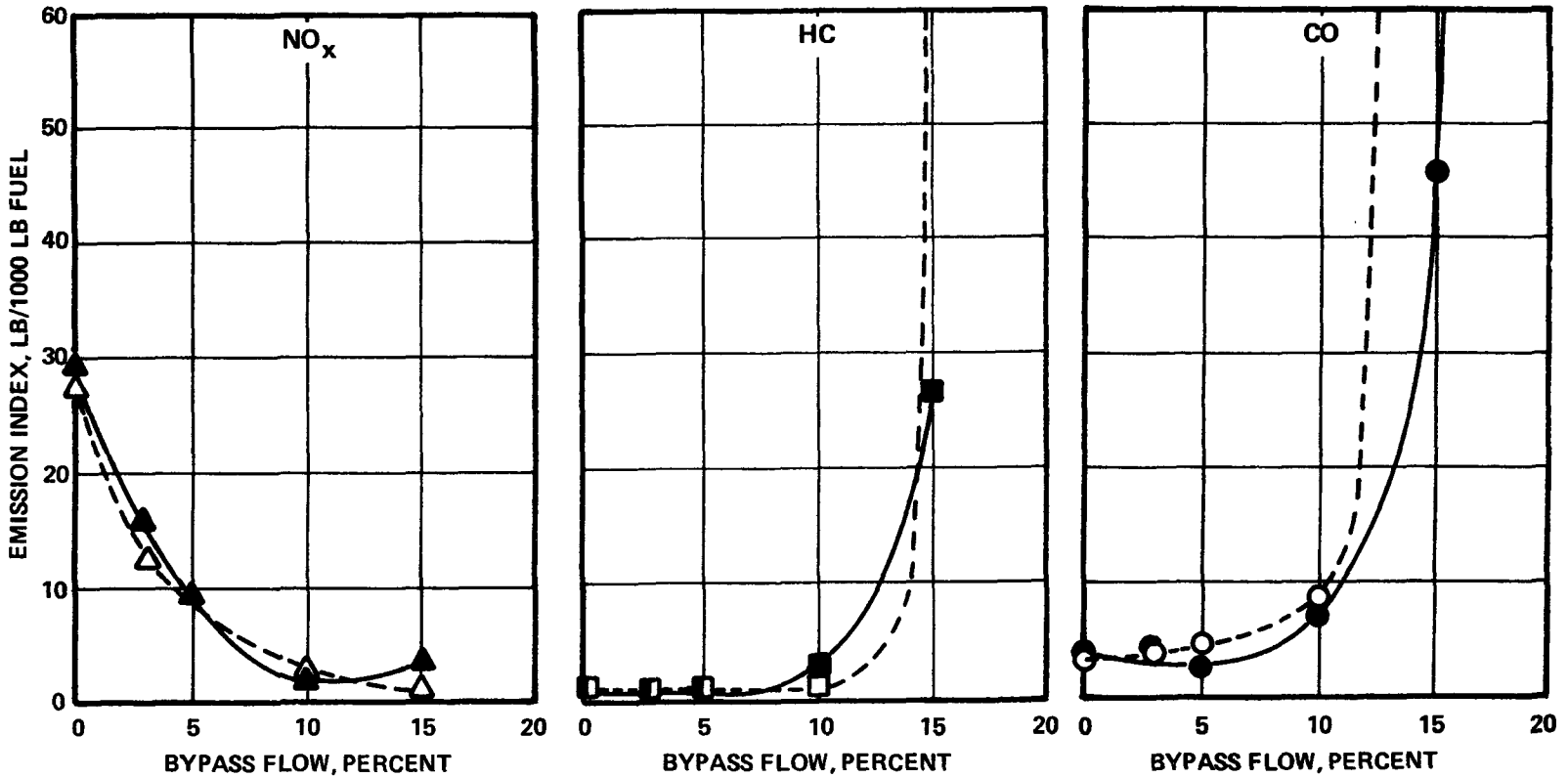

L-PIPE VAPORIZER (STAGED DOME) WITH BYPASS TO L-PIPE

SAME EXCEPT WITH BYPASS TO L-PIPE AND TO DOME

FIGURE 5-50

VAPORIZER COMBUSTOR SKP26489-SD

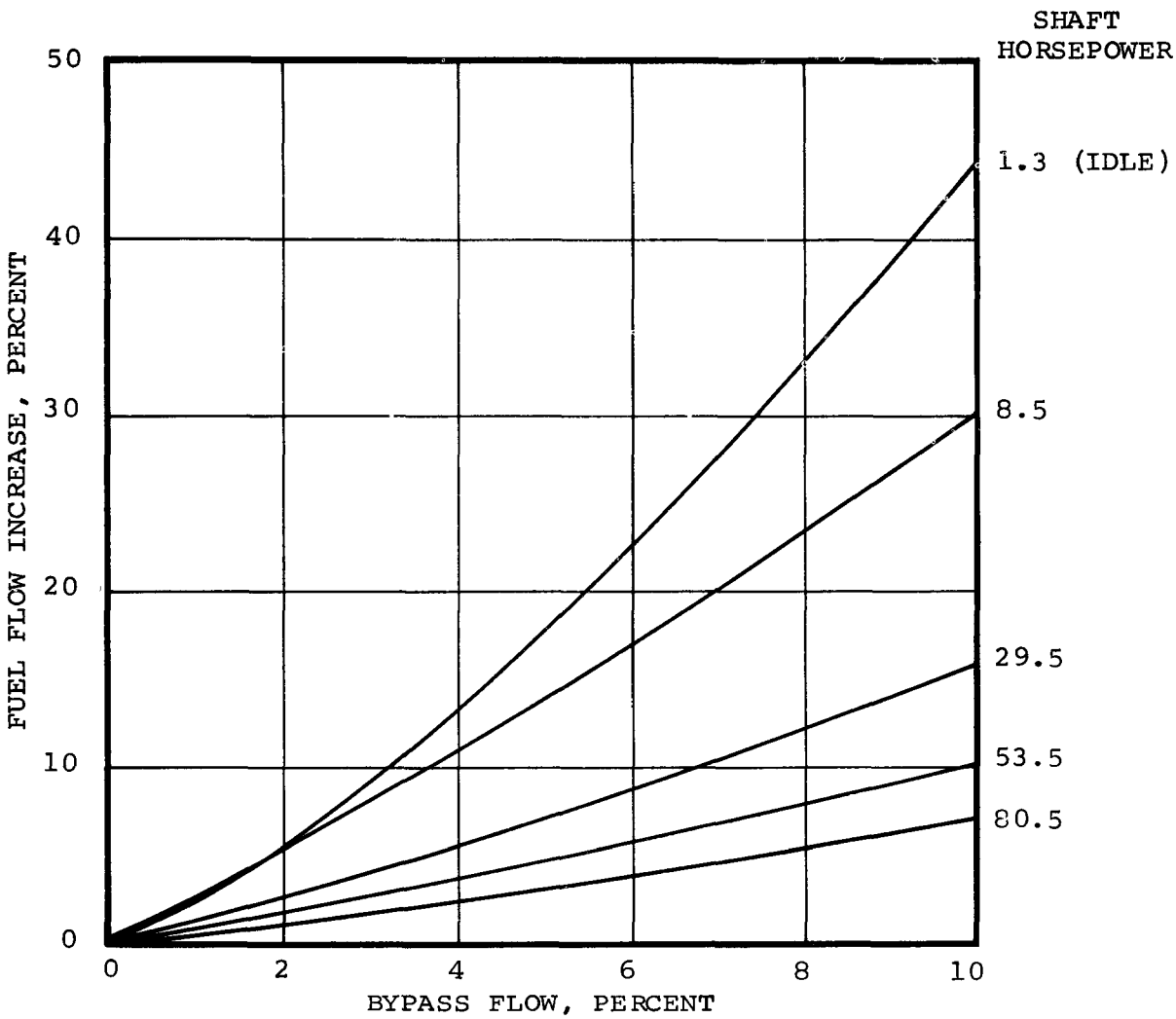

EFFECT OF RECUPERATOR BYPASS ON
FUEL CONSUMPTION AT PART-LOAD OPERATING CONDITIONS

FIGURE 5-51

It was intended that emissions data would be taken at constant airflow, fuel flow, bypass flow, and combustor inlet pressure at each of three inlet temperatures up to the capability of the facility in order to establish a means by which data could be extrapolated to the inlet temperatures defined by the cycle. While at the maximum combustor inlet temperature conditions, the facility preheater tube bundle developed an internal leak that precipitated a failure in the test rig combustor as a result of diverting air from the rig. The loss of air to the rig at constant fuel flow was accompanied by a step increase in the discharge temperature at which time the facility was shut down, but by that time the combustor was already destroyed.

Subsequent disassembly of the rig and visual inspection of the combustor indicated that failures had occurred in the baseplate and in the combustor liner at the first cooling skirt. Photographs of these failures are shown in Figures 5-52 and 5-53.

In order to complete the final test, both the preheater and the combustor required repair. A period of two months elapsed while repairs were being completed. The final testing was subsequently reinitiated in October, 1972.

(d) L-Pipe Vaporizer With Staged Dome, SKP26489SD - Final Calibration - This configuration is shown in Figure 5-54. Results of the continued final test are presented in Figures 5-54, 5-55, 5-56, and 5-57. The zero bypass data are shown in Figure 5-58 for reference. It can be seen from the data that a substantial reduction in NO_x emission is available with recuperator bypass with significant changes to CO and unburned hydrocarbon emissions.

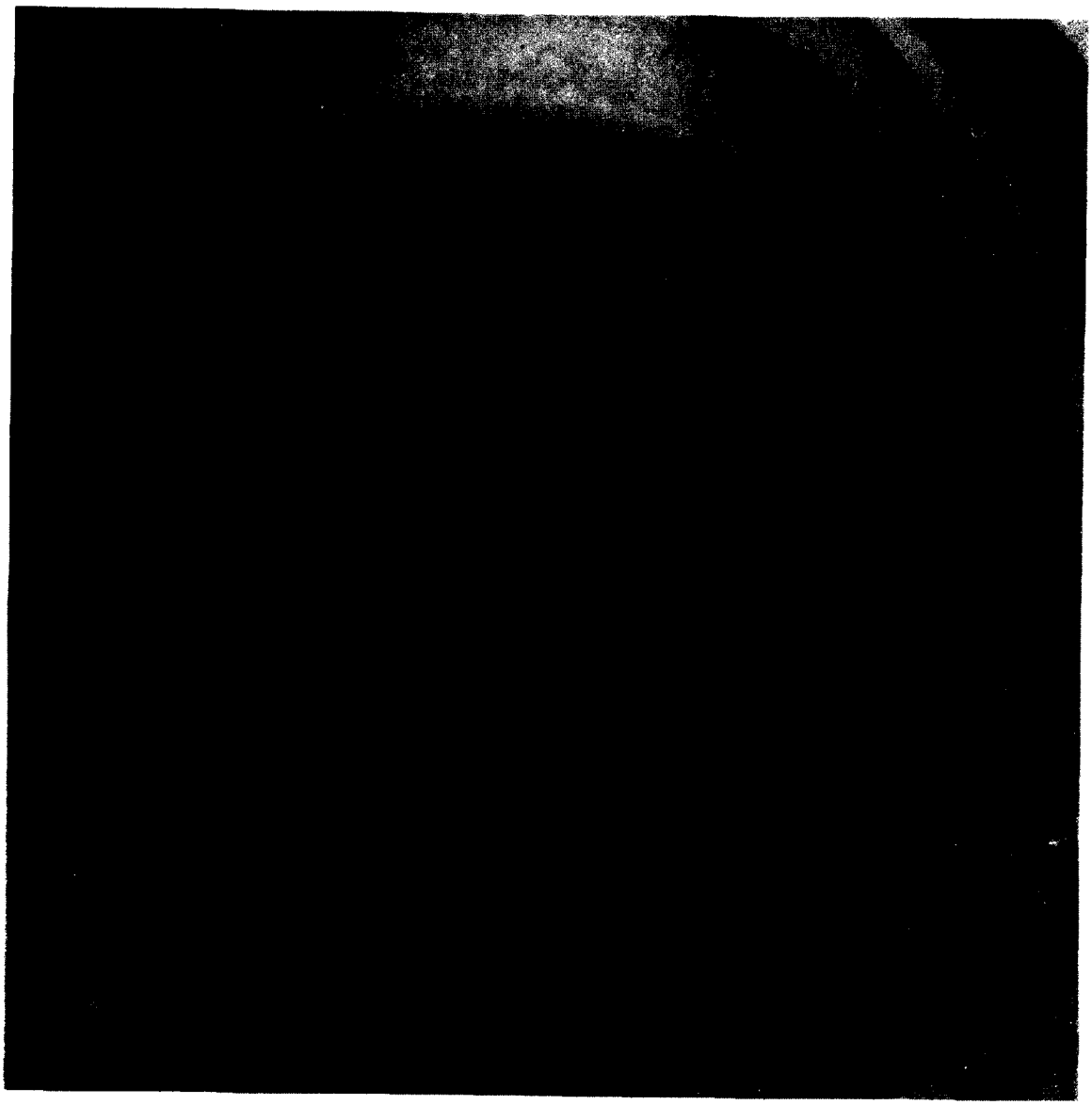

SKP26489-SD COMBUSTOR BASEPLATE FAILURE

FIGURE 5-52

SKP26489-SD COMBUSTOR LINER FAILURE

FIGURE 5-53

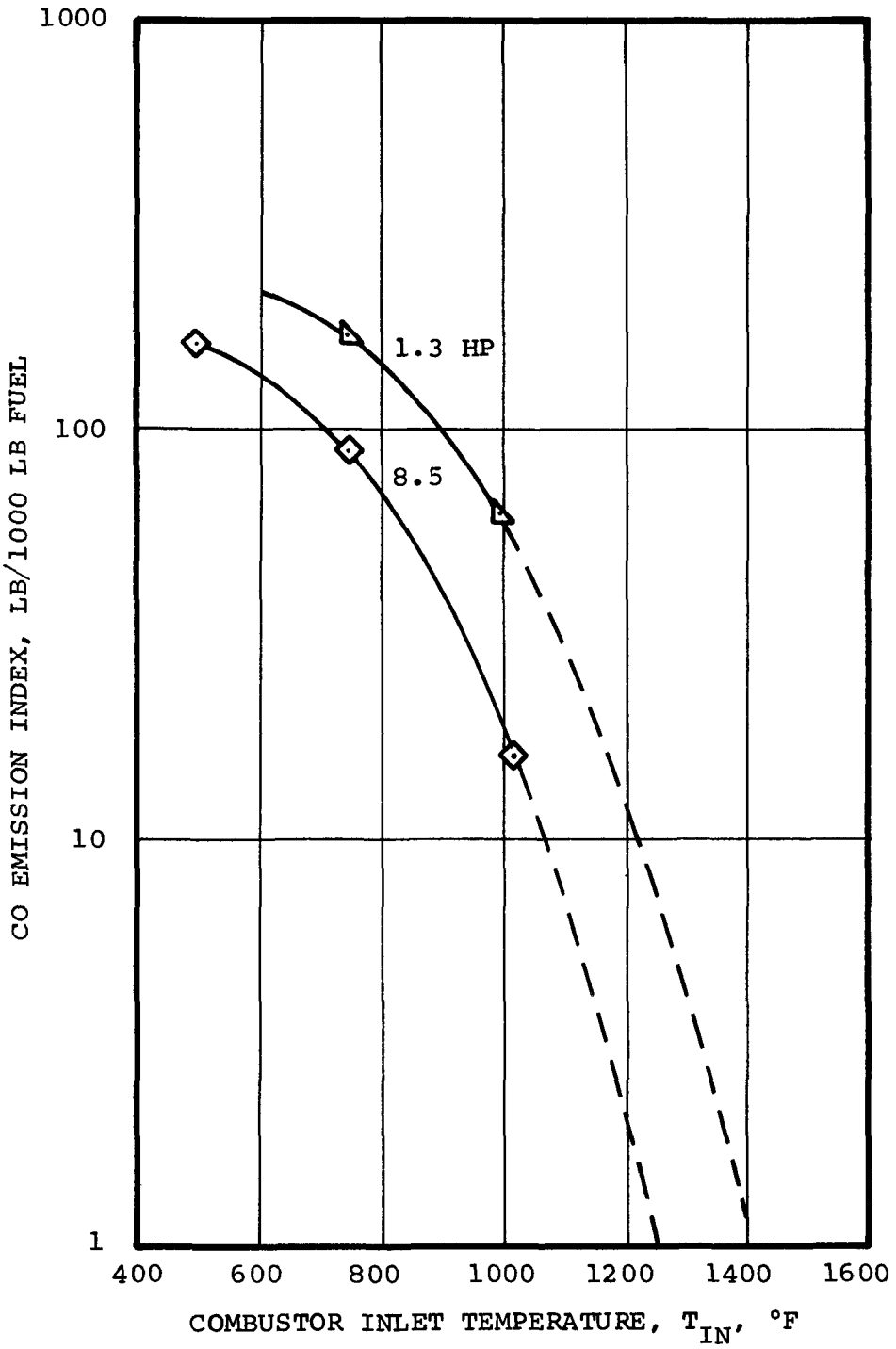

CO EMISSION RESULTS FROM COMBUSTOR SKP26489-SD
WITH 10% BYPASS AIR THROUGH PRIMARY PIPE ONLY

FIGURE 5-54

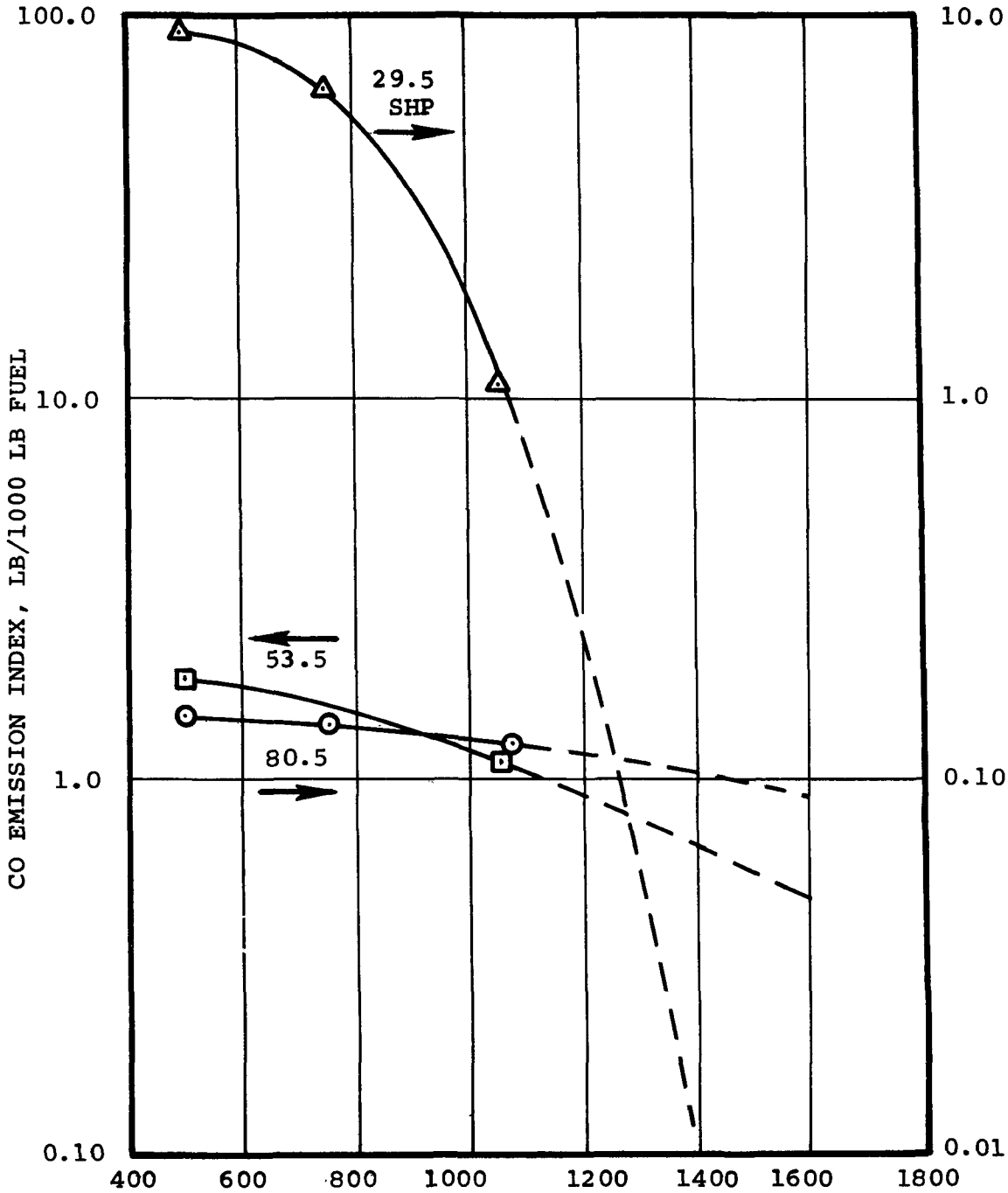

CO EMISSION RESULTS FROM COMBUSTOR SKP26489-SD
WITH 10 PERCENT BYPASS AIR THROUGH PRIMARY PIPE ONLY

FIGURE 5-55

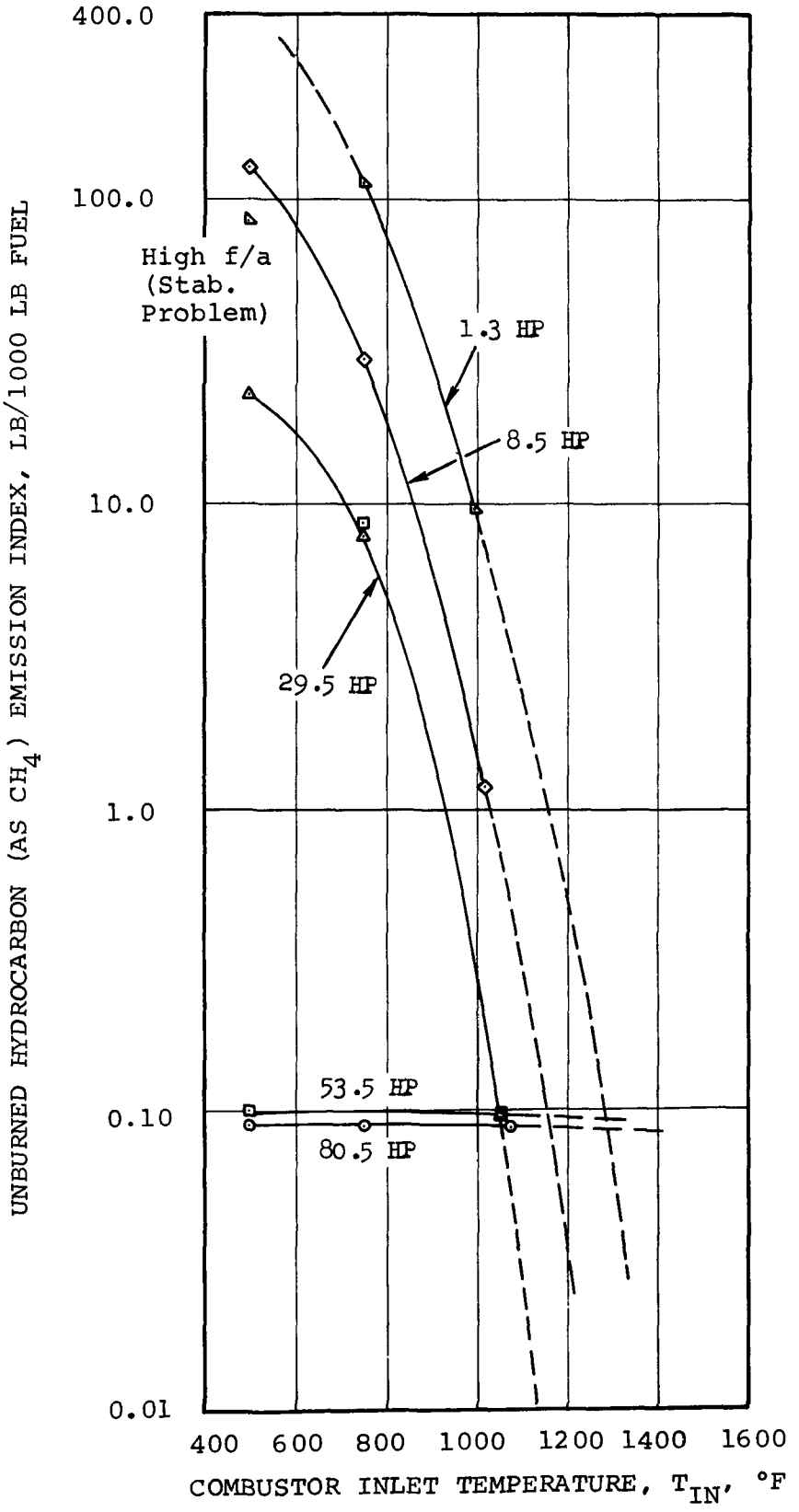

HYDROCARBON EMISSION RESULTS FROM COMBUSTOR
SKP26489-SD WITH 10 PERCENT BYPASS AIR THROUGH PRIMARY PIPE ONLY

FIGURE 5-56

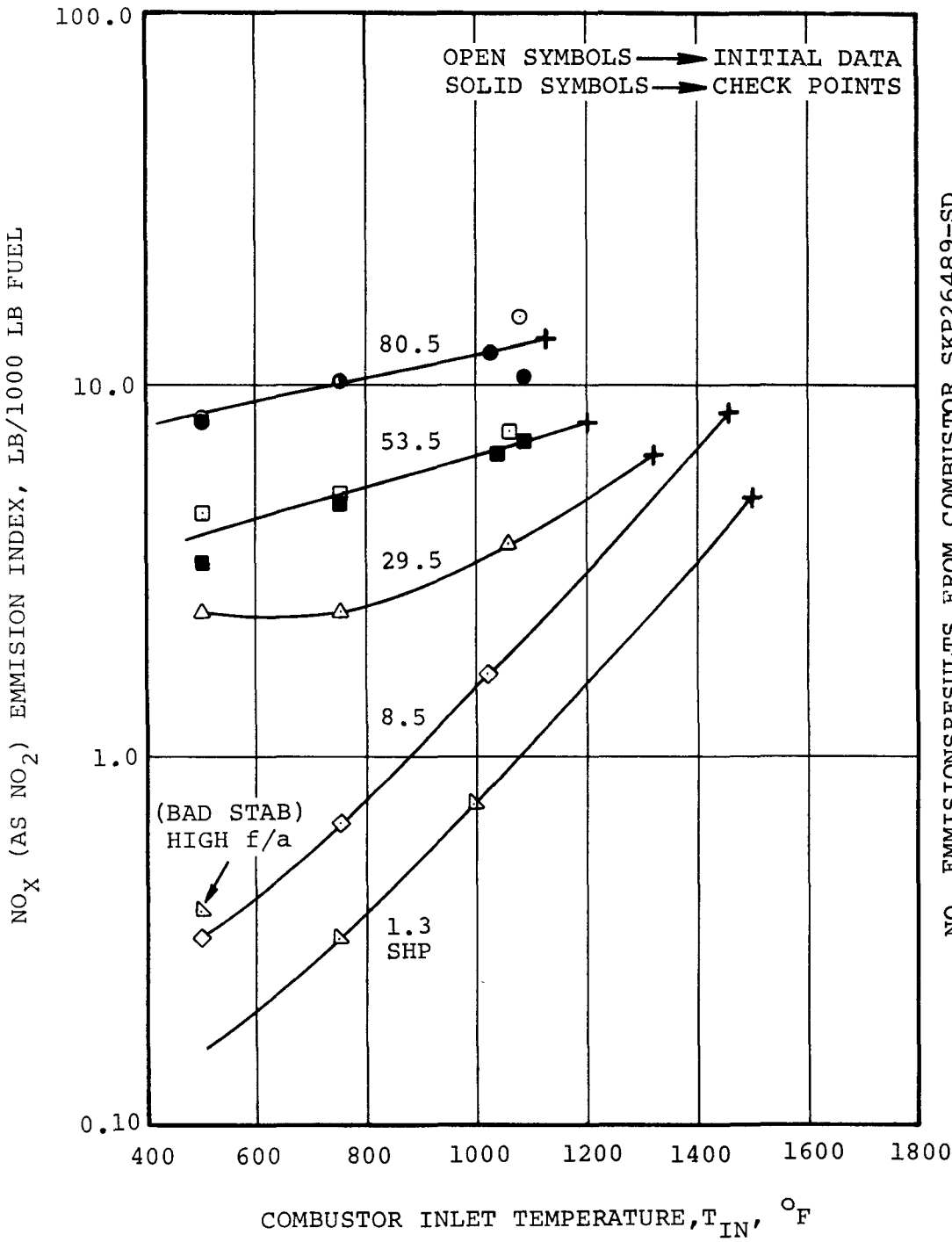

NOx EMMISIONSRESULTS FROM COMBUSTOR SKP26489-SD
WITH 10 PERCENT BYPASS AIR THROUGH PRIMARY PIPE ONLY

FIGURE 5-57

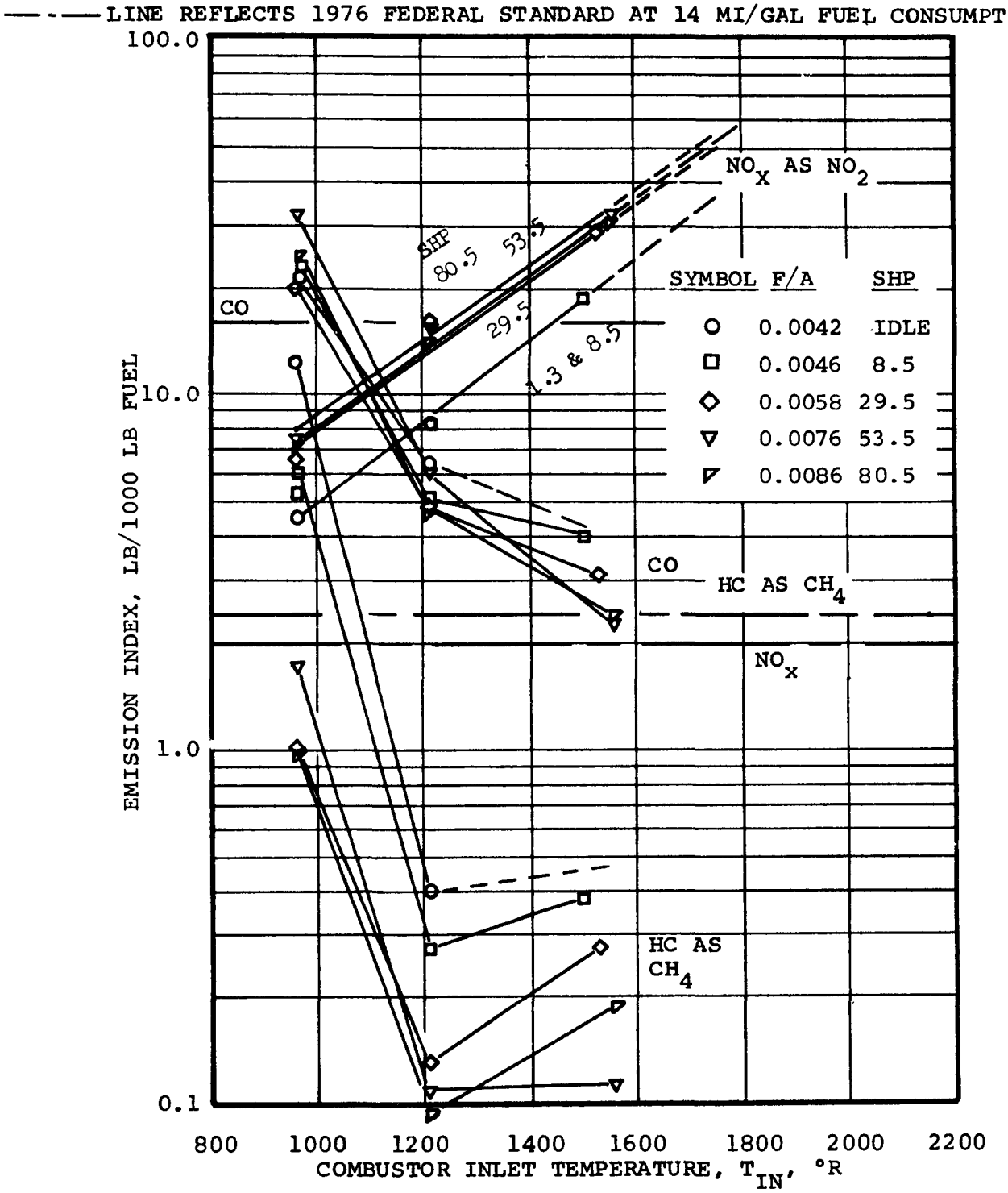

VAPORIZER COMBUSTOR - SKP26489SD
(ZERO BYPASS)

FIGURE 5-58

(e) SKP26489SD Vaporizer - OAP 6-Point FDC Simulation - After completion of the initial final calibration testing of the L-pipe vaporizer combustor with staged dome, represented by the initial data shown on Figure 5-57, a test was conducted using the OAP 6-point simulation procedures. Some operating conditions of the AiResearch 5-point test and the OAP 6-point test were then repeated by additional runs to determine if the emissions performance had changed because of distortion of the dome by the combustion. The check run results for the AiResearch 5-point testing are superimposed on Figure 5-57. Significant emissions differences were measured during these check runs, and it was decided to repeat the OAP test with a newly fabricated dome of identical design.

The OAP test results and calculations are tabulated in Figure 5-59 for the five test points at 10 percent bypass with the distorted dome. The emission index values are given for each test condition. Fuel flows and fuel-air ratios were adjusted during the test to account for the estimated fuel consumption penalty, as in all previous testing.

All emissions were above the 1976 standards. However, it can be seen that 98 percent of the HC and 94 percent of the CO comes from points 2 and 3. It was thought that dome distortion in combination with a high bypass ratio may have been excessively leaning out the primary zone during these low heat-release points.

The dome was then replaced with a new one of identical design. The test was repeated and extended to include variable bypass operation (6 percent, 8 percent, and 10 percent) at OAP test points 2 and 3. Figures 5-60 and 5-61 show the variable bypass results for points 2 and 3, respectively. These figures, along with the EI values from the other test points, were then used to predict the emission at several assumed variable-bypass schedules. The results were as follows:

OAP 6-POINT SIMULATED FEDERAL DRIVING CYCLE MASS EMISSIONS
WITH 10-PERCENT RECUPERATOR BYPASS AIR
(DISTORTED DOME)

NO_x

POINT	EI	X	KFc*	=	EIxKxFc	EIxKxFc/7.5
1	0.96		0.045		0.043	(0.0058)
2	0.394		0.580		0.228	(0.0305)
3	1.14		0.447		0.453	(0.0679)
4	1.84		0.478		0.880	68% { (0.117)
5	4.25		0.447		1.900	{ (0.253)
6	13.28		0.035		0.465	(0.061)
					3.969	÷ 7.5 = 0.53 gm/mi

(At 0% bypass, the gm/mi was 4.67 or a 77% reduction from the original burner NO_x emission)

CO

POINT	EI	X	KFc	=	EIxKxFc	EIxKxFc/7.5
1	<1.0		0.045		<0.045	(<0.006)
2	58.4		0.580		33.87	94% { (4.514)
3	8.5		0.447		3.80	{ (0.507)
4	3.84		0.478		1.84	(0.245)
5	<0.1		0.447		0.045	(<0.006)
6	12.72		0.035		0.445	(0.059)
					40.05	÷ 7.5 = 5.3 gm/mi

HC

POINT	EI	X	KFc	=	EIxKxFc	EIxKxFc/7.5
1	<0.1		0.045		<0.0045	(<0.0006)
2	7.1		0.580		4.118	98% { (0.549)
3	3.58		0.447		1.600	{ (0.213)
4	0.24		0.478		0.115	(0.015)
5	<0.01		0.447		<0.0045	(<0.0006)
6	0.29		0.035		0.010	(0.0013)
					5.852	÷ 7.5 = 0.78 gm/mi

*Fc = W_f at 10% BP/W_f at 0% BP

FIGURE 5-59

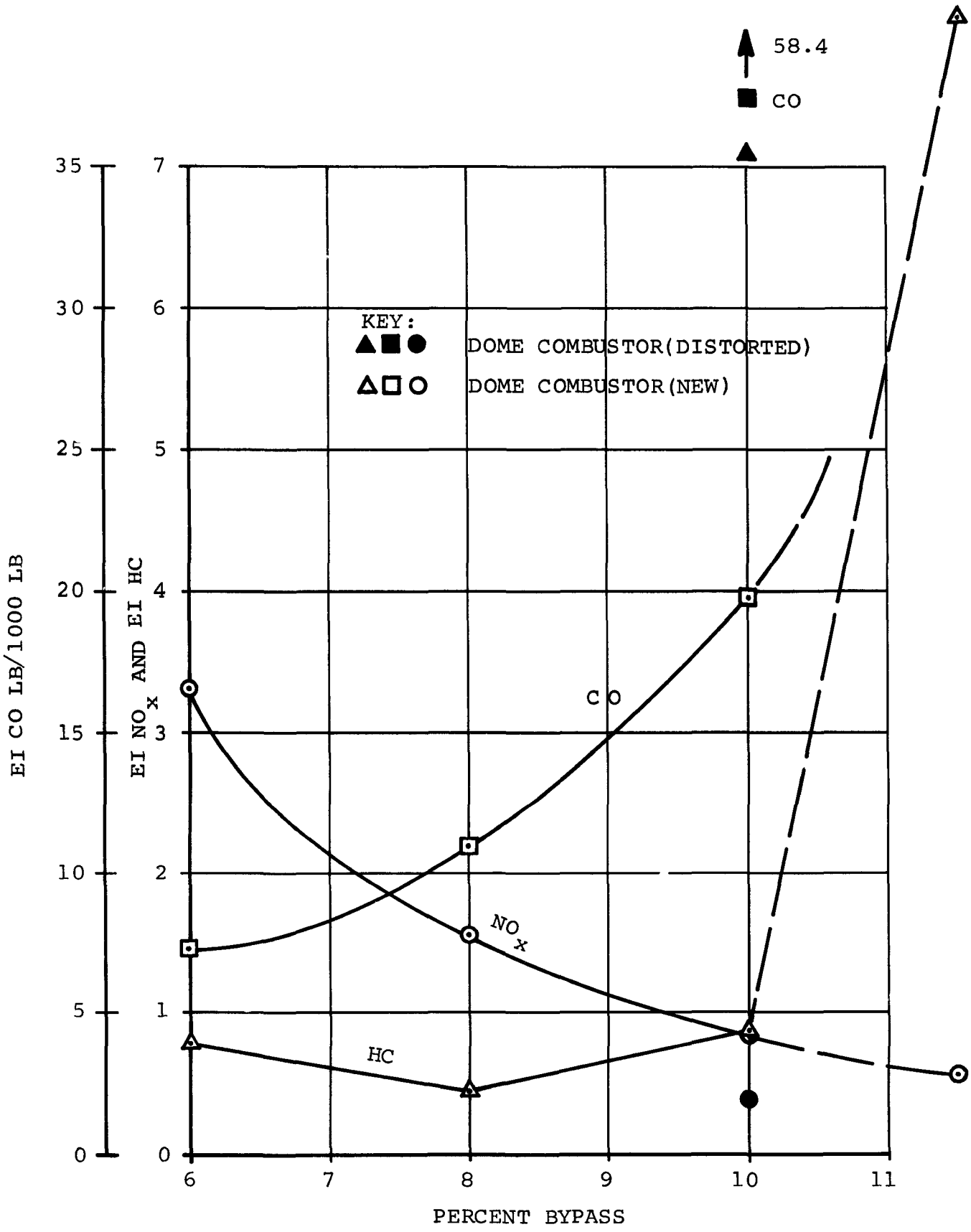

EFFECT OF BYPASS AT OAP CONDITION 2

FIGURE 5-60
AT-6097-R12
Page 5-96

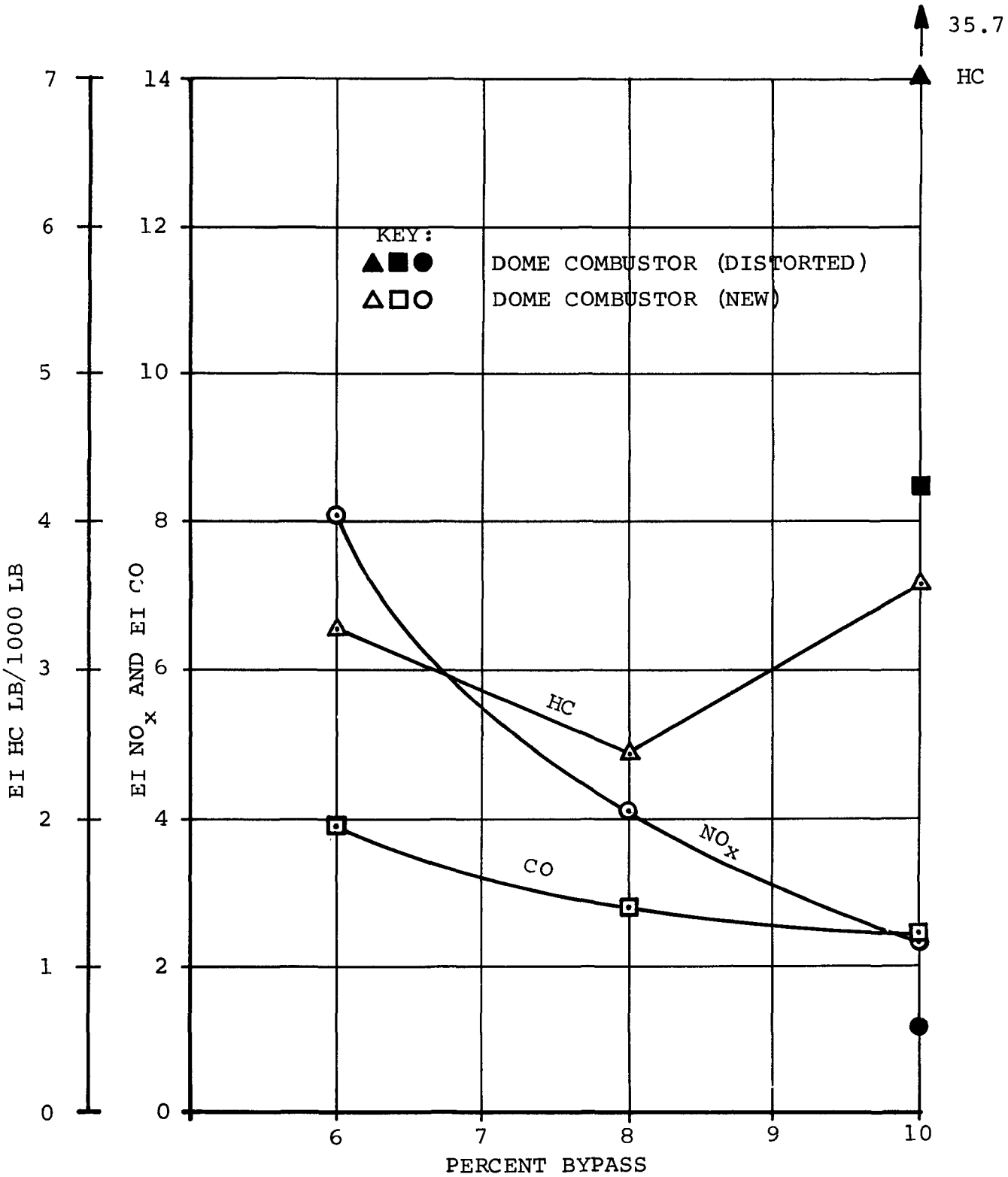

EFFECT OF BYPASS AT OAP TEST CONDITION 3

FIGURE 5-61

TABLE 5-6

EFFECT OF VARIABLE BYPASS

Schedule No.	Configuration	Assumed BY Variations		Emissions, gm/mi		
		OAP Test Point	Percent Bypass	NO_x	HC	CO
1	Distorted dome	All	10	0.53	0.78	5.3
1	New dome	All	10	0.66	0.12	1.90
2	New dome	1,3,4,5,6 2	10 9 1/2+	0.66	0.09	1.82
3	New dome	1,3,4,5,6 2	10 7	0.78	0.09	0.90
4	New dome	1,4,5,6 2,3	10 8	0.80	0.06	1.19

5.4.2 Discussion of Test Results

The various tests conducted on Class A vaporizer combustors, in conjunction with the recuperator bypass concept, established several trends that warrant further investigation. These findings are discussed below in the order in which the tests were conducted.

(a) Bypass Simulation Plus Transverse Primary Jets - Figure 5-45 presents additional NO_x reduction over and above that available from bypass alone and appears to be attainable at low bypass percentages, with primary air jets. Specifically, the data show that the NO_x emission reduction in percent, changes from 46 to 66 at 3 percent bypass and from 68 to 76 at 5 percent bypass with the addition of primary jets at the 29.5 hp test condition flow and inlet pressure and maximum available test temperature. These data suggest that this combined method of NO_x control might be attractive in an automotive application with a schedule of combustor inlet

temperatures optimized with respect to the reduction of NO_x emissions over the range of engine operating conditions. The bypass flow percentage required would then be optimized to the lowest value to minimize the fuel consumption penalty associated with bypass operation thereby improving overall engine performance.

Note that the benefit derived from the primary jets decreases with increasing bypass percentage. This is attributed to the effects of the bypass operation and the primary jets simultaneously acting to reduce primary zone equivalence ratio (hence, combustion efficiency). At the lower bypass percentages the primary pipe internal fuel-air ratio is above the rich extinction level and the air injected through the primary jets is required to complete combustion. At 10 percent bypass, however, the internal fuel-air ratio is slightly below stoichiometric such that combustion can be completed prior to the point of influence of the primary jets. The bypass ratio at which the primary pipe internal fuel-air ratio decreases to stoichiometric is the apparent point at which there is no further effect of transverse primary jets. For example, the internal fuel-air ratios at 3, 5, and 10 percent bypass are approximately 0.21, 0.13, and 0.065 at the 29.5 hp test conditions.

(b) Bypass to Primary Pipe and Combustor Dome - As was illustrated in Figure 5-46 the dual bypass arrangement appears to have potential for additional NO_x emission reduction at bypass percentage in excess of 10 percent. This is in contradiction with the test results for the single bypass system in which a NO_x emission increase was noted in going from 10 to 15 percent bypass. Further testing is required to establish the validity of these trends and to determine the ultimate benefit available from recuperator bypass.

In the event that such a program is undertaken, methods would have to be explored to delay the drop-off in combustion efficiency associated with high bypass percentages. In particular it can be seen from Figure 5-46 that carbon monoxide and unburned hydrocarbon emissions at 15 percent bypass for the dual delivery system are much greater than for the primary pipe bypass only. If cycle studies demonstrate that bypass percentages greater than 10 percent are feasible from an engine performance standpoint, then a dual delivery system with combustion efficiency control is an attractive candidate NO_x control system. Efficiency drop-off point might be predictable from primary zone aerodynamic loading considerations.

(c) L-Pipe Vaporizer With Staged Dome (SKP264895D) - Final Calibration - The data from the final calibration test with SKP26489SD were converted to grams-per-mile by the method described in Section 2.2 and compared to the zero bypass values of the best vaporizer, SKP26489M2.

This comparison is the most conservative comparison possible. The emissions at 10 percent bypass for a vaporizer combustor which had high zero-bypass emissions (SKP26489 SD) are compared with the zero-bypass emissions of the vaporizer combustor that had the lowest zero-bypass emissions. The values are tabulated in Tables 5-7 and 5-8 below.

TABLE 5-7

MASS EMISSIONS PREDICTION OVER THE SIMULATED FEDERAL DRIVING CYCLE

(for a vaporizer combustor with and without recuperator bypass)

GRAMS/MILE				
EMISSION	ZERO BYPASS (SKP26489M2)	10 PERCENT BYPASS (SKP26489 SD)	GOALS	REDUCTION (%)
CO	0.13	0.071	3.4	45
HC (as CH_4)	0.012	0.005	0.47	58
NO_x (as NO_2)	6.38	1.73	0.4	73

The emission index to grams-per-mile conversion constants at each power level as tabulated in Section 2.2 were multiplied by the fuel consumption penalty factors resulting from bypass operation as determined from engine cycle calculations. The penalty factor is the ratio of the fuel flow required at the specified power output with 10 percent bypass to the fuel flow required with no bypass. The fuel flow increase for bypass operation is plotted versus bypass percentage in Figure 5-47 for lines of constant engine power. Tabulated below is a comparison of the zero bypass conversion constants with those corrected for 10 percent bypass operation.

TABLE 5-8

EFFECT OF 10 PERCENT RECUPERATOR BYPASS ON EI CONVERSION CONSTANTS AND REQUIRED FUEL FLOW

POWER SHP	CONSTANT, K_0 (NO BYPASS)	FUEL FLOW PENALTY FACTOR, Fc	CONSTANT, K_{10} (10 PERCENT BYPASS)
1.3	0.0103	1.441	0.0148
8.5	0.0881	1.303	0.1144
29.5	0.0565	1.158	0.0650
53.5	0.0246	1.099	0.270
80.5	0.0038	1.067	0.0041

Bypass operation at the low power conditions results in a larger fuel flow penalty because the combustor inlet temperature is effectively reduced and is reflected as a greater percentage of the combustor overall temperature rise at the lower fuel-air ratios. The fuel flow increase, is, therefore, a greater percentage of the zero bypass fuel flow in order to bring the combustor discharge temperature back up to its initial value.

While the absolute value of the NO_x emission in grams-per-mile is still in excess of the 1976 standard, the magnitude of the reduction achieved with the recuperator bypass concept is highly significant. A 73 percent reduction in NO_x emission was realized with 10 percent bypass over the best configuration of the SKP26489 vaporizer combustor without bypass, namely the M2 configuration with secondary pipes. The magnitude of the reduction is greater than 75 percent compared with the zero bypass value of the staged-dome configuration currently in use. Furthermore, realize that the SKP26489 vaporizer combustor with no bypass generated the greatest amount of NO_x of all the baseline combustors tested. The potential to meet the 1976 standards still exists with other combustor configurations, particularly if the variable engine geometry of the automotive engine cycle is exercised to optimize the combustor inlet temperature from an emissions standpoint.

Figure 5-62 shows the NO_x emission index plots for the best SKP26489 zero bypass configuration (M2) and the 10 percent bypass staged-dome configuration (SD) superimposed. Note that the reduction available with bypass decreases with increasing power level. The significance to this is that the engine/vehicle spends greater than 50 percent of its operating time at power levels below 10 HP over the Federal Driving Cycle (FDC). A comparison between the emission

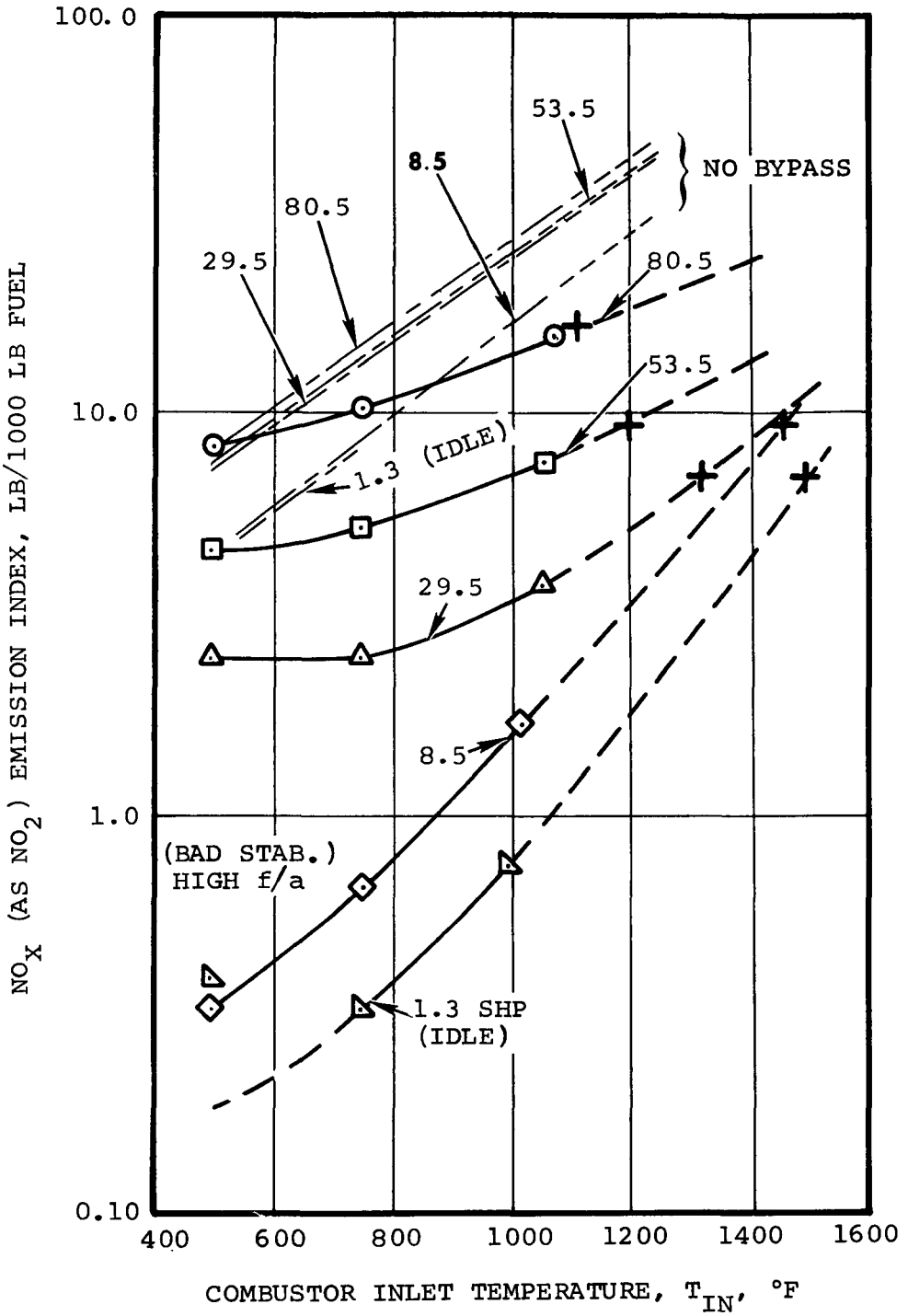

NO_X EMISSION COMPARISON BETWEEN COMBUSTOR SKP26489-SD WITH 10 PERCENT BYPASS AIR AND SKP26489 M2 COMBUSTOR WITH NO BYPASS

FIGURE 5-62

indices extrapolated to the combustor inlet temperatures specified by off-design engine performance analysis and the percent reductions achieved with 10-percent bypass are shown in Table 5-9 as follows:

TABLE 5-9

NO_x REDUCTION ACCOMPLISHED WITH 10 PERCENT RECUPERATOR BYPASS			
POWER, SHP	EMISSION INDEX ZERO BYPASS (SKP26489 M2)	EMISSION INDEX 10 PERCENT BYPASS (SKP26489 SD)	PERCENT REDUCTION
1.3	41.6	7.0	83.2
8.5	38.0	9.4	75.2
29.5	31.3	7.0	77.6
53.5	29.4	9.4	68.0
80.5	31.0	16.2	47.7

A significant reduction potential exists at the low power levels typical of vehicle operation over the Federal Driving Cycle. The data suggests that a variable bypass arrangement might be effective in maximizing the NO_x reduction as a function of part load power level. This possibility could be explored by conducting a bypass evaluation test at each of the five conditions chosen to simulate the FDC to determine whether the optimum bypass percentage varies as a function of power output.

The reduction in bypass effectivity with increasing power level is believed to be related to the primary zone equivalence ratio. Since the bypass air is delivered with the fuel through the primary pipe, the system tends to function similar to a premix combustor in that the primary zone equivalence ratio is strongly influenced by the equivalence ratio in the primary pipe (fuel plus bypass air).

At low power levels, 10-percent bypass air is sufficient to reduce the primary pipe fuel-air ratio well below stoichiometric with a corresponding decrease in primary zone temperature. For instance, at the 1.3 and 8.5 hp test points, the equivalence ratio in the primary pipe is 0.45 and 0.58, respectively. Corresponding equilibrium flame temperatures would be below 2700°F resulting in low NO_x formation rates even if no further dilution of the primary pipe mixture is assumed to occur prior to combustion. Dilution would further reduce this temperature.

At high power levels (above 40 hp), the primary pipe fuel-air ratio with 10-percent bypass is slightly greater than stoichiometric yielding higher primary zone temperatures and corresponding higher NO_x emissions. At the 53.5 and 80.5 hp test points the equivalence ratio in the primary pipe is 1.13 and 1.32 respectively. Corresponding equilibrium flame temperatures would be in the range of 3700°F to 3800°F provided the amount of additional primary air, over that supplied in the primary pipe, is not greater than about 20 percent for the 53.5 hp test point and not greater than about 50 percent for the 80.5 hp test point. These high primary zone temperatures yield high NO_x formation rates.

A variable bypass system would offer the potential of maintaining the beneficial effect of a lean primary premix system throughout the load range. Previous attempts to control primary zone equivalence ratio without premixing or burner variable geometry have been unsuccessful, except for bypass operation. Such results are typical of combustors that operate with diffusion flames.

A further indication that variable bypass or premix with bypass might be effective as a NO_x control technique is illustrated by a comparison of the effect of overall fuel-air ratio on NO_x emission for the zero bypass configuration as shown on Figure 5-63 for the maximum inlet temperature test conditions. The data show that at the higher fuel-air ratios there is a strong dependence of NO_x emission on fuel-air ratio. The smaller difference in NO_x emission index between zero and ten percent bypass at the high fuel-air ratios implies that the bypass percentage could be optimized at the higher power levels to obtain additional reduction.

(d) L-Pipe Vaporizer - OAP 6-Point FDC Simulation - A conclusion of the test was that the distorted dome had caused excessively lean operation of the primary zone with resultant high values of HC and CO.

The results further illustrate that variable bypass can be used to achieve desireable compromizes in total Federal Driving Cycle emissions. NO_x and CO emissions would be further reduced by operation of several of the points at bypass ratios greater than ten percent. This is illustrated by Figure 5-61.

The desirable CO and NO_x combination from assumed Schedule 3 from Table 5-6 (7 percent bypass at point 2, 10 percent bypass at all other points) should be noted. It should be possible to achieve the 76 FDC emissions standards by; 1.) reducing the combustor volume to increase the loading, thus achieving lower NO_x and higher CO and HC, 2.) additional optimization on the combustor fuel delivery systems and 3.) combined optimization of the engine cycle and the combustor characteristics.

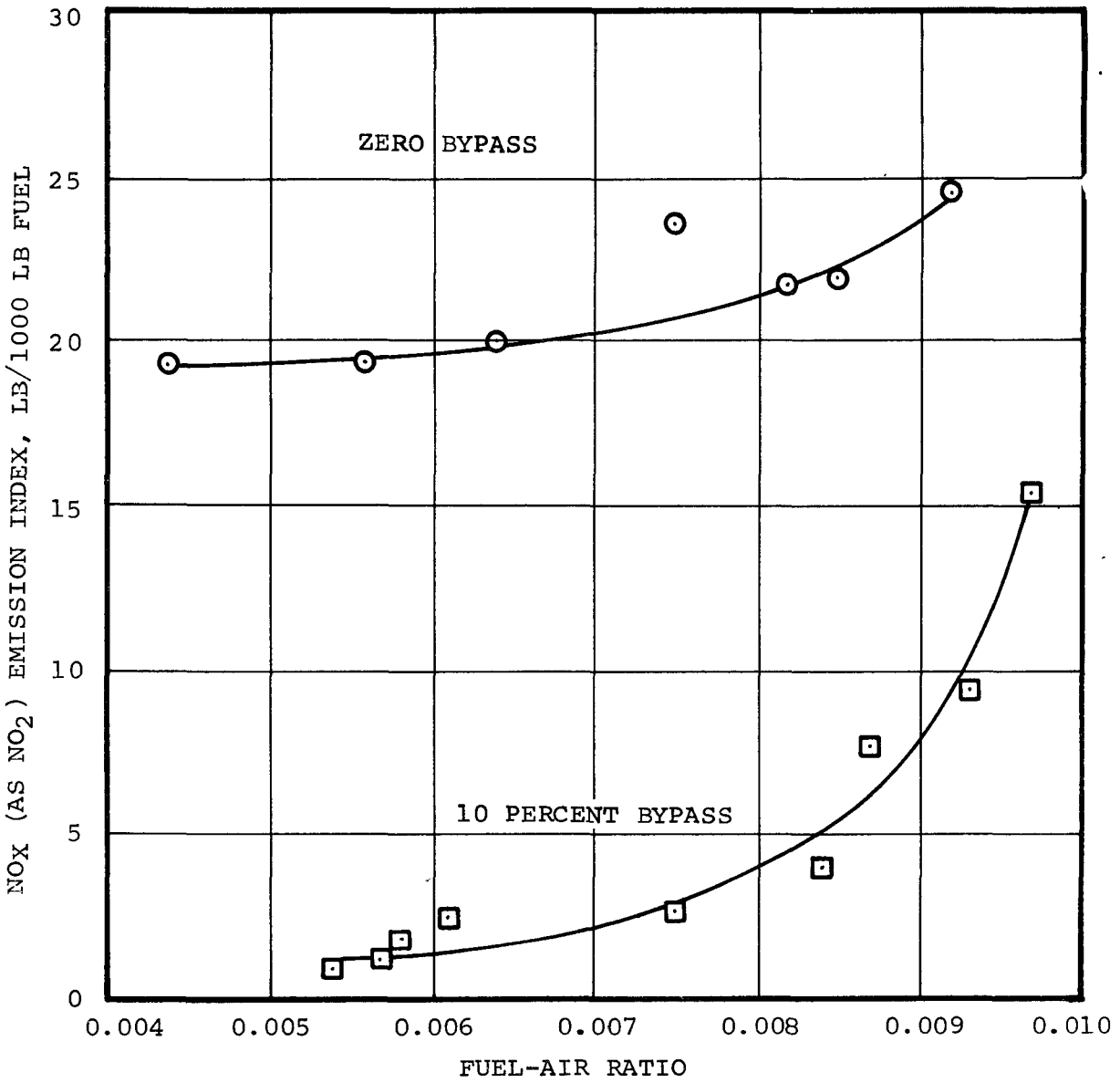

EFFECT OF FUEL-AIR RATIO ON NO_X EMISSION FROM COMBUSTOR SKP26489-SD WITH 10 PERCENT BYPASS AND ZERO BYPASS

FIGURE 5-63

5.5 Effect of Inlet Temperature on NO_x Over FDC

The computer simulation of an automobile performing over the Federal Driving Cycle (FDC) involves a number of assumptions which affect the predicted emissions. Obviously, the type, size, and configuration of the vehicle's engine have important influences. The type of transmission selected has a strong influence. Another of the most important influences is the part-load operational schedule that is selected for the engine. Once the transmission is defined in a fixed-geometry gas turbine engine, the part-load operational schedule is fixed. However, in variable-geometry turbine engines, the designer has the freedom to select, within limits, the part-load operational schedule which optimizes the engine in a desired manner. This optimization could be for best fuel economy, lowest NO_x emissions or various tradeoffs of these or other desirable performance qualities.

The part-load operational schedule used in the AiResearch mission simulation program was optimized for good part-load fuel economy as determined for the NII2V engine studied in the Automobile Gas Turbine Optimization Study.* Good part-load fuel economy was achieved by maintaining high combustor discharge temperatures at reduced power levels by the use of variable inlet guide vanes. This selected schedule has high combustor inlet temperatures at reduced power levels as shown in Schedule A on Figure 5-64.

NO formation is exponentially dependent on local combustion temperature. The fuel-air ratio, heat loss rate to the combustor walls, combustor inlet air temperature, bypass rate and bypass air temperature all have an important influence on the NO_x formation and emission rates.

*Automobile Gas Turbine Study, EPA Contract 68-04-0012, Final Report (AT-6100-R7), July 14, 1972.

The emissions shown in Figures 5-55, 5-56, and 5-57 may be used to illustrate the effect of selected combustor inlet temperature on the simulated FDC emissions at constant bypass rate (10 percent) and bypass air temperature (300°F).

Figure 5-64 presents, for example, two combustor inlet temperature (CIT) schedules, A and D as a function of output power.

- Schedule A reflects the AiResearch 5-point FDC simulation procedure selected for best fuel economy. (Defined in Section 2.2)

- Schedule D corresponds to arbitrarily defined schedule at lower combustor inlet temperatures.

Table 5-10 presents the computation of simulated NO_x, CO, and HC emissions over the Federal Driving Cycle for the two CIT schedules.

The predicted NO_x emissions for these schedules are 1.73 and 0.85 grams/mile for Schedules A and D, respectively. Thus, a NO_x reduction of 50 percent is predicted for changing the CIT schedule from the schedule used in the AiResearch 5-point simulation procedure to Schedule D. Concurrently, the CO increases from 0.044 to 0.65 grams/mile and the HC increases from 0.004 to 0.25 grams/mile. Even at the increased values of the lower CIT schedule D, the CO is only 19 percent of the 1976 Federal Standard and the HC is only 6 percent of the 1976 standard. These margins would permit further reduction in NO_x while continuing to meet the emission standards for CO and HC. The fuel economy reduction was estimated at 6 percent for the FDC and has been accounted for in the results. This would reduce this predicted advantage. However, this illustrates the potential for significant FDC NO_x reductions by the optimum selected

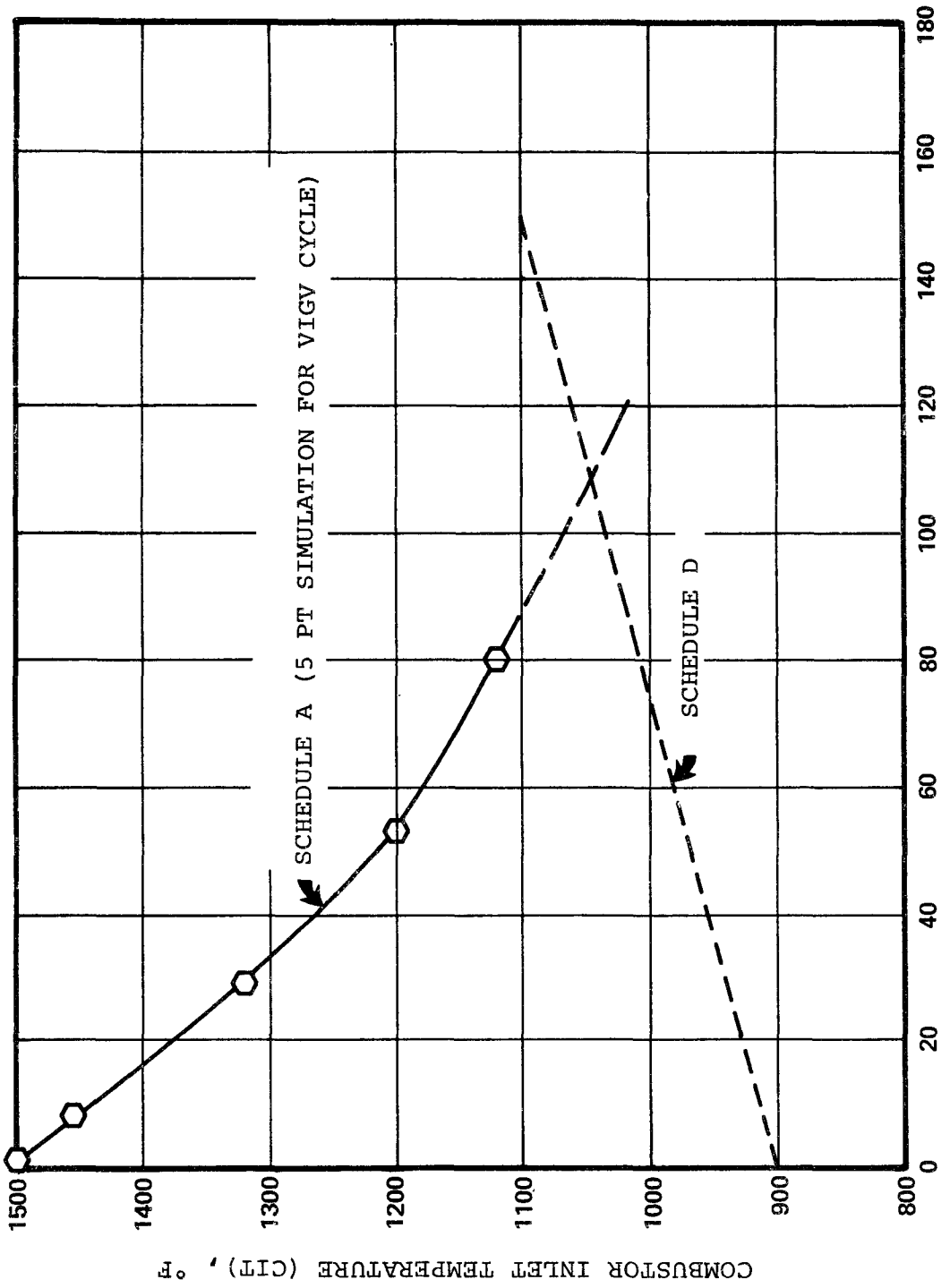

COMBUSTOR INLET TEMPERATURE SCHEDULES

FIGURE 5-64

Output Power hp	Combustor Inlet Temperature °F	K_0 at Zero Bypass	K_{10} Corrected For 10% Bypass	K_{10} Corrected For 10% Bypass and Low CIT	NO_x E1	CO E1	AC E1	NO_x E1 . K_{10}	CO E1 . K_{10}	HC E1 . K_{10}
SCHEDULE A (5 POINT SIMULATION AT BEST FUEL ECONOMY)										
1.3	1500	0.0103	0.0148	Not Applicable	5.0	0.4	∿0.005	0.074	0.0059	0.0001
8.5	1455	0.0881	0.1144		8.4	0.1	∿0.005	0.961	0.0114	0.0006
29.5	1320	0.0565	0.0650		6.5	0.03	∿0.005	0.423	0.0020	0.0003
53.5	1200	0.0246	0.0270		8.0	0.9	0.095	0.216	0.0243	0.0026
80.5	1120	0.0038	0.0041		13.1	0.12	0.09	0.054	0.0005	0.0004
					TOTALS (GM/MILE)			1.73	0.044	0.004
SCHEDULE D										
1.3	1200	0.0103	0.0148	0.0158	1.6	12	0.5	0.025	0.190	0.0079
8.5	1160	0.0881	0.1144	0.1224	2.7	3	0.09	0.330	0.367	0.0110
29.5	1070	0.0565	0.0650	0.0690	3.8	0.9	0.04	0.262	0.062	0.0028
53.5	970	0.0246	0.0270	0.0286	6.3	1.2	0.095	0.180	0.034	0.0028
80.5	1010	0.0038	0.0041	0.0042	12.1	0.12	0.09	0.051	0.001	0.0004
					TOTALS (GM/MILE)			0.85	0.65	0.025

TABLE 5-10

combustor inlet temperature schedule in combination with bypass ratio. Since reduced CITs and the use of recuperator bypass, both have detrimental effects on fuel economy, a complete part-load analysis with various combinations of bypass ratio and CIT is necessary to arrive at the optimum trade off between minimum NO_x emissions and reduced fuel economy.

5.6 Development Test Summary

Table 5-11 presents a Summary of Test Results for the combustor development program.

During development testing, an examination was made of various methods of measured NO_x emissions data presentation. Preliminary indications suggest a suitable NO_x correlating parameter in the form of an aerodynamic loading parameter

$$Q = \frac{W}{P^n \text{ Vol. } e^{T/540}}$$

where W = combustor inlet airflow, lb/sec
P = combustor inlet pressure, atmosphere
T = combustor inlet temperature, °R
Vol. = combustor volume, ft^3
n = exponent

The following Figure 5-65 is an example of a machine plot of NO_x emission index as a function of the combustor loading parameter based on data obtained from the vaporizing combustor, SKP26489. It is significant to note that as combustor aerodynamic loading is increased, by a corresponding decrease in combustor volume, lower NO_x emissions should result for this combustor configuration. However, additional study should be conducted on this and other NO_x correlating parameters for a number of combustor configurations prior to making any generalizations about combustor emissions performance.

TABLE 5-11
SUMMARY OF TEST RESULTS

Combustor P/N and Model	Type	Description	Emission Index at T_{IN}=1000°F LB/1000 LB FUEL			FDC Mass Emissions, Grams/Mile			FDC Simulation Procedure	Comments
			NO_x (as NO_2)	CH_x (as C_6H_{14})	CO	NO_x (as NO_2)	CH_x (as C_6H_{14})	CO		
SKP26312	Vaporizer	GTP30/Shelldyne H/Cone								ATM pressure rig
SKP26312	Vaporizer	GTP30/Shelldyne H/STD								ATM pressure rig
SKP26312 M_0	Vaporizer	GTP30/Shelldyne H/Cone	7*	0.4*	7*	5.0	NA	NA	ME (B)	High pressure rig, *Class B conditions (740°F BIT)
SKP26259 M_0	Vaporizer	Cone dome	8*	4*	18*	14	0.005	0.05	ME (A)	*EI at 740°F
SKP26259 M_1	Vaporizer	Cone dome/blocked ports	9*	0.9*	20*					*EI at 740°F
SKP26259 M_2	Vaporizer	Flat dome (full ports)	8*	4.0*	25*	6.6	0.48	0.28	ME (A)	*EI at 740°F
SKP26259 M_3	Vaporizer	Flat dome/primary injection	6*	3.4*	44*	3.1	0.25	0.58	ME (A)	*EI at 740°F
PAP218770 M_0	Premix	Premix chamber	4.5*	0.075*	14*	1.4	0.003	1.7	ME (A)	*EI at 740°F, NG fuel
PAP218770 M_0	Premix	Premix chamber	2.0			0.8	18	24	ME (A)	JP-4 fuel, new hot rig
PAP218770 M_1	Premix	Primary holes removed	4.5*	0.1	8.7*	2.2	0.014	4.8	ME (A)	*EI at 740°F, NG fuel
SKP26489 M_0	Vaporizer	Secondary pipe	14	<0.1	4.2	5.1	0.003	0.28	ME (A)	
SKP26489 M_1	Vaporizer	Secondary pipes/impinge plate	13*	0.5*	4.5*	6.2	0.0004	0.41	ME (A)	*EI at 740°F
SKP26489 M_1	Vaporizer	Secondary pipes/impinge plate	14*	0.093*	2.1*	4.2	0.10	0.51	TE (A)	New hot air supply, *at 27 hp
SKP26489 PI	Pneu impact		5.2*	8.8* (as CH_4)	26*		(as CH_4)			*EI at 500°F and 0.0065 f/a
899930	Pres atomizer	GTCP85-115 combustor	13*	7.2*	36*	4.2	1.3	5.6	TE (A)	*EI at 27 hp (1000°F)
SKP26489	Vaporizer		16*	0.1*	2.0*	3.4	0.04	2.0	TE (A)	*EI at 27 hp (1000°F)
976074-2 (1)	Pres atomizer	GTPR36-61 STD can	20	NA	NA					Engine tests (GTCP36-61)
PAP226608 (2)	Vaporizer	Hot L-pipe air	24	NA	NA					Engine tests (GTCP36-61)
PAP226608 (3)	Vaporizer	Cold L-pipe air	23	NA	NA					Engine tests (GTCP36-61)
PAP226608 (4)	Vaporizer	Cold L-pipe and dome air	19	NA	NA					Engine tests (GTCP36-61)
PAP226608 (5)	Vaporizer	As 3, no L-pipe insert	20	NA	NA					Engine tests (GTCP36-61)
PAP226608 (6A)	Vaporizer	As 5, cooling to L-pipe	20	NA	NA					Engine tests (GTCP36-61)
PAP226608 (6B)	Vaporizer	As 6A, low N_2 dissolved fuel	No Reduction	NA	NA					Engine tests (GTCP36-61)
PAP226608 (7)	Vaporizer	As 6A, with 3 prim tubes added	16	NA	NA					Engine tests (GTCP36-61)
PAP226608 (8)	Vaporizer	As 7, bellmouth entry	14	NA	NA					Engine tests (GTCP36-61)
PAP226608 (9)	Vaporizer	As 8, revised pri/sec ports	12	NA	NA					Engine tests (GTCP36-61)
SKP26489 M_2	Vaporizer	Original M_1 + cooling skirt	16*	0.009*	1.3*	6.38			TE 5 PT	*EI at 29.5 hp (1000°F)
SKP26489 SD	Vaporizer	Staged dome	24*	0.23*	3.4*	9.89	0.012	0.13	TE 5 PT	*EI at 29.5 hp (1000°F)
SKP26489 NL	Vaporizer	Weir L-pipe (' dome)	20*	0.14*	3.0*					*EI at 29.5 hp (1000°F)
SKP26489 SD	Vaporizer	Variable bypass (29.5 hp)				0.45*	0.7*	1.6*	TE 1 PT	Data at 29.5 hp only, *10% BP
SKP26489M_3 SD	Vaporizer	Prim zone ports plus bypass	1.5*	0.2*	27*				TE 1 PT	Variable bypass, *at 10% BP
SKP26489 SD	Vaporizer	Bypass to L-pipe and dome	3.0*	0.6*	8.6*				TE 1 PT	Variable bypass, *at 10% BP
SKP26489 PIM_1	Pneu impact	Improved fuel injection	19*	0.15*	1.4*	8.14			TE 5 PT	*EI at 29.5 hp (1000°F)
SKP26489 SD	Vaporizer	Staged dome	3.4	0.33	1.7	1.73			TE 5 PT	Final calibration at 10% BP
SKP26489 SD	Vaporizer	Staged dome	-	-	-	0.53	0.78	5.3	OAP 6 PT	Final calibration at 10% BP
SKP26489 SD	Vaporizer	Staged dome	-	-	-	0.78	0.09	0.90	OAP 6 PT	Variable bypass, 7-10% new dome
SKP26489 SD	Vaporizer	Staged dome	-	-	-	0.66	0.09	1.82	OAP 6 PT	Variable bypass, 9-10% new dome

FDC simulation procedures:

ME - AT6097 cycle, 4 point, multiple extrapolation, (A) or (B) indicates combustor class

TE - AT6097 cycle, 4 point, temperature extrapolation, (A) or (B) indicates combustor class

TE 5 PT - NII2V cycle, 5 point, temperature extrapolation, Class A only

TE 1 PT - NII2V cycle, 29.5 hp only, temperature extrapolation, Class A only

OAP 6 PT - OAP supplied, 6 point, temperature extrapolation, Class A only

*Asterisk data refers to comment across the page.

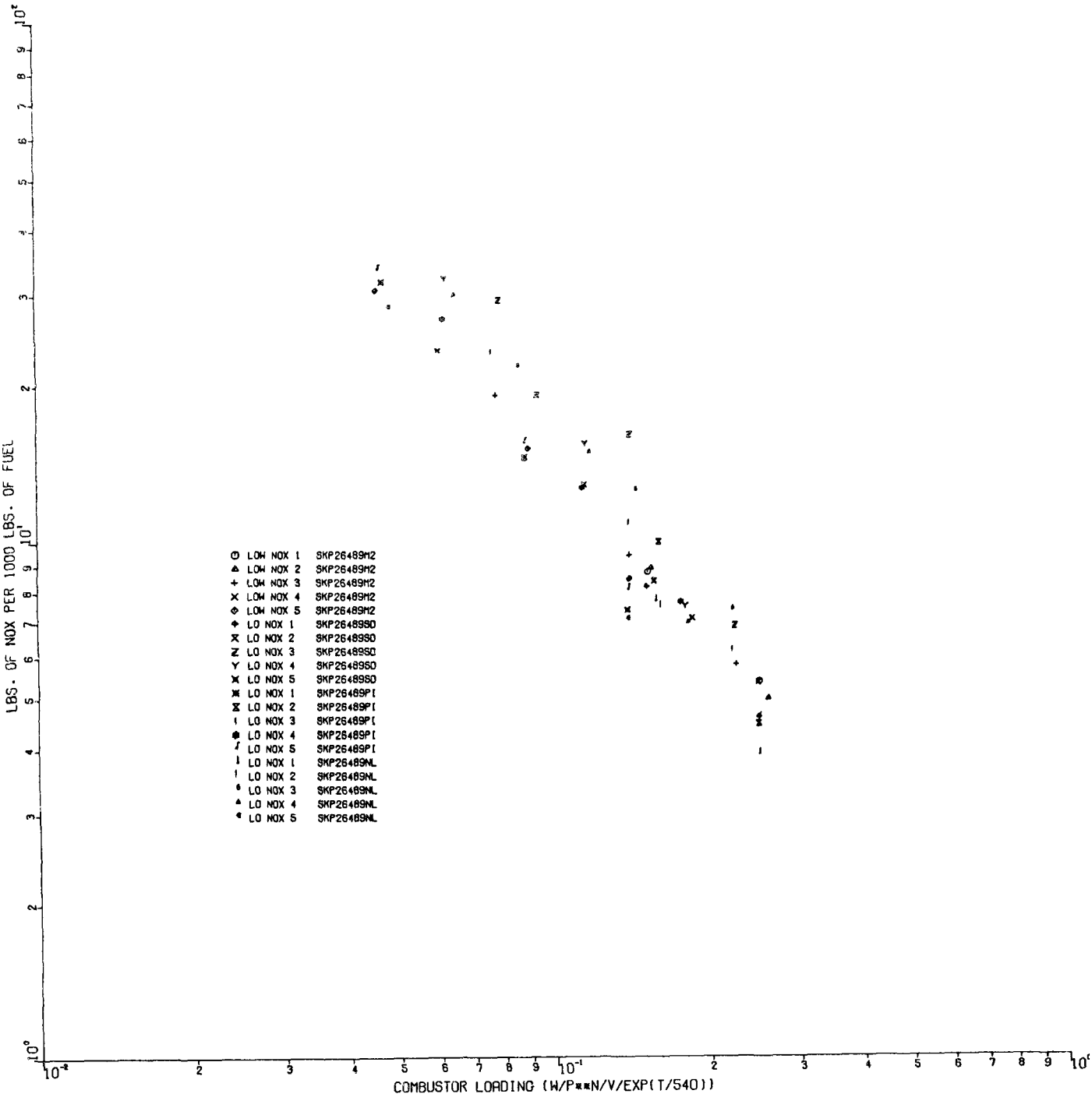

EPA-OAP LO-NOX COMBUSTOR PROGRAM

FIGURE 5-65

6. CONCLUSIONS AND RECOMMENDATIONS

6.1 Conclusions

An analytical model was formulated and programmed for a digital computer. The model predicts the formation of the trace species nitric oxide (NO) and nitrogen dioxide (NO_2) for a specified two-dimensional flow field in a gas turbine combustor.

Comparison of the nitrogen oxide concentrations with one test case incorporating more rigorous calculations using a one-dimensional flow model showed good agreement (see Appendix I, Pages 33 through 35).

In the experimental program, a variety of combustor configurations were rig tested, including vaporizers, atomizers, radiant, pneumatic impact and premix combustors. Both an atomizer combustor and a vaporizer combustor with various recuperator bypass ratios were tested in an engine. Significant test conclusions have been identified and discussed under Section 5 Combustor Development and Evaluation.

Conclusions reached regarding the relative merits of each system tested are presented below

- The conventional gas turbine pressure-atomizing combustor would require some modification to be applicable to a low emission automotive engine. This is because of the problem of off-design combustion efficiency as well as relatively high NO_x emissions. Such modification would probably include some type of air assisted atomization.

- A film-vaporizing combustion system, by itself, offers significant improvement over a pressure atomizing system with respect to combustion efficiency, and its fuel delivery system is more adaptable to NO_x emission reduction by inlet temperature and fuel-air ratio control.

- The premix combustion system shows potential for reduced NO_x emission. This is due to control over the primary zone fuel-air ratio inherent with this design, as opposed to pure diffusion flame combustors of the atomizing or vaporizing types. Flashback is a potential hazard with this system, however, particularly at the high inlet temperature characteristic of recuperated engine cycles.

- Insufficient data were generated for the pneumatic impact fuel injection system from which to draw legitimate conclusions. The baseline NO_x emission level for this configuration was generally higher than the other systems. By virtue of its design, however, the pneumatic impact atomizer is an attractive system on which to apply the recuperator bypass technique because by injecting all primary air and all bypass air through the injector venturi the designer can at once control both primary zone inlet temperature and fuel-air ratio.

The experimental program was able to achieve high combustion efficiencies, significant reductions in NO_x emissions while maintaining acceptable low HC and CO emissions, and low temperature spread factors in practical combustor designs.

The concept of recuperator bypass to the combustor was evaluated both in an engine and on the combustion test rig. NO_x reductions of up to a 97-percent reduction were measured at individual test conditions. The predicted NO_x reductions over simulated Federal Driving Cycles were from 72 to 77 percent depending on the simulation method used.

When a high (10 percent) and fixed bypass ratio was used in a vaporizer combustor at all operating points selected to simulate the Federal Driving Cycle, the low power conditions with low combustor

inlet temperatures yield excessive HC and CO emissions. This is believed to be caused by excessive lean fuel-air ratio and by excessive cooling or quenching in the primary combustion zone. Two methods of alleviating this condition could be used.

(a) Using a lower, but fixed, bypass ratio for all operating conditions

(b) Using a bypass ratio which is varied as a function of engine load (that is, reduced bypass-ratio at the low power conditions)

Based on the test data taken during the program, it is reasonable to postulate that at any operating condition, a bypass ratio exists where major NO_x reductions are possible and where CO and HC emission increases are acceptable.

The predicted values of emissions from a gas turbine powered automobile when driven over the Federal Driving Cycle were found to be as much as an order-of-magnitude difference (for HC and CO) depending on whether a particular pollutant was predicted using the EPA/OAP simulation method or the AiResearch-developed 5-point simulation method. (NO_x predictions were different by a factor of 3 to 1, with the AiResearch 5-point method predicting the higher values.)

The predicted values for the Federal Driving Cycle emissions are also very sensitive to the assumed part-load operating schedule for the hypothetical gas turbine engine assumed. A part-load operating schedule which is optimized on minimum fuel consumption, as was done in the cycle analysis performed for this study, will generally result in low values of HC and CO emissions. Because of the strong dependence of NO_x formation on burner inlet temperature, this optimization on fuel consumption will generally result in adverse rates of NO_x formation. The variable geometry gas turbine, such as provided by VIGVs,

provides the ability to select the burner outlet temperature (thus, also burner inlet temperature) at part load so as to optimize on the desired low NO_x emissions.

There is considerable potential for optimizing the bypass technique in combination with other NO_x reduction techniques and for simultaneously optimizing the schedule of burner inlet temperature as a function of load at low power levels so as to minimize the formation and emission of NO_x. The potential exists for meeting the required total emission goals over the FDC with less fuel consumption than the 1976 spark ignition engine and with a fixed burner geometry in a gas turbine engine.

Summary of Conclusions

(a) Recuperator bypass, correctly applied, is an effective NO_x control technique

(1) An 82 percent reduction in NO_x using 10 percent bypass was demonstrated on a vaporizer combustor (SKP26489 SD) during AiResearch 5-point FDC simulation. The calculated fuel consumption penalty for 10 percent bypass compared to zero-bypass over the FDC was 18 percent.

(2) A 73-percent reduction using 10-percent bypass was demonstrated during AiResearch 5-point FDC simulation. This result was determined from two vaporizer combustor configurations; a vaporizer that exhibited the best zero-bypass emissions compared to a vaporizer that exhibited the highest zero-bypass emissions.

(b) Recuperator bypass as a NO_x control technique is applicable to a variety of combustor concepts including the following:

(1) Premix
(2) Air-Blast Atomizer
(3) Vaporizer
(4) Pneumatic Impact

(c) An engine cycle can be optimized to provide the best balance of the emission constituents and fuel economy

(d) Variable recuperator bypass is a simple and convenient alternative to variable combustor geometry, with the required control system being simpler and with the potential of having:

(1) Lower cost
(2) Higher reliability
(3) Better maintainability
(4) Higher fuel consumption

6.2 Recommendations

On the basis of the potential demonstrated by the test results obtained, it is recommended that additional development activity be conducted in the following areas.

(a) Combustor Optimization:

(1) Exploratory testing on the combustor to develop the optimum baseline configuration varying the following parameters:

- Volume
- Primary Zone F/A (Lean)
- Fuel delivery
- Mixing

(2) Baseline configuration optimization for each of the following combustor types:

- Vaporizer
- Premix
- Pneumatic Impact
- Air-Blast Atomizer

The relative potential of candidate combustor types for achieving low NO_x emissions is relative to achieving a highly homogeneous mixture in the combustion zone that can be controlled at an optimum lean equivalence ratio.

This objective can be realized by striving to achieve the following combustion system characteristics:

- Premix the fuel and air before entry into the combustion zone
- Ensure a homogeneous fuel-air mixture by providing a suitable fuel presentation system (vaporizer or atomizer)
- Provide a high degree of air turbulence throughout the mixture to ensure a uniform fuel dispersal through the mixture

The following preferred list of candidate combustor types are listed relative to their predicted NO_x reduction potential based on their ability to match these design considerations:

- Premix, preferably prevaporized as well
- Vaporizer
- Air blast atomizer
- Pneumatic impact

(3) Optimize the bypass air delivery system on the most promising baseline combustor type varying the quantity and distribution of bypass flow.

(4) Develop complete emissions performance maps of selected combustor type.

(b) Match selected combustor design with Optimized Engine Cycle to arrive at optimized emissions at minimum fuel consumption penalty for FDC operating condition. The following order of analysis is recommended:

(1) Optimize bypass percentage at all load conditions for fixed bypass

(2) Optimize bypass percentage at all load conditions for variable bypass

(3) Optimize combustor inlet temperature schedule at part load with VIGV for minimum NO_x emission

(4) Combine 1 and 3 or 2 and 3.

6.2.1 Recommendations for Future Programs Include the Following:

- All experimental data should be obtained at the correct combustor inlet conditions to avoid uncertainties associated with extrapolated results. AiResearch has recently ordered an indirect-fired heater capable of simulating recuperated engine operation with nonvitiated air up to 1700°F at the heater discharge flange. Projected availability of this heater is May 1, 1973.

- Additional effort should be expended to improve the simulation procedure for the Federal Driving Cycle. Specifically, a more adequate representation of the power levels associated with acceleration transients and of ignition emissions is required.

- A special study on emissions correlation should also be conducted to determine a suitable NO_x correlating parameter. Preliminary indications at AiResearch suggest that the aerodynamic loading parameter used for combustion efficiency correlations may be suitable with additional development.

APPENDIX I

TWO-DIMENSIONAL MATHEMATICAL MODEL OF NITRIC OXIDE AND NITROGEN DIOXIDE FORMATION

By
C.A. Bodeen, J.G. Sotter, and V. Quan
K V B Engineering, Inc.

Prepared for

AiResearch Manufacturing Company of Arizona

October 15, 1971

TABLE OF CONTENTS

TWO-DIMENSIONAL MATHEMATICAL MODEL OF NITRIC OXIDE AND NITROGEN DIOXIDE FORMATION

The work described in this report was completed in support of the low non-emission combustor study for automobile engines being carried out by the AiResearch Manufacturing Company of Arizona for the Environmental Protection Agency.

The task was to provide a mathematical model to predict the formation rates of oxides of nitrogen, given AiResearch's two-dimensional analysis of the combustor flow field including local heat release rates. The nitrogen oxides model was to be based on chemical kinetics, and was required to be valid under any or all of the following conditions:

a. Both nitric oxide (NO) and nitrogen dioxide (NO_2) being formed.
b. Either fuel-rich or fuel-lean combustion.
c. Local zones in which the nitrogen oxide reactions may be either near to or far from equilibrium.
d. Local zones in which the major heat-releasing reactions may be either near to or far from equilibrium.
e. Significant amounts of the nitrogen oxides being formed in regions of recirculating flows, where the average streamlines form closed loops.
f. Large spatial variations in temperature and concentrations so that different chemical reactions may predominate at various locations or under certain operating conditions.

The model which was chosen to meet these requirements is described in Section 1 of this report. Section 2 describes how the programming of the model for digital computer was

accomplished. In Section 3, some suggestions for further refinements to the model, in possible future efforts, are outlined. Finally, results of test cases run using the present version of the program are given in the Appendix.

In its present form the model, when coupled with the AiResearch flow-field analysis, appears to be the most advanced method available for analytical study of pollutant formation in combustion systems.

1. NITRIC OXIDE AND NITROGEN DIOXIDE FORMATION RATES

Expressions describing the formations of nitric oxide, NO, and nitrogen dioxide, NO_2, in combustion products of hydrocarbon-air mixtures are given below. These expressions can be used as source terms in the NO and NO_2 two-dimensional mass conservation equations. The mass conservation equations, which contain the convection and diffusion terms in addition to the source term, can then be integrated simultaneously to obtain the NO and NO_2 concentrations in a given flow field by using the same computer program (Ref. 1) which has been modified by AiResearch to do the combustor flow field analysis.

The reactions of importance for NO and NO_2 formation are considered to be:

$$N + NO \rightleftharpoons N_2 + O \quad (1)$$

$$N + O_2 \rightleftharpoons NO + O \quad (2)$$

$$N + OH \rightleftharpoons NO + H \quad (3)$$

$$H + N_2O \rightleftharpoons N_2 + OH \quad (4)$$

$$O + N_2O \rightleftharpoons N_2 + O_2 \quad (5)$$

$$O + N_2O \rightleftharpoons NO + NO \quad (6)$$

$$NO + O + M \rightleftharpoons NO_2 + M \quad (7)$$

$$NO_2 + O \rightleftharpoons NO + O_2 \quad (8)$$

Reactions (1) to (6) account for NO production, while (7) and (8) account for NO_2 production. Among reactions (1) to (6), which have been considered in Reference 2, (1) and (2) are the dominant ones when NO is far below equilibrium and are usually referred to as the Zeldovich mechanism. Under fuel-rich conditions, (3) may be significant. For lean mixtures under relatively low temperatures (4) to (6) may dominate over (1) to (3); although NO is nearly frozen at low temperatures. Since production of NO_2 is significant only under fuel-lean conditions, it is believed that (7) and (8) are the major reactions for NO_2.

The rate equations for NO, N, N_2O, and NO_2 can be written as

$$\begin{aligned}(\dot{NO}) &= k_{1b}(N_2)(O) + k_{2f}(N)(O_2) + k_{3f}(N)(OH) \\ &+ 2k_{6f}(O)(N_2O) + k_{7b}(NO_2)(M) + k_{8f}(NO_2)(O) \\ &- k_{1f}(N)(NO) - k_{2b}(NO)(O) - k_{3b}(NO)(H) \\ &- 2k_{6b}(NO)(NO) - k_{7f}(NO)(O)(M) - k_{8b}(NO)(O_2) \end{aligned} \quad (9)$$

$$\begin{aligned}(\dot{N}) &= k_{1b}(N_2)(O) + k_{2b}(NO)(O) + k_{3b}(NO)(H) \\ &- k_{1f}(N)(NO) - k_{2f}(N)(O_2) - k_{3f}(N)(OH) \end{aligned} \quad (10)$$

$$\begin{aligned}(\dot{N_2O}) &= k_{4b}(N_2)(OH) + k_{5b}(N_2)(O_2) + k_{6b}(NO)(NO) \\ &- k_{4f}(H)(N_2O) - k_{5f}(O)(N_2O) - k_{6f}(O)(N_2O) \end{aligned} \quad (11)$$

$$\begin{aligned}(\dot{NO_2}) &= k_{7f}(NO)(O)(M) + k_{8b}(NO)(O_2) \\ &- k_{7b}(NO_2)(M) - k_{8f}(NO_2)(O) \end{aligned} \quad (12)$$

where (X) indicates concentration of X in moles per unit volume; the dot denotes creation rate per unit time; and k_{if} and k_{ib} (which are functions of temperature) are the forward and backward reaction rate constants, respectively, of reaction i. Any molecule in the system can act as the third body, M, so that the concentration (M) = ρ/M_g, where ρ is the density and M_g is the molecular weight of the gas.

It is assumed that (N) and (N_2O) are at steady state; i.e., the net (N) produced in reactions (1), (2), and (3) and the net (N_2O) produced in reactions (4), (5), and (6) are zero. With $(\dot{N}) = 0$ and $(\dot{N_2O}) = 0$, Equations (10) and (11) yield

$$(N) = \frac{k_{1b}(N_2)(O) + k_{2b}(NO)(O) + k_{3b}(NO)(H)}{k_{1f}(NO) + k_{2f}(O_2) + k_{3f}(OH)} \quad (13)$$

$$(N_2O) = \frac{k_{4b}(N_2)(OH) + k_{5b}(N_2)(O_2) + k_{6b}(NO)(NO)}{k_{4f}(H) + k_{5f}(O) + k_{6f}(O)} \qquad (14)$$

In addition to the rate constants k_{if} and k_{ib} where i = 1 to 8, one needs (N_2), (O_2), (O), (OH), and (H) to solve for (NO) and (NO_2). For hydrocarbon-air combustion, it is assumed that (N_2), (O_2), (H_2O), (CO), and (CO_2) are known. The following reactions are assumed to be infinitely fast in adjusting the concentrations (O), (OH), and (H):

$$CO + OH \rightleftharpoons CO_2 + H \qquad (15)$$

$$O + OH \rightleftharpoons O_2 + H \qquad (16)$$

$$OH + OH \rightleftharpoons H_2O + O \qquad (17)$$

Note that this is not the same as assuming equilibrium values for all the species involved in these reactions. The non-equilibrium values for (H_2O), (CO), and (CO_2), computed in the combustion analysis, are used to get the concentrations of the much more reactive species O, OH, and H by assuming that a quasi-equilibrium is established for reactions (15) through (17). Thus, for example, although (OH) may be present in such a small concentration that a large percentage change of (CO) takes a comparatively long time, H and OH are highly reactive and the ratio of their concentrations is assumed to be rapidly adjusted according to the ratio of CO_2 to CO so that the relationship

$$\frac{(CO_2)(H)}{(CO)(OH)} = K_{eq}$$

is satisfied. The equilibrium constant K_{eq} is a function of temperature only. Reactions (15), (16), and (17) yield

$$(O) = \frac{K_{15}}{K_{16}} \frac{(CO)(O_2)}{(CO_2)} \qquad (18)$$

$$(OH) = \left[K_{17}^{-1}(H_2O)(O)\right]^{\frac{1}{2}} \tag{19}$$

$$(H) = K_{15}\,\frac{(CO)(OH)}{(CO_2)} \tag{20}$$

where K_i are the equilibrium constants for reaction i.

Equations (13), (14), (18), (19), and (20) allow one to evaluate the source terms for (NO) and (NO_2) which are given by equations (9) and (12), respectively. To convert moles per unit volume to mass fraction for species X, one merely multiplies (X) by the molecular weight of species X and divides by the local fluid density. The terms ($\dot{N}O$) and ($\dot{N}O_2$), multiplied by the molecular weights of NO and NO_2, respectively, constitute the source terms in units of mass of NO and NO_2 per unit volume per unit time to be used in the differential equations describing conservations of mass of NO and NO_2, respectively.

2. MODIFICATIONS MADE TO THE GOSMAN-SPALDING PROGRAM

A. General Technique

Nitric oxide (NO) and nitrogen dioxide (NO_2) are treated as trace species being formed kinetically in a flowfield in which temperature, density, and the concentrations of N_2, O_2, H_2O, CO, and CO_2 are specified. These concentrations need not be equilibrium values, but it is assumed that the formation of NO and NO_2 does not significantly affect the concentrations of the other species. The iterative solution for the trace species concentrations is performed separately from that for the fluid mechanics and hydrocarbon kinetics.

The NO-NO_2 source terms as used in the program are derived using the following definitions:

$$
\begin{aligned}
G_1 &= k_{1b}(N_2)(O) \\
G_2 &= k_{2b}(O) + k_{3b}(H) \\
G_3 &= k_{2f}(O_2) + k_{3f}(OH) \\
G_4 &= k_{4b}(N_2)(OH) + k_{5b}(N_2)(O_2) \\
G_5 &= k_{4f}(H) + k_{5f}(O) \\
G_6 &= k_{6f}(O) \\
G_7 &= k_{7b}(M) + k_{8f}(O) \\
G_8 &= k_{7f}(O)(M) + k_{8b}(O_2)
\end{aligned}
\tag{21}
$$

In terms of the G's, equations (9) and (12) become

$$
\begin{aligned}
(\dot{NO}) = {} & G_1 + G_3(N) + 2G_6(N_2O) + G_7(NO_2) \\
& - k_{1f}(N)(NO) - G_2(NO) - 2\,k_{6b}(NO)^2 - G_8(NO)
\end{aligned}
\tag{22}
$$

$$
(\dot{NO_2}) = G_8(NO) - G_7(NO_2) \tag{23}
$$

Equations (13) and (14) become

$$(N) = \frac{G_1 + G_2(NO)}{G_3 + k_{1f}(NO)} \tag{24}$$

$$(N_2O) = \frac{G_4 + k_{6b}(NO)^2}{G_5 + G_6} \tag{25}$$

Substitution of equations (24) and (25) into (22) yields

$$(\dot{NO}) = 2\left[\frac{G_1G_3 - k_{1f}G_2(NO)^2}{G_3 + k_{1f}(NO)} + \frac{G_4G_6 - k_{6b}G_5(NO)^2}{G_5 + G_6}\right] - G_8(NO) + G_7(NO_2) \tag{26}$$

Unnecessary repeated evaluation of terms in equation (26) can be avoided by defining

$$\begin{aligned} Z_1 &= k_{1f} \\ Z_2 &= 2G_1G_2 \\ Z_3 &= G_3 \\ Z_4 &= 2k_{1f}G_2 \\ Z_5 &= \frac{2k_{6b}G_5}{(G_5+G_6)} \\ Z_6 &= \frac{2G_4G_6}{(G_5+G_6)} \\ Z_7 &= G_7 \\ Z_8 &= G_8 \end{aligned} \tag{27}$$

Equations (26) and (23) can now be written as

$$(\dot{NO}) = \frac{Z_2 - Z_4(NO)^2}{Z_3 + Z_1(NO)} + Z_6 - Z_5(NO)^2 - Z_8(NO) + Z_7(NO_2) \tag{28}$$

$$(\dot{NO}_2) = Z_8(NO) - Z_7(NO_2) \qquad (29)$$

B. Subroutine NOXCON

The subroutine NOXCON contains all reaction rate data and performs the function of evaluating the Z's of equations (27).

Data for the reactions directly involved in the production of NO and NO_2 include: (1) logarithms of eleven equilibrium constants as functions of temperature and (2) lists of activation energies β_j, frequency factors A_j, and temperature exponents N_j for calculation of eight reaction rates according to the equation

$$k_{fj} = A_j \, T^{-N_j} \, \exp(-\beta_j/RT) \qquad (30)$$

These data are given in Table 1. The eight kinetic reactions are equations (1) through (8) and the required equilibrium constants are for these plus equations (15) through (17).

The logarithms (base 10) of the equilibrium constants are stored for several values of temperature (°R). Except for K_{7e} the equilibrium constants are dimensionless; K_{7e} has units of (moles per unit volume). A list of values of K_{7e}^* was taken in units of cm^3/g-mole, and the logarithms of these values are stored in the data statement. Before these values can be used, they must be converted to values of logarithms of K_{7e}, which has units of ft^3/lb-mole used in the program. The relationship is

$$K_{7e} = K_{7e}^* \frac{cm^3}{g\text{-mole}} \frac{1000 \text{ g-mole}}{2.20462 \text{ lb-mole}} \frac{ft^3}{(12 \times 2.54)^3 cm^3}$$

$$= .0160185 \, K_{7e}^* \qquad (31)$$

TABLE I

CHEMICAL REACTIONS, RATE CONSTANT EXPRESSIONS, AND REFERENCES

j.	Reaction	A_j $cm^3/mole\ sec$, or $cm/mole^2 sec$.	N_j	B_j kcal/mole	Ref. for k_{fj}	Ref. for K_p
1.	$N+NO \rightleftharpoons N_2+O$	3.10×10^{13}	0	0.334	3	3
2.	$N+O_2 \rightleftharpoons NO+O$	6.43×10^{9}	-1	6.250	4	4
3.	$N+OH \rightleftharpoons NO+H$	4.22×10^{13}	0	0.0	5	8, 3*
4.	$H+N_2O \rightleftharpoons N_2+OH$	2.95×10^{13}	0	10.77	12	9, 10, 11*
5.	$O+N_2O \rightleftharpoons N_2+O_2$	3.82×10^{13}	0	24.1	12	9, 10*
6.	$O+N_2O \rightleftharpoons NO+NO$	4.58×10^{13}	0	24.1	12	10
7.	$NO+O+M \rightleftharpoons NO_2+M$	1.05×10^{15}	0	-1.870	6	10
8.	$NO_2+O \rightleftharpoons NO+O_2$	1.0×10^{13}	0	0.600	7	7
9.	$CO+OH \rightleftharpoons CO_2+H$	-	-	-	-	13
10.	$O+OH \rightleftharpoons O_2+H$	-	-	-	-	14
11.	$OH+OH \rightleftharpoons H_2O+O$	-	-	-	-	15

*K_p for these reactions were calculated from data given for other reactions in the cited references.

Subroutine NOXCON adds $\log_{10}$ .0160185 to the tabulated values of $\log_{10} K_{7e}^{*}$ and overstores the new values.

The β_j of equation (30) are stored in the DATA Statements in kcal/g-mole, and they are used in conjunction with the universal gas constant R. NOXCON continues data conditioning by overstoring and redefining β_j' as

$$\beta_j' = \frac{\beta_j}{R} \tag{32}$$

where R is given by

$$R = .001987 \frac{\text{kcal}}{\text{g-mole } ^\circ\text{K}} \cdot \frac{5\ ^\circ\text{K}}{9\ ^\circ\text{R}}$$

$$= .001104 \frac{\text{kcal}}{\text{g-mole } ^\circ\text{R}} \tag{33}$$

β_j' then has units of °R.

The units of the A_j (with the exception of A_7) as stored in the DATA statements are $cm^3\ ^\circ K^{N_j}/(\text{g-mole sec})$. For consistency of units, we convert these to $ft^3\ ^\circ R^{N_j}/(\text{lb-mole sec})$, overstoring the original values according to

$$A_j' \equiv A_j \frac{cm^3 \cdot ^\circ K^{N_j}}{\text{g-mole sec}} \cdot \frac{ft^3}{(12 \cdot 2.54)^3 cm^3} \cdot \frac{1000\ \text{g-mole}}{2.20462\ \text{lb-mole}} \cdot \left(\frac{9\ ^\circ R}{5\ ^\circ K}\right)^{N_j}$$

or

$$A_j' = A_j \times 0.0160185 \times \left(\frac{9}{5}\right)^{N_j} \tag{34}$$

Again, equation (7) is the exception to the rule. The stored units of A_7 are $(cm^3/\text{g-mole})^2$, so the conversion factor .0160185 is applied twice.

Reaction 7 requires (M), the molecular concentration of the gas as a whole. This quantity is given by

$$(M) = \frac{p}{RT} \tag{35}$$

and numerically becomes

$$(M) = \left(p \frac{lb_f}{ft^2}\right) \frac{lb\text{-mole } °R}{1545 \text{ ft } lb_f} \quad \frac{1}{T\ °R} \tag{36}$$

The forward reaction rate constants are next evaluated according to

$$k_{fj} = A_j\ T^{-N_j} \exp\left(-\beta'_j/T\right) \tag{37}$$

where it will be remembered that β'_j contains the factor 1/R.

Backward rates are required for reactions 1 through 8, and these are calculated according to

$$k_{jb} = \frac{k_{jf}}{K_{je}} \tag{38}$$

Subroutine NOXCON next converts the species mass fractions (produced by the main iteration of the Garrett-modified Gosman-Spalding program) into molar concentrations in lb-mole/ft^3 (used in the NO-NO_2 source terms). Then the functions G (Equation (21)) and Z (Equation (27)) are evaluated.

C. Subroutine SORCCK

The source term subroutine SORCC1 was modified to include the terms for NO and NO_2, which are assumed to be called "Mass Fraction 5" and "Mass Fraction 6" within the structure of Garrett's program.

The Gosman, et al text (Ref. 1) describes a technique in using source terms which serves to avoid divergence or to improve convergence in many cases. The source term, d_ϕ, which appears in the algebraic statement of the equation is represented within the program as (in cylindrical coordinates)

$$d_\phi = -rR_\phi = -SOURCE + ZQ \cdot \phi \tag{39}$$

where

r is the local radius;

R_ϕ is the rate of production of ϕ, in this case NO or NO_2, $lb_m/(ft^3 sec)$;

ϕ is the mass fraction of NO or NO_2;

SOURCE and $ZQ \cdot \phi$ are an artificial separation of terms such that SOURCE is not a function of ϕ.

In the case of NO_2 the basic concept in the separation of $d\phi$ into the two terms, $-SOURCE + ZQ \cdot \phi$, is well illustrated:

NO_2

$$SOURCE = rM_{NO_2} Z_8(NO) \tag{40}$$

$$ZQ = \frac{rM_{NO_2} Z_7(NO_2)}{m_{f6}} = r\rho Z_7 \tag{41}$$

where M_{NO_2} is the molecular weight of NO_2, m_{f6} is the mass fraction of NO_2, and ρ is the local density.

In the case of NO the task is not quite so simple since the NO rate function is nonlinear in (NO). After

discarding one attempt which sometimes exhibited instability, the following definitions were found to be satisfactory:

$$\text{SOURCE} = rM_{NO}\left\{Z_6 + Z_7(NO_2) + \frac{Z_2}{Z_3+Z_1(NO)}\right\} \qquad (42)$$

NO

$$Z_Q = \frac{rM_{NO}}{m_{f5}}\left\{\left[Z_5 + \frac{Z_4}{Z_3+Z_1(NO)}\right](NO)^2 + Z_8(NO)\right\}$$

$$= r\rho\left\{\left[Z_5 + \frac{Z_4}{Z_3+Z_1(NO)}\right](NO) + Z_8\right\} \qquad (43)$$

where M_{NO} is the molecular weight of NO and m_{f5} is the mass fraction of NO.

D. Subroutine SOLVCK

The subroutine SOLVC1 was modified to avoid certain unnecessary functions during the NO-NO_2 iterations. Furthermore SOLVCK rearranges and restores the solution matrix "A" and a number of other lists to facilitate the trace species iteration using the same program log'c as the main iteration.

E. Subroutine BLOCKK

The input subroutine BLOCK1 was modified to read a new card_which controls the behavior of the program with the three variables IOLD, INEW, INOX according to the following schedule:

IOLD — Absolute value of IOLD is the logical unit number of a magnetic tape (or other peripheral device) which contains the solution to a previously worked problem.
IOLD = 0 implies "no such tape exists"
IOLD<0 implies "read in the tape, but do not iterate - just generate plots".

INEW Logical unit of tape on which solution is to be saved.
INEW = 0 implies "do not save solution."

INOX Absolute value of INOX is the number of trace species equations to be solved: 1 → NO only
2 → NO & NO_2
0 → neither
INOX < 0 implies "do not do the main Gosman iteration...the solution has been recovered from tape."

F. Subroutines BOUNC1 and FDEQC1

These routines were modified to avoid the generation of negative mass fractions which seriously affect the ability of the NO-NO_2 system to converge.

G. Main Program GOSNOK

The main program GOSAR1 was modified to control the solution according to the user's requests with IOLD,INEW, INOX card (see Section E).

H. Subroutine LININT

This is a linear interpolation subroutine. An entry point, MOREYS allows for multiple dependent variables to be a function of a single independent variable. The routine extrapolates off the low-subscript end of the independent variable list and uses the high-end value if the independent variable is off the list at the opposite end. The independent variable list must be monotonic, but may be either increasing or decreasing.

3. SUGGESTIONS FOR FUTURE IMPROVEMENTS

Two improvements to the Gosman computer program are suggested for future efforts. One is the computation of the effective chemical species production terms. Since the formation rate of nitric oxide is an exponential function of temperature, the rate computed using the average temperature in an element of volume as currently done is always lower than the effective rate for which the temperature variation in the element of volume is taken into account. The error can be substantial, since the temperature variation within the element is often of the order of hundreds of degrees. A method of calculating the effective rate has already been developed by KVB Engineering. The method consists of integrating analytically the chemical species source terms over the element of volume considering the variation of temperature in both of the coordinate directions. It is recommended that this method be implemented in the computer program in a form suitable for gas turbine analyses. The effective rate computation is not only useful for nitric oxide evaluation, but it can be applied to more accurate computation of fuel-oxidizer combustion as well.

Another recommended modification to the current computer program is the inclusion of heat transfer. Although gas turbine walls are nearly adiabatic, there is great spatial variation of temperature in the fluid. Radiation can reduce the peak temperature to the extent that nitric oxide production is substantially reduced. Therefore, heat transfer by radiation and convection should be incorporated into the computer program.

If calculations made with the present version of the program indicate that reactions 3 through 8 and the backward directions of reactions 1 and 2 are of little importance, a simpler algebraic expression for the nitric oxide source term can be utilized and the nitrogen dioxide solution can be omitted.

The calculation of the improved effective source term mentioned above is also considerably simplified. These changes are quite easily made and could be added as an option in the present program. It is recommended that this possibility be investigated because a substantial saving in computer time, as well as improved accuracy in the source term, may be possible.

REFERENCES

1. Gosman, A. D., et al., Heat and Mass Transfer in Recirculating Flows, Academic Press, London, 1969.

2. Lavoie, G. A., et al, "Experimental and Theoretical Study of Nitric Oxide Formation in Internal Combustion Engines," Combustion Science and Technology, Vol. 1, pp 313-326, 1970.

3. Baulch, D.L., et al., "Critical Evaluation of Rate Data for Homogeneous Gas-Phase Reactions of Interest in High-Temperature Systems," Dept. of Physical Chemistry, The University, Leeds, England, Vol. 4, p. 1.

4. ibid., Vol. 4, p. 11.

5. Roberts, R., et al., "An Analytical Model for Nitric Oxide Formation in a Gas Turbine Combustion Chamber," presented at AIAA Seventh Propulsion Joint Specialist Conference, Salt Lake City, 15 June 1971.

6. Baulch, et al., op. cit., Vol. 5, p. 15.

7. ibid,, Vol. 5, p. 1.

8. ibid., Vol. 3, p. 14.

9. ibid.,Vol. 4, p. 40.

10. ibid., Vol. 4, p. 44.

11. ibid., Vol. 3, p. 1.

12. Schofield, K., "An Evaluation of Kinetic Rate Data for Reactions of Neutrals of Atmospheric Interest," Planet. Space Sci. 15, 1967, p. 654.

13. Baulch, et al., op. cit., Vol. 1, p. 1.

14. ibid., Vol. 3, p. 14.

15. ibid., Vol. 2., p. 20.

16. Kliegel, J.R., Frey, H. M., One-Dimensional Reacting Gas Nonequilibrium Performance Program, TRW Systems Group, Redondo Beach, CA, 1967.

APPENDIX A

TEST CASES

1. SMAC.1

Garrett supplied KVB with a sample test case for the program. A small premixed methane-air burner was modeled under the name "SMAC .1". The program input for this case is given in Table 2 and the results of the basic Gosman solution are shown graphically in Figures 1 through 5.

Solutions for NO and NO_2 mass fractions are shown in Figures 6 and 7.

The NO-NO_2 iteration system was also tested on several simple modifications of the basic problem results. Figures 8 and 9 give NO and NO_2 mass fractions for the basic case with 500°R added to the temperature field. Figures 10 and 11 give similar results for the basic case with all densities multiplied by 10. Finally, Figures 12 and 13 present NO and NO_2 solutions for the combination of the 500°R temperature increase and the 10-fold density increase.

The NO-NO_2 iteration scheme converged to 1% relative residual in 59 or fewer iterations for all four test cases.

TABLE 2

INPUT FOR SMAC .1 TEST CASE

```
SMAC.1
CARTESIAN
TURBULENT
NON-UNIFORM DENSITY
CONSTANT PRESSURE
DEP VARIABLES ARE:
   VORTICITY  - A(I,J,NW)
   STREAM FUNCTION - A(I,J,NF)
   MASS FRACTION NO 1
   MASS FRACTION NO 2
GEOMETRY:
   8 ROWS    8 COLUMNS
   J      IMIN      IMAX
   1         1         8
   2         1         8
   3         1         8
   4         1         8
   5         1         8
   6         1         8
   7         1         8
   8         1         8
  JA, JA1,  JB,  JC, IAB,  IC
   3    3    3    8    1    8
        RADA,     RADA1,     RADB,     RADC,     RADN
       1.000     1.000     1.000     1.000     1.000
          DA,       DA1,       DB,      DCN,       DN
       .0000     .0000     .0000   .9845-01  .9845-01

      X2AXIS     X1CONV     X2CONV
       1.000      .2813      .1142
 I OR J        X1(I)        X2(J)
      1      .0000        .0000
      2      .1406-01     .4167-02
      3      .2813-01     .8336-02
      4      .4219-01     .1459-01
      5      .5626-01     .2284-01
      6      .7032-01     .2855-01
      7      .8439-01     .3426-01
      8      .9845-01     .3997-01
PHYSICAL DATA:
   V PRI      1233.      V SEC      .0000
   ROREF      .7500-01   P REF      2116.
   ZMUREF     .2000-04   T REF      3000.
   CP REF     .2400
   GC         32.20      ZJC        778.0

   STC        17.16      HC         17415.
   HP(FU)     17856.     HS(OX)     441.00
```

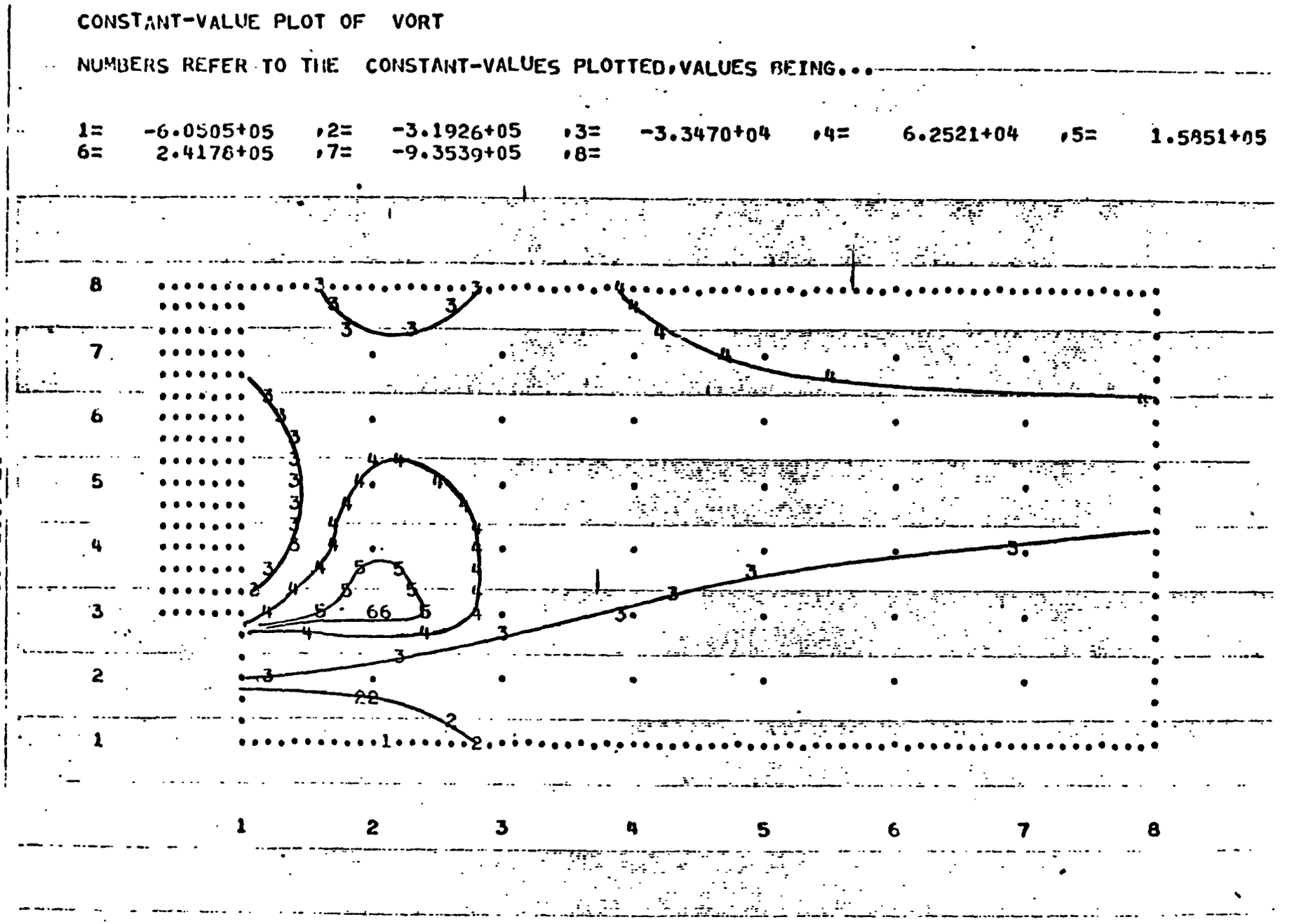

Figure 1. SMAC.1 Basic Case rticity.

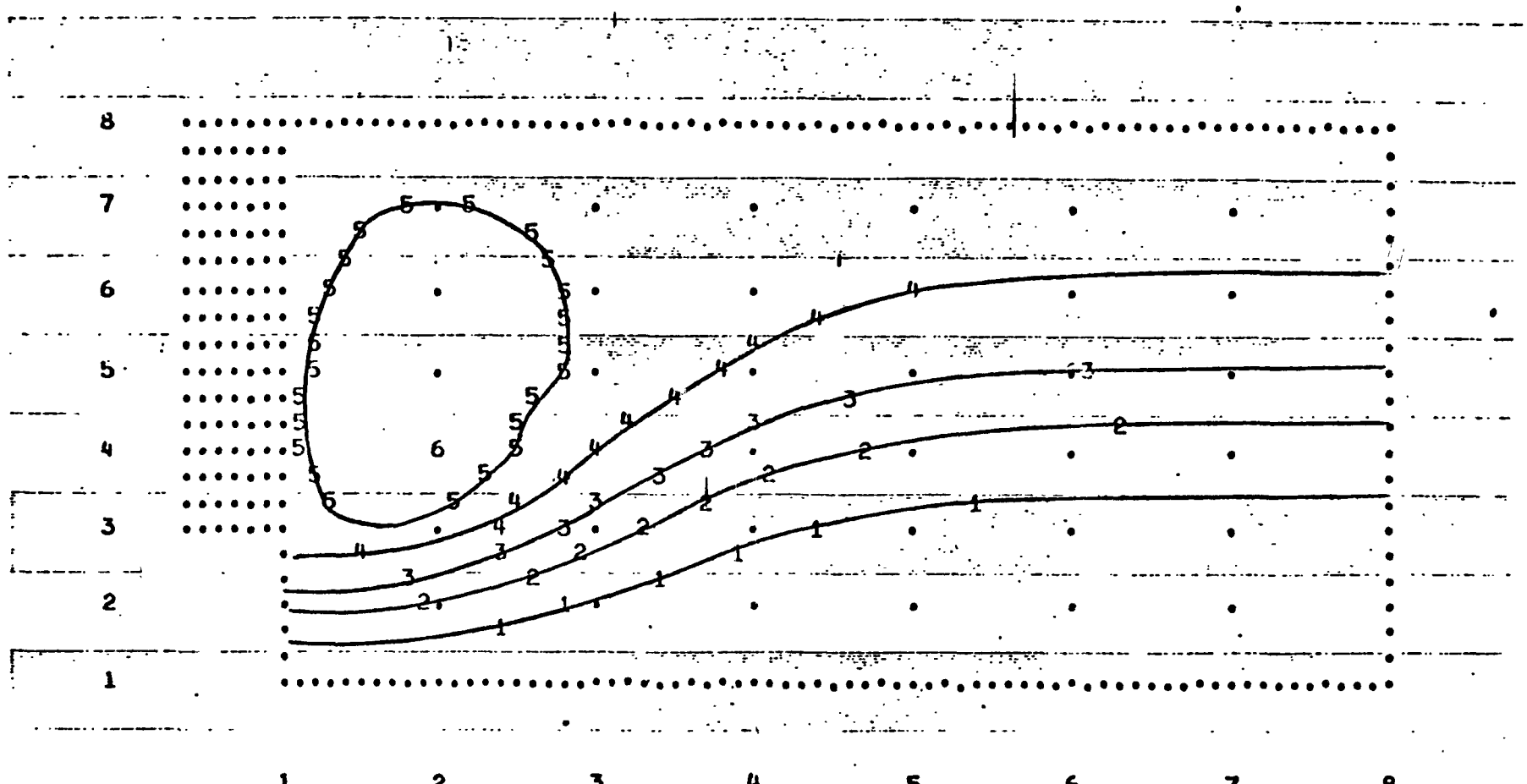

Figure 2. SMAC.1 Basic Case Stream Function.

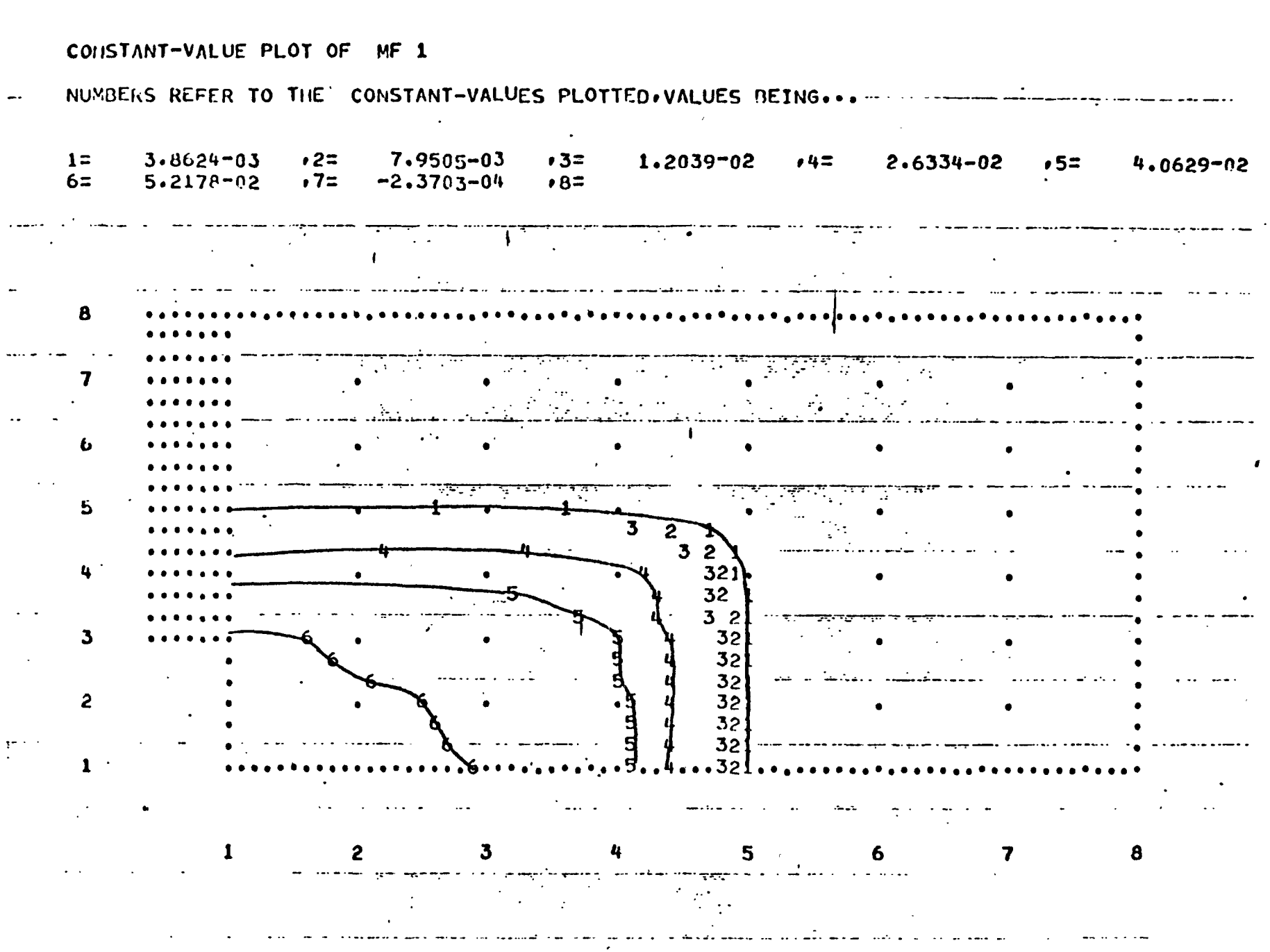

Figure 3. SMAC.1 Basic Case Fuel Mass Fraction.

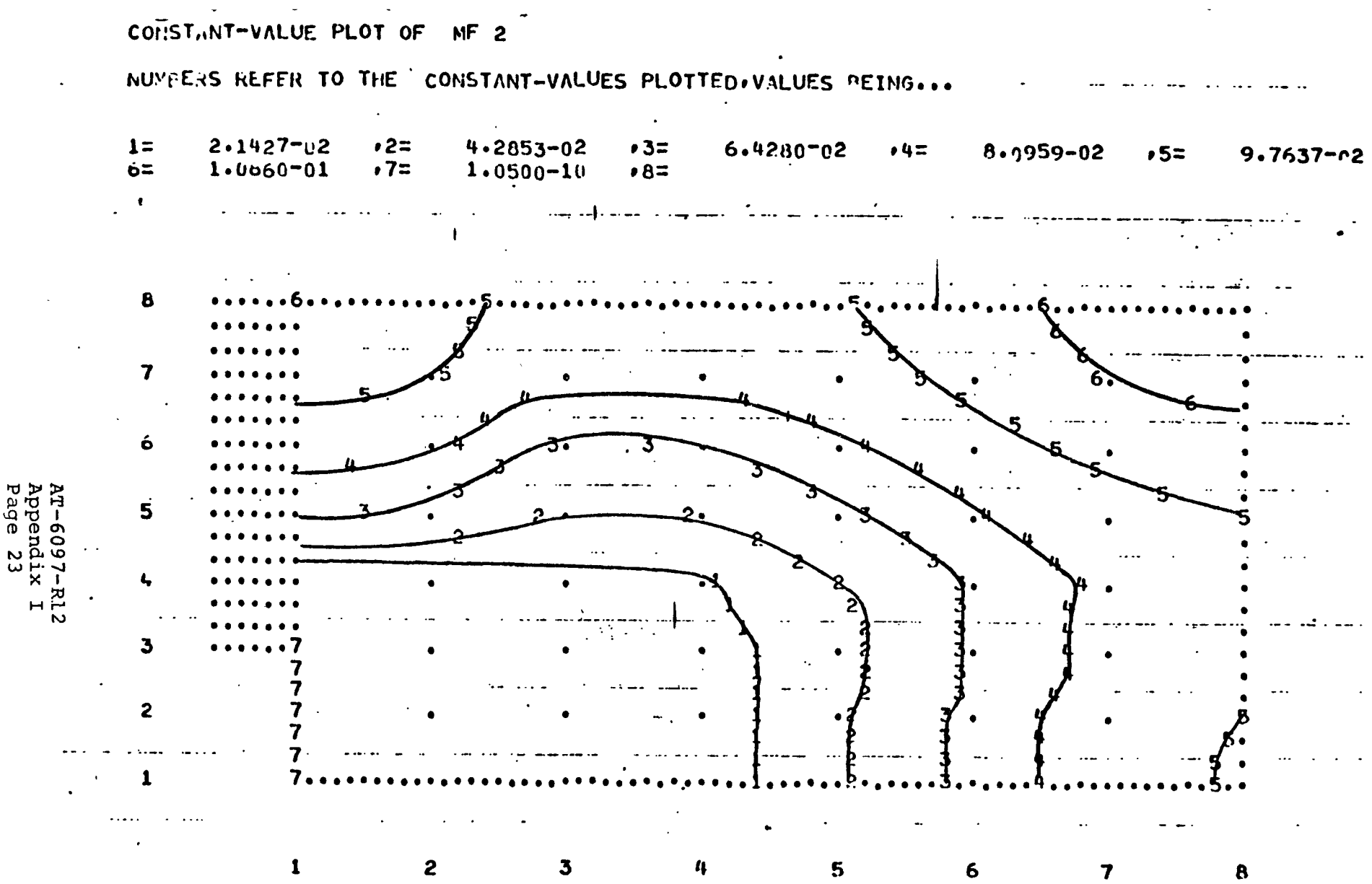

Figure 4. SMAC.1 Basic Case CO_2 Mass Fraction.

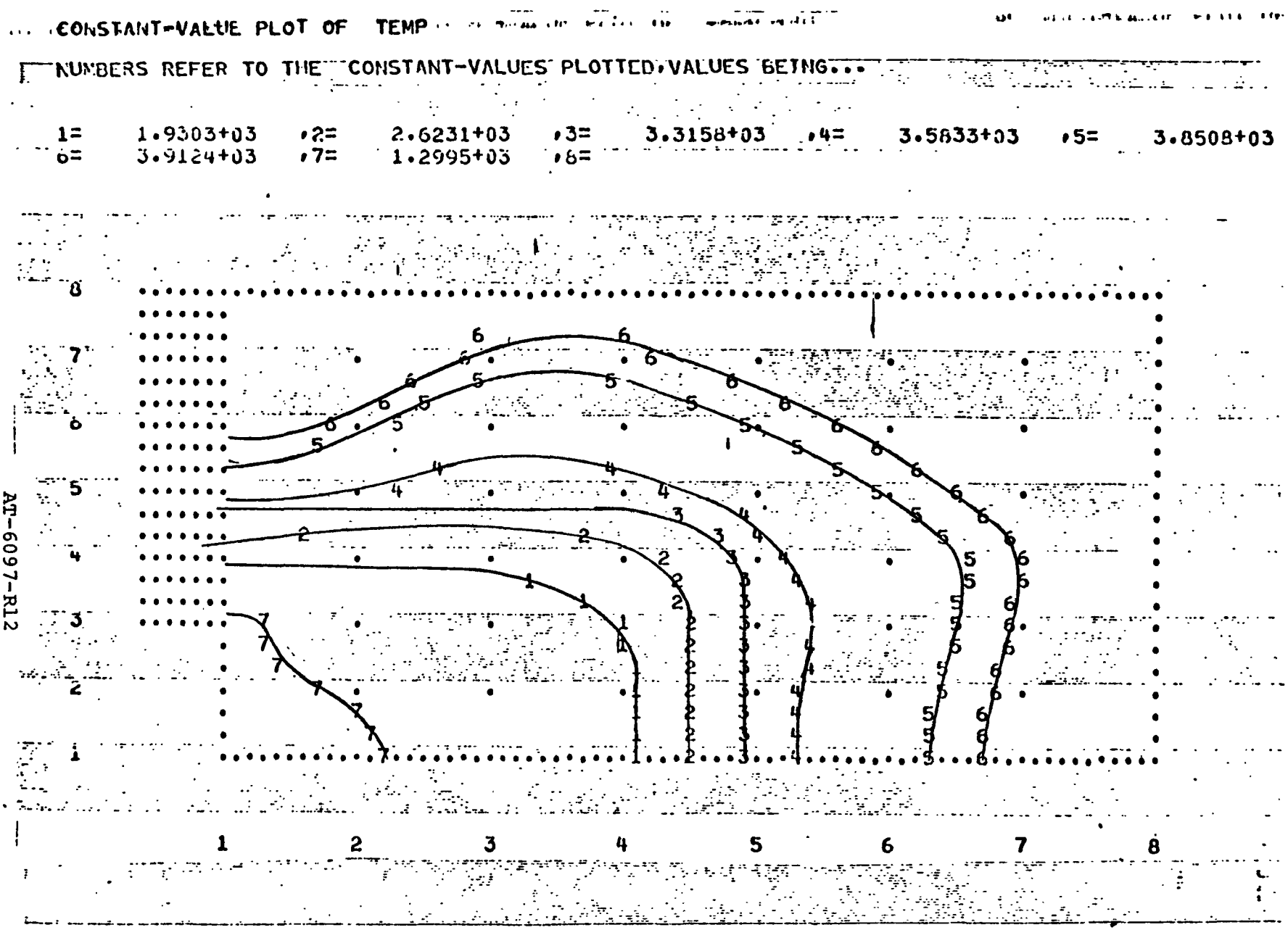

Figure 5. SMAC.1 Basic Case Temperature.

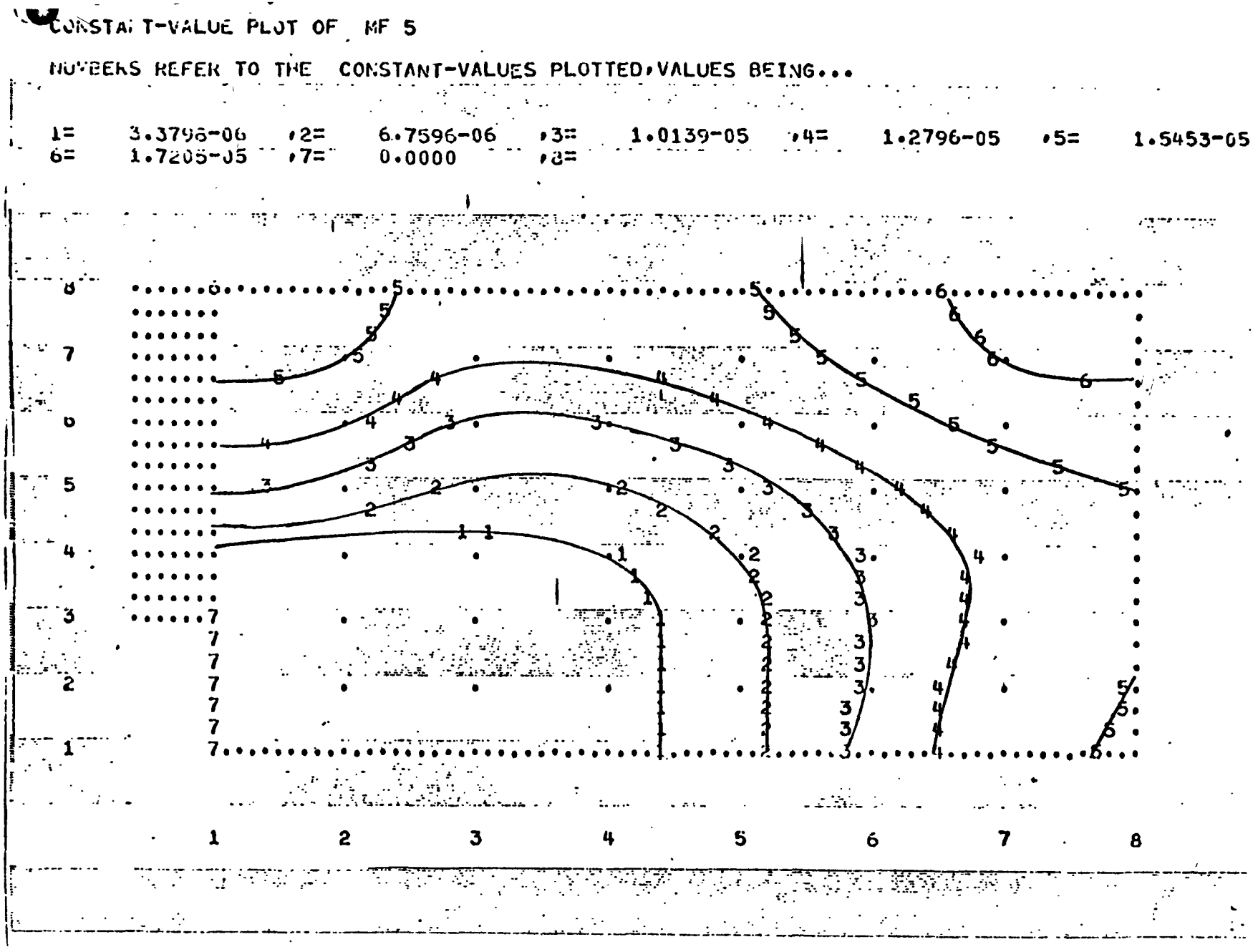

Figure 6. SMAC.1 Basic Case NO Mass Fraction.

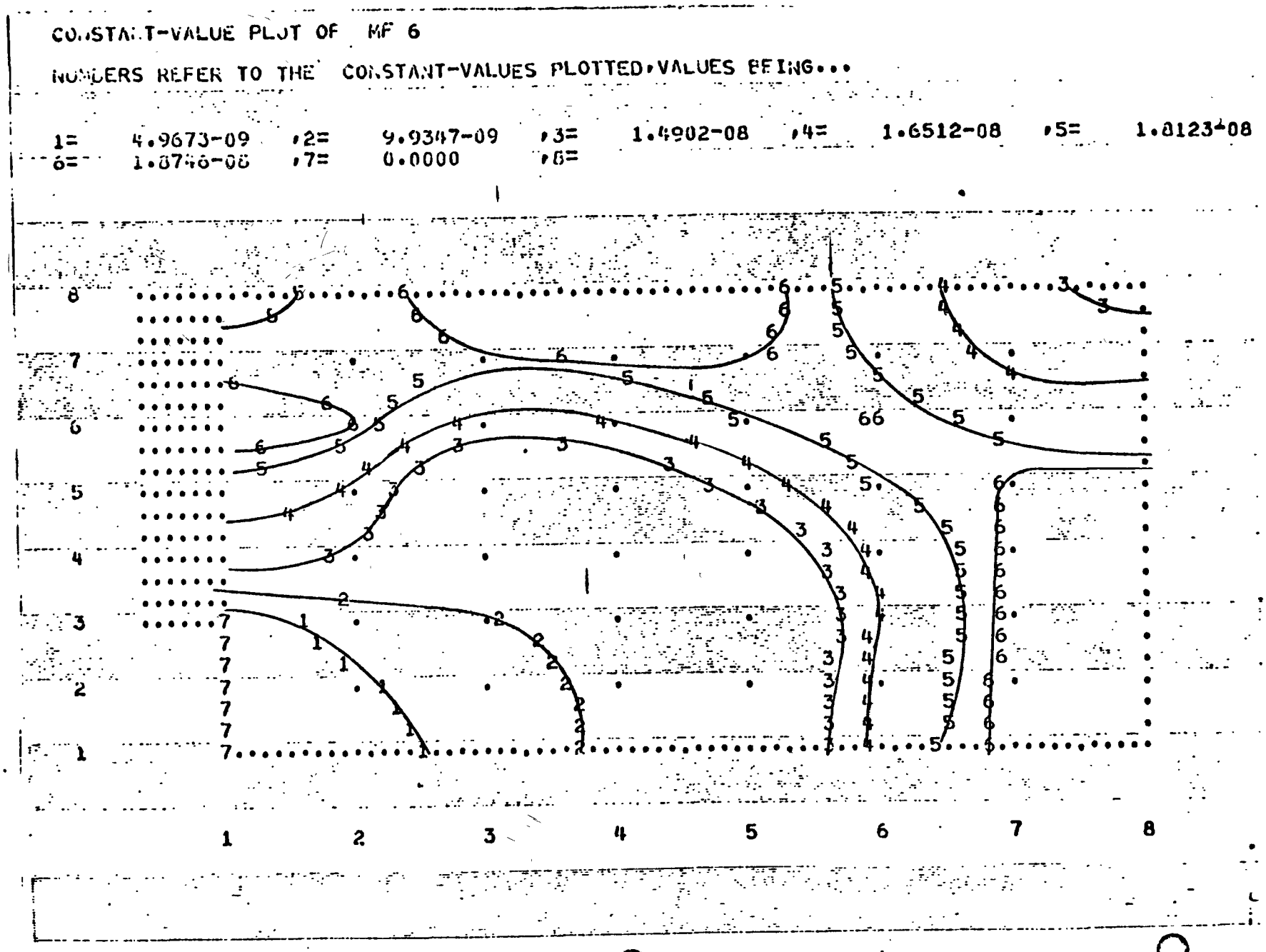

Figure 7. SMAC.1 Basic Case O_2 Mole Fraction

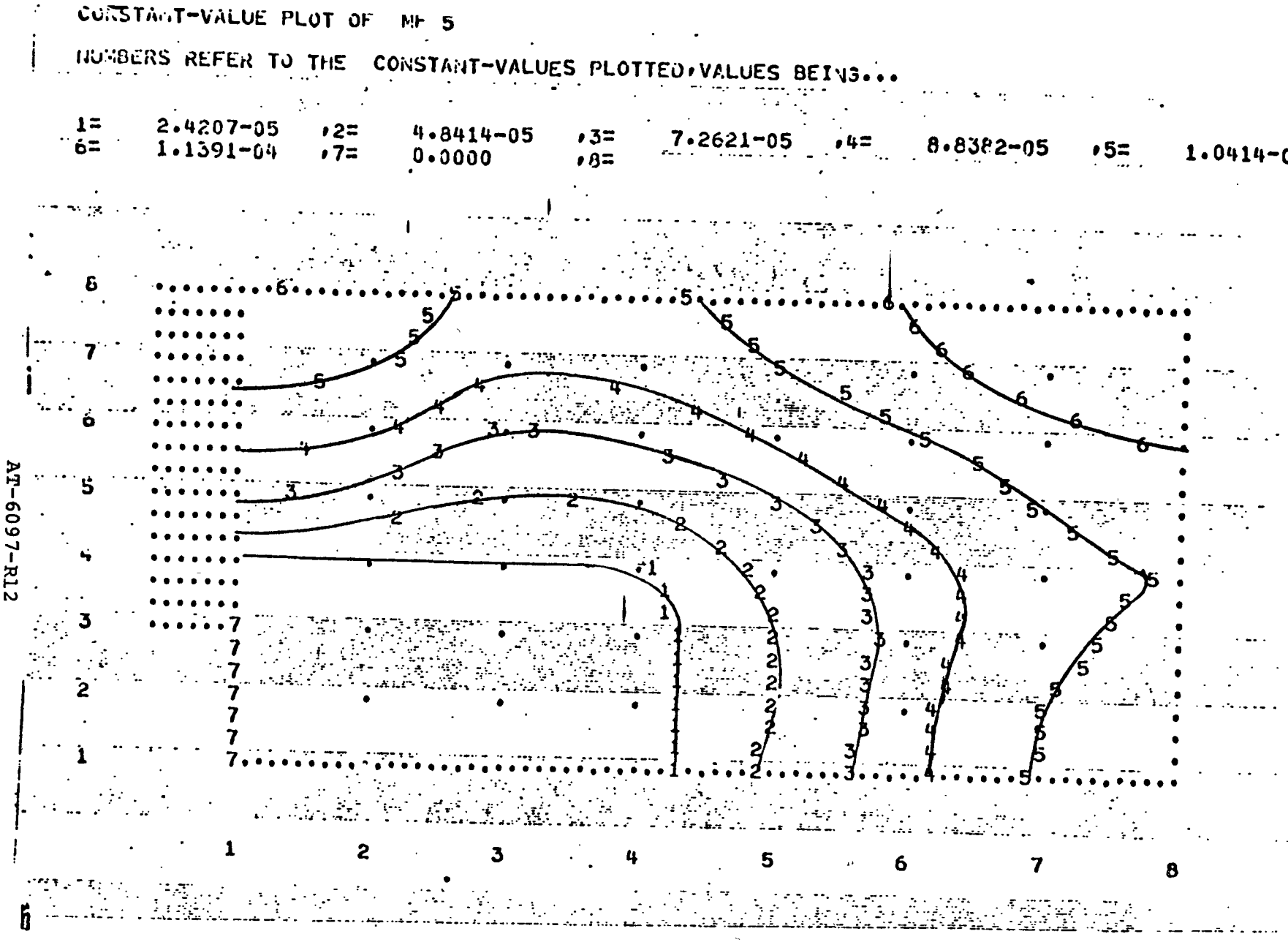

Figure 8. SMAC.1 T+500 NO Mass Fraction.

CONSTANT-VALUE PLOT OF MF 6

NUMBERS REFER TO THE CONSTANT-VALUES PLOTTED, VALUES BEING...

1= 2.0139-08 ,2= 4.0279-08 ,3= 6.0418-08 ,4= 7.1389-08 ,5= 8.2240-03
6= 1.8493-08 ,7= 0.0000 ,8=

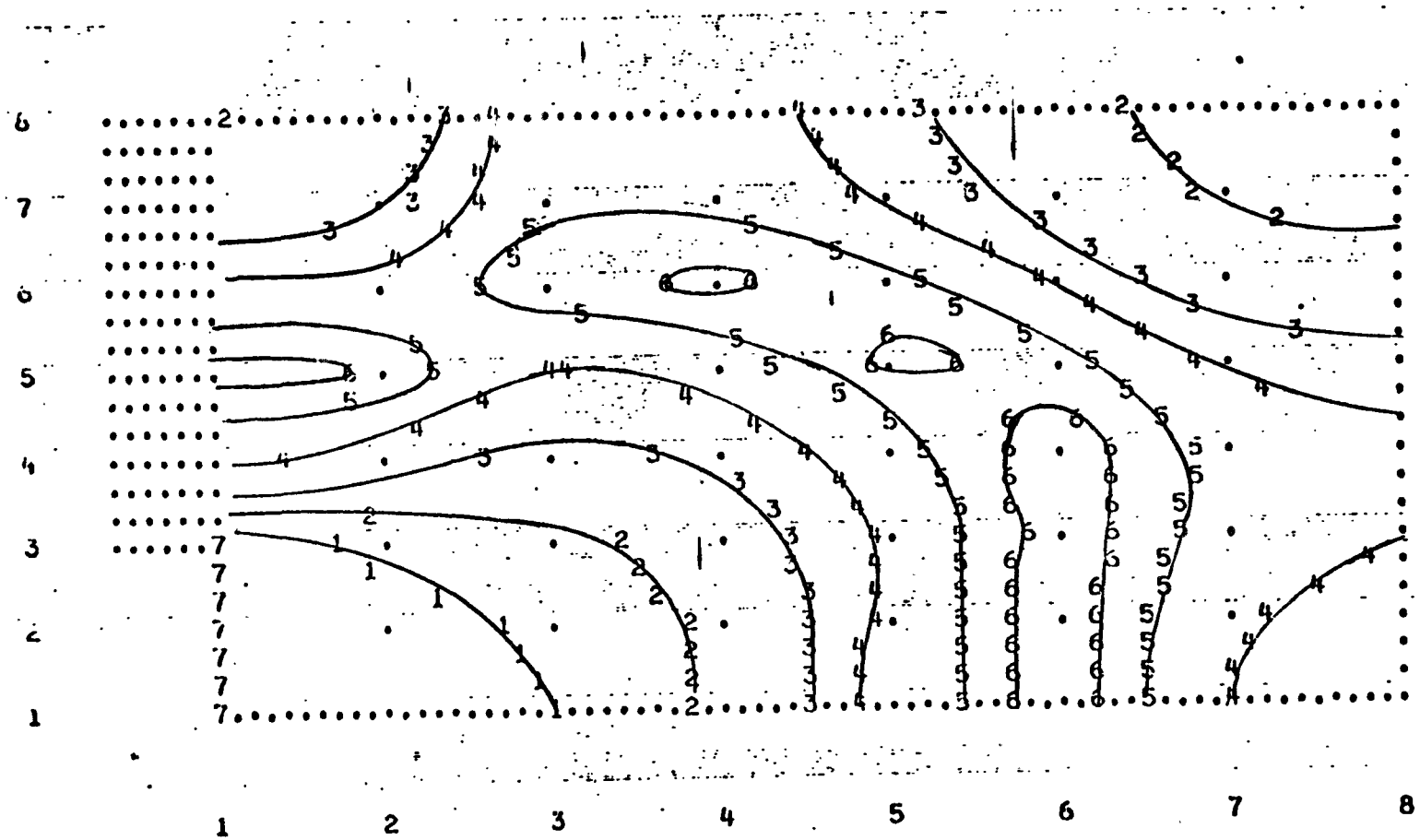

Figure 9. SMAC.1 T+500 NO_2 Mass Fraction.

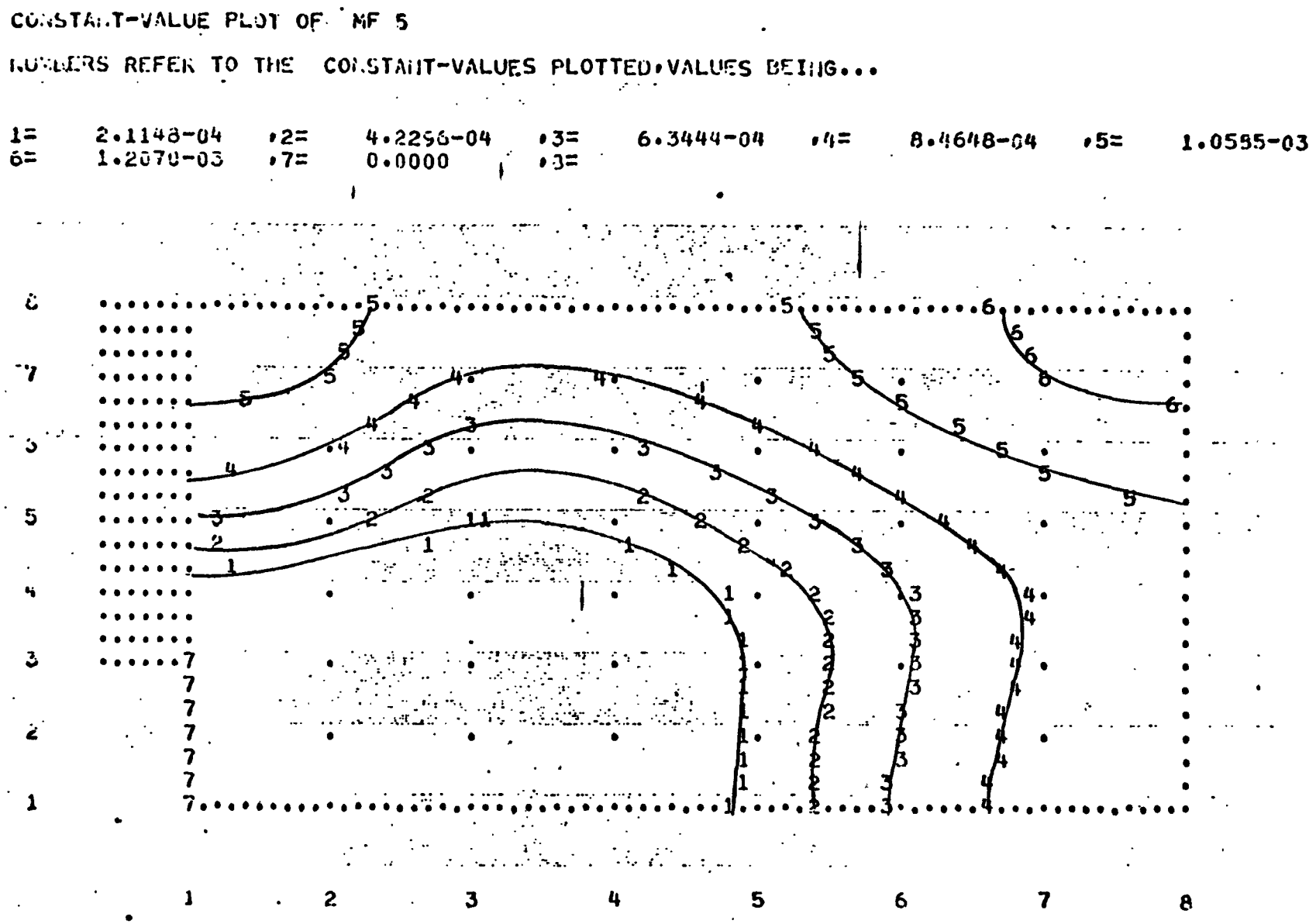

Figure 10. SMAC.1 ρx10 NO Mass Fraction.

CONSTANT-VALUE PLOT OF NF 6

NUMBERS REFER TO THE CONSTANT-VALUES PLOTTED, VALUES BEING...

1= 2.6649-06 ,2= 5.3697-06 ,3= 8.0543-06 ,4= 9.9213-06 ,5= 1.1708-05
6= 1.2972-05 ,7= 0.0000 ,8=

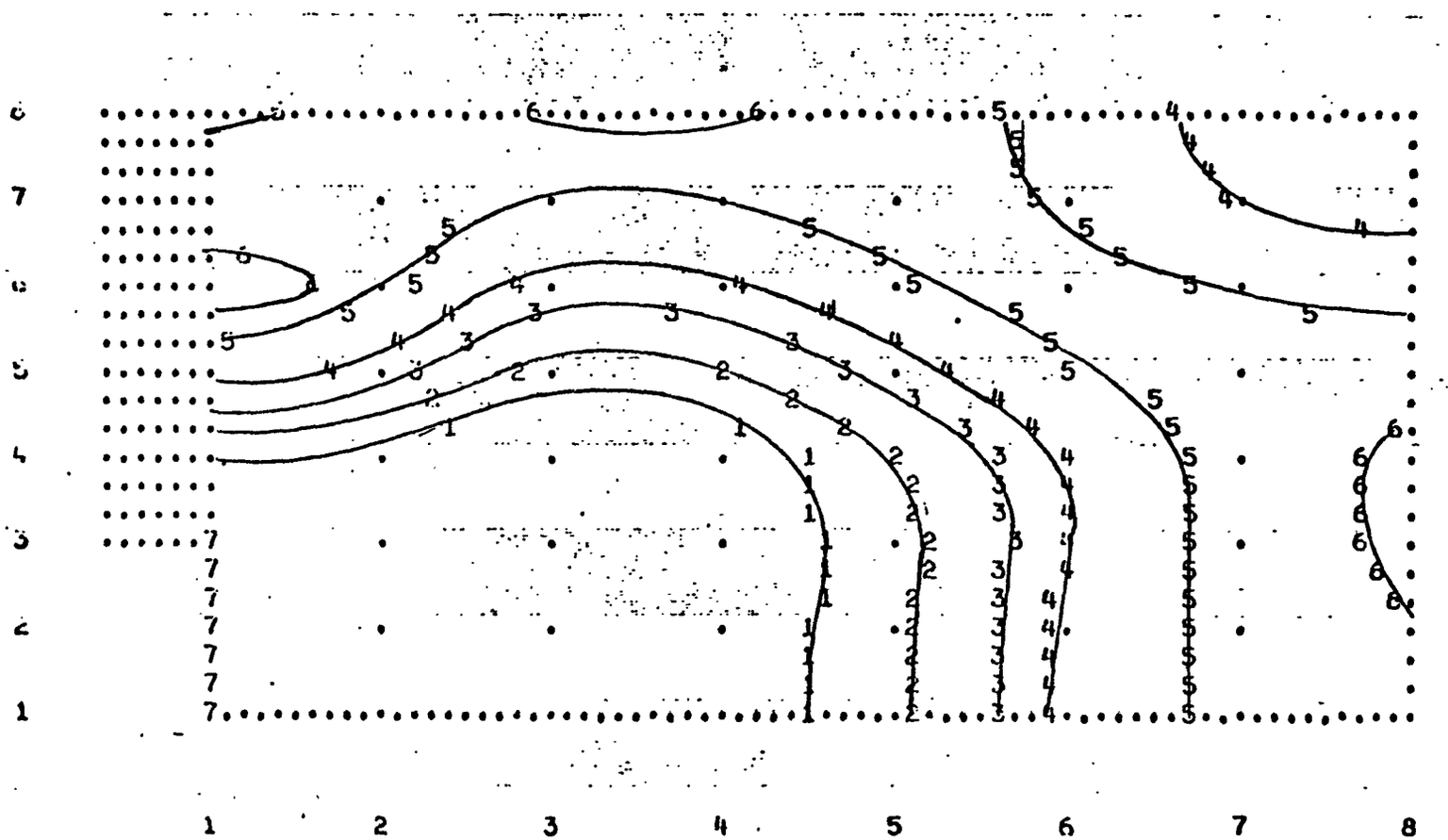

Figure 11. SMAC.1 ρ_{x10} NO_2 Mass Fraction.

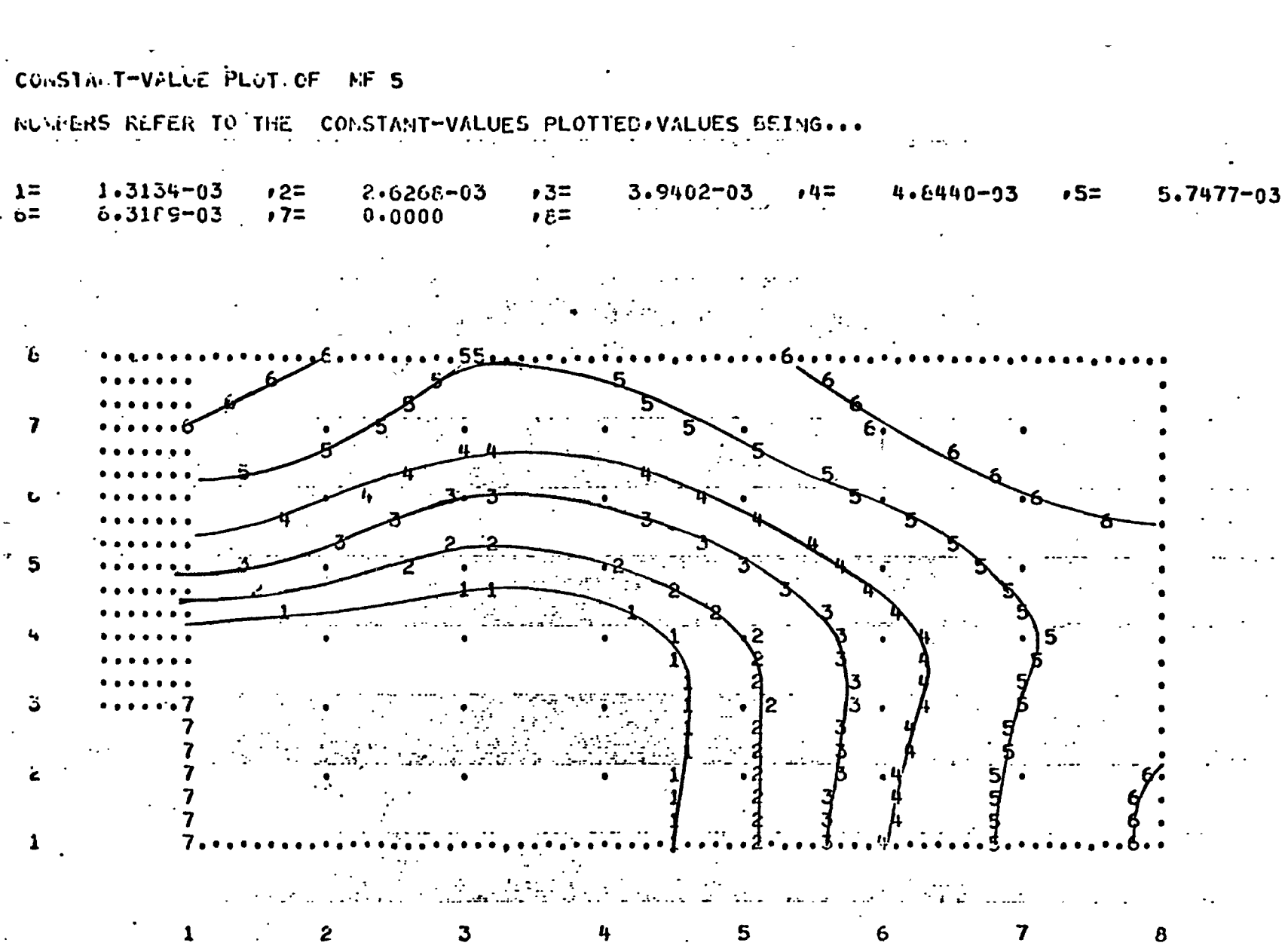

Figure 12. SMAC.1 T+500, ρx10 NO Mass Fraction.

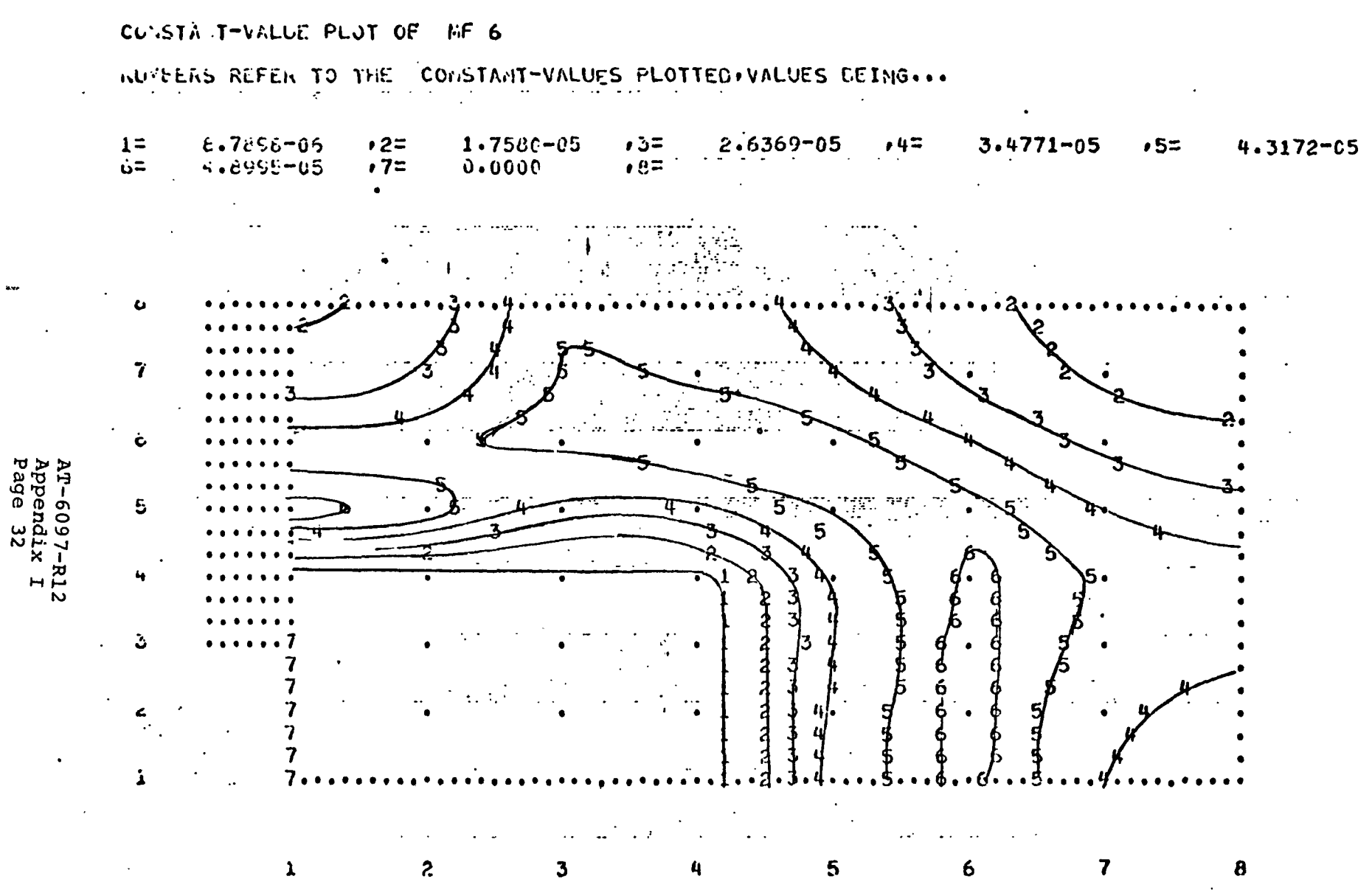

Figure 13. SMAC.1 T+500, ρx10 NO_2 Mass Fraction.

2. ONE-DIMENSIONAL KINETICS COMPARISON

The one-dimensional chemical kinetics program (ODK) of Reference 16 was run for 26 reactions involving 13 species as given in Table 3. The pressure was constant at 10 atmospheres and the initial temperature was 4300°R.

Temperatures, densities, and mass fractions of CO, CO_2,H_2O,O_2, and N_2 from the kinetics run were preloaded into a slightly modified version of the Gosman program in which one-dimensional flow was simulated. Since ODK assumes inviscid flow with no diffusion or heat transfer, similar assumptions were introduced into the Gosman comparison case by setting the viscosity to an extremely small value and the Prandtl and Schmidt numbers to unity.

The results shown in Table 4 and Figure 14 show very good agreement between ODK and the Gosman program. The quasi-equilibrium and steady state assumptions concerning the species O, OH, H, N, and N_2O are not exactly valid. The worst case is that of N_2O, which does not really react fast enough to be in steady state on the time scale of this example. Still, the assumptions seem to be adequate for the calculation of NO and NO_2.

TABLE 3

REACTIONS AND INITIAL COMPOSITION FOR ODK-GOSMAN COMPARISON

SPECIES TABLE INPUT ODK START CONDITIONS

		Mass Fractions
1	N2	.7501
2	O2	.2259
3	N	.2441-7
4	NO	.2600-3
5	O	.1590-2
6	H	.2863-5
7	OH	.1566-2
8	NO2	.1171-5
9	N2O	.9951-5
10	H2O	.5380-2
11	CO	.3062-3
12	CO2	.1483-1
13	H2	.3442-5

```
REACTION CARDS
 NO + O = NO2,          A=1.05E15,   N=0.,  B=-1.870,   RX 7,LEEDS 4.1
 O2 = O + O    , A=2.85E19,  N=1.00,  B=118.7,  RX 21,JOHNSTON(1968)
 N2 = N + N,    A=3.70E21,  N=1.60,  B=226.0,  RX 22,APPELTON(1968)
 H2 = H + H,    A=7.00E12,  N=-.50,  B=92.60,  RX 23,BROKAW (1970)
 H + OH = H2O,  A=3.00E19,  N=1.00,  B=0.00,   RX 25,PREHN (1967)
 N + O = NO,    A=1.00E20,  N=1.50,  B=0.00,   RX 26,WRAY (1963)
 O + N2 = N2O,  A=1.00E16,  N=1.00,  B=0.00,   RX 28,BORTNER(1967)
 CO + O = CO2, A=6.30E15, N=0.00, B=2.50,  RX29, BAULCH(1968)
END TBR REAX
 N + NO = N2 + O,       A=3.10E13,   N=0.,  B=0.334,    RX 1,LEEDS 4.11
 N + O2 = NO + O,       A=6.43E9,    N=-1.,  B=6.250,   RX 2, ROBERTS
 N + OH = NO + H,       A=4.22E13,   N=0.,  B=0.0,      RX 3,ROBERTS
 H + N2O =N2 +OH,       A=2.95E13,   N=0.,  B=10.77,    RX 4,ROBERTS
 O + N2O = N2 + O2,     A=3.82E13,   N=0.,  B=24.1,     RX 5  ROBERTS
 O + N2O = NO + NO,     A=4.58E13,   N=0.,  B=24.1,     RX 6  ROBERTS
 NO2 + O = NO + O2,     A=1.0E13,    N=0.,  B=0.600,    RX 8  LEEDS 5.1
 CO + OH = CO2 + H,     A=5.6E11,    N=0.,  B=1.080,    RX 9 L1.1
 O + OH = O2 + H,       A=1.3E13,    N=0.,  B=0.,       RX 10 L3.14
 OH + OH = H2O + O,     A=5.75E12,   N=0.,  B=.780,     RX 11 L2.20
 CO + OH = CO2 + H,     A=5.60E11,  N=0.00,  B=1.08,   RX31,BAULCH(68)
 H + O2 = OH + O,      A=1.44E14,  N=0.00,  B=16.60,    RX38,BELLES(70)
  O + H2 = H + OH   ,  A=2.96E13,  N=0.00,  B=9.80,   RX39 BRABBS 70
 OH + H2 = H + H2O,     A=2.19E13,  N=0.00,  B=5.15,    RX40,BAULCH(68)
 OH + OH = O + H2O,     A=5.75E12,  N=0.00,  B=0.78,    RX41,BAULCH(68)
 NO2 + H = NO + OH,      A=7.20E14, N=0.00,  B=1.93,    RX48,SCHOFELD(67)
 N + CO2 = NO + CO,     A=1.93E11,  N=0.00,  B=3.40,   RX 50,AVRAMENK(65)
 CO2 + O = CO + O2,     A=1.90E13,  N=0.00,  B=54.15,   RX51,BAULCH(68)
LAST REAX
THIRD BODY REAX RATE RATIOS
ALL EQUAL 1.0
LAST CARD
```

TABLE 4.

COMPARISON OF ONE-DIMENSIONAL KINETICS AND GOSMAN NO_x CALCULATIONS

t(msec)	Program	Mass Fractions						
		$NOx10^3$	NO_2x10^5	$Ox10^4$	$OHx10^4$	$Hx10^7$	$Nx10^9$	N_2Ox10^6
0	ODK	.26	.12	15.90	15.66	28.63	24.41	9.95
	Gosman	.26	.12	14.29	14.41	24.30	17.78	1.10
.375	ODK	1.16	.50	6.95	10.47	8.62	10.06	4.72
	Gosman	1.31	.55	6.58	10.16	7.93	9.53	2.57
3.553	ODK	6.37	2.77	6.50	10.06	7.96	10.77	4.76
	Gosman	6.03	2.56	6.15	9.76	7.32	9.98	2.73
7.553	ODK	10.69	4.68	6.15	9.74	7.46	10.90	4.46
	Gosman	10.61	4.53	5.82	9.45	6.87	10.01	3.11
9.948	ODK	12.46	5.47	6.01	9.60	7.26	10.87	4.42
	Gosman	12.52	5.36	5.69	9.32	6.68	9.98	3.37

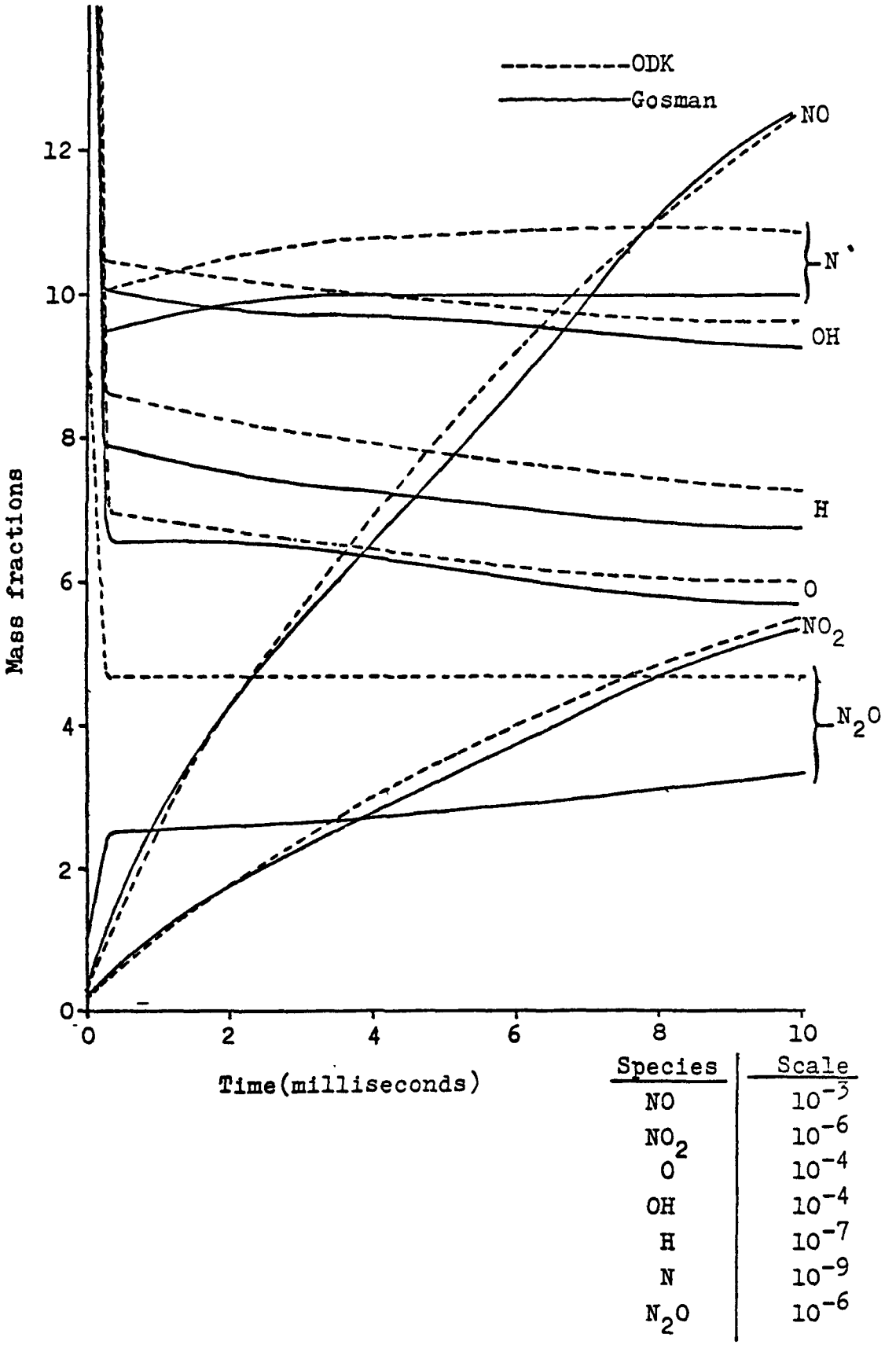

Species	Scale
NO	10^{-3}
NO_2	10^{-6}
O	10^{-4}
OH	10^{-4}
H	10^{-7}
N	10^{-9}
N_2O	10^{-6}

Figure 14. Comparison of One-Dimensional Kinetics and Gosman NO_x Calculations.

APPENDIX II

EMISSIONS ANALYZERS PRINCIPLES OF OPERATION

A. ANALYZER INSTRUMENTATION

This section reviews the gas analyzers and their principles of operation as used to conduct emissions measurements at AiResearch facilities.

A.1 Heated Hydrocarbon Analyzer (Beckman Model 402)

The hydrocarbon analyzer, Figure A-1, is designed to measure the total hydrocarbon contents of exhaust emissions from gasoline, diesel, gas turbine, and jet engines. The analysis is based on flame ionization, a highly sensitive detection method.

The instrument consists of:

(1) Heated, temperature-controlled sample line.

(2) Analyzer unit, incorporating a flame-ionization detector and associated sample-handling system, with critical sample-handling components contained within a temperature-controlled oven.

(3) Electronics unit, containing an electrometer amplifier and associated circuitry, readout meter, and recorder output provisions. The electronics unit is attached directly to the analyzer unit as shown in Figure A-1.

Sample from the source is drawn into the analyzer through the sample line. To prevent the loss of higher-molecular-weight hydrocarbons, the sample is maintained at an elevated temperature during its passage through the sample line and the interior of the analyzer. Temperature setpoint for the sample line and the analyzer oven will be approximately 350°F for the tests carried out according to the plan.

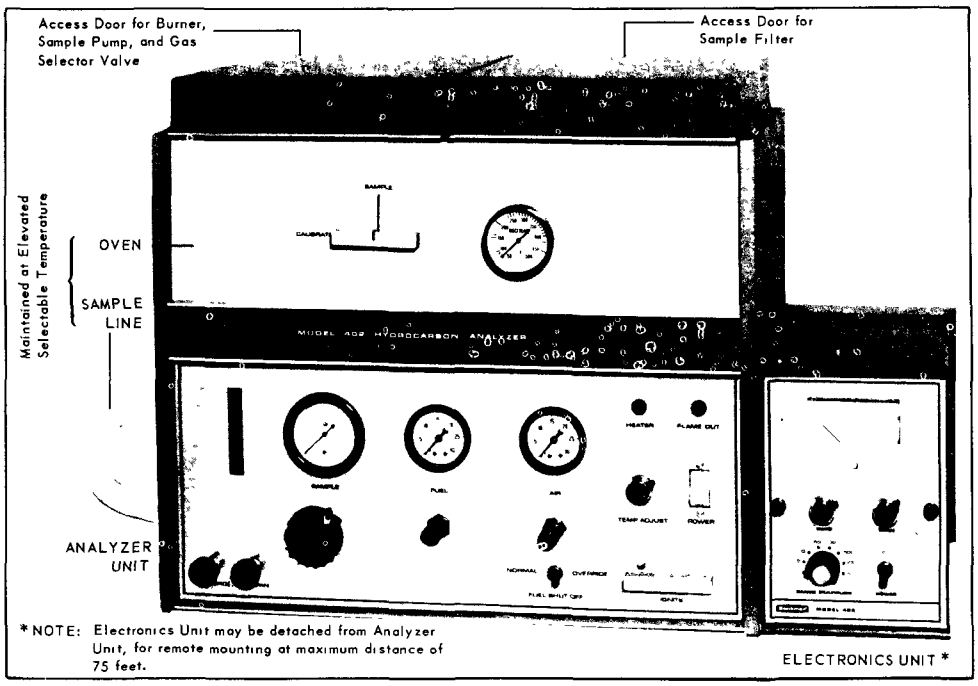

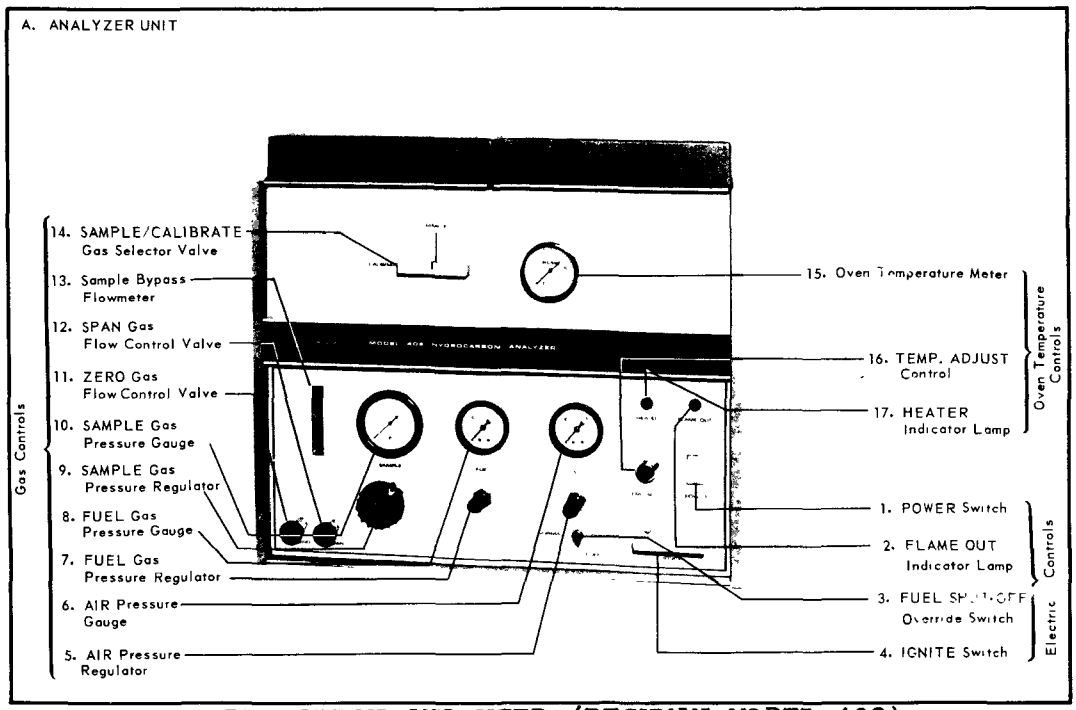

HYDROCARBON ANALYZER (BECKMAN MODEL 402)
(COURTESY BECKMAN INSTRUMENTS, INC.)

FIGURE A-1

MP-30224

The hydrocarbon sensor is in a burner where a regulated flow of sample gas passes through a flame sustained by regulated flows of a fuel gas and air. The flame formed when fuel gas (hydrogen diluted with an inert gas) burns in air contains an almost negligible number of ions. Introduction of traces of hydrocarbons into such a flame, however, produces a large amount of ionization. Within the flame, the hydrocarbon components of the sample stream undergo ionization, producing electrons and positive ions. Polarized electrodes collect these ions, causing current to flow through measuring circuitry located in the electronics unit. The ionization current is proportional to the rate at which carbon atoms enter the burner and is therefore a measure of the concentration of hydrocarbons in the original gas sample.

The flow diagrams for the analyzer and burner are shown in Figure A-2 A stainless-steel bellows-type positive displacement pump of four cu ft/min capacity draws the sample into the analyzer and through a glass fiber filter that removes particulate matter. The sample is then supplied to the burner under positive pressure. An internal sample-bypass arrangement provides high-velocity sample flow through the analyzer, thus minimizing system response time. A front-panel flowmeter indicates bypass flow. Since the ionization level is related to the flow rate of sample through the flame, the flowmeter must be set to read a sample flow identical to the calibration gas flow. The analyzer has rear-panel inlet ports for connection of suitably pressurized zero and span standard gases. Flow of each standard gas is controlled by a corresponding front-panel needle valve. A front-panel three-way valve permits selection of either the actual sample or the desired standard gas (i.e., "zero gas" or "span gas" referenced in Figure A-2) used in calibrating the instrument.

The oven, which uses air-bath heating, is maintained at the selected temperature by a solid-state temperature controller utilizing a thermistor sensor. A vertical partition divides the oven into

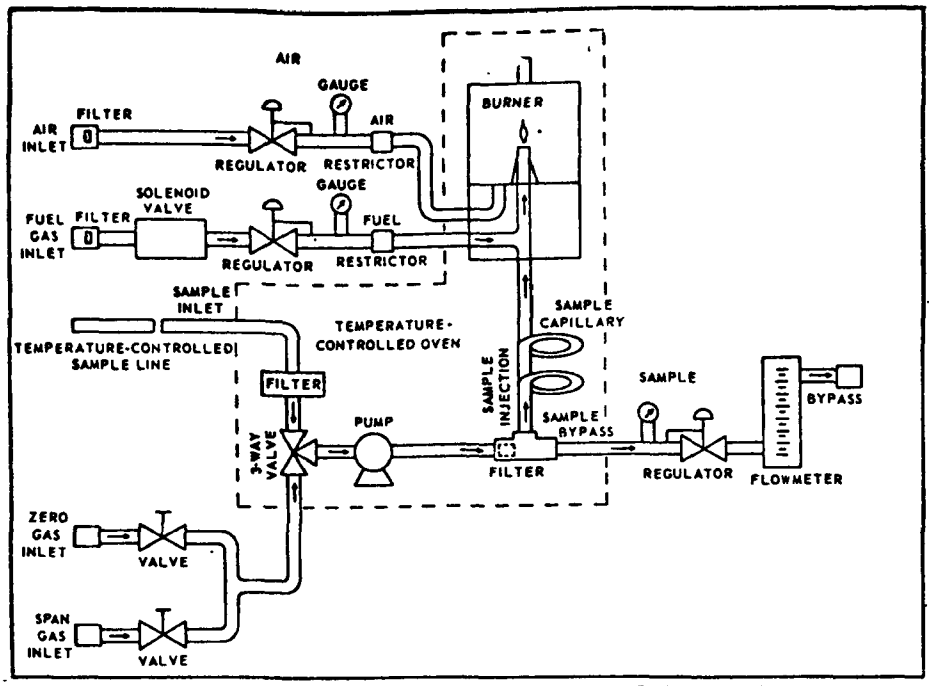

FLOW DIAGRAM

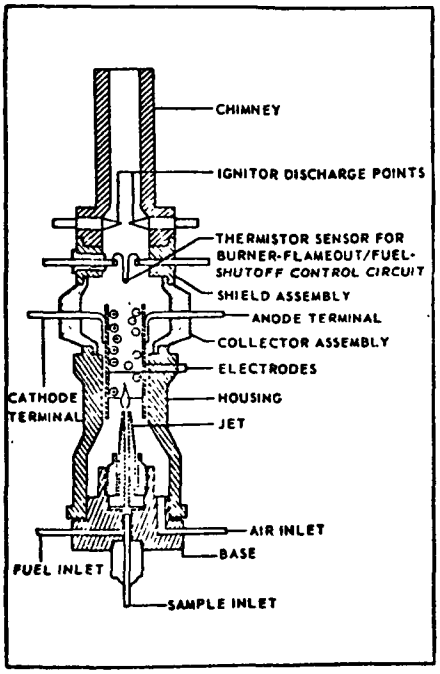

BURNER DIAGRAM

SPECIFICATIONS

Analysis Temperature	Adjustable from 200°F to 400°F
Line Voltage	107-127 VAC 50/60 Hz, 1000 watts max.
Ambient Operational Temperature	32°F to 110°F
Ambient Operational Humidity	95% R.H.
Potentiometric Output	10 mV, 100 mV, 1V
Sensitivity	5 ppm to 10% full scale as CH_4 with H_2/N_2 or H_2/He Fuel
Ranges	X1, X5, X10, X50, X100, X500, X1000, X5000 with continuous electronic span adjustment
Response	Less than 1 second for 90% of final reading (with CH_4 from analyzer input without sample probe)
Electronic Stability	±1% full scale/24 hrs. with less than 10° ambient temperature change
Repeatability	±1% full scale for successive samples
Temperature Controlled Probe	10 ft. length, teflon surface in contact with sample (proportional temperature controlled and adjustable from 200°F to 400°F)

HEATED HYDROCARBON ANALYZER SPECIFICATIONS AND DIAGRAMS
(FIGURES COURTESY OF BECKMAN INSTRUMENTS, INC.)

FIGURE A-2

two compartments with separate doors. The left-hand compartment contains the burner, the sample pump, and the three-way gas-selector valve. The right-hand compartment contains only the sample filter and permits access to the filter without disturbing temperature equilibrium of the other elements.

Within the analyzer, the fuel gas is routed to the burner through a solenoid valve controlled by the burner-flameout/fuel-shutoff circuitry. A thermistor sensor continuously monitors the status of the burner flame. In event of flameout, the valve closes to stop the flow of fuel gas; simultaneously, a front-panel indicator illuminates to alert the operator.

The electronics unit has front-panel controls for range selection and adjustment of zero and span. Readout is on a front-panel meter calibrated linearly from 0 to 100. In addition, a selectable output of 10 mv, 100 mv, or 1 volt is available to drive a voltage-type recorder.

A.2 Chemiluminescent/NO - NO_x Analyzer

The chemiluminescent analyzer is packaged as four separate units: (1) control unit, (2) an analyzer unit, (3) a reaction chamber mechanical vacuum pump, and (4) a converter for the thermal conversion of NO_2 to NO. For these tests, a Thermo Electron Corporation analyzer model 10A was used, which was operated in the NO_x and NO modes.

A typical arrangement of the Model 10A chemiluminescent analyzer is shown in Figure A-3. Other equipment needed for use with the analyzer are the NO and NO_2 standard gases, an oxygen source for the ozone generator, and an accumulator and suitable sample bypass pump to provide two to two and one-half cu ft/hr sample flow.

The control unit contains the switch for selection of sensitivity from seven available full-scale ranges (10, 25, 100, 250, 1000, 2500, and 10,000 ppm) and potentiometers which provide for instrument calibration.

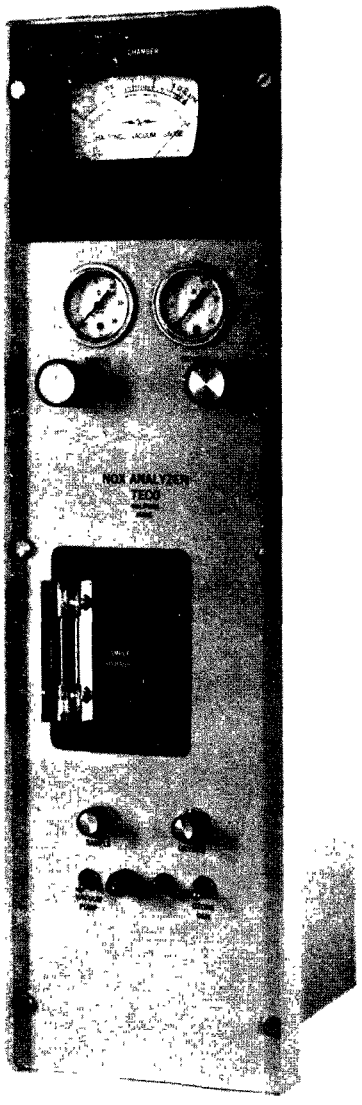

ANALYZER UNIT

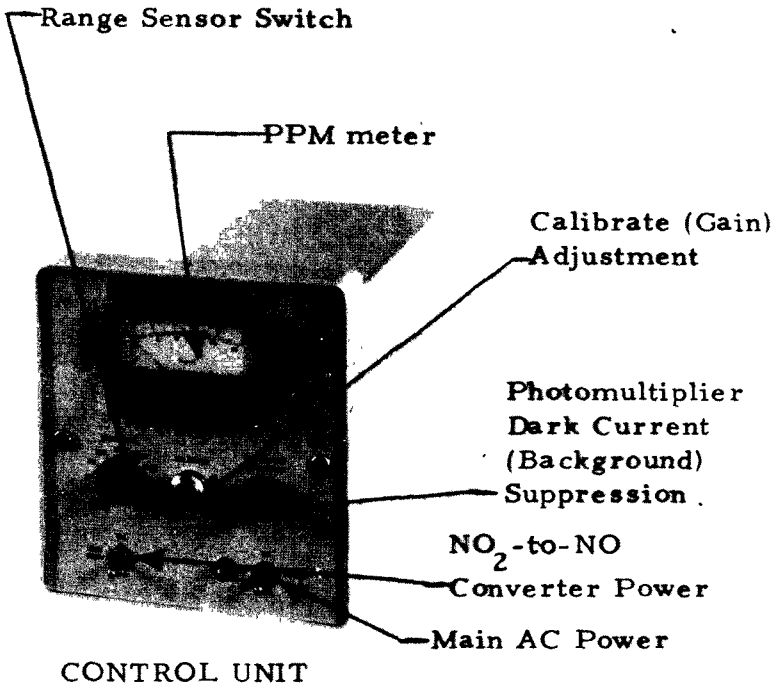

CONTROL UNIT

MODEL 10 CHEMILUMINESCENT ANALYZER (CONTROL AND ANALYZER UNITS)

FIGURE A-3

MP-30252

The analyzer unit contains the reaction chamber, the photomultiplier tube, the ozonator, the ozonator power supply, the oxygen and gas sample lines, capillaries, and pressure regulators.

Figure A-4 presents a schematic drawing of the entire chemiluminescent instrument with the portion inside the dashed rectangle representing the analyzer unit. The heart of the analyzer is the cylindrical reaction chamber where sample gas containing NO molecules mixes with O_3 molecules from the ozonator. Electronically excited NO_2 molecules are created that emit light (chemiliminescence) as the orbital electrons decay to their ground states.

The chemiluminescence is monitored through an optional filter by a high sensitivity photomiltiplier positioned at one end of the reactor. The filter-photomultiplier combination responds to light in a narrow wavelength band unique to the desired electron decay. Sample flow is controlled so that the output from the photomultiplier is linearly proportional to the NO concentration.

Oxygen, O_2, enters the analyzer unit, passing through a pressure regulator that is used to regulate the flow rate, and enters the ozonator. A fraction of the O_2 is converted to O_3, and the mixture passes through an orificing glass capillary to the reaction chamber.

Sample gas enters the instrument, passing through another glass capillary, and is bled off to the reaction chamber. That portion of the entering sample not diverted to the reaction chamber passes through a front panel flowmeter adjusted to two standard cubic feet per hour and a regulator to the instrument exhaust system. A bypass pump is used to pull the sample through the instrument. That portion of the entering gas sample diverted toward the reaction chamber is directed to the rear of the analyzer unit, where the sample gas will

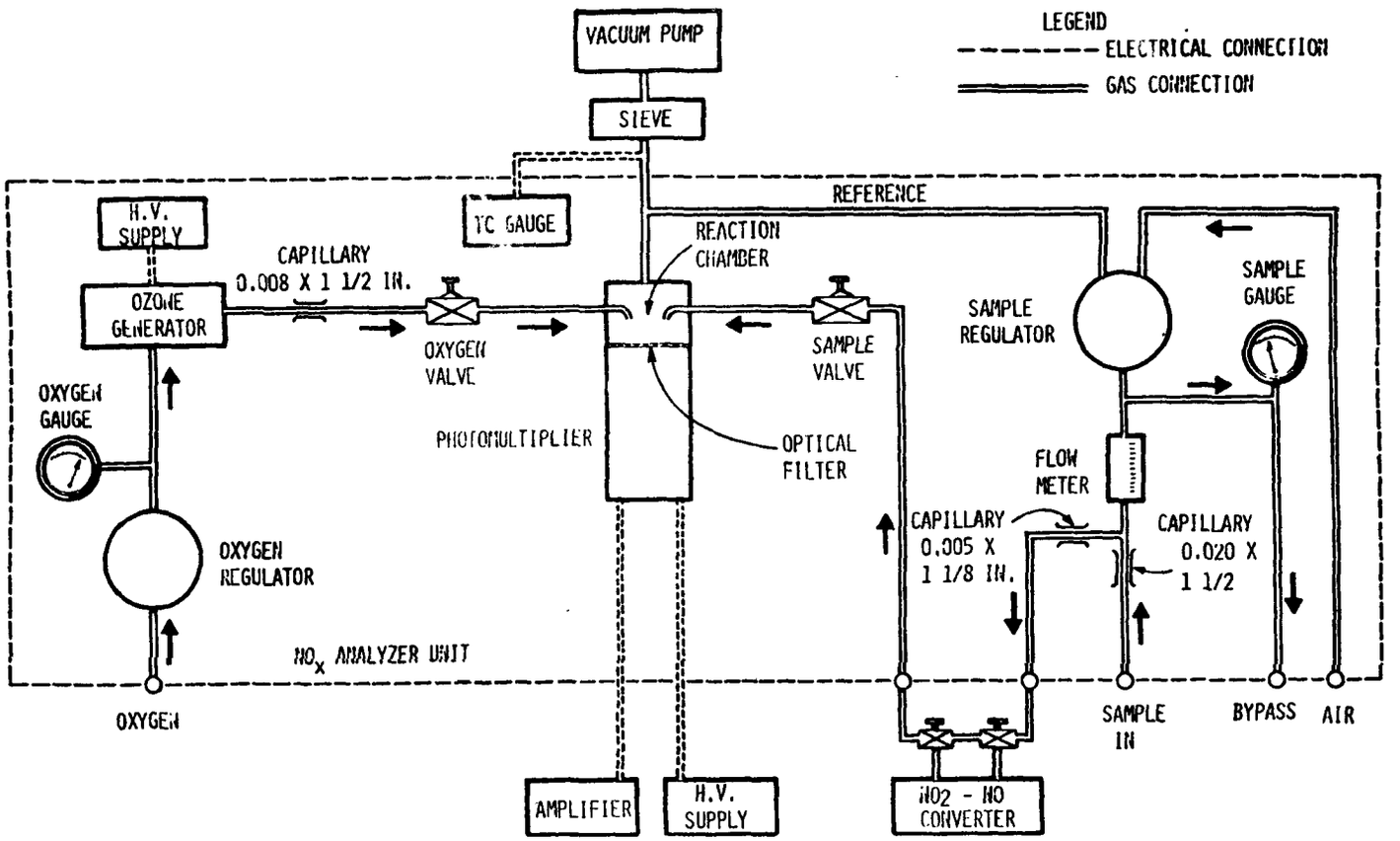

CHEMILUMINESCENT ANALYZER

FIGURE A-4

enter the converter if the instrument is operating in the NO_x mode (i.e., NO - NO_2 mixture mode). As explained below, use of the converter is unnecessary if the instrument is operating in the NO mode.

The basic chemiluminescent analyzer is only sensitive to NO molecules, as opposed to NO_2 molecules, since O_3 does not react with NO_2 to create chemiluminescence. Therefore, to measure NO_x (NO_2 + NO), the NO_2 must first be converted to NO. The conversion is accomplished by passing the sample gas through the converter, a thermally-insulated resistance-heated stainless steel coil at 1292°F. With the application of heat, NO_2 molecules in the sample gas are reduced to NO molecules. Two three-way valves located on the front of the converter direct the sample gas either through the converter to measure NO_x or past the converter to measure NO.

A mechanical vacuum pump is supplied to evacuate the analyzer reaction chamber to pressures in the 12 torr range. A metal bellows hose connects to a molecular sieve installed above the mechanical pump. The purpose of this sieve is to absorb O_3 in order to prevent breakdown of the pump oil.

The gas sample is pulled through the instrument by a small dynapump, after which it is exhausted to ambient. This pump improves the overall system response by moving the flow in the main sample line by about 20 liters per minute, while each instrument in the analyzer group removes flow from the main sample line at a much lower rate.

A.4 Non-Dispersive Infrared (NDIR) Analyzers for CO - CO_2

To measure the differential absorption of infrared energy, this instrument employs a double-beam optical system contained in the analyzer section. A simplified functional diagram and instrument specifications are shown in Figure A-5

Two infrared sources are used, one for the sample energy-beam, the other for reference energy-beam. The beams are blocked simultaneously ten times per second by the chopper, a two-sigmented blade rotating at five revolutions per second. In the unblocked condition, A of Figure A-5 each beam passes through the associated cell and into the detector.

The sample cell is a flow-through tube that receives a continuous stream of sample. The reference cell is a sealed tube filled with a reference gas. This gas is selected for negligible absorption of infrared energy of those wavelengths absorbed by the sample component of interest.

The detector consists of two sealed compartments separated by a flexible metal diaphragm. Each compartment has an infrared-transmitting window, to permit entry of the corresponding energy-beam. Both chambers are filled, to the same sub-atmospheric pressure, with the vapor of the component of interest. Therefore, each chamber will absorb infrared energy from its source and will respond.

The response of the two detector chambers differs, since in operation the presence of the infrared-absorbing component of interest in the sample streams leaves less energy available for the corresponding detector chamber. There is, thus, a difference in energy levels between the sample (containing the component of interest) and the reference (non-absorbing) sides of the system. This energy difference results in the following sequence of events.

SPECIFICATIONS

MAXIMUM ZERO DRIFT:
±1% of full scale per 8 hours.

MAXIMUM SPAN DRIFT:
±1% of full scale per 24 hours.

SENSITIVITY:
0.5% of full scale.

ACCURACY:
±1%.

AMPLIFIER RESPONSE SPEED:
90% response in 0.5 second.

AMBIENT TEMPERATURE RANGE:

IR315, IR315L, −20° to +120°F.

OUTPUT (Options Available):
Current output—0 to 5 ma into 500 ohms maximum.
Voltage output—Adjustable to match any potentiometric recorder having a span of between 1 and 100 mv.

VOLTAGE AND FREQUENCY (Options Available):
115 ±15 volts, 60 ±0.5 Hz (cps); or
115 ±15 volts, 50 ±0.5 Hz (cps).

MAXIMUM POWER CONSUMPTION

IR315, 530 watts; IR315L, 640 watts.

MAXIMUM SEPARATION OF AMPLIFIER CONTROL SECTION AND ANALYZER SECTION
500 feet.

SHIPPING WEIGHT:

IR315S, 115 pounds; IR315L, 170 pounds.

NET WEIGHT:

IR315S, 85 pounds; IR315L, 120 pounds.

CATALOG NUMBERS:
95700 Model IR315S Infrared Analyzer (Short Path)
95701 Model IR315L Infrared Analyzer (Long Path)

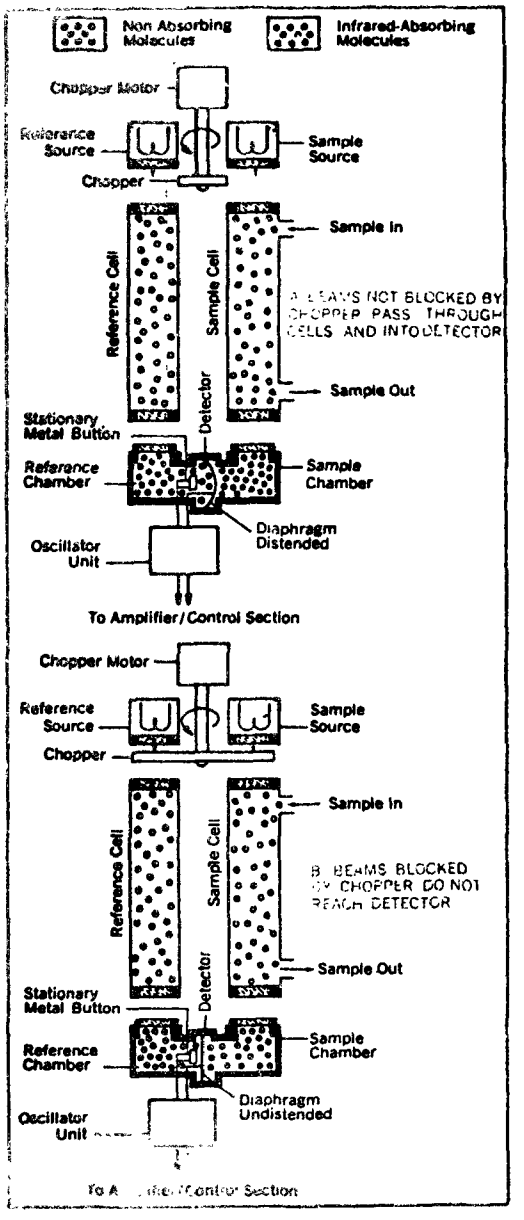

NON-DISPERSIVE INFRA-RED
ANALYZER SECTION SPECIFICATIONS
AND FUNCTIONAL DIAGRAM

FIGURE A-5

(1) Radiant energy absorption: In the sample cell through which the infrared radiation passes on the way to the sample chamber of the detector, part of the original energy of the sample infrared beam is absorbed by the component of interest present in the sample. In the reference cell, however, absorption of infrared energy from the reference beam is negligible, and the energy of this reference beam is higher.

(2) Temperature effect: Inside the detector, each beam heats the gas in the corresponding chamber, because of absorption of infrared energy by the component of interest. The gas in the reference chamber is heated to a higher temperature, however, since the energy available from the reference beam is higher.

(3) Pressure effect: The higher gas temperature in the reference chamber raises the pressure of this compartment above that of the sample chamber.

(4) Mechanical energy effect: The higher gas pressure in the reference chamber distends the diaphragm toward the sample chamber. The energy difference between the two chambers in thus expended in flexing the diaphragm.

(5) Capacitance effect: The diaphragm and an adjacent stationary metal button (see Figure A-5) constitute a two-plate variable capacitor. Distention of the diaphragm away from the button decreases the capacitance.

When the chopper blocks the beams, as in B of Figure A-5, pressures in the two chambers equalize, and the diaphragm returns to the undistended condition. As the chopper alternately blocks and unblocks the beams, therefore, the diaphragm pulses, thus changing detector

capacitance cyclically. The detector signal is passed through the electronic circuitry, where it is treated and sent to a meter and recorder.

The meter reading is a function of the concentration of the component of interest in the sample stream. When the instrument is put into operation, it is adjusted so that a reading of zero or any desired arbitrary reading corresponds to a concentration of zero percent of the component of interest, while a fullscale reading corresponds to the highest concentration in the operating range covered. Each instrument is provided with a calibration curve for converting meter readings to concentrations.

APPENDIX III

SAMPLE DATA SHEETS

DATE: 9 Oct '7[illegible] COMBUSTION CHAMBER LINER P/N: [illegible] IGNITION UNIT P/N: ______ TEST CELL: [illegible]

EWO: [illegible] FUEL ATOMIZER P/N: [illegible] IGNITION LEAD P/N: ______ TEST CREW: [illegible]

TEST REQUEST NO. [illegible] FUEL: [illegible] IGNITER PLUG P/N: ______

	UNITS	CD	LOC	A	B	C	D	E	F	G	H	I	J	K	L	M	N	
TIME				11H	10L	10M	10H	9L	9M	9H	8L	8M	8H	7H	7M	7L	6H	6M
BAROMETER	IN. Hg A	X2	1	[illegible]	28.68	[illegible]	28.68	[illegible]	[illegible]	[illegible]	[illegible]	[illegible]	[illegible]	28.68	[illegible]	28.68	28.68	28.68
4. AIR ORIFICE INLET PRESSURE	PSIG		13	[illegible]	150.	150.	150.	[illegible]	105.	[illegible]	100.	[illegible]	[illegible]	50.	[illegible]	50.	50.	50
ORIFICE INLET TEMPERATURE	°F		25	[illegible]	50.	45.	45.	48.	48.	[illegible]	48.	48.	48.	52.	52.	50.	45.	45
" " "	°F		37															
ORIFICE ΔP	IN. H_2O		49	[illegible]	24.0	24.7	24.7	22.[illegible]	21.6	22.[illegible]	11.4	11.4	11.2	3.8	9.0	9.0	6.0	6.3
4. DUCT DIAMETER	INCHES		61	[illegible]	→	→	→	→	→	→	→	→	→	→	→	→	→	→
4. ORIFICE DIAMETER	INCHES	X3	1	[illegible]	→	→	→	→	→	→	→	→	→	→	→	→	→	→
COMBUSTOR STATIC ΔP	IN. H_2O		13															
COMBUSTOR STATIC ΔP	IN. Hg		25	[illegible]	1.80	1.87	1.72	1.45	1.40	1.50	.90	.90	.55	.60	.60	.55	.35	.35
COMBUSTOR TOTAL ΔP	IN. H_2O		37															
COMBUSTOR TOTAL ΔP	IN. Hg		49															
COMBUSTOR INLET STATIC PRESS. (CISP)			61	[illegible]	72.1	72.0	72.0	48.5	48.6	47.8	31.3	31.5	31.5	16.9	16.7	16.4	13.4	13.2
" " " "		X4	1															
" " " "			13															
COMBUSTOR DISCH. STATIC PRESS. (CDSP)			25	[illegible]	70.5	70.7	70.1	46.9	47.1	46.5	31.1	31.3	31.4	16.3	16.2	16.0	13.0	13.0
" " " "			37															
" " " "			49															
COMBUSTOR INLET TOTAL PRESS. (CITP)			61	[illegible]	71.8	71.5	71.7	48.2	45.[illegible]	47.7	30.5	30.7	32.7	16.7	16.6	16.3	13.3	13.2
" " " "		X5	1															
" " " "			13															
COMBUSTOR DISCH. TOTAL PRESS.																		
" " " "																		
" " " "					758		[illegible]	[illegible]			[illegible]							
COMBUSTOR INLET TEMP.	°F	X5	25	[illegible]	[illegible]	[illegible]	[illegible]		[illegible]	[illegible]	[illegible]	[illegible]	[illegible]	[illegible]	[illegible]	[illegible]	[illegible]	[illegible]
" " "	°F	X5	37	[illegible]	[illegible]	[illegible]	725	[illegible]	760	760	760	770	770	750	[illegible]	[illegible]	750	750
FUEL PRESSURE	PSIG			[illegible]	332	380	430	144	170	195	50	54	65	17	17	15	10	9
OBSERVED FUEL FLOW	LB/HR	X5	49	[illegible]	42.3	45.	47.8	24.5	31.8	33.7	18.2	19.2	21.0	11.0	10.4	9.7	7.7	7.2
LIQ. FUEL ROTOMETER NO.	--			[illegible]	LR6	LR6	LR6	LR6	LR6	LR6	LR5	LR6	LR6	LR5	LR5	LR5	LR5	LR5
GAS ORIFICE INLET PRESSURE	PSIG	X5.1	1	[illegible]	62.	61.	61.	52.	50.	50.	31.5	31.5	31.5	17.5	17.5	17.5	13.5	13.5
ORIFICE INLET TEMP	°F		13	[illegible]	279	370	371.	312	313.	302.	260.	270.	268.	190.	192.	200.	186	188
" " "	°F		25															
ORIFICE ΔP	IN. H_2O		37	[illegible]	51.0	52.[illegible]	51.1	30.7	38.5	36.4	26.5	26.3	26.1	15.8	15.8	11.3	11.6	11.9
DUCT DIAMETER	INCHES		49	[illegible]	→	→	→	→	→	→	→	→	→	→	→	→	→	
ORIFICE DIAMETER	INCHES		61	[illegible]	→	→	→	→	→	→	→	→	→	→	→	→	→	

NOTES:
1. CARDS X2, X3, X4, X5 MUST HAVE AT LEAST ONE ENTRY.
2. IF COLUMNS ARE SKIPPED, RELETTER COLUMNS.
3. DECIMAL POINT MUST APPEAR FOR ALL NUMBERS.
4. FOR BELLMOUTH: AIR ORIFICE INLET PRESSURE = 0. (J6031P2 ONLY) DUCT DIAMETER = BELLMOUTH C D; ORIFICE DIAMETER = BELLMOUTH THROAT DIAMETER

DATA SHEET ORIGINAL RECEIVED BY: [illegible]

ALTITUDE EQUIPMENT DIVISION — CALCULATED / RECORDED / DRAWN / CHECKED / APPROVED

COMPUTER PROBLEM NO. J6031 J6031P1 J6031P2

MODEL NO. EPA

TEST TITLE Emission Study

DATA SHEET [illegible] A

DATE: [illegible]

EWO: [illegible]

		UNITS	CD	LOC	A	B	C	D	E	F	G	H	I	J	K	L	M	N	
1	COMBUSTOR DISCH. TEMP. STA 1 (1)	°F	X6.1	1	[illegible]	1310.	[illegible]	[illegible]	1240.	[illegible]	[illegible]	[illegible]	[illegible]	[illegible]	[illegible]	[illegible]	955.	[illegible]	1015
[illegible]	" " " " (2)			13	[illegible]	[illegible]	[illegible]	[illegible]	[illegible]	[illegible]	[illegible]	[illegible]	[illegible]	[illegible]	[illegible]	[illegible]	910.	[illegible]	1010
[illegible]	" " " " (3)			25	[illegible]	[illegible]	[illegible]	[illegible]	[illegible]	1240.	[illegible]	[illegible]	[illegible]	[illegible]	[illegible]	[illegible]	975.	[illegible]	1015
[illegible]	" " " " (4)			37	[illegible]	[illegible]	[illegible]	[illegible]	[illegible]	[illegible]	[illegible]	[illegible]	[illegible]	[illegible]	[illegible]	[illegible]	960.	[illegible]	930
[illegible]	" " " " (5)			49	[illegible]	[illegible]	[illegible]	[illegible]	[illegible]	[illegible]	[illegible]	[illegible]	[illegible]	[illegible]	[illegible]	[illegible]	[illegible]	[illegible]	920
[illegible]	" " " " (6)			61	[illegible]	[illegible]	[illegible]	[illegible]	[illegible]	[illegible]	[illegible]	[illegible]	[illegible]	[illegible]	[illegible]	[illegible]	[illegible]	[illegible]	970
[illegible]	" " " " (7)		X6.2	1	845.	[illegible]	[illegible]	[illegible]	[illegible]	[illegible]	[illegible]	[illegible]	[illegible]	[illegible]	[illegible]	[illegible]	[illegible]	[illegible]	1025
[illegible]	" " " " (8)			13	[illegible]	[illegible]	1290.	[illegible]	1195.	[illegible]	[illegible]	[illegible]	[illegible]	[illegible]	[illegible]	1050.	[illegible]	[illegible]	1010
[illegible]	" " " " (9)			25	[illegible]	[illegible]	[illegible]	[illegible]	[illegible]	[illegible]	[illegible]	[illegible]	[illegible]	[illegible]	113.	[illegible]	995.	[illegible]	1035
[illegible]	" " " " (10)			37	[illegible]	[illegible]	[illegible]	[illegible]	[illegible]	[illegible]	[illegible]	[illegible]	[illegible]	[illegible]	[illegible]	[illegible]	995.	[illegible]	1035
[illegible]	" " " " (11)			49	[illegible]	[illegible]	[illegible]	[illegible]	[illegible]	[illegible]	[illegible]	[illegible]	[illegible]	[illegible]	[illegible]	[illegible]	[illegible]	1100.	[illegible]
[illegible]	" " " " (12)			61	[illegible]	[illegible]	[illegible]	[illegible]	[illegible]	[illegible]	[illegible]	[illegible]	[illegible]	[illegible]	[illegible]	[illegible]	[illegible]	[illegible]	965
[illegible]	" " " " (13)		X6.3	1	[illegible]	[illegible]	[illegible]	[illegible]	[illegible]	[illegible]	[illegible]	[illegible]	[illegible]	[illegible]	[illegible]	[illegible]	[illegible]	[illegible]	[illegible]
[illegible]	" " " " (14)			13	[illegible]	[illegible]	[illegible]	[illegible]	[illegible]	[illegible]	[illegible]	[illegible]	[illegible]	[illegible]	[illegible]	[illegible]	915.	[illegible]	[illegible]
[illegible]	" " " " (15)			25	[illegible]	[illegible]	[illegible]	[illegible]	[illegible]	[illegible]	[illegible]	[illegible]	[illegible]	[illegible]	[illegible]	[illegible]	965.	[illegible]	1020
[illegible]	" " " " (16)			37	[illegible]	[illegible]	[illegible]	[illegible]	[illegible]	[illegible]	[illegible]	[illegible]	[illegible]	[illegible]	[illegible]	[illegible]	985.	[illegible]	1025
	" " " " (17)			49															
	" " " " (18)			61															
	" " " " (19)		X6.4	1															
	" " " " (20)			13															
	" " " " (21)			25															
	" " " " (22)			37															
	" " " " (23)			49															
	" " " " (24)			61															
	COMBUSTOR DISCH. TEMP. STA 2 (1)	°F	X7.1	1															
	" " " " (2)			13															
	" " " " (3)			25															
	" " " " (4)			37															
	" " " " (5)			49															
	" " " " (6)			61															
	" " " " (7)		X7.2	1															
	" " " " (8)			13															
	" " " " (9)			25															
	" " " " (10)			37															
	" " " " (11)			49															
	" " " " (12)			61															

NOTES: 1. DECIMAL POINT MUST APPEAR FOR ALL NUMBERS.
2. RELETTER COLUMNS IF ANY ARE SKIPPED.

DATA SHEET ORIGINAL RECEIVED BY: [illegible]

ALTITUDE EQUIPMENT DIVISION
CALCULATED
RECORDED
DRAWN
CHECKED
APPROVED

COMPUTER PROBLEM NO. J6031 J6031P1 J6031P2
MODEL NO. EPA
TEST TITLE: EMISSION STUDY

DATA SHEET 14 B

Appendix III
Page 2

FUEL SPECIFICATION

FX7133-1

NOV 15 1972 L. G. Brandt

	OIL & FUEL ANALYSIS 11877
	MATERIALS ENGINEERING

Requestor Hellekson Dept. 93-20
Copies To FINKELSTEIN 93-20
E. H. JONES 93-20

Manufacturer
Date OCT. 27, 1972

Customer
Engine Serial No. 3304 BUILD 6
Operating Hours 5 MINUTES
Sample Origin LACC-2
Charge No. 3309-410019-04-2000
Date Required OCT. 30, 1972

RECEIVED NOV 14 1972 MATERIALS ENGINEERING

☒ B. P. Distillation

IBP	152	°F
5%	198	
10%	312	
20%	328	
30%	349	
40%	364	
50%	352	% @ 400°F
60%	306	
70%	353	
80%	380	
90%	450	
95%	493	
E.P.	522	
% distilled	98	

☐ Flash Point

COC _____ °F

☐ T.A.N. _____

☒ L.H.V.

18,520 BTU/lb

☐ Other

☒ Specific Gravity

49.5 °API @60°F

Sp. Gr. = .782 @60°F

☒ Reid Vap. Press. 2.10 psi

☐ Viscosity

cs.	@ °F
	77
	100
	210

All tests performed conform to MIL-T-5624 H Spec grade JP-4.

AT-6097-R12
Appendix IV
Page 1

Analyst Jim Moore

APPENDIX V

SAMPLE EMISSIONS RECORDING

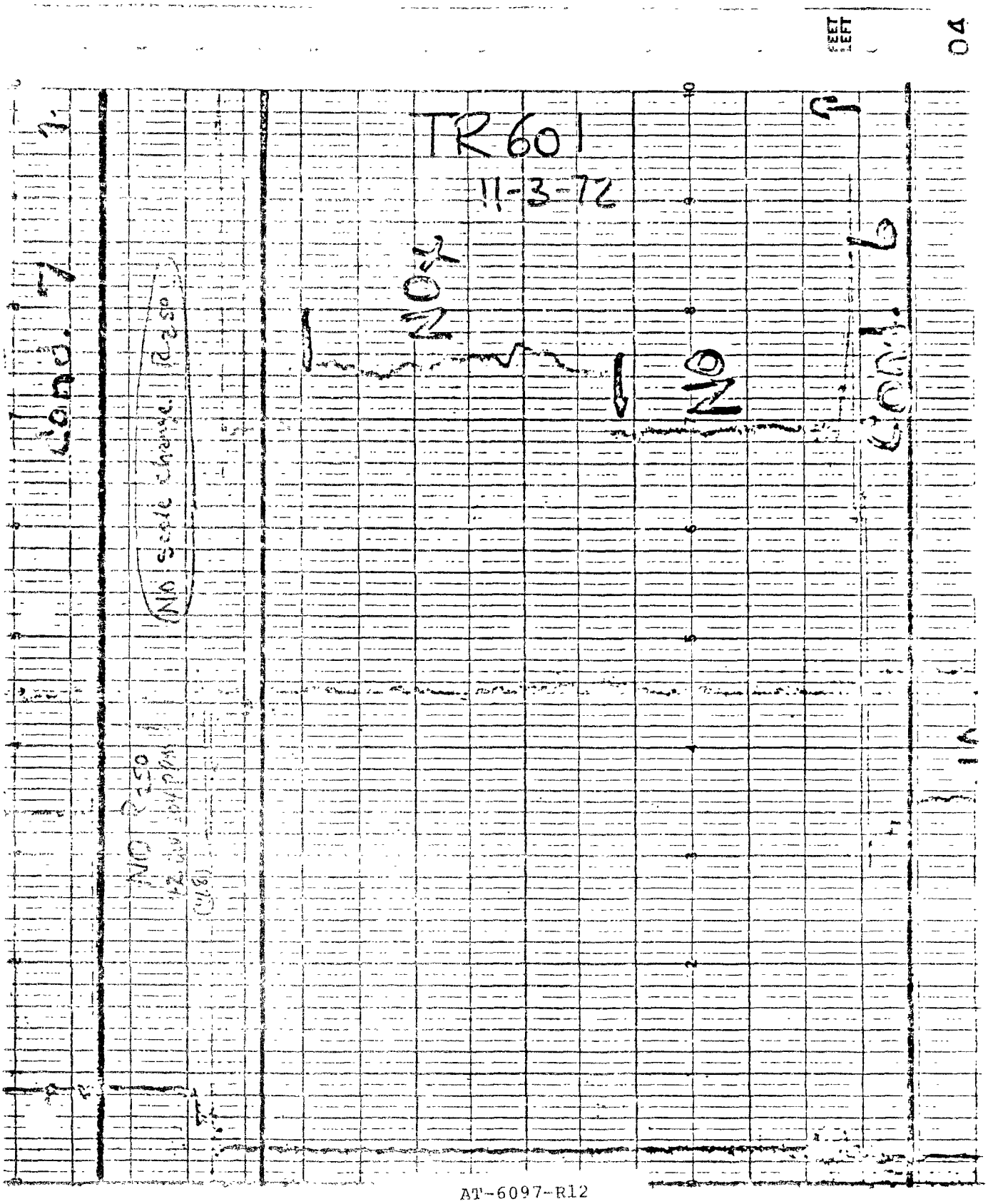

APPENDIX VI

COMBUSTOR PHOTOS

PHOTOGRAPHS

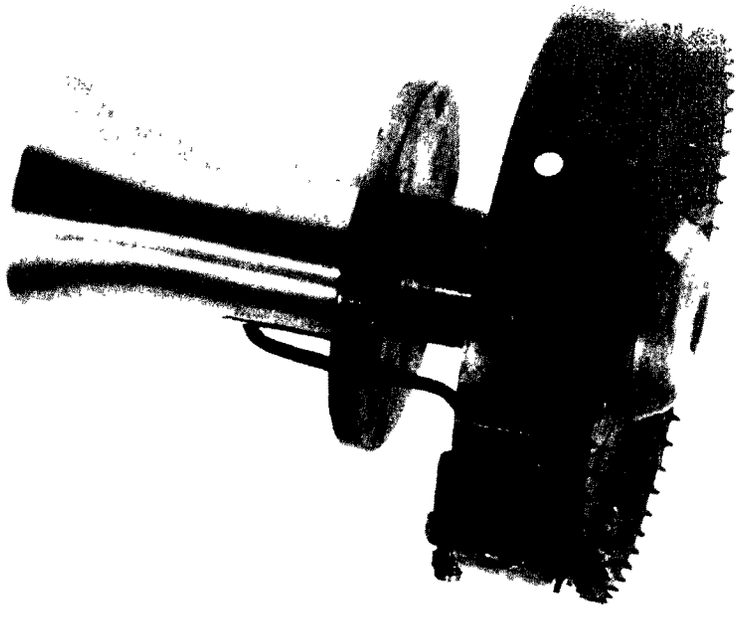

MP-38424

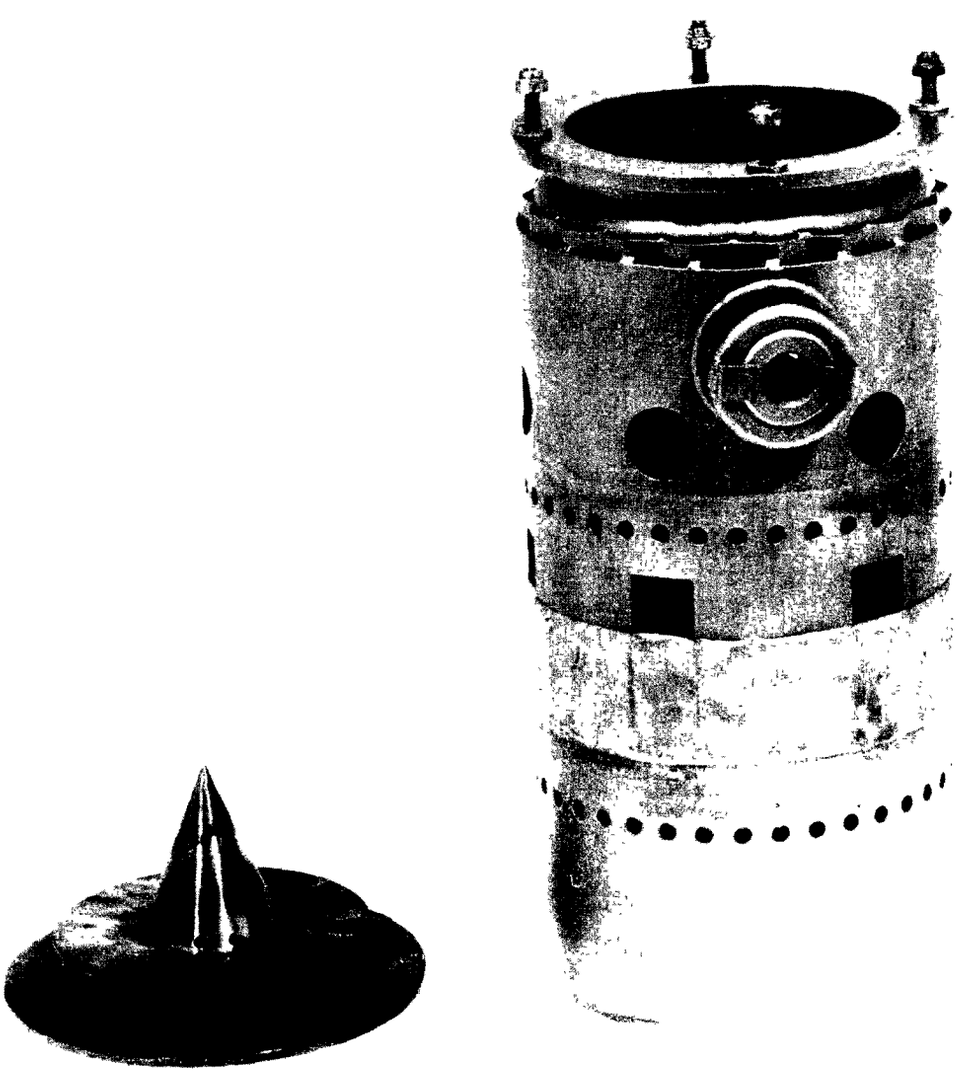

MP-38425

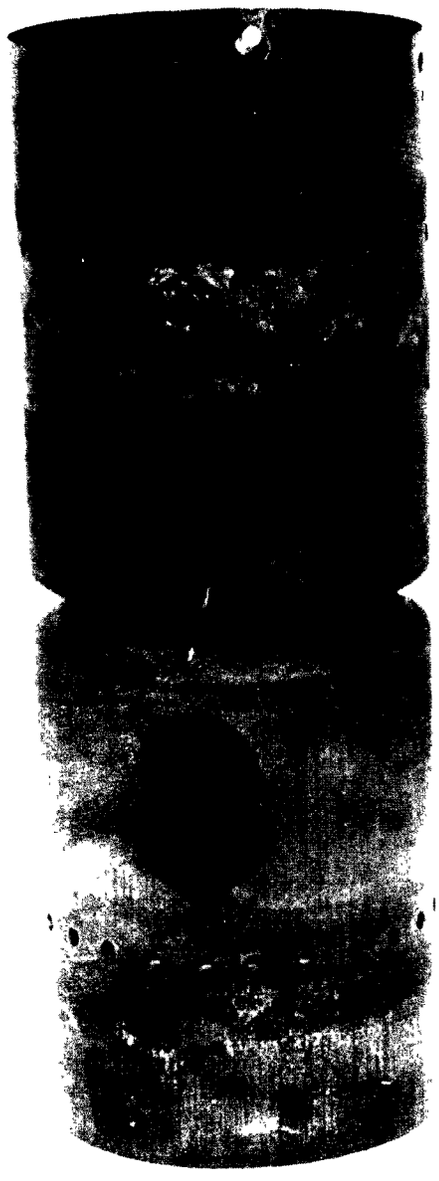

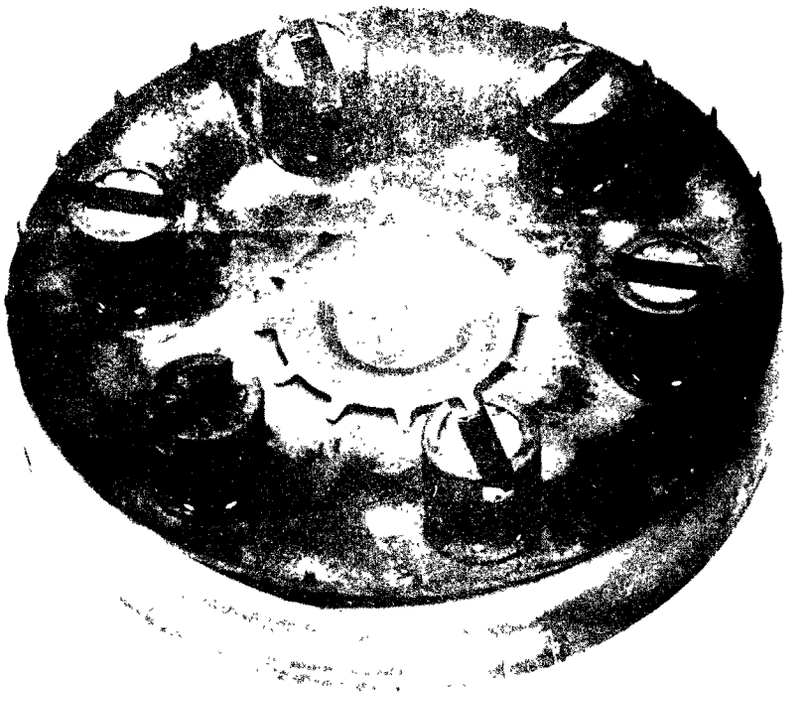

☆ G. P. O. 1973 — 747-788 / 328, REGION NO. 4